Rosette Nanotubes Supported Catalytic Metal Nanoparticles

by

Mohammad Rokib Hassan

A thesis submitted in partial fulfillment of the requirements for the degree of

Doctor of Philosophy

Department of Chemistry
University of Alberta

Abstract

In recent years, there has been considerable interest in gaining a fundamental understanding of nanoparticle (NP) synthesis and reactivity due to their wide applicability in the fields of biomedicine, optoelectronics and catalysis. Although metal NPs with a small and narrow size distribution tend to have high performance, their inherent heterogeneity generally results in less reactivity compared to their homogeneous counterparts. Hence, it is crucial to develop support systems, which not only permit the synthesis of uniform sized NPs and improve their solubility, but also provide a system suitable for "Green" catalysis.

Towards the effort of developing green catalysts, we have designed water-soluble, biocompatible rosette nanotube (RNT) supported Pd NPs composites. The RNT is a biocompatible tubular architecture that is self-assembled under aqueous conditions from a self-complementary guanine-cytosine (G∧C) DNA hybrid molecule. The hierarchical self-assembly process involves the initial formation of hexameric rosettes through intermolecular H-bonding interactions. These hydrophobic macrocycles then π-π stack to form the RNT. The *in-situ* formation of the M NPs occurs within 1 minute upon mixing the corresponding metal salt with the RNTs at ambient temperature in the absence of a reducing agent. On our quest to investigate the origin of the M NP formation, it was determined that water oxidation is responsible for the M^0 formation. Further studies on the kinetics of the M NPs formation showed that their nucleation and growth are very rapid and occur through a step-wise process. The intellectual design of the surface

functionalization and their well-defined structural features allow for the growth of the M NPs to be controlled to a certain size and prevent their further agglomeration. The studies showed that once the nucleation takes place, the NPs continue to grow until each nucleation pocket restricts further growth. Followed by the complete growth, a new nucleation takes place in an empty nucleation site.

Based on the success of the developed synthetic protocol, we then applied our M NPs/RNTs catalyst (M = Au, Pd and Pt) for olefin hydrogenation and Suzuki-Miyaura cross-coupling reactions. The results showed that we could perform such catalytic reactions smoothly under environmentally benign and mild conditions with a wide range of functional group tolerance. The utility of our Pd NPs/RNTs catalyst was also evaluated for the synthesis of a drug intermediate, an agrochemical, and various organic materials for solar cell, OLED and sensor applications. As the supramolecular chirality of the RNT is also translated in the presence of the M NPs on its surface, the asymmetry induction of the Pd NPs/RNTs catalyst was investigated. Unfortunately, only poor chirality induction was observed under the optimized conditions of the Suzuki-Miyaura cross-coupling reaction. The M NPs/RNTs catalysts were characterized by using standard materials characterization techniques including spectroscopy as well as microscopy.

To conclude this work, further research directions of this thesis work are also briefly discussed and suggested.

Dedication

To all prophets (especially Prophet Mohammad saas.) who

sacrificed their lives showing mankind the right path of life

Acknowledgments

First and foremost, I thank Almighty God for giving me the energy, passion, and patience to complete my PhD studies. I thank him for enlightening my way to achieve this goal.

I am thankful to Professor Hicham Fenniri to act as my supervisor and his support during my studies. Beside my advisor, I would like to thank the rest of my thesis committee members: Professor Jeffrey M. Stryker, Professor Arthur Mar, Professor Richard L. McCreery and Professor Natalia Semagina for their encouragement, insightful comments and hard questions.

My sincere thanks also go to Dr. Rahul Chhabra for initial discussion and introduction to the synthesis of rosette nanotube supported metal nanoparticle. I especially thank to Dr. Rachel Beingessner for the valuable scientific discussions that we had during this studies, valuable advises and finally for the thesis corrections. I am so grateful to my wonderful friends Dr. Mounir El Bakkari and Dr. Alaaeddin Alsbaiee, with whom I spent a wonderful and unforgettable time. I thank Dr. Jae-Young Cho for microscopy imaging studies, Dr. Zhimin Yan for an initial NMR training and Dr. Takeshi Yamazaki for the modeling studies. To all of the members of SNAG group, I thank you for assistance and fun in lab.

Table of Contents

Chapter 3. Hydrogenation Catalysis

List of Figures

xiv

List of Tables

List of Schemes

List of Abbreviations

ACSES	Alberta Centre for Surface Engineering and Science
CNT	Carbon nanotube
CV	Cyclic voltammetry
DNA	Deoxyribonucleic acid
DLVO	Derjaguin-Landau-Verwey-Overbeek
ES	Electrospray
G∧C	Guanine-cytosine
ΔG	Gibbs free energy change
GPC	Gel permeation chromatography
HPLC	High performance liquid chromatography
ISI	Institute for Scientific Information
JACS	Journal of American Chemical Society
K_a	Acid dissociation constant
LAA	Lysine amino acid
M NP	Metal nanoparticle
M41S	Mesoporous molecular sieves no. 41
MCM-41	Mobil composition of matter no. 41
MALDI	Matrix-assisted laser desorption ionization
MeOH	Methanol
Mn	Number average molar mass

M	Molar
MCF-17	mesostructured cellular foam no. 17
mL	Milliliter
NP	Nanoparticle
NINT	National Institute for Nanotechnology
NPY-5	Neuropeptide Y type 5
NMR	Nuclear magnetic resonance
OLED	Organic light emitting diode
PVP	poly(N-vinyl-2-pyrrolidone)
PEG	polyethylene glycol
PPO	poly(2,5-dimethylphenylene oxide)
PAMAM G4-OH	Hydroxyl-terminated fourth-generation poly(amidoamine)
RNT	Rosette Nanotube
SAC	Sample analytical chamber
SEM	Scanning electron microscopy
SAM	Self-assembled monolayer
TEM	Transmission electron microscopy
TM-AFM	Tapping mode atomic force microscopy
ToF SIMS	Time-of-flight secondary ion mass spectrometry
TOF	Turnover frequency
THF	Tetrahydrofuran

TLC	Thin layer chromatography
TGA	Thermogravimetric analysis
U	Potential energy
UV-Vis	Ultraviolet-visible spectroscopy
VT-CD	Variable temperature circular dichroism
XPS	X-ray photoelectron spectroscopy

Chapter 1

Introduction

1.1 Background

In recent years, nanosciences have evolved as a major research direction in modern science. In general, there are two different well-established processes to construct nanostructured materials: "top-down" and the "bottom-up" approaches (Figure 1.1).[1-3] In the top-down approach, a macrosized material is essentially reduced in size to the nanoscale dimensions. The bottom-up approach alternatively, is a strategy whereby molecular building blocks are assembled to obtain the desired nanostructure. Certainly, the bottom-up approach became more popular in recent years over the top-down approach due to better control of the size and properties of the nanomaterials.[1-3] The bottom-up approach can be applied to construct supramolecular architectures through the self-assembly of simple building blocks. Metal nanoparticles (M NPs) can also be synthesized from the corresponding metal salt precursors.

This thesis proposes an approach for the combinatorial synthesis and screening of the rosette nanotube (RNT) supported M NPs catalysts for the olefin hydrogenation and Suzuki-Miyaura cross-coupling reactions under environmentally benign and mild conditions. We will present the strategy to synthesize M NPs/RNTs catalysts by water oxidation reaction by a very simple, quick and one-pot process followed by their detailed characterization and kinetic studies. In addition, we will demonstrate the scope and the utility of our catalyst for olefin hydrogenation and Suzuki coupling reactions.

As an overview of the entire project, this first chapter describes the background of this thesis work. We will then showcase the properties as well as the synthesis of the M NPs in the presence different support systems including traditional supports such as metal oxides, polymers and dendrimers, as well as bio- and/or inspired supports. Finally, we will describe the properties of RNTs and their potential as a bio-inspired support for the synthesis of M NPs.
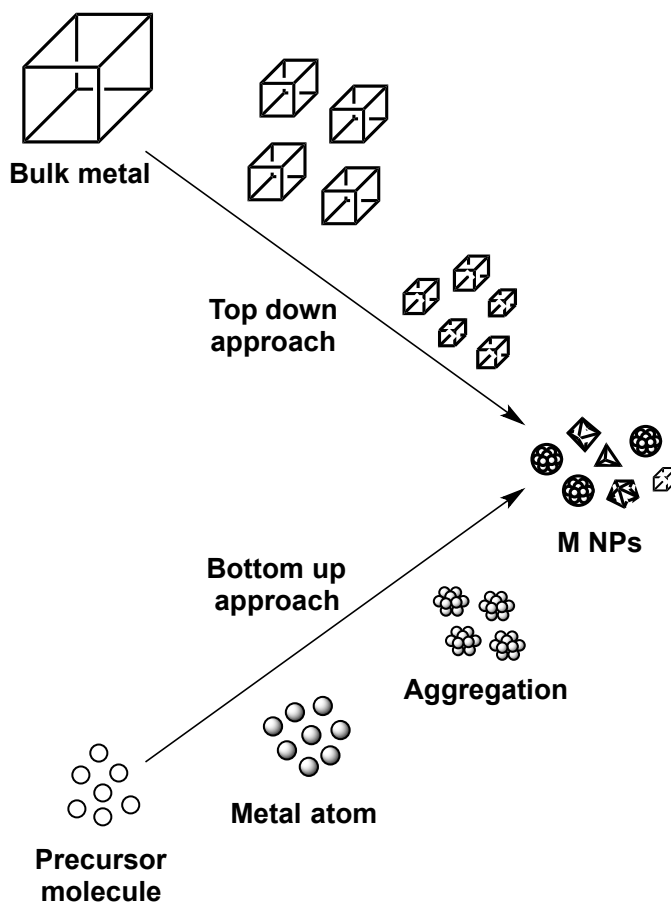
Figure 1.1: Schematic representation of the top down and the bottom up approaches for the synthesis of M NPs.

1.2 Metal Nanoparticles

1.2.1 Overview and Scope

M NPs are a class of materials, which exhibit properties that differ significantly from those observed in their bulk and molecular counterparts. Due to the high surface-to-volume ratio, M NPs provide a larger number of active sites per unit area.[4] As the size of the NP goes smaller the % of the surface atom increases. These surface atoms located on the vertices, edges and faces in a NP have lower coordination numbers (or nearest neighboring atoms) than in the bulk and provide high catalytic activity. Sometimes, M NPs are referred to as "artificial atoms" because of their atom-like behaviors.[5,6] M NPs show typical quantum size behavior for a particle size below 2 nm. As a result, they tend to have discrete energy levels instead of overlapping electronic bands characteristic of a bulk metal.[6] The size of M NPs can vary from 1 to 100 nm, and they usually consist of ten to a thousand metal atoms. The advantages of M NPs include reproducible synthetic protocol with well-defined composition, and potential recycling.[7] In recent years, M NPs have been actively investigated due to their high potential in catalysis[5,8-13], sensors[14], nanoscale electronics[15], fuel cell[16], cosmetics[17] and optoelectronics.[18] Semiconducting NPs with a particle size of 3 nm or less can be defined as "quantum dots". This is because the electrons in a smaller size NPs are confined and behave like particles-in-a-box. These bound state electrons can tune the optoelectronic properties of the NPs in such a way, which is impossible in bulk material electronic structure.

1.2.2 Synthesis and Stabilization of M NPs

1.2.2.1 Synthesis of M NPs

The literature review demonstrates that the M NPs designed for catalysis can be synthesized by following two main protocols, either the reduction of the corresponding metal salt precursors or the decomposition of the zerovalent organometallic compounds (Figure 1.2).[7,19] Moreover, a number of techniques have been developed over the last few years such as impregnation, co-precipitation, deposition-precipitation, sol-gel, gas-phase organometallic deposition, electrochemistry, laser ablation, sonochemistry, microemulsion and cross-linking.[19] However, the actual size and shape of the resulting NP is defined by a number of factors such as the type of reducing agent, metal precursor, solvent, concentration, temperature and reaction duration.[20]

$$K_m M^{n+} X_{n+m} \xrightarrow{\text{Reducing agent}} M\ NP \xleftarrow{\text{Decomposition}} M^0 L_n$$

M = group 8-10 metal
X = Cl or Br
n = number of charge
m = 1, 2

L = ligand
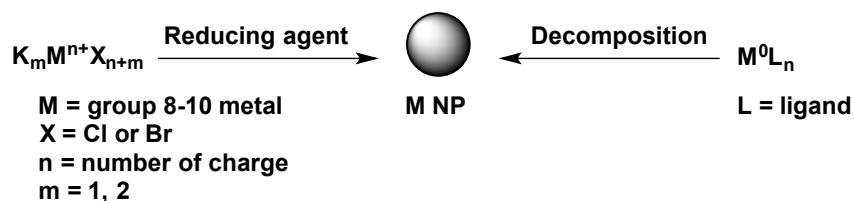
Figure 1.2: Two main methods for the synthesis of M NPs.

1.2.2.1.1 Chemical Synthesis of the M NPs

To date, the synthesis of M NPs by the reduction of the corresponding metal salt precursors using various reductants is the most widely used method. In general, this method is very simple to implement for the production of M NPs on a laboratory as well as on an industrial scale. A variety of reducing agents have been successfully applied for the synthesis of M NPs, including sodium, hydrogen, alcohols, hydrazine, hydrides and salts such as sodium borohydride or sodium citrate.[20,21] The possible oxidation process of some common reductants is presented in Figure 1.3.[22,23] In most cases upon oxidation, the

reductants produce protons in solution beside reducing the metal ions to metal atoms (M^0). These metal atoms nucleate to form stable nuclei, which then upon growth form the NPs. The generation of protons in solution results in a drop of the solution pH and is thereby indicative of the NP formation.[24] In 1857, Faraday first reported the synthesis of gold (Au) NPs by the reduction of $HAuCl_4$ with phosphorus.[25] Turkevich *et al.* demonstrated the first reproducible synthesis of uniform Au NPs with a particle size of 13 nm. They used sodium citrate as both the reductant and stabilizer.[26-28] Later, following this pioneering work, the wet chemical reduction process was routinely applied for the synthesis of M NPs. Besides aqueous solution phase synthesis, a range of methods has also been reported for the phase transfer of M MPs from aqueous to organic media. Though the technique has an advantage of large-scale preparation, the resulting nanomaterials lack detailed compositional analysis.[21]

$$H_2 \longrightarrow 2H^+ + 2e^-$$

$$RCH_2OH \longrightarrow RCHO + 2H^+ + 2e^-$$

$$N_2H_4 \longrightarrow N_2 + 4H^+ + 4e^-$$

$$NaBH_4 + 2H_2O \longrightarrow NaBO_2 + 8H^+ + 8e^-$$
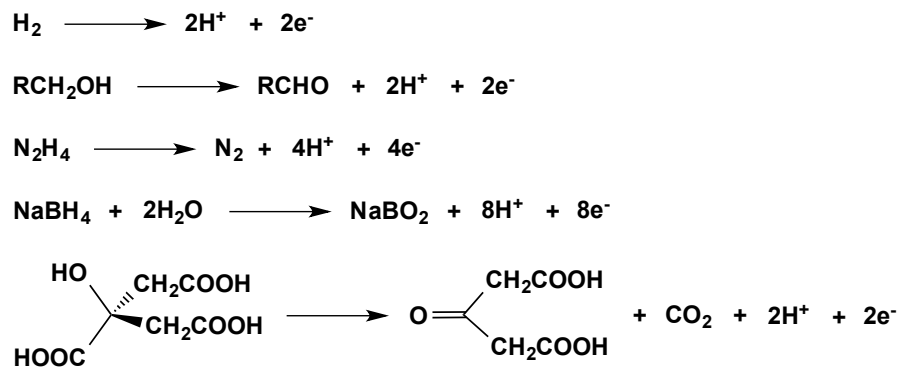
Figure 1.3: Possible oxidation process of the commonly used reductants.

1.2.2.1.2 Synthesis of the M NPs by Thermal Decomposition

The thermal decomposition method involves the injection of organometallic compounds in a hot surfactant solution. The surfactant facilitates the formation of monodisperse NPs of various materials by preventing rapid agglomeration. This protocol has several advantages such as (i) the use of the reductant is absolutely not required as the

metal is already zerovalent, (ii) the use of organic solvent, which replaces the phase transfer synthesis, and (iii) high crystallinity and monodispersity of the NPs with excellent dispersibility in organic solvent.[20] However, the main challenge in this method is the choice of the surfactant to stabilize the NP. Bawendi and co-workers first demonstrated the synthesis of monodisperse CdE (E = S, Se and Te) NPs by using the thermal decomposition technique.[29] Later, the protocol was extended for the synthesis of monodisperse NPs of various metals and alloys including Fe, Ni, Au, Pd, Pt and FePt.[20] However, the main drawback of this process is the size selective precipitation of the NP, which is very laborious and tedious.

1.2.2.1.3 Nucleation and Growth of the M NPs

The process of nucleation and growth of the NPs, plays an important role in determining the crystal structure, shape, size and distribution of the NPs. Hence, it is important to understand the mechanism of the NP formation to synthesize monodisperse NPs. For several decades, the nucleation and growth of the NPs were best described using the LaMer burst nucleation process followed by Ostwald ripening.[30-32] Later in 1997, Watzky and Finke proposed a two-step model of constant slow nucleation followed by autocatalytic growth of the M NPs.[33] The nucleation process is considered as the first step towards the crystal growth from nuclei, which act as templates.[34] While the homogeneous nucleation occurs in the absence of a surface, the heterogeneous nucleation takes place at nucleation sites on surfaces contacting the liquid or vapor.[34,35] However, the heterogeneous nucleation is much faster than the homogeneous counterpart because of the lower nucleation free energy barrier at a surface.[36] The homogeneous nucleation is a thermodynamic process, which is expressed in terms of the free energy of nucleus

6

formation.[34] The total free energy is the sum of the two competing terms, the surface free energy and the bulk free energy (equation 1.1). The bulk free energy is negative, which favors the formation of a stable nucleus. On the other hand, the surface free energy is positive, which is unfavorable to the stable nucleus formation.[23,34]

$$\Delta G = \frac{4}{3}\pi r^3 \Delta G_v + 4\pi r^2 \gamma \text{----------------(1.1)}$$

The equation is based on the assumption of a spherical nucleus. Here, ΔG is the total free energy, r is the radius of the NP, ΔG_v is the crystal free energy, and γ is the surface energy. In equation 1.1, when the surface free energy is negligible the total free energy ΔG becomes negative which favors the nucleation (Figure 1.4a). On the other hand, there is no nucleation for a very high surface free energy. A stable particle with a critical radius r^* forms when the nuclei overcome the critical free energy (ΔG^*) barrier (Figure 1.4a). At this stage the NP can survive in solution without being redissolved.[34] Later, the fresh and continuous supply of more nuclei facilitates the growth of the NP.
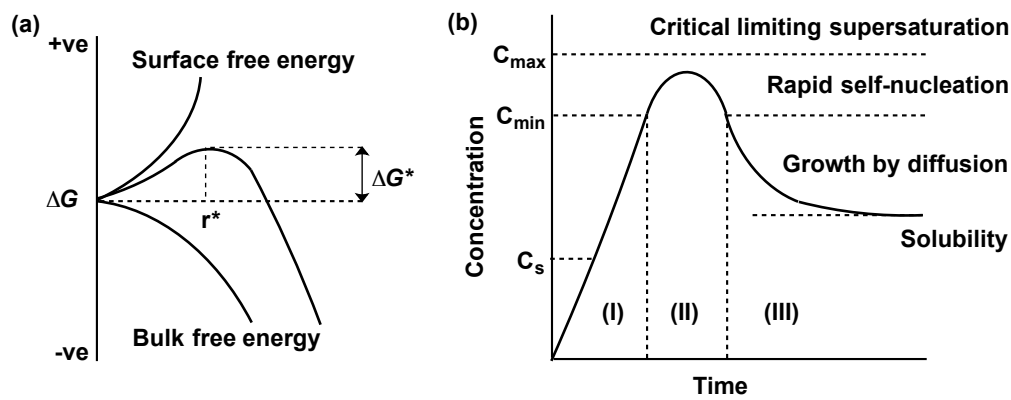
Figure 1.4: Schematic representation of the (a) nucleation free energy diagram, and (b) LaMer diagram.

In 1950, LaMer and co-workers proposed a model of the particle formation based on the nucleation theory.[30] This mechanism became the most famous and widely cited

7

mechanism to explain the phenomenon of particle formation for almost 50 years. The LaMer mechanism first separated the concept of nucleation and growth of the particles into two stages. The mechanism was not originally formulated for the M NP formation.[23] Instead, LaMer *et al.* applied the classical nucleation theory to describe the sulfur sol formation.[30] In the first step, the decomposition of the sodium thiosulfate in hydrochloric acid led to the free sulfur formation. Finally, the aggregation of the free sulfur resulted in sulfur sol in solution. The model shows the concentration of sulfur as a function of time (Figure 1.4b). The mechanism can be best described in three portions: (I) an increase in the free sulfur concentration in solution up to a critical supersaturation level, (II) burst nucleation occurs at this level, which significantly drops the concentration of the free sulfur in solution, and (III) growth of the particle occurs by the diffusion of sulfur atoms throughout the solution.[34] The Ostwald ripening, which was proposed in 1900, can describe the growth mechanism of the NP.[32] The mechanism explains how the growth is affected by the size dependent solubility change of the NPs. Compared to the larger sized NPs, the smaller NPs have high solubility and surface energy. Hence, the smaller NPs can redissolve in solution and integrate to the larger particles to grow even bigger.[34]

1.2.2.2 Stabilization of the M NPs

In solution, the naked NPs are kinetically and thermodynamically unstable because of the high surface energy.[20] Hence the key issue for the synthesis of M MPs is their stability, which is independent of the synthetic route chosen.[7] This is because the smaller NPs have high surface energy resulting in very reactive surface atoms. Therefore, two smaller NPs can attract each other by the van der Waals force at short interparticle distances.[21] The smaller NPs then can aggregate into larger particles in the absence of any

repulsive forces, which could oppose the van der Waals force.[21] Usually, the stabilization of the M NPs is achieved by applying protective agents, which oppose the van der Waals attractive force and block the agglomeration of the metal atoms at the colloidal stage to avoid bulk metal formation.[7,19-21] The stability of the M NPs in solution can be described by the Derjaguin-Landau-Verwey-Overbeek (DLVO) theory. The theory suggests that the stability of a NP in solution is defined by its total potential energy (U), which is the sum of the van der Waals attractive force (U_A) and the repusive force (U_R) (equation 1.2).

$$U = U_A + U_R = - \frac{A}{12\pi D^2} + 2\pi\varepsilon a\zeta^2 e^{-\kappa D} \quad \text{-----------------------(1.2)}$$

Here, A is the Hamaker constant, D is the interparticle distance, a is the radius of the particle, π is the solvent permeability, ζ is the zeta potential and κ is a function of the ionic composition. The magnitude of the zeta potential defines the stability of a colloidal system. A high zeta potential value either positive or negative confers the well dispersion of the colloidal NPs in suspension. The zeta potential is a potential measured at the boundary located on the slipping plane between the diffuse layer of the colloidal NP and the bulk solution (Figure 1.5a).
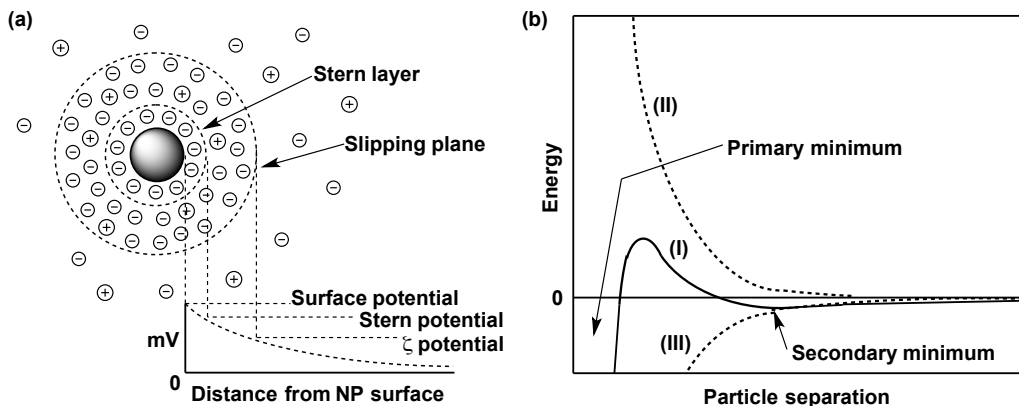
Figure 1.5: Schematic representation of (a) ζ potential and (b) energy diagram of the stability of the particles according to the DLVO theory.

9

The attractive and the repulsive forces exist when two particles approach each other because of the Brownian motion. There is a minimum potential energy barrier, which arises from the repulsive forces, that the interacting particles have to overcome. Hence, if the two particles can overcome this energy barrier they will flocculate together (Figure 1.5b, condition (I)). In the case of high repulsive forces, there is no flocculation and the colloidal system is stable (Figure 1.5b, condition (II)). On the other hand in the absence of any repusive forces, the colloidal system would be unstable and a rapid coagulation would take place. There are two different types of stabilization possible depending on the nature of the protective agents, electrostatic stabilization and steric stabilization (Figure 1.6). The electrostatic stabilization can be obtained by using ionic complexes such as ammonium halides (Figure 1.6a). On the other hand, the steric stabilization can be achieved by using neutral molecules including polymers and other bulky molecules (Figure 1.6b). While the electrostatic stabilization provides the stability of the M NPs in aqueous solution, the steric stabilization can be applied in both organic and aqueous solvents. As the stabilizer has significant influence on the stability and the reactivity of the M NPs, the use of stabilizers is always a compromise between the stability and the reactivity of the M NPs.[19]

Electrostatic stabilization   **Steric stabilization**
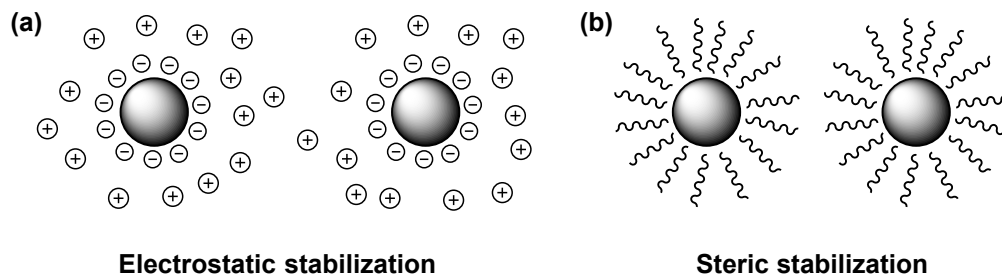
Figure 1.6: Schematic representation of the electrostatic (a) and steric (b) stabilization of the M NPs.

1.2.3 Synthesis of Supported M NPs

An interesting and alternative method for the synthesis of M MPs is the use of a support system. This includes the use of both inorganic and organic supports.[5,7,19-21] While the classic organic support uses polymers and dendrimers, the inorganic supports include the use of silica and other metal oxides of Al, Ti, Zr, Ca, Mg and Zn.[7,19-21] In addition, significant efforts have been made for the immobilization of the colloidal M NPs on carbon materials such as activated carbon, carbon nanotubes and graphenes.[37-39] The immobalization of the M NPs on a support involves - (i) the synthesis of a stable colloidal metal suspension by reduction, (ii) impregnation of the M NPs on the support, and (iii) purification of the supported M NPs. The size of the NPs synthesized by this protocol is independent of the support.[7,21] On the other hand, in the case of heterogeneous catalyst synthesis, the reduction step takes place after the impregnation of the metallic precursor.

A large number of recent reports have been documented on the synthesis of M NPs supported on metal oxides and their potential application in catalysis.[12,40,41] The metal oxide support offers several advantages including facile synthesis, high thermal and chemical stabilities, a well-defined porous structure and high surface areas (>100 m^2g^{-1}).[40,41] The commonly used metal oxides include those of Si, Al, Ti, Zr, Ca, Mg, Zn and Ce. Depending on the chemical reactivity, the metal oxide supports can be inert such as SiO_2, or reactive such as CeO_2.[40,41] Despite the large variety of supports, most deal with some form of silica such as SiO_2 aerogels or sol–gels, M41S silicates and alumimosilicates, MCM-41 mesoporous silicates, SiO_2 microemulsions, hydroxyapatite, hydrotalcite, zeolites, molecular sieves and alumina membranes.[12] Recently,

11

superparamagnetic oxide (Fe_3O_4) has also been employed to immobilize catalytic M NPs with improved separation capabilities. The M NPs/Fe_3O_4 catalyst can easily be isolated by using a permanent magnet from the reaction mixture and recycled back for further use.[40,41] Very recently, Dai and co-workers have reported the synthesis of Au NPs immobilized on metal phosphates as a support and tested their catalytic activity and stability towards CO oxidation.[42]
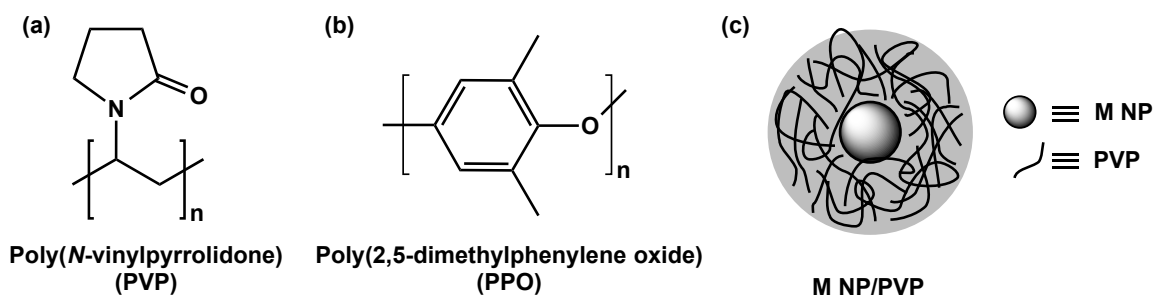
Figure 1.7: Structures of (a) PVP and (b) PPO. (c) Schematic representation of the PVP supported M NP.

Beside the use of metal oxide supports, a large number of organic supports such as polymers and dendrimers have been employed to synthesize M NPs.[19,20,40,41] The polymers and dendrimers offer the opportunity to modify the functional groups, which can provide specific reactive sites for controling the growth and size of the resulting M NPs.[20] Among the other polymers, poly(*N*-vinyl-2-pyrrolidone) (PVP) is the most studied polymer employed for the synthesis of M NPs (M = Pd, Pt, Rh and Ag) (Figure 1.7a). The PVP stabilized M NPs are synthesized by the reduction of the corresponding metal halide in refluxing ethanol (Figure 1.7c).[12,43] Later, a myriad of polymers have been successfully employed for the synthesis of M NPs, which includes poly(2,5-dimethylphenylene oxide) (Figure 1.7b),[12,19] polyurea,[44] polyacrylonitrile,[45] polyacrylic acid,[45] polysilane shell-cross-linked micelles,[46] polysiloxane,[47] oligosaccharides,[48]

12

poly(4-vinylpyridine),[49] poly(N,N-dialkylcarbodiimide),[50,51] polyethylene glycol (PEG),[52] chitosan,[53] and aramids.[54]

Another interesting and commonly used organic support are dendrimers, which are monodispersed macromolecules that have well-defined branched three-dimensional architechtures. In 1998, several groups reported that dendrimers can stabilize the NPs either by encapsulating within a single dendrimer or by blocking the surface of the NPs with several dendrimers.[55-57] The synthesis involves the initial complexation of the corresponding metal salt (M^{n+}) precursors with the positively charged tertiary amines of the dendrimer followed by the reduction with $NaBH_4$ to M^0.[58] The water solubility of the dendrimers allows the dispersion and catalysis of the resulting M NPs in aqueous condition. El-Sayed *et al.* reported comparative study of the support effect between PAMAM G4-OH dendrimer, and PVP- or polystyrene-poly(sodium acrylate) block copolymers on the stability and the catalytic activity of the M NPs.[59] They found that the dendrimer supported M NP possesses higher stability but lower catalytic activity than the copolymer supported M NP.
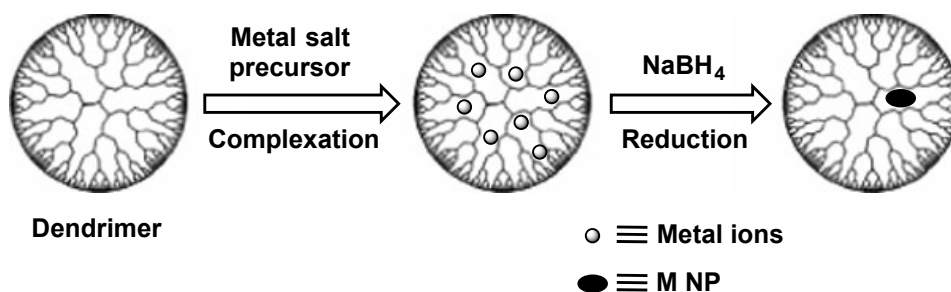
Figure 1.8: Synthesis of the dendrimer supported M NPs. Partially adapted with permission from Wiley Interscience.[58]

In recent years, a significant effort has been made regarding the synthesis of M NPs using carbonaceous materials including activated carbon, starbon, carbon nanotubes

and graphenes. As a support, the carbonaceous materials offer several advantages such as well-defined porosities, high surface areas and surface functionalization. One of the most commonly and commercially available carbon support for the M NPs is activated carbon. Bönnemann and co-workers demonstrated the synthesis of activated carbon supported M NPs from the reduction of quaternary ammonium salts of corresponding metal cations in THF followed by the impregnation into charcoal.[60,61] Later, following the same protocol, they dispersed electrochemically reduced M NPs on the surface of charcoal.[62] Recently, Budarin *et al.* have reported the preparation of M NPs on a novel family of mesoporous carbonaceous materials called "Starbon", which are the sulfonic acid derivatives of activated carbon.[63,64]
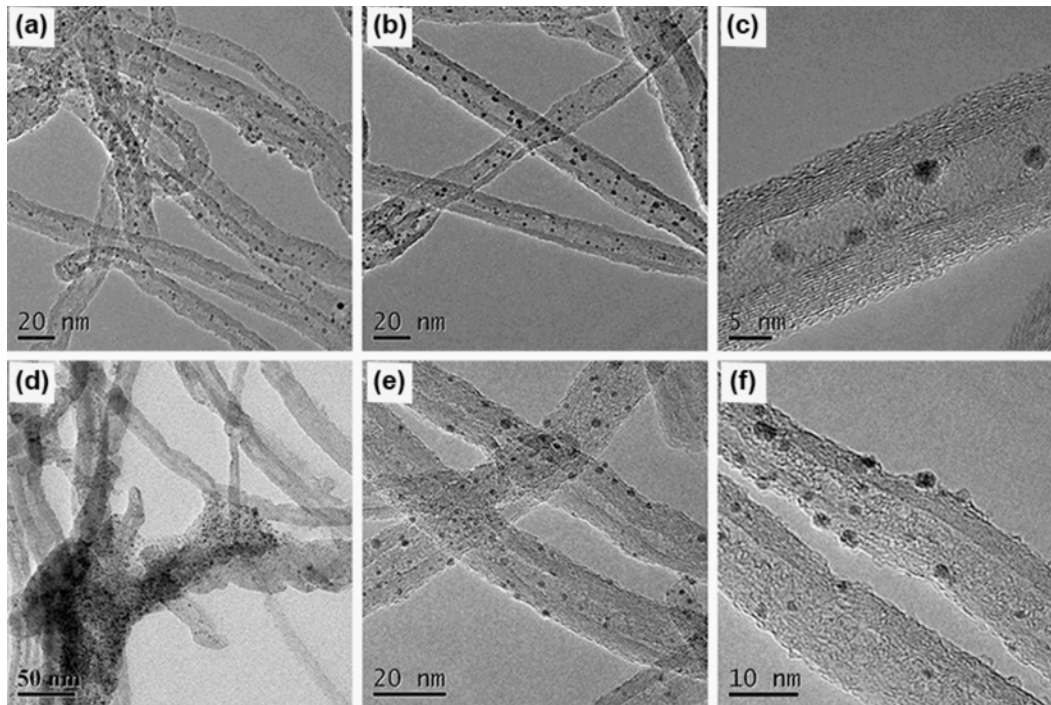
Figure 1.9: TEM images of the Ru NPs inside the CNT channels (a-c) and on the CNT exterior surfaces (d-f). Adapted with permission from Wiley Interscience.[68]

Carbon nanotubes (CNTs) including both single- and multi-walled, have also been employed as supports for M NPs.[65-69] Though they offer several intrinsic properties such as high surface areas, unique physical properties and morphologies, high electrical conductivity and inherent size and hollow geometry, it is hard to obtain monodispersed M NPs (Figure 1.9).[68] Very recently, graphene materials have also been employed as supports to synthesize M NPs, including Ag, Au, Pd and Pt.[70-80] The graphene supported M NPs can be prepared either by (i) the reduction of the metal ions and graphene oxide separately followed by deposition, or (ii) one-pot reduction of the metal ions and graphene oxide through chemical or electrochemical means.[72]
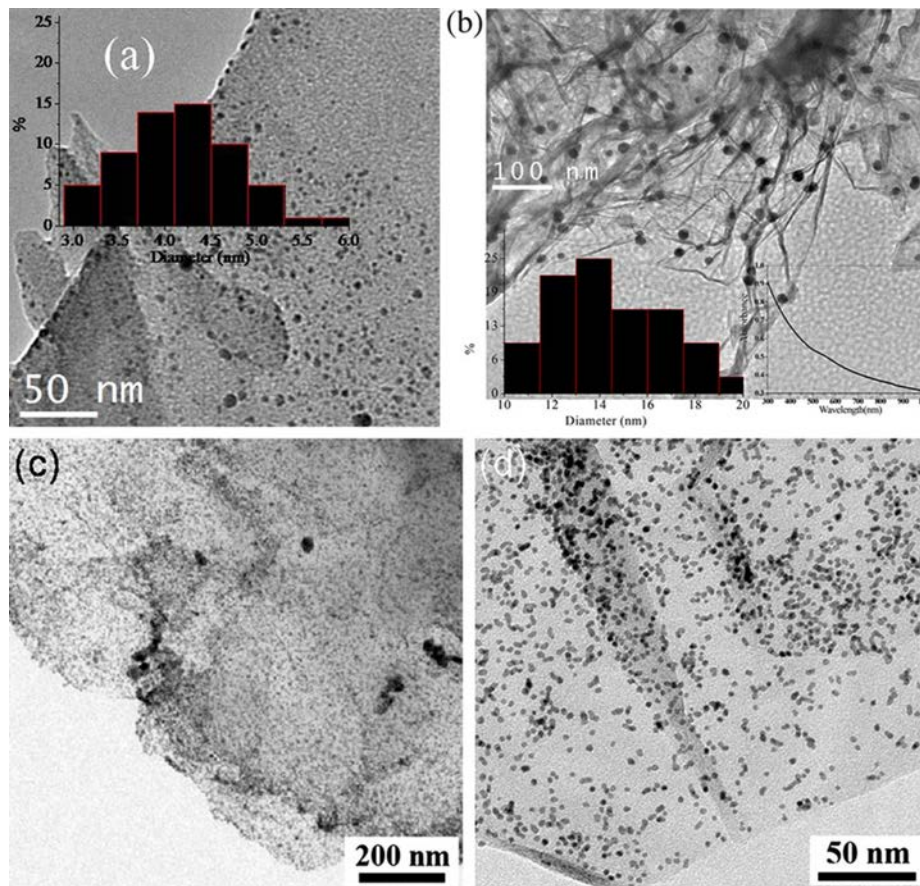
Figure 1.10: TEM images of the reduced graphene oxide supported Ag (a), Au (b), and Pt (c, d) NPs. Adapted with permission from Elsevier and RSC publishing.[70,71]

1.2.3.1 Synthesis of Bio- and/or Inspired Supported M NPs

Taking inspiration from Mother Nature, many researchers have demonstrated the design and fabrication of M NPs using bio- and/or inspired supports under ambient conditions.[81,82] In living organisms, naturally occurring proteins contribute to the bio-mineralization of inorganic materials. The bio- and/or inspired supports offer several advantages such as mild preparation condition, low toxicity and cost, high biocompatibility, availability and abundance.[41,82] The hallmarks of this approach include the use of protein,[82-84] enzymes,[85,86] DNA,[87] peptides including collagen fiber,[81,82,88-98] bacteria,[99-104] virus,[105-108] oligo- and polysaccharides such as cyclodextrins and gum acacia,[109-112] and banana peel extract.[113] Although the bio- and/or inspired supports offer several advantages for the synthesis of bio-inorganic hybrid materials, they possess some limitations on their applicability. One major problem often encountered with the bio-templates such as protein, enzyme, DNA and microorganism is their instability in the absence of physiological conditions.[81,84] To address this issue, several bio-inspired supports have been introduced to prepare M NPs, including peptides, and other biopolymers. Though the bio-inspired supports show selective binding interactions with the inorganic precursor, it remains a challenge to control the size of the M NPs and provide high monodispersity. This is due to the lack of well-defined nucleation pocket or sites on the surface of the bio-support, which can control the growth of the M NP to a certain size and prevent Ostwald ripening.

1.2.3.2 Rosette Nanotube (RNT) as a New Bio-inspired Support

Towards this effort of designing bio-inspired supports, Fenniri group have introduced RNTs as a mimic of DNA.[114-118] RNTs are biocompatible tubular architectures

that are self-assembled under aqueous conditions from a self-complementary guanine-cytosine (G∧C) DNA hybrid molecule (Figure 1.11a). The hierarchical self-assembly process involves the initial formation of hexameric rosettes (Figure 1.11b), which are maintained through intermolecular H-bonding interactions. These hydrophobic macrocycles then π-π stack to form the RNT (Figure 1.11c), which have an internal diameter of *ca.* 1 nm. The RNTs can be modified on their surface with different functional groups including amino acids, crown ethers and other organic groups, which determines their solubility in aqueous or organic solvents.[114-118]
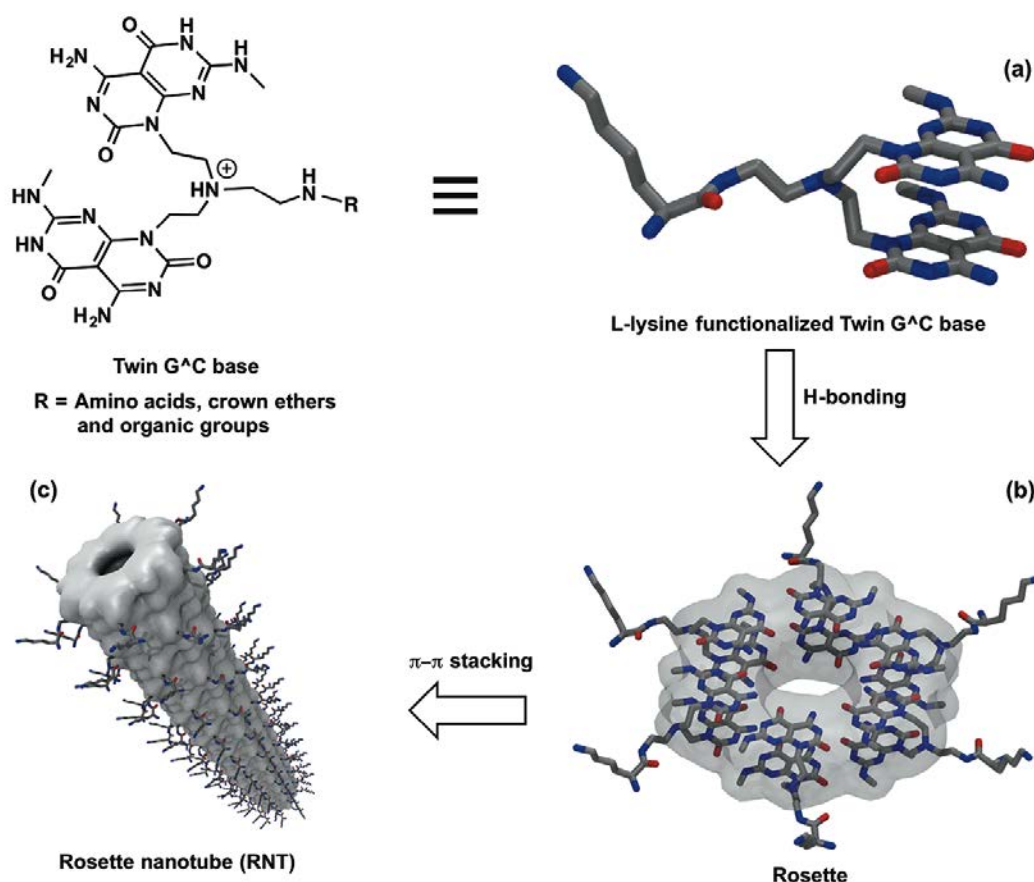
Figure 1.11: Schematic representation of RNT formation – (a) twin G∧C base (called "G0"); (b) hexameric rosette; and (c) RNT.

As our concern is to develop green M NPs/RNTs composite catalysts, initially Fenniri and coworkers employed a L-lysine functionalized twin G∧C base to form water soluble RNTs (called "G0").[118] The positively charged lysine, which is addressed on the surface of the RNT upon formation, results in complete solubility and stability of the RNT in water. In addition, the positively charged lysine has the advantage of undergoing complexation through electrostatic interaction with the metal salt precursor before reduction. This complexation can facilitate the directed continuous fresh supply of the metal salt precursors for M NP formation on the surface of the RNT followed by reduction. To provide a viable solution for obtaining highly monodispersed M NPs, it was hypothesized that the lysine functionalization will offer well-defined nucleation and growth sites to form highly monodispersed M NPs on the surface of the RNT. Indeed, the initial studies showed that the G0-RNT could nucleate and passivate the formation of highly monodispersed Au NPs upon reduction and the results will be summarized in chapter 2.[118] Besides this, I will summarize some initial results obtained by a former group member (Dr. Rahul Chhabra) on the synthesis and characterization of M NPs/RNTs (M = Au, Pd and Pt) composites. Later, I will introduce further optimization of the synthetic protocol of the M NPs/RNTs (M = Au, Pd and Pt) composites followed by a detail studies on the origin and kinetics of the Pd NPs/RNTs formation in the absence of a reducing agent. In addition, I will discuss the application of Pd NPs/RNTs catalyst in olefin hydrogenation and Suzuki-Miyaura cross-coupling reactions.

1.2.4 Nanoparticle Catalysis

Research on nanoparticle catalysis has grown intensively due to its vital role in pharmaceuticals, automotive and food industries. The synthesis of transition M NPs for

catalysis has received considerable interest over traditional catalysts since they mimic metal surface activation and provide reactivity at the nanoscale level. Hence, they can impart selectivity and high efficiency to catalytic reactions under mild conditions.[5] The importance of nanoparticle catalysis in the scientific community has been demonstrated by the rapid growth of publications. The ISI web of science citation database over the 1995-2014 periods (collected up to November 02, 2014) shows a statistics on how the nanoparticle catalysis is becoming a popular and major research areas of interest in nanotechnology (Figure 1.12). Therefore, because of a large volume of research articles published on nanoparticle catalysis, we will instead present a summary of the relevant works in each individual catalysis chapter. Among the other catalytically active transition M NPs, palladium NPs are the most studied because of their high degree of catalytic activity towards the C-C bond formation and olefin hydrogenation.[90,91]
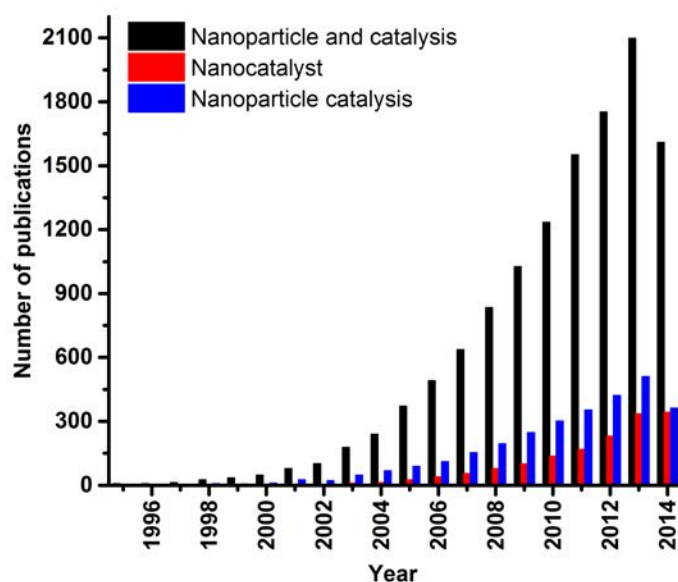
Figure 1.12: The trend in published research articles on the topic of nanoparticle and catalysis (black), nanocatalyst (red) and nanoparticle catalysis (blue).

1.3 Organization of the thesis

The primary goal of this thesis is to establish a simple and green protocol for the synthesis of RNT supported M NPs (M = Au, Pd and Pt) followed by their potential application in catalysis under environmentally benign and mild reaction conditions. The key steps involved in synthesizing the M NPs/RNTs composite materials are the reaction condition optimization. This includes the ratio of the metal salt precursor and RNT concentrations, and the choice of appropriate RNT surface functionalization. The scope and utility of the M NPs/RNTs catalysts were evaluated towards industrially important olefin hydrogenation and Suzuki-Miyaura cross-coupling reactions.

Chapter 2 introduces a brief summary of the initial results obtained on the M NPs/RNTs (M = Au, Pd and Pt) composite material by Fenniri and co-workers. Later, it describes further optimization of the synthetic protocol and a detailed characterization of the Pd NPs/RNTs catalyst addressing the kinetics and the origin of the NP formation on the surface of the RNT. Usually, the presence of more than two reactants in the reaction medium complicates the kinetic study. As I established a modified one-pot synthetic protocol of Pd NPs/RNTs catalyst by water oxidation in the absence of a reducing agent, it simplified the kinetic study. I also found that the supramolecular chirality of the RNTs is even preserved in the presence of the M NPs on the surface of the RNTs.

Chapter 3 describes the application of the M NPs/RNTs catalysts towards styrene hydrogenation under environmentally benign and mild reaction conditions. Because of the poor catalytic activity of the Pd NPs/RNTs catalyst synthesized by over night incubation, I had to modify the catalyst preparation method by reducing the Pd NPs with hydrogen in the presence of the RNTs. The newly modified Pd NPs/RNTs catalyst

showed quantitative hydrogenation of different styrene derivatives as well as selectivity. A detailed characterization of the catalyst is also reported in chapter 3.

In chapter 4, the Suzuki-Miyaura cross-coupling reaction using M NPs/RNTs catalysts is reported. The reaction shows tolerance to a variety of functional groups leading to very high coupling product conversion. Later, the utility of the Pd NPs/RNTs catalyst was examined for the synthesis of drug and agrochemical intermediates. In addition, the catalysis was also extended for the preparation of benzothiadiazole based materials for solar cell, OLED and sensor applications. The properties of the Pd NPs/RNTs catalyst are also investigated under the catalytic conditions including base and temperature effect. Chapter 5 describes the supramolecular chiral catalysis by using the Pd NPs/RNTs catalyst. The studies suggest poor chirality induction of the catalyst to the coupling product.

Finally, chapter 6 presents a summary of chapters 2, 3, 4 and 5 followed by brief potential research directions of this thesis work.

1.4 References

(1)   Siegel, R. W.; Hu, E; Roco, M. C. Eds. *Nanostructure Science and Technology-A Worldwide Study*. *Prepared under the guidance of the IWGN and NSTC*, WTEC: Loyola College, Maryland, 1999.

(2)   Mansoori, G. A. *Principles of Nanotechnology: Molecular Based Study of Condensed Matter in Small Systems*, World Scientific: New York, 2005.

(3)   Mansoori, G. A.; George, T. F.; Assoufid, L.; Zhang, G. *Molecular Building Blocks for Nanotechnology: from Diamondoids to Nanoscale Materials and Applications*, Springer: New York, 2007.

(4)   Ranu, B. C.; Chattopadhyay, K.; Adak, L.; Saha, A.; Bhadra, S.; Dey, R.; Saha, D. *Pure Appl. Chem.* **2009**, *81*, 2337−2354.

(5)   Astruc, D. In *Nanoparticles and Catalysis*; Weinheim: Wiley-VCH, 2008.

(6)   Schmid, G.; Fenske, D. *Phil. Trans. R. Soc. A* **2010**, *368*, 1207–1210.

(7)   Balanta, A.; Godard, C.; Claver, C. *Chem. Soc. Rev.* **2011**, *40*, 4973−4985.

(8)   Roduner E. In *Nanoscopic Materials: Size-dependent Phenomena*; Cambridge: The Royal Society of Chemistry, 2006.

(9)   Davies, P. R.; Roberts, M. W. In *Atom Resolved Surface Reactions: Nanocatalysis*; Cambridge: The Royal Society of Chemistry, 2008.

(10)   Johánek, V.; Laurin, M.; Grant, A. W.; Kasemo, B.; Henry, C. R.; Libuda, J. *Science* **2004**, *304*, 1639−1644.

(11)   Ertl, G. *J. Mol. Catal. A: Chem.* **2002**, *182*, 5−16.

(12)   Astruc, D.; Lu, F.; Aranzaes, J. R. *Angew. Chem. Int. Ed.* **2005**, *44*, 7852−7872.

(13) Wieckowski, A.; Savinova, F. R.; Vayenas, C. G. In *Catalysis and Electrocatalysis at Nanoparticle Surfaces*; New York: Dekker, 2003.

(14) Valentini, F.; Biagiotti, V.; Lete, C.; Palleschi, G.; Wang, J. *Sensor Actuat. B: Chem.* **2007**, *128*, 326−333.

(15) Tsoukalas, D. *Int. J. Nanotechnol.* **2009**, *6*, 35−45.

(16) Sevilla, M.; Sanchis, C.; Valdés-Solís T.; Morallón, E.; Fuertes, A. B. *Electrochim. Acta* **2009**, *54*, 2234−2238.

(17) Gutiérrez, J. M.; González, C.; Mastr, A.; Solè, I.; Pey, C. M.; Nola, J. *Curr. Opin. Colloid Interface Sci.*, **2008**, *13*, 245−251.

(18) Enoch, S.; Quidant, R.; Badenes, G. *Opt. Express* **2004**, *12*, 3422−3427.

(19) Astruc, D. *Inorg. Chem.* **2007**, *46*, 1884−1894.

(20) Jia, C. -J.; Schüth, F. *Phys. Chem. Chem. Phys.* **2011**, *13*, 2457−2487.

(21) Roucoux, A.; Schulz, J.; Patin, H. *Chem. Rev.* **2002**, *102*, 3757−3778.

(22) Redón, R.; Rendón-Lara, S. K.; Rernández-Osorio, A. L. Ugalde-Saldivar, V. M. *Rev. Adv. Mater. Sci.* **2011**, *27*, 31−42.

(23) Finney, E. E.; Finke, R. G. *J. Colloid Interface Sci.* **2008**, *317*, 351−374.

(24) Lim, J. -S.; Kim, S. -M.; Lee, S. -Y.; Stach, E. A.; Culver, J. N.; Harris, M. T. *Nano Lett.* **2010**, *10*, 3863−3867.

(25) Faraday, M. *Phil. Trans. R. Soc. London* **1857**, *147*, 145−153.

(26) Turkevich, J.; Stevenson, P. C.; Hillier, J. *Discuss. Faraday Soc.* **1951**, *11*, 55–75.

(27) Turkevich, J.; Kim, G. *Science* **1970**, *169*, 873–879.

(28) Turkevich, J. *Gold Bull.* **1985**, *18*, 86–91.

(29)   Murray, C. B.; Norris, D. J.; Bawendi, M. G. *J. Am. Chem. Soc.* **1993**, *115*, 8706–8715.

(30)   LaMer, V. K.; Dinegar, R. H. *J. Am. Chem. Soc.* **1950**, *72*, 4847–4854.

(31)   LaMer, V. K. *Ind. Eng. Chem.* **1952**, *44*, 1270–1277.

(32)   Ostwald, W. *Z. Phys. Chem.* **1900**, *34*, 495–503.

(33)   Watzky, M. A.; Finke, R. G. *J. Am. Chem. Soc.* **1997**, *119*, 10382–10400.

(34)   Thanh, N. T. K.; Maclean, N.; Mahiddine, S. *Chem. Rev.* **2014**, *114*, 7610−7630

(35)   Pruppacher, H. R.; Klett, J. D. *Microphysics of Clouds and Precipitation*, Kluwer: Massachusetts, 1997.

(36)   Sear, R. P. *J. Phys.: Condens. Matter* **2007**, *19*, 033101.

(37)   Guerra, J.; Herrero, M. A. *Nanoscale* **2010**, *2*, 1390−1400.

(38)   Zhuo, Q.; Ma, Y.; Gao, J.; Zhang, P.; Xia, Y.; Tian, Y.; Sun, X.; Zhong, J.; Sun, X. *Inorg. Chem.* **2013**, *52*, 3141−3147.

(39)   Shang, L.; Bian, T.; Zhang, B.; Zhang, D.; Wu, L. -Z.; Tung, C. -H.; Yin, Y.; Zhang, T. *Angew. Chem. Int. Ed. Engl.* **2014**, *53*, 250−254.

(40)   White, R. J.; Luque, R.; Budarin, V. L.; Clark, J. H.; Macquarrie, D. J. *Chem. Soc. Rev.* **2009**, *38*, 481–494.

(41)   Campelo, J. M.; Luna, D.; Luque, R.; Marinas, J. M.; Romero, A. A. *ChemSusChem* **2009**, *2*, 18–45.

(42)   Ma, Z.; Yin, H.; Overbury, S. H.; Dai, S. *Catal. Lett.* **2008**, *126*, 20–30.

(43)   Gallezot, P.; Richard, D.; Bergeret, G. In *Novel Materials in Heterogeneous Catalysis*; Baker, R. T. K., Murrell, L. L., Eds.; ACS Symposium Series No. 437; American Chemical Society: Washington DC, 1990, 150–159.

(44)   Ley, S. V.; Mitchell, C.; Pears, D.; Ramarao, C.; Yu, J. -Q.; Zhou, W. -Z. *Org. Lett.* **2003**, *5*, 4665–4668.

(45)   Demir, M. M.; Gulgun, M. A.; Menceloglu, Y. Z.; Erman, B.; Abramchuk, S. S.; Makhaeva, E. E.; Khokhlov, A. R.; Matveeva, V. G.; Sullman, M. G. *Macromolecules* **2004**, *37*, 1787–1792.

(46)   Kidambi, S.; Dai, J. -H.; Lin, J.; Bruening, M. L. *J. Am. Chem. Soc.* **2004**, *126*, 2658–2659.

(47)   Chauhan, B. P. S.; Rathore, J. S.; Bandoo, T. *J. Am. Chem. Soc.* **2004**, *126*, 8493–8500.

(48)   Sanji, T.; Ogawa, Y.; Nakatsuka, Y.; Tanaka, M.; Sakurai, H. *Chem. Lett.* **2003**, 32, 980–981.

(49)   Drelinkiewicza, A.; Waksmundzka, A.; Makowski, W.; Sobczak, J. W.; Krol, A.; Zieba, A. *Catal. Lett.* **2004**, *94*, 143–156.

(50)   Liu, Y. -B.; Khemtong, C.; Hu, J. *Chem. Commun.* **2004**, 398–399.

(51)   Hu, J.; Liu, Y.-B. Langmuir 2005, 21, 2121–2123.

(52)   Pillai, U. R.; Sahle-Demessie, E. *J. Mol. Catal. A: Chem.* **2004**, *222*, 153–158.

(53)   Adlim, M.; Abu Bakar, M.; Liew, K. Y.; Ismail, J. *J. Mol. Catal. A: Chem.* **2004**, *212*, 141–149.

(54)   Tabuani, D.; Monticelli, O.; Chincarini, A.; Bianchini, C.; Vizza, F.; Moneti, S.; Russo, S. *Macromolecules* **2003**, *36*, 4294–4301.

(55)   Zhao, M.; Sun, L.; Crooks, R. M. *J. Am. Chem. Soc.* **1998**, *120*, 4877–4878.

(56)   Balogh, L.; Tomalia, D. A. *J. Am. Chem. Soc.* **1998**, *120*, 7355–7356.

(57)   Esumi, K.; Susuki, A.; Aihara, N.; Usui, K.; Torigoe, K. *Langmuir* **1998**, *14*,

3157–3159.

(58) Pachón, L. D.; Rothenberg, G. *Appl. Organometal. Chem.* **2008**, *22*, 288–299.

(59) Narayanan, R.; El-Sayed, M. A. *J. Phys. Chem. B* **2004**, *108*, 8572–8580.

(60) Bönnemann, H.; Brijoux, W.; Brinkmann, R.; Dinjus, E.; Joussen, T.; Korall, B. *Angew. Chem. Int. Ed. Engl.* **1991**, *30*, 1312–1314.

(61) Bönnemann, H.; Brijoux, W. In *Active Metals: Preparation, Characterization, Applications*; Fürstner, A. Ed.; VCH, Weinheim, 1996.

(62) Niederer, J. P. M.; Arnold, A. B. J.; Hölderich, W. F.; Tesche, B.; Reetz, M.; Bönnemann, H. *Top. Catal.* **2002**, *18*, 265 269.

(63) Luque, R.; Budarin, V.; Clark, J. H.; Macquarrie, D. J. *Appl. Catal. B* **2008**, *82*, 157–162.

(64) Budarin, V.; Clark, J. H.; Hardy, J. J. E.; Luque, R.; Milkowski, K.; Tavener, S. J.; Wilson, A. J. *Angew. Chem. Int. Ed.* **2006**, *45*, 3782–3786.

(65) Pan, X.; Bao, X. *Chem. Commun.* **2008**, 6271–6281.

(66) Terrones, M. *Int. Mater. Rev.* **2004**, *49*, 325–377.

(67) Wildgoose, G. G.; Banks, C. E.; Compton, R. G. *Small* **2006**, *2*, 182–193.

(68) Wang, C.; Guo, S.; Pan, X.; Chen, W.; Bao, X. *J. Mater. Chem.* **2008**, *18*, 5782–5786.

(69) Li, X.; Qin, Y.; Picraux, S. T.; Guo, Z. -X. *J. Mater. Chem.* **2011**, *21*, 7527–7547.

(70) Subrahmanyam, K. S.; Manna, A. K.; Pati, S. K.; Rao, C. N. R. *Chem. Phys. Lett.* **2010**, *497*, 70–75.

(71) Kundu, P.; Anumol, E. A.; Ravishankar, N. *Nanoscale* **2013**, *5*, 5215–5224.

(72) Oyama, M.; Chen, X.; Chen, X. *Anal. Sci.* **2014**, *30*, 529–538.

(73)   Muszynski, R.; Seger, B.; Kamat, P. V. *J. Phys. Chem. C* **2008**, *112*, 5263–5266.

(74)   Kamat, P. V. *J. Phys. Chem. Lett.* 2010, 1, 520–527.

(75)   Raghuveer, M. S.; Agrawal, S.; Bishop, N.; Ramanath, G. *Chem. Mater.* **2006**, *18*, 1390–1393.

(76)   Jasuja, K.; Berry, V. *ACS Nano* **2009**, *3*, 2358–2366.

(77)   Lu, L.; Randjelovic, I.; Capek, R.; Gaponik, N.; Yang, J.; Zhang, H.; Eychmuller, A. *Chem. Mater.* **2005**, *17*, 5731–5736.

(78)   Hassan, H. M. A.; Abdelsayed, V.; El-Rahman, A.; Khder, S.; AbouZeid, K. M.; Terner, J.; El-Shall, M. S.; Al-Resayes, S. I.; El-Azhary, A. A. *J. Mater. Chem.* **2009**, *19*, 3832–3837.

(79)   Li, J.; Liu, C. *Eur. J. Inorg. Chem.* **2010**, 1244–1248.

(80)   Yoo, E.; Okata, T.; Akita, T.; Kohyama, M.; Nakamura, J.; Honma, I. *Nano Lett.* 2009, 9, 2255–2259.

(81)   Bhandari, R.; Coppage, R.; Knecht, M. R. *Catal. Sci. Technol.* **2012**, *2*, 256–266.

(82)   Dickerson, M. B.; Sandhage, K. H.; Naik, R. R. *Chem. Rev.* **2008**, *108*, 4935–4978.

(83)   Guerra, J.; Burt, J. L.; Ferrer, D. A.; Mejía, S.; José-Yacamán, M. *J. Nanopart. Res.* **2011**, *13*, 1723–1735.

(84)   Behrens, S.; Heyman, A.; Maul, R.; Essig, S.; Steigerwald, S.; Quintilla, A.; Wenzel, W.; Bürck, J.; Dgany, O.; Shoseyov, O. *Adv. Mater.* **2009**, *21*, 3515–3519.

(85)   Smith, G. P.; Baustian, K. J; Ackerson, C. J.; Feldheim, D. L. *J. Mater. Chem.* **2009**, *19*, 8299–8306.

(86)   Virkutyte, J.; Varma, R. S. *Chem. Sci.* **2011**, *2*, 837–846.

(87)   Ohara, S.; Hatakeyama, Y.; Umetsu, M.; Tan, Z.; Adschiri, T. *Adv. Power Technol.* **2011**, *22*, 559–565.

(88)   Chiu, C. -Y.; Li, Y.; Huang, Y. *Nanoscale* **2010**, *2*, 927–930.

(89)   Seker, U. O. S.; Demir, H. V. *Molecules* **2011**, *16*, 1426–1451.

(90)   Bhandari, R.; Knecht, M. R. *ACS Catal.* **2011**, *1*, 89–98.

(91)   Jakhmola, A.; Bhandari, R.; Pacardo, D. B.; Knecht, M. R. *J. Mater. Chem.* **2010**, *20*, 1522–1531.

(92)   Coppage, R.; Slocik, J. M.; Briggs, B. D.; Frenkel, A. I.; Heinz, H.; Naik, R. R.; Knecht, M. R. *J. Am. Chem. Soc.* **2011**, *133*, 12346–12349.

(93)   Pacardo, D. B.; Sethi, M.; Jones, S. E.; Naik, R. R.; Knecht, M. R. *ACS Nano* **2009**, *3*, 1288–1296.

(94)   Pacardo, D. B.; Knecht, M. R. *Catal. Sci. Technol.* **2013**, *3*, 745–753.

(95)   Briggs, B. D.; Pekarek, R. T.; Knecht, M. R. *J. Phys. Chem. C* **2014**, *118*, 18543−18553.

(96)   Pacardo, D. B.; Slocik, J. M.; Kirk, K. C.; Naik, R. R.; Knecht, M. R. *Nanoscale* **2011**, *3*, 2194−2201.

(97)   Ramezani-Dakhel, H.; Mirau, P. A.; Naik, R. R.; Knecht, M. R.; Heinz, H. *Phys. Chem. Chem. Phys.* **2013**, *15*, 5488−5492.

(98)   Wu, H.; Wu, C.; He, Q.; Liao, X.; Shi, B. *Mater. Sci. Eng. C* **2010**, *30*, 770−776.

(99)   Hennebel, T.; Verhagen, P.; Simoen, H.; Gusseme, B. D.; Vlaeminck, S. E.; Boon, N.; Verstraete, W. *Chemosphere* **2009**, *76*, 1221−1225.

(100)   Bennett, J. A.; Creamer, N. J.; Deplanche, K.; Macaskie, L. E.; Shannon, I. J.;

Wood, J. *Chem. Eng. Sci.* **2010**, *65*, 282−290.

(101) Søbjerg, L. S.; Gauthier, D.; Lindhardt, A. T.; Bunge, M.; Finster, K.; Meyer, R. L.; Skrydstrup, T. *Green Chem.* **2009**, *11*, 2041−2046.

(102) Hennebel, T.; Gusseme, B. D.; Boon, N.; Verstraete, W. *Trends Biotechnol.* **2008**, *27*, 90−98.

(103) Søbjerg, L. S.; Lindhardt, A. T.; Skrydstrup, T.; Finster, K.; Meyer, R. L. *Colloids Surf. B* **2011**, *85*, 373−378.

(104) Murugesan, K.; Bokare, V.; Jeon, J. -R.; Kim, E. -J.; Kim, J. -H.; Chang, Y. -S. *Bioresour. Technol.* **2011**, *102*, 6019−6025.

(105) Manocchi, A. K.; Seifert, S.; Lee, B.; Yi, H. *Langmuir* **2011**, *27*, 7052−7058.

(106) Manocchi, A. K.; Horelik, N. E.; Lee, B.; Yi, H. *Langmuir* **2010**, *26*, 3670−3677.

(107) Yang, C.; Yi, H. *Biochem. Eng. J.* **2010**, *52*, 160−167.

(108) Yang, C.; Manocchi, A. K.; Lee, B.; Yi, H. *Appl. Catal. B* **2010**, *93*, 282−291.

(109) Bricout, H.; Hapiot, F.; Ponchel, A.; Tilloy, S.; Monflier, E. *Sustainability* **2009**, *1*, 924−945.

(110) Alvarez, J.; Liu, J.; Román, E.; Kaifer, A. E. *Chem. Commun.* **2000**, 1151−1152.

(111) Senra, J. D.; Malta, L. F. B.; Michel, R. C.; Cordeiro, Y.; Simão, R. A.; Simas, A. B. C.; Aguiar, L. C. S. *J. Mater. Chem.* **2011**, *21*, 13516−13523.

(112) Sreedhar, B.; Reddy, P. S.; Devi, D. K. *J. Org. Chem.* **2009**, *74*, 8806−8809.

(113) Bankar, A.; Joshi, B.; Kumar, A. R.; Zinjarde, S. *Mater. Lett.* **2010**, *64*, 1951−1953.

(114) Fenniri, H.; Mathivanan, P.; Vidale, K. L.; Sherman, D. M.; Hallenga, K.; Wood, K. V.; Stowell, J. G. *J. Am. Chem. Soc.* **2001**, *123*, 3854−3855.

(115)   Fenniri, H.; Deng, B. -L.; Ribbe, A. E.; Hallenga, K.; Jacob, J.; Thiyagarajan, P. *Proc. Natl. Acad. Sci. USA* **2002**, *99*, 6487–6492.

(116)   Fenniri, H.; Deng, B. -L.; Ribbe, A. E. *J. Am. Chem. Soc.* **2002**, *124*, 11064–11072.

(117)   Moralez, J. G.; Raez, J.; Yamazaki, T.; Motkuri, R. K.; Kovalenko, A.; Fenniri, H. *J. Am. Chem. Soc.* **2005**, *127*, 8307–8309.

(118)   Chhabra, R.; Moralez, J. G.; Raez, J.; Yamazaki, T.; Cho, J. -Y.; Myles, A. J.; Kovalenko, A. Fenniri, H. *J. Am. Chem. Soc.* **2010**, *132*, 32–33.

Chapter 2

Catalyst Synthesis and Characterization

2.1 Introduction

Over the last two decades metal nanoparticles (M NPs) have emerged as an interesting field of research because of their numerous applications in catalysis, [1-8] energy production and storage,[6,9-15] optoelectronics,[6,16-18] and medicine including biomedical diagnostics.[9,17,19-24] The fascinating unique catalytic, electronic and photonic properties of M NPs are derived from their high surface-to-volume ratio and quantum size effects.[17] Most of these properties are strongly influenced by the size, shape and composition of the M NPs.[9,25] Recent studies revealed that monodisperse M NPs with a size variation of <5% display unique properties and enhanced activity compared to polydisperse M NPs.[26] Monodisperse M NPs result in equal reactivity instead of average reactivity observed for their polydisperse counterpart. Hence, one of the main objectives of the current research is to synthesize highly monodisperse and smaller (1-2 nm) M NPs.[25] However, as the size of the NP decreases it becomes more challenging to control their stability, because the high surface energy of the smaller NP unfavorably dominates their aggregation.[17,25,27]

To address the challenges of controlling the NP size and preventing the aggregation of NPs into larger structures, a variety of supports have been introduced. The supports usually passivate the surface to provide stable and reactive NPs.[9] To date, many synthetic protocols have been developed for producing monodisperse M NPs in solution. These methods include ligand-surface passivation, template-based methods, and seed-mediated techniques.[28] However, the most successful techniques use nonaqueous

systems, toxic chemicals and require energy input such as temperature and pressure.[29,30] Therefore, the development of a green synthetic procedure is highly desired, which uses (i) less toxic chemicals and preferably water as a solvent, (ii) fewer synthetic steps and (iii) low temperature such as ambient condition.[31] It is worth noting that the solution process synthesis has a greater advantage of controlling the nucleation and growth of the NP over other traditional methods. Both the nucleation and growth play a vital role in dictating the monodispersity of the supported NP.[25,26] However, only a few reports have documented the synthesis of NPs smaller than 10 nm in aqueous solution.[32,33]

In addition to the development of aqueous synthetic protocols, the introduction of biomaterials as scaffolds makes the systems even more attractive and eco-friendly. Biomaterials offer several interesting features including renewability, energy efficiency, hydrophobic/hydrophilic properties, and high sorption and stabilization of metal ions.[16,17,30] Several biomolecules such as proteins,[10,30] DNA,[10,34] viruses[10,15,35,36] and peptides[9,37] have successfully been exploited as templates to synthesize monodisperse M NPs. These biomolecules afford regular arrays in aqueous solution, which could template the critical nucleation step, tune the size of the NPs and provide enhanced functionality.[10,29] The synthesis of NPs in aqueous solution takes place in two major steps.[9,28,38,39] First upon addition, the metal ions undergo complexation with the surface functional groups of the biotemplates through electrostatic interaction. Then, the metal ions are chemically reduced to give the NPs following a nucleation and growth mechanism. The templates play a vital role in the reactivity of the materials and dictate the size and composition of the NP.

In this chapter, the synthesis of M NPs (M = Au, Pd and Pt) has been demonstrated by introducing the rosette nanotube (RNT) as a template. It was expected that the well-defined array of the RNTs formed through a self-assembly process, would play a vital role in dictating and providing monodisperse NPs. Initially, the NPs were synthesized by applying a reducing agent in the presence of the RNTs.[40] Later, it was determined that M NPs/RNTs could be synthesized in the absence of a reducing agent. This later discovery encouraged us to investigate the detail kinetic studies and the origin of the NP formation. The size tuning of the NP was also achieved by surface functionalization of the RNTs.

2.2 Results and Discussion

2.2.1 Synthesis of Au NPs/RNTs by Using Reducing Agent

The following discussion in this section is based on an article previously published by Fenniri and co-workers.[40] The article demonstrates the initial approach for the synthesis of RNT supported Au NPs. As RNTs are water-soluble the total synthetic procedure is based on a water-mediated system. To synthesize Au NPs, a pre-made self-assembled solution of RNTs was used. The RNT consists of twin G∧C base (called "G0") containing lysine as a side chain (Figure 2.1). The amines on the side chain are positively charged existing as ammonium ions and are counter balanced by trifluoroacetate (CF_3COO^-) anions (1, Figure 2.1). As the trifluoroacetate anion acts as a weak conjugate base upon addition of tetrachloroaurate ($AuCl_4^-$), they undergo a rapid anion exchange reaction. Because of this exchange reaction, the complexation of $AuCl_4^-$ and RNT takes place through electrostatic interaction. Previously, several groups have observed similar types of support−metal ion complexation prior to the reduction step forming the

NPs.[9,28,38,39] It was expected that the lysine side chains on the surface of RNT could act a nucleation point for the formation of Au NPs upon reduction with hydrazine hydrate ($N_2H_4.H_2O$).
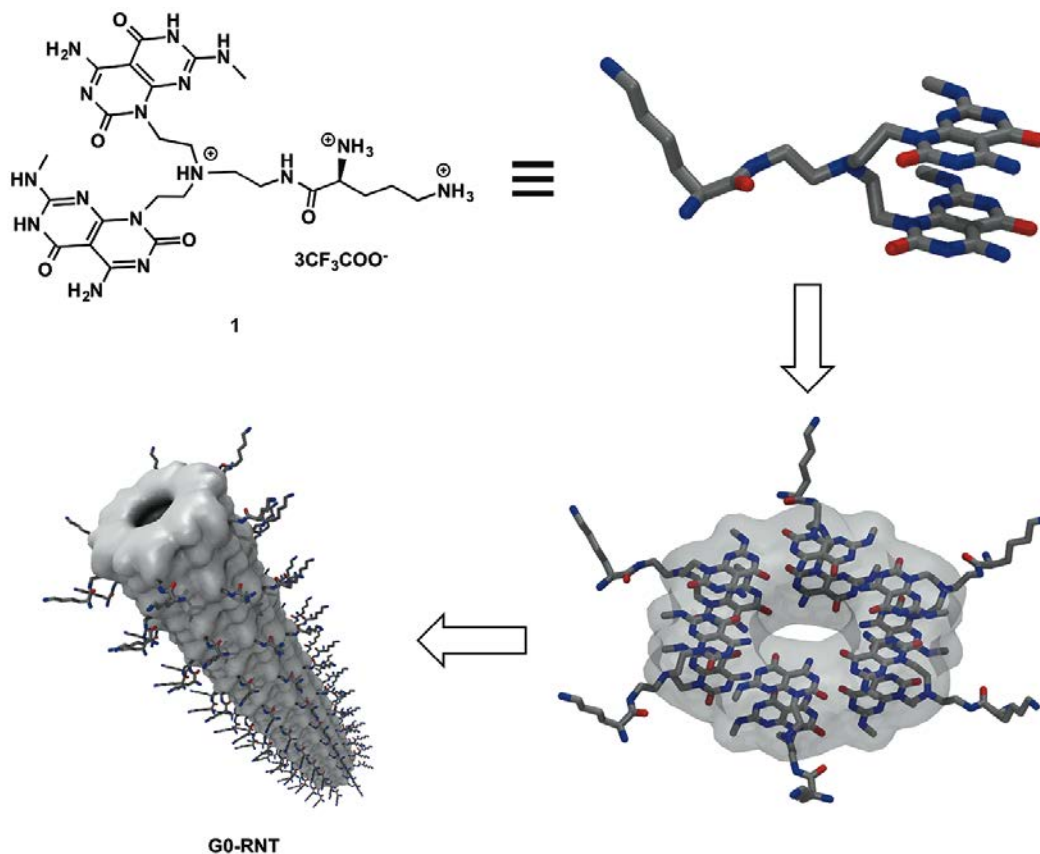
Figure 2.1: Schematic representation of G0-RNT formation through the self-assembly of twin G∧C base.

To maximize the loading of the Au NPs on the surface of the RNTs, the ratio of $AuCl_4^-/1$ was optimized to 20:1. It has been observed that at lower salt concentration (<20 fold excess), the deposition of Au NPs is less than the possible maximum loading. On the other hand a higher salt concentration (>20 fold excess) leads to the formation of polydispersed Au aggregates. To obtain monodisperse Au NPs was optimization of the ratio of $AuCl_4^-/N_2H_4.H_2O$ to 10:1 fold. The pH of the final solution was maintained at ~3.

The size of the Au NPs was measured by transmission electron microscopy (TEM), revealing a mean diameter of 1.4±0.2 nm, while the mean interparticle distance found to be 3.8±0.8 nm (B, Figure 2.2). The inset shows a helical orientation of Au NPs on the surface of RNT (B, Figure 2.2). The red lines indicate the pitch angle while the blue lines indicate the distance between the two adjacent Au NPs (scale bar = 10 nm). The TM-AFM images of the Au NPs/RNTs composite showed a height of ~4.6 nm, which is in very good agreement with the calculated diameter. A detailed analysis of the organization of the Au NPs on the surface of the RNTs showed that the NPs are oriented in a helical fashion with a pitch angle of 40.1±2.3°. The shortest distance between the adjacent NPs was found to be 3.5±0.3 nm along the long axis of the RNT and to be 4.2±0.3 nm across the RNT.
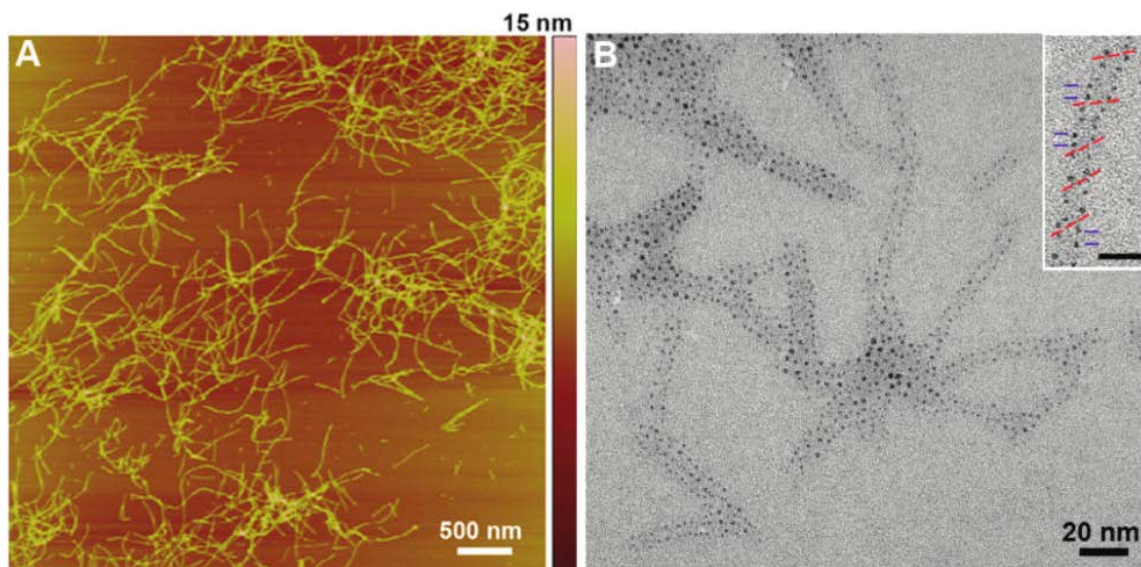
Figure 2.2: TM-AFM (A) and TEM (B) images of Au NP/RNT composite. Used with permission from ACS publishing.[40]

Based on the TEM analysis, a model of Au NPs/RNTs composite was developed (Figure 2.3). The model showed that four adjacent lysine side chains could act as a

nucleation pocket with a cross section of 1.6 nm (c, Figure 2.3). Each nucleation pocket could accommodate a 1.4-1.5 nm size Au NP, and prevent further growth and aggregation leading to larger sized NPs. The model also showed that the next available pocket is 1.4-1.6 nm away along the long axis of RNT. This results in an interparticle distance of ~3.2 nm which is in fairly good agreement with the observed value.
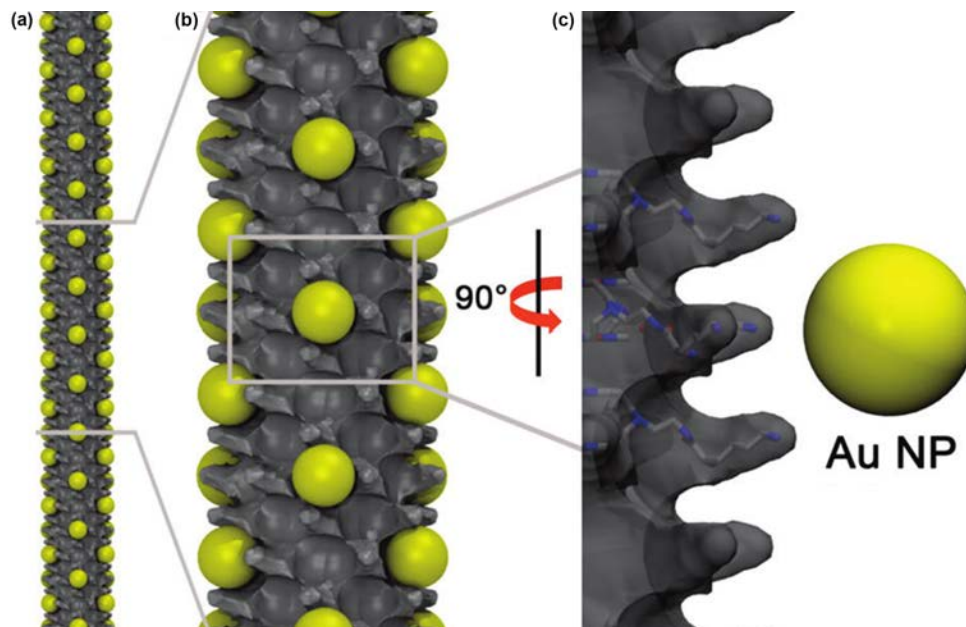
Figure 2.3: Models of Au (gold spheres) NP/RNT composite (a, b), Close-up view of a nucleation pocket containing an Au NP (c). Used with permission from ACS publishing.[40]

A statistical analysis of the TEM images of the Au NPs/RNTs showed that the available maximum numbers of nucleation sites are 188/100 nm and only ~30% of the total nucleation sites were loaded with the Au NPs (58 sites/100 nm). To gain more insight into the loading of the Au NPs on the surface of the RNTs, two models were developed based on the TEM analysis such as a – (i) maximum occupancy model, and (ii) zigzag model. While the maximum occupancy model shows the presence of NPs into all the available nucleation pockets, the zigzag model displays the presence of NPs

36

maintaining the interparticle distance measured by TEM. In comparison to the maximum

occupancy model, the zigzag model supports the observed ~30% loading and measured

interparticle distance while confirming the reduced interparticle repulsion.
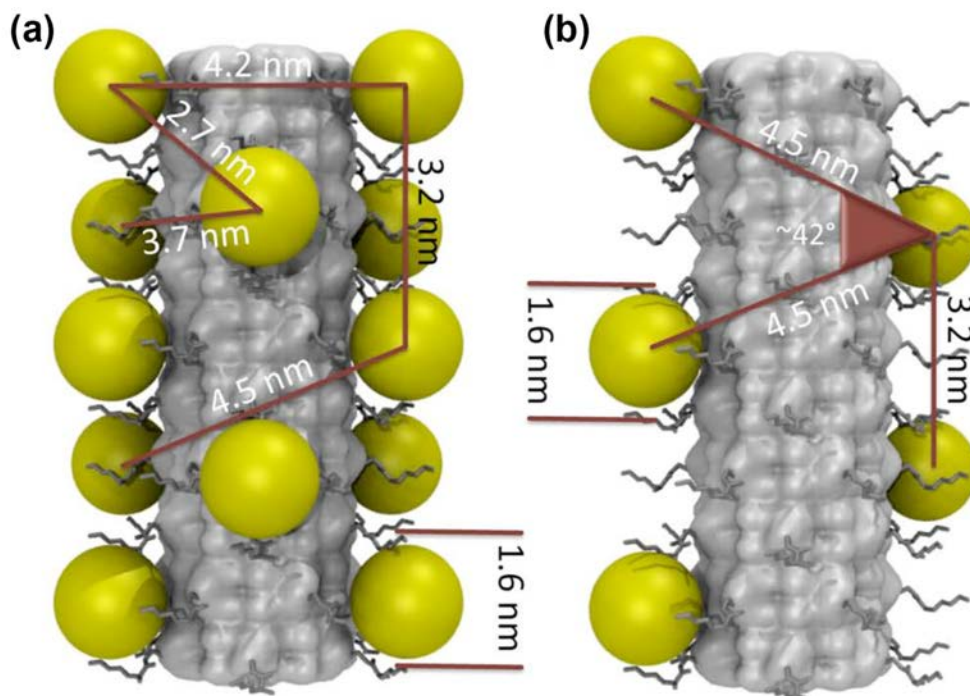
Figure 2.4: Maximum occupancy (a), and zigzag (b) models of Au NP/RNT composite.

Used with permission from ACS publishing.[40]

2.2.2 Synthesis of M NPs/RNTs (M = Au, Pd and Pt) in the Absence of a Reducing Agent

Being inspired by the previous work, Fenniri and coworkers successfully

extended the studies for preparing Au, Pd and Pt NPs using RNT as a scaffold. They

speculated that similar to that of $AuCl_4^-$, the positively charged lysine side chains would

also interact with $PdCl_4^{2-}$ and $PtCl_4^{2-}$, and facilitate the NP formation. It was

hypothesized that upon reduction with hydrazine, RNTs would also nucleate and control

the growth of Pd and Pt NPs in well-organized fashions. Previous studies suggested that

the molar ratios of twin G∧C base, $AuCl_4^-$ and hydrazine should be maintained at 1:20:2

for maximum loading of Au NPs on the surface of the RNTs.[41] However, the statistical

analysis of the occupied nucleation pockets revealed a maximum of ~30% loading of Au

NPs nucleated along the axis of RNT in a zigzag fashion. Based on this observation, it

was calculated that for every twin G∧C base ~4.1 equivalents of $AuCl_4^-$ and 6.2

equivalents of hydrazine are required. To understand the details of the NP formation,

three different metal salt concentrations such as 5, 10 and 20 equivalents with respect to

the RNT concentration were used. Also, equimolar ratios of hydrazine were used as a

reducing agent with respect to that of the metal salt concentrations.

Aqueous solutions of RNTs containing 5, 10 and 20 equivalents of $PdCl_4^{2-}$ were

initially incubated for 24 hours in the dark at ambient temperature. Based on the previous

calculation, it suggested that if Pd NPs would also occupy ~30% of the available pockets

then 5 fold excess of $PdCl_4^{2-}$ should be sufficient to form the NPs. However, additional

equivalents of $PdCl_4^{2-}$ were also examined in attempts to improve the loading of the NPs

on the surface of RNT. Finally, the $PdCl_4^{2-}$/RNT composite was treated with equimolar

ratios of $N_2H_4.H_2O$ for 24 hour to ensure complete reduction. The microscopy

characterization of the Pd NPs/RNTs by both SEM and TEM showed the presence of tiny

dots of Pd NPs templated on the surface of the RNTs. The statistical analyses of the

particle diameter by TEM were carried out on several hundred random RNT templated Pd

NPs and reported in Table 2.1. The sample containing 5 equivalents of $PdCl_4^{2-}$ revealed

an average diameter of 1.6±0.2 nm (Figure 2.5) whereas for the samples with 10 and 20

equivalents of $PdCl_4^{2-}$ the average diameters were estimated to be 1.5±0.1 and 1.7±0.2

nm, respectively (Figure 2.6). A slight increase in the size of the NPs was observed with

increased loading of $PdCl_4^{2-}$. This could be attributed to the over deposition on the

surface of the NP due to the fresh supply of more Pd^0. However, the size differences were found to be insignificant, indicating that the nucleation pockets reached their maximum capacity of holding ~1.5 nm size NPs.
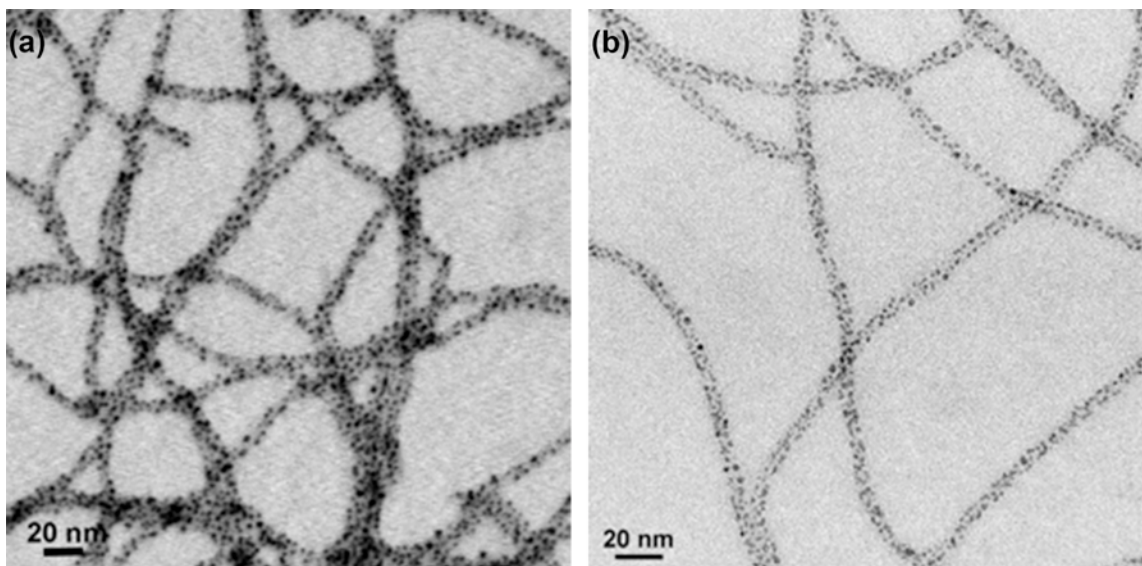
Figure 2.5: STEM (a), and TEM (b) images of K_2PdCl_4/RNTs (250:50 μM) reduced by $N_2H_4.H_2O$.

The average diameter of the Pd NPs/RNTs composite (5 eqvs.) was measured at ~4.5 nm, while it ranges from 10-14 nm for higher equivalents of $PdCl_4^{2-}$ (Figure 2.6). This is perhaps resulted from multilayer coating of different Pd oxo/chloro species on the surface of RNT. In a separate experiment to understand the interaction between RNT and $PdCl_4^{2-}$, and their subsequent consequences on NP formation, we incubated an aqueous solution of RNT containing 5-fold excess of $PdCl_4^{2-}$ for 24 hours in the absence of hydrazine. Surprisingly, both SEM and TEM analyses confirmed the presence of tiny dots of Pd NPs on the surface of the RNTs with an average particle size of 1.5±0.1 nm. This discovery led us to extend our investigation even further and into a new direction. Hence we further studied the formation of NPs with 10 and 20 equivalents of $PdCl_4^{2-}$ and

their effect on the NP size. The TEM analysis showed an average NP size of 1.6±0.2 and

1.7±0.2 nm for the samples containing 10 and 20 equivalents of $PdCl_4^{2-}$ respectively.
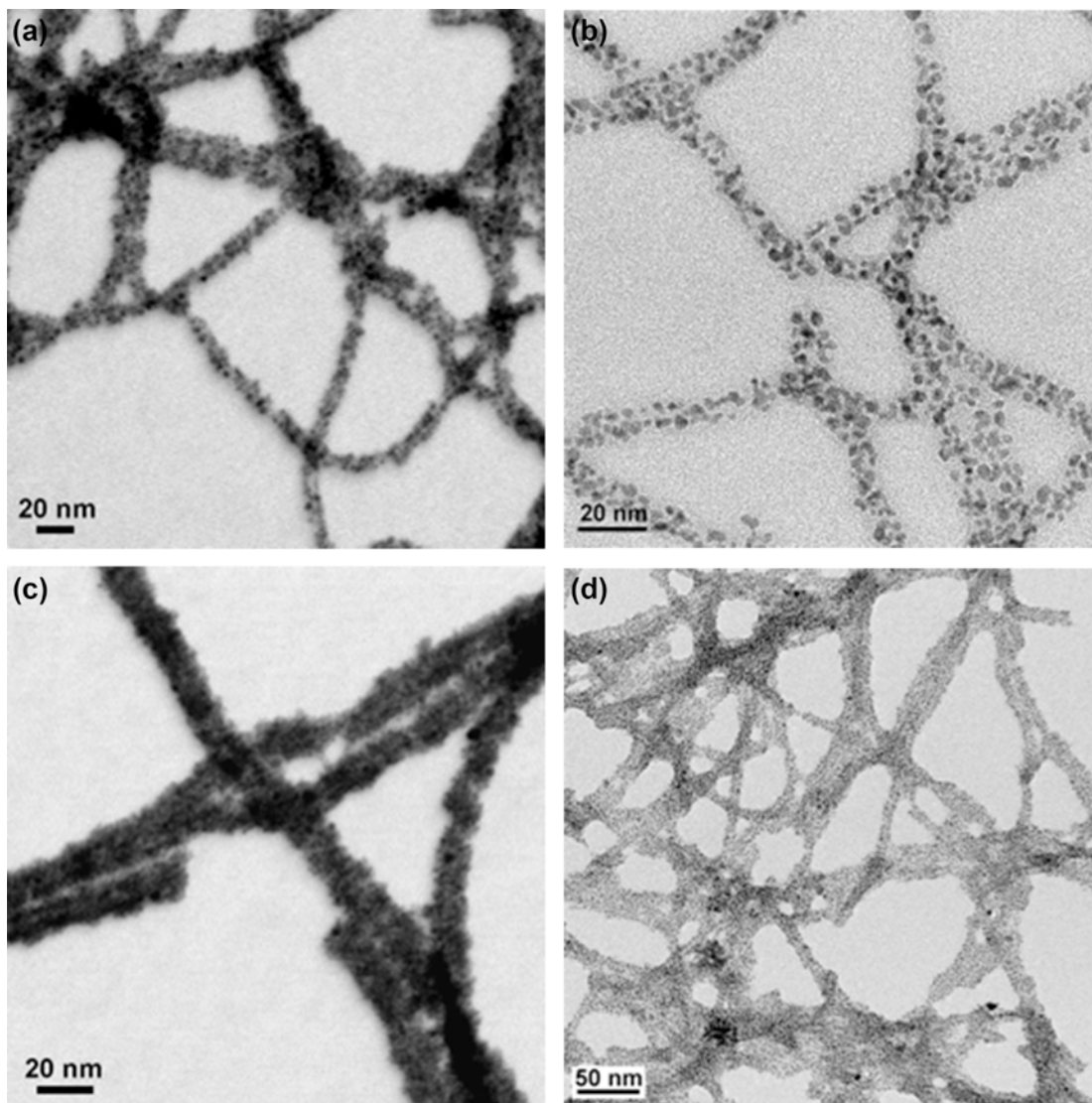
Figure 2.6: STEM and TEM images of K_2PdCl_4/RNTs (500:50 (a, b) and 1000:50 (c, d)

μM) reduced by $N_2H_4.H_2O$.

Similar to the previous observations, there was no significant increase in the

particle size with increasing the $PdCl_4^{2-}$ concentration with respect to that of the RNT,

suggesting that the NPs have grown to the maximum size accommodated by the

nucleation pockets. At higher concentrations, dense loadings of the NPs as well as multi-

layer coatings were also observed. The coating was due to the deposition of excess palladium chloro/oxo complexes, which was confirmed by XPS analysis and will be discussed in a later section in this chapter. Detailed studies of the Pd NP formation at three different concentrations of $PdCl_4^{2-}$ with or without reduction by hydrazine led to several conclusions- (i) the nucleation pockets played a vital role in dictating the size of the Pd NPs formed, (ii) the growth process was controlled by the nucleation pockets and (iii) the NPs have comparable size obtained from both processes.

Table 2.1: Summary of the NP size templated on the surface of the RNTs.

Samples	NP size (nm)	
	With reduction	Without reduction
$PdCl_4^{2-}$/RNT (1:5 fold)	1.6±0.2	1.5±0.1
$PdCl_4^{2-}$/RNT (1:10 fold)	1.5±0.1	1.6±0.2
$PdCl_4^{2-}$/RNT (1:20 fold)	1.7±0.2	1.7±0.2
$AuCl_4^{-}$/RNT (1:5 fold)	1.2±0.1	1.2±0.1
$AuCl_4^{-}$/RNT (1:10 fold)	1.1±0.1	1.2±0.2
$AuCl_4^{-}$/RNT (1:20 fold)	1.2±0.2	1.2±0.2
$PtCl_4^{2-}$/RNT (1:5 fold)	1.3±0.1	1.3±0.2
$PtCl_4^{2-}$/RNT (1:10 fold)	1.4±0.1	1.4±0.1
$PtCl_4^{2-}$/RNT (1:20 fold)	1.4±0.1	1.3±0.1
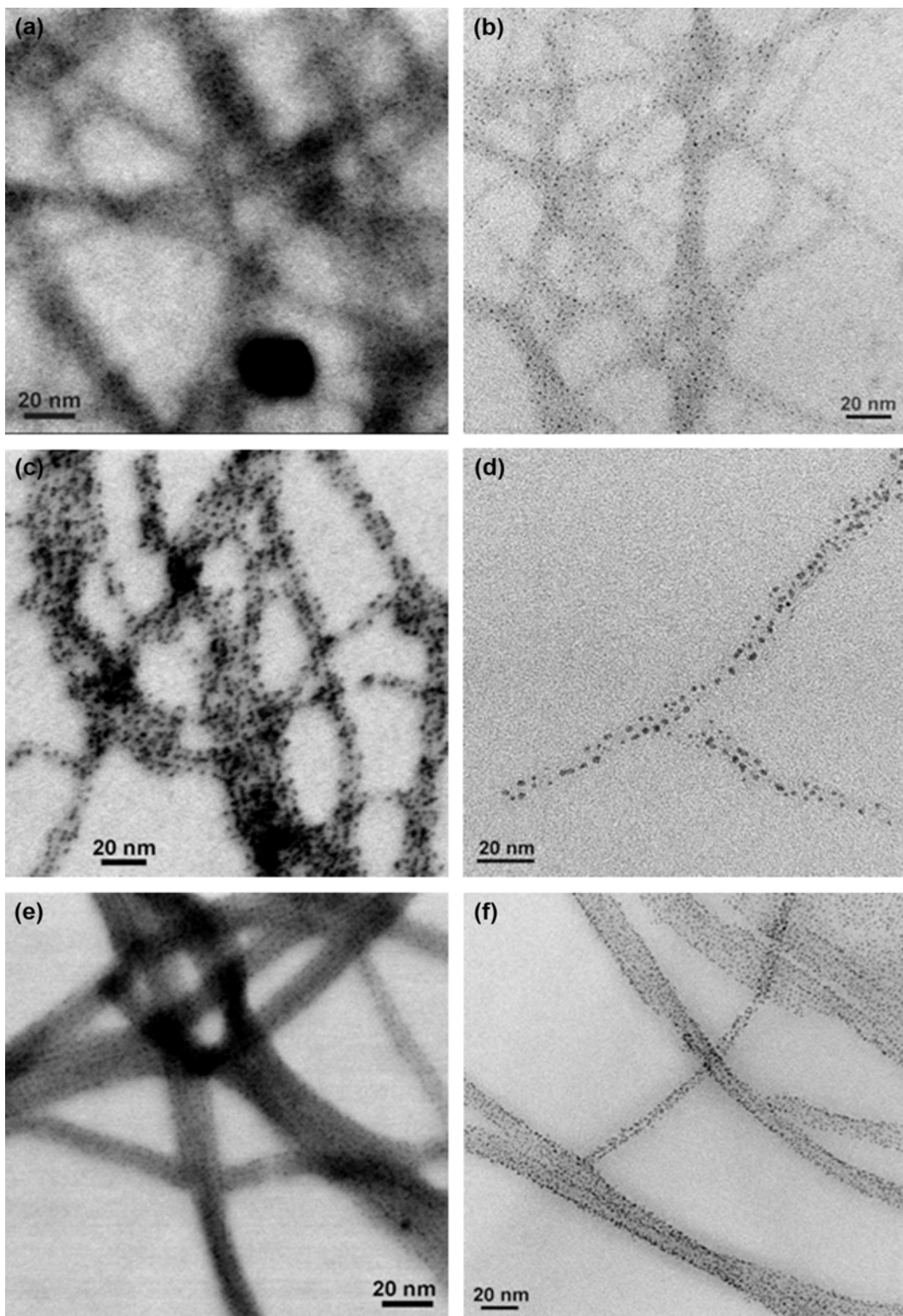
Figure 2.7: STEM and TEM images of K_xMCl_4 (x = 1, 2)/RNTs (500:50 μM, M = Au (a, b), Pd (c, d) and Pt (e, f)) without the addition of $N_2H_4.H_2O$.

Similarly, $AuCl_4^-$ and $PtCl_4^{2-}$ were also employed as precursors for the synthesis of Au and Pt NPs with and without using hydrazine as a reducing agent. Firstly, aqueous solutions of RNT containing 5, 10 and 20 equivalents of $AuCl_4^-$ and $PtCl_4^{2-}$ were allowed to incubate for 24 hours. To ensure complete reduction, the samples were treated with hydrazine for 1 hour before the SEM and TEM analyses. Later, the same experiments were repeated without the reduction step (Figure 2.7). Samples from both experiments were analyzed by SEM and TEM, which confirmed the presence of both Au and Pt NPs nucleated on the surface of the RNTs. The size of the Au and Pt NPs were measured by TEM and reported in Table 2.1.
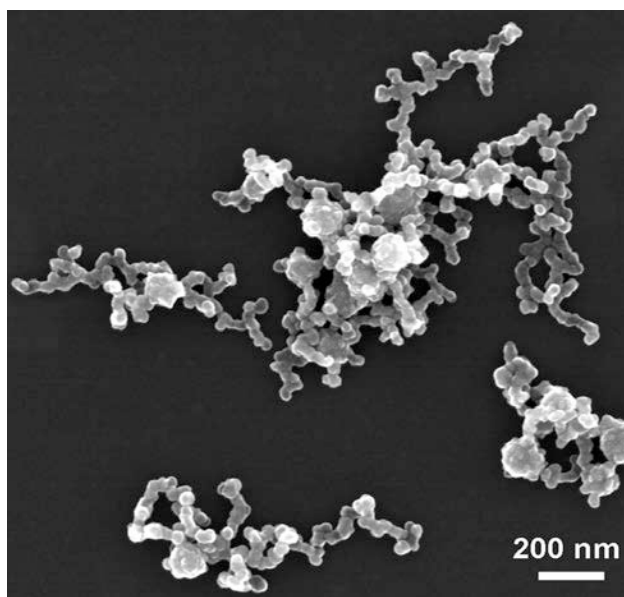
Figure 2.8: SEM image of K_2PdCl_4/L-LAA (250:50 μM) without the addition of $N_2H_4.H_2O$.

Initially, we speculated that the supramolecular organization of the RNT and the nucleation pockets formed by the lysine side chains play a key role in dictating the narrow size distribution of metal NPs. To prove this hypothesis, we employed L-lysine amino acid (L-LAA) instead of RNT. As control experiments, aqueous solutions of lysine

43

amino acid were incubated with a 5 and 20 fold excess of $PdCl_4^{2-}$. After an incubation period of 24 h, the samples were analyzed by SEM and the images clearly showed that lysine amino acid was unable to form Pd NPs, but rather produced random large aggregates (Figure 2.8). This observation suggests that the supramolecular organization of the RNTs and the subsequent nucleation pocket formation indeed play a vital role in providing monodispersed Pd NPs.

To confirm the nature and composition of RNT templated M NPs (M = Au, Pd and Pt), Fenniri and coworkers performed X-ray Photoelectron Spectroscopy (XPS) on M NPs/RNTs with or without reduction by hydrazine. As expected, the XPS analysis confirmed the presence of M^0 in M NPs/RNTs samples reduced by hydrazine. Besides this, the analysis also unambiguously revealed the metallic nature of all three metal NPs formed without the addition of $N_2H_4.H_2O$. The metallic nature of M NPs was confirmed by the corresponding binding energies associated with each M NPs (Au^0, $4f_{5/2}$ = 87.7 eV and $4f_{7/2}$ = 84.0 eV; Pd^0, $3d_{3/2}$ = 340.4 and $3d_{5/2}$ = 335.1; and Pt^0, $4f_{5/2}$ = 74.5 eV and $4f_{7/2}$ = 71.2 eV).[41-43] Additionally, these results were also confirmed by Auger Electron Spectroscopy (AES) analysis. The AES data showed the characteristic peaks correspond to specific metals (M^0) such as Au^0 (1741 eV, 2011 eV and 2097 eV), Pd^0 (325 eV), and Pt^0 (1698 eV, 1960 eV and 2039 eV). An excellent match of the peaks of M NPs/RNTs was observed for the samples treated with or without $N_2H_4.H_2O$. This observation further demonstrates that the RNTs are acting as a support in providing highly monodispersed M NPs as well as contributing to the reduction of corresponding metal salt. Also the energy dispersive X-ray (EDX) analysis and selective area electron diffraction (SAED) of M NPs/RNTs support the previous observation.

Earlier, Fenniri and coworkers have found that RNTs could nucleate and allow the growth of NPs to a specific size dictated by the nucleation pockets formed by the lysine side chains in the absence of hydrazine. Hence, it was crucial to investigate the reason for the NP formation as the system only contains RNTs as a support, water as a solvent and metal chloride as the precursor of the corresponding M NP. Therefore, I decided to perform a detail studies to evaluate the origin of the NP formation. It is well established that a redox reaction is a simultaneous process. This means that when a reduction reaction takes place, an oxidation reaction also occurs at the same time. Considering this scenario, if the metal salt is reduced to form the NP then in the system something else has to be oxidized. For this system, as I do not use any additional reducing agent the possible suspect could be either RNT or water.
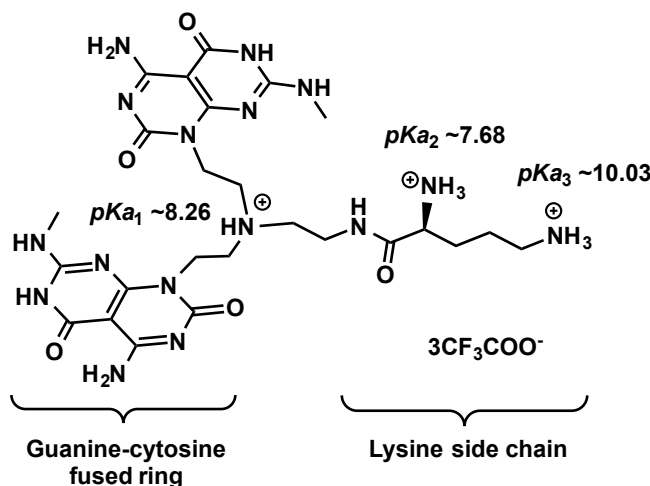
Figure 2.9: Structure of the G∧C base, building block of RNT.

The twin G∧C base building block of RNT, used for this studies consists of two parts- (i) guanine-cytosine fused rings and (ii) a L-lysine dangling side-chain (Figure 2.9). Hence it is possible that either the guanine-cytosine fused ring or lysine undergoing

oxidation affords the required electrons to reduce the metal ions. It is well documented that the oxidation of DNA takes place at the guanines.[44] This is due to the fact that guanine has a low oxidation potential.[44,45] Since the twin G∧C base contains the fused guanine-cytosine rings, it is possible that the fused ring is responsible for the reduction of the metal ions. Alternately, the dangling lysine side chains addressed on the surface of RNT could contribute to the reduction of the metal ions as they contain amines. It has been reported earlier that the primary and secondary amines can act as reducing agents and stabilizers after the formation of NPs.[46,47] Depending on the amines used, the oxidized product could be imines,[48] or oligomeric and polymeric species.[46,49] Similarly, if RNTs are not involved in the reduction process then alternately, water could be oxidized and provide the required electrons.[50] One of the trivial facts of NP formation is the drop in pH of the solution due to the generation of protons in solution.[51] For the current studies I used $PdCl_4^{2-}$ as the precursor to Pd NP formation and employed a ten fold excess to that of the RNTs concentration (Table 2.2). Initially, I measured the pH of a 0.01 mM aqueous solution of RNTs and found it to be 6.72, while for a 0.1 mM solution of $PdCl_4^{2-}$ the pH was 4.67 (Figure 2.2). Hence it is expected that upon Pd NP formation the pH of the $PdCl_4^{2-}$/RNT solution would drop below the pH of the individual solution. As expected, the pH measurement of $PdCl_4^{2-}$/RNT solution showed that the pH rapidly dropped to 4.31 within 1 min of mixing (Table 2.2). This indicates that perhaps the NP formation followed by the nucleation on the surface of RNT could be a very quick process. The pH of the solution further continued to drop slowly to 4.18 over a period of 1 h. This observation includes both the possibilities that either RNT or water are involved in the reduction of metal ions.

Table 2.2: pH measurement of the RNT, $PdCl_4^{2-}$ and $PdCl_4^{2-}$/RNT solutions.

Samples	pH
RNT (0.01 mM)	6.72
$PdCl_4^{2-}$ (0.1 mM)	4.67
$PdCl_4^{2-}$/RNT (0.1:0.01 mM)	4.31 (1 min)
	4.23 (30 min)
	4.18 (60 min)

To gain more insight into the process, I carried out cyclic voltammetry (CV) studies to investigate the redox properties of RNTs and K_2PdCl_4 in water. A detail list of reduction potentials of water and palladium species is reported in Table 2.3.[52] Recently, Chen and coworkers have investigated the CV of an aqueous solution of K_2PdCl_4 (1 mM) using 0.5 M H_2SO_4 as the supporting electrolyte.[52a] They found the reduction potential of Pd^{2+} in K_2PdCl_4 is 0.38 V vs Ag/AgCl.[52a] As the system does not contain any acid, it is important evaluate the reduction potential of Pd^{2+} in K_2PdCl_4 in the absence of acid. Therefore, the CV studies of K_2PdCl_4 in water containing 0.1 M KCl as the supporting electrolyte, showed a reduction potential of Pd^{2+} in K_2PdCl_4 is 0.03 V vs Ag/AgCl (Figure 2.10a). However, it is expected that the presence of RNT in solution would influence the reduction potential of Pd^{2+} to form the Pd NPs. If RNTs are involved in the reduction of Pd^{2+}, then they should have an oxidation potential close to the reduction potential of Pd^{2+}. It is crucial that the oxidation potential of a reducing agent is higher than the reduction potential of the metal precursor in order for a spontaneous redox reaction to proceed.[46] Earlier, I stated that one of the options for RNT to reduce Pd^{2+} is through the oxidation of the guanine-cytosine ring. Previously, several groups have investigated the redox properties of guanine. The studies suggested that guanine could be readily oxidized to a radical cation, which has an oxidation potential of 1.06 V vs

Ag/AgCl.[53] As the oxidation potential of guanine is closer and higher than the reduction potential of Pd^{2+} this makes the guanine-cytosine ring a suitable candidate as a reducing agent. Considering this, the CV studies were performed in water over a scan rate of 0.1 Vs^{-1} at a temperature of 21±1 °C.

Table 2.3: The standard reduction potentials ($E°$) of water and palladium species.[52]

Half-reaction			$E°$ (V)
Oxidation		Reduction	
$O_2 + 4H^+ + 4e^-$	$\rightleftharpoons$	$2H_2O$	1.229^a
$Pd^{2+} + 2e^-$	$\rightleftharpoons$	Pd^0	0.951^a
$[PdCl_4]^{2-} + 2e^-$	$\rightleftharpoons$	$Pd^0 + 4Cl^-$	0.591^a
$[PdCl_4]^{2-} + 2e^-$	$\rightleftharpoons$	$Pd^0 + 4Cl^-$	0.380^b
$[PdCl_4]^{2-} + 2e^-$	$\rightleftharpoons$	$Pd^0 + 4Cl^-$	0.030^c

^{a} $E°$ (V) vs SHE at T = 25 °C, P = 1 atm and acid concentration = 1 M; ^{b} $E°$ (V) vs Ag/AgCl using glassy carbon electrode from 0.5 M H_2SO_4 containing K_2PdCl_4 (1 mM); ^{c} $E°$ (V) vs Ag/AgCl using glassy carbon electrode from 0.1 M KCl containing K_2PdCl_4 (1 mM).
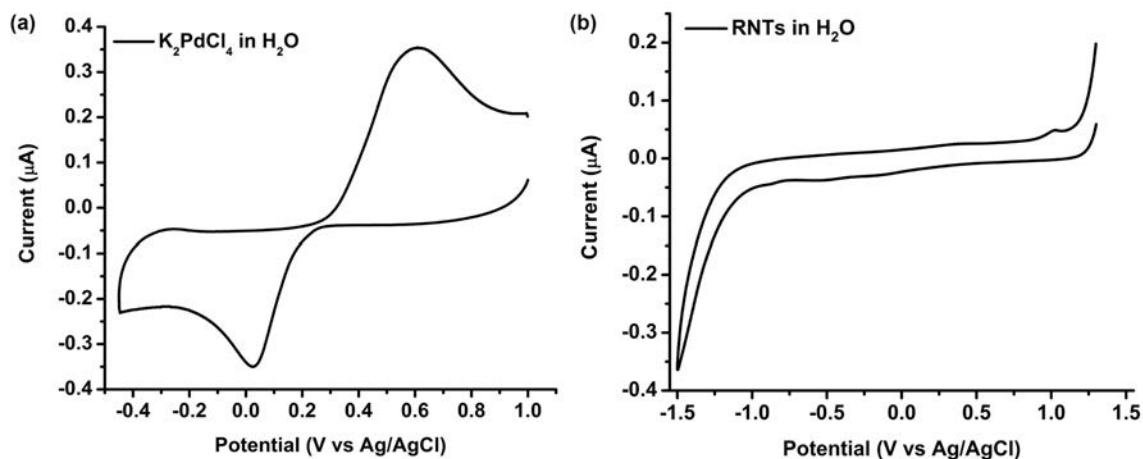
Figure 2.10: CV of (a) K_2PdCl_4, and (b) RNT in water (1 mM). The potential was first swept in the negative direction.

48
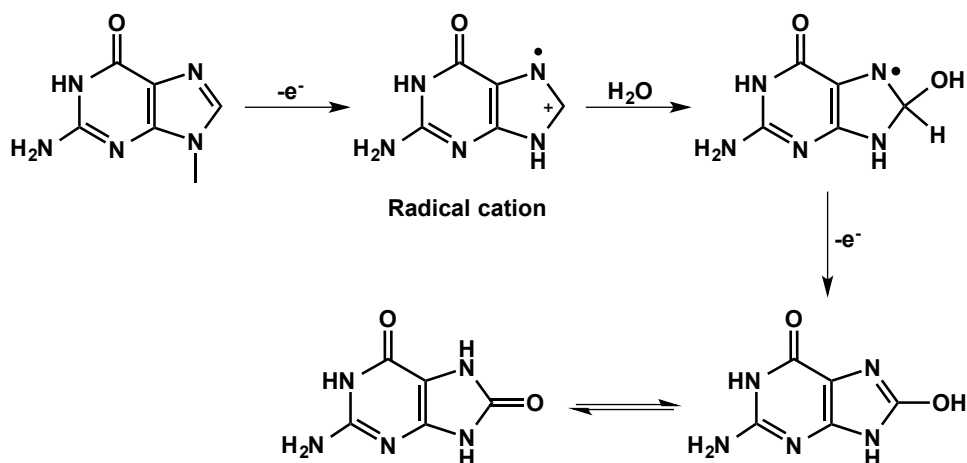
Figure 2.11: A more facile oxidation route of guanine and subsequent products formation.

The data showed that the RNTs in water with KCl (0.1 M) as the supporting electrolyte gave rise to no redox activity within the potential window of ±1.5 V (Figure 2.10b). The observed result suggests that perhaps RNT is not involved in providing the electrons to form Pd^0. A careful examination at the oxidation scheme of guanine reveals that the oxidation reactions are more susceptible on the pentacycle ring leaving the hexacycle ring undisturbed (Figure 2.11).[53] The guanine-cytosine ring of RNT is composed of the hexacycle portion of the guanine molecule. Hence it is more likely that the heterocyclic ring of the RNTs will not undergo oxidation supporting the observed CV results. The second option for the RNTs to reduce Pd^{2+} is by the oxidation of amines of the lysine. However, the CV studies also ruled out this option as well. Usually, to give electrons the lone pair of electrons of nitrogen should be available. In the case of the RNTs, the amines of the lysine exist as ammonium ions, which are already in the oxidized form. However, ammonium ions could give up protons and be converted back to the amines and finally contribute to the reduction process.[48] This conversion could be strongly influenced by the pKa value of the amines and the pH of the solution. Earlier,

Fenniri and coworkers reported the pKa values of the amines of the lysine, which found to be very high (Figure 2.9; *pKa₁* ~8.26, *pKa₂* ~7.68 and *pKa₃* ~10.03).[40] This indicates that the ammonium ions are very weak acids and there are fewer chances for these ammonium ions to give up the protons at pH ~4.0. The pH studies also suggest that the amines will prefer to stay as ammonium ions instead of giving up the protons under acidic condition (Table 2.2). Hence it is very unlikely that the amines would contribute to the reduction of Pd^{2+} ions to form Pd NPs.

As discussed earlier, the theoretical calculation showed that the size of the nucleation pocket formed by four adjacent lysine side chains was 1.6 nm. Hence, each nucleation pocket could spontaneously accommodate a NP with a particle size of ~1.6 nm. If the NP consists of Pd atoms then by using equation (1) we could calculate the number of Pd atoms present in a ~1.6 nm size NP. The calculation shows that a ~1.6 nm size Pd NP contains 132 Pd atoms. The Pd has +2 oxidation state in $PdCl_4^{2-}$, which requires $2e^-$ to form each Pd^0. Hence it requires a total of 264 e^- to form 132 Pd atoms in a single NP. Earlier, from the model studies we found that RNTs contain a total of 188 nucleation pockets within a length of 100 nm. Based on the ~30% loading of the Pd NPs onto the surface of RNT, Pd NPs could occupy a maximum of 58 nucleation sites within the length of 100 nm. This indicates that to form 58 NPs with an average particle size of ~1.6 nm, 15,312 e^- (264×58) are required. The model studies show that each 100 nm length of RNT consists of 125 rosette stacks formed by the self-assembly of 750 (125×6) twin G∧C bases. Unfortunately, it is quite impossible to afford 20 e^- (15,312÷750) by each twin G∧C base to form 58 NPs within the 100 nm length of RNT. The RNTs could not provide this large number of electrons either by the oxidation of the guanine-cytosine

fused ring or amines of the lysine. Both the experimental and theoretical analyses ruled out the option for RNT to act as a reducing agent. However, perhaps RNT could facilitate the Pd NP formation because of the supramolecular organization.

$$N = \frac{\pi \rho D^3}{6 M} N_A \quad \text{---------------(1)}$$

N = No. of atoms/NP

π = 3.14

ρ = Density of Pd in a face centered cubic (fcc) unit cell = 12.0 g/cm^3 = 12.0×10^{-20} g/nm^3

D = Diameter of the NP = 1.55 nm

N_A = Avogadro number = 6.023×10^{23} atoms/mol

M = Atomic mass of Pd = 106.42 g/mol

Hence this leads the solvent "water" as the potential candidate to act as a reducing agent to form Pd NPs. As will be discussed below water oxidation may occur in the presence of K_2PdCl_4 and RNT. If water is involved in the reduction, then the use of D_2O would display the kinetic isotopic effect on the NP formation. The kinetic isotope effect originates from the difference in the zero point energy resulting in the different bond dissociation energies. Usually, heavier isotopes have higher bond dissociation energies than their lighter isotopes. For H_2O, the average bond dissociation energy is 458.9 KJ/mol, while for D_2O it is 466.4 KJ/mol. Hence, because of high bond dissociation energy, the oxidation of D_2O would be slower leading to smaller sized NPs compared to that of in water. To justify this hypothesis, we repeated the synthesis of Pd NPs/RNTs in D_2O under the identical conditions in water. The size of the NPs were evaluated by TEM and compared with those from water.
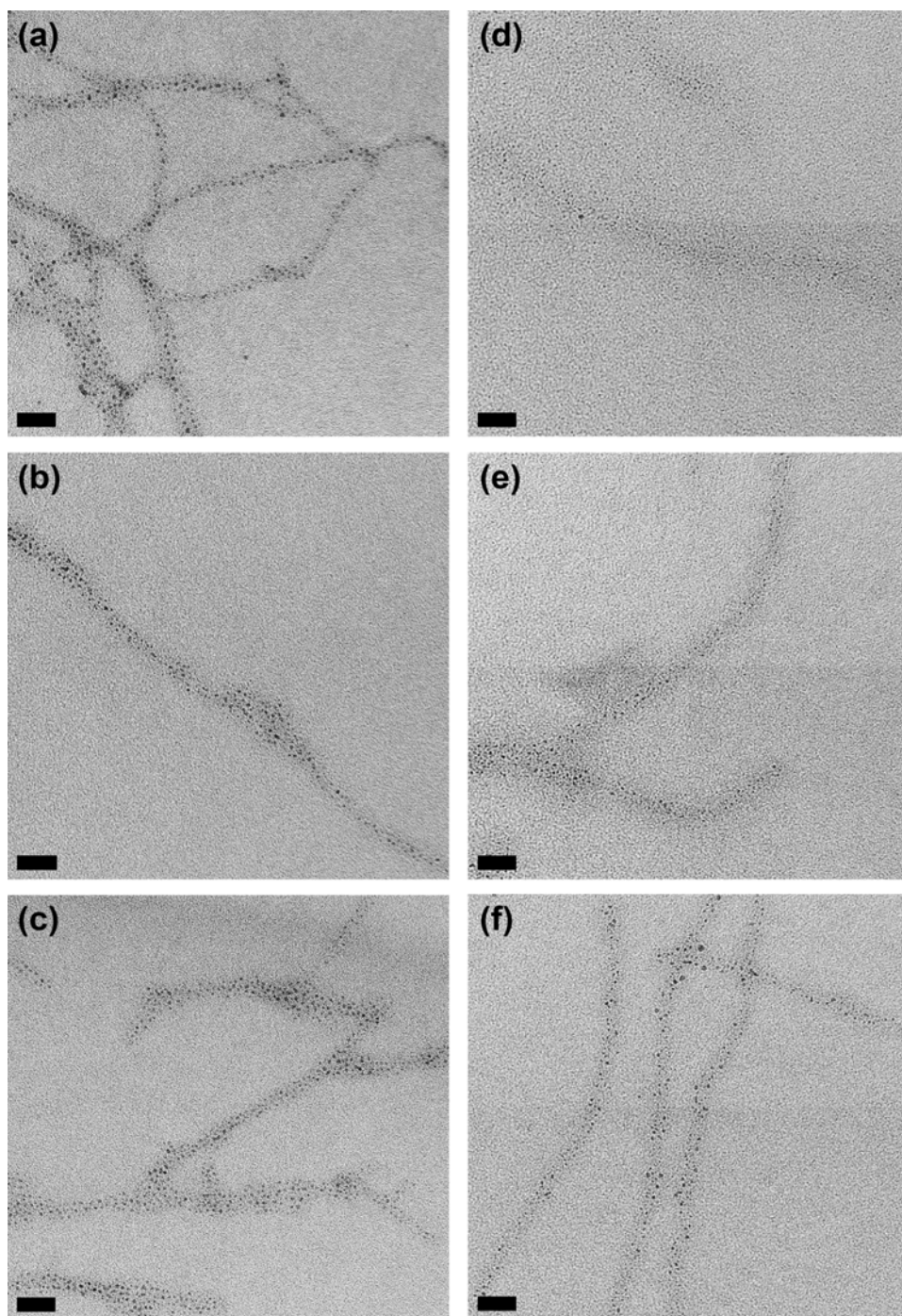
Figure 2.12: TEM images of Pd NPs/RNTs in H_2O (a-c) and D_2O (d-f). Scale bar – 20 nm. The samples incubated for 1 min (a, d), 30 min (b, e) and 60 min (c, f).

Table 2.4: TEM analysis of Pd NPs/RNTs in H_2O and D_2O.

Pd NPs/RNTs	Incubation time (min)		
	1	30	60
H_2O	1.5±0.1 nm	1.5±0.1 nm	1.6±0.1 nm
D_2O	0.6±0.1 nm	1.0±0.1 nm	1.4±0.1 nm

Three samples from the D_2O experiment were analyzed by TEM based on the aging time (1 min, 30 min and 60 min) (Figure 2.12). The results from the analysis are summarized in Table 2.4. When compared, the TEM measurement showed that the size of the Pd NP was smaller in D_2O than in H_2O. This observation indeed supports the hypothesis of water oxidation causing the Pd NP formation. The TEM analysis revealed that the NP formation was a very rapid process in water, which was slowed down in D_2O.
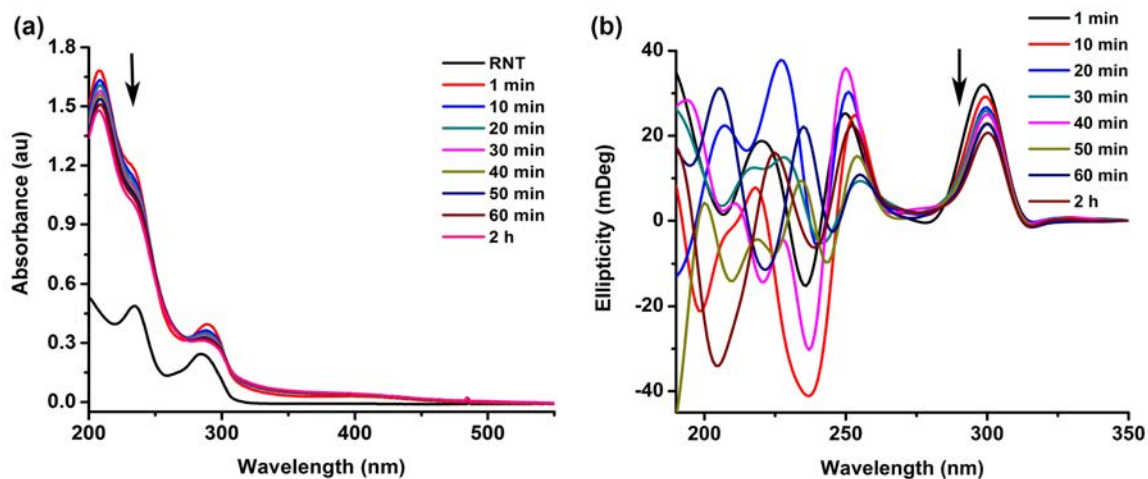
Figure 2.13: Kinetics of the Pd NP/RNT formation in D_2O studied by UV-Vis (a), and CD (b) spectroscopy.

The solution characterization such as the time dependent UV-Vis studies of Pd NPs/RNTs in D_2O also showed slow kinetics (Figure 2.13a) compared to that in water (Figure 2.23a), which also supported the TEM analysis affording the smaller size NPs.

The UV spectrum of the D_2O sample displayed a slow drop in absorbance at 208, 234 and 289 nm within 1 hour. It is worth noting that the absorption at 208 nm corresponds to the $Pd(D_2O)Cl_3^-$ anion. On the other hand, the water sample showed a rapid drop in absorbance within the first 10 mins and leveled off after 1 hour (Figure 2.23a). The slow kinetics was also reflected in the circular dichroism (CD) at a higher wavelength around 300 nm (Figure 2.13b). To gain further insight into the nature of palladium in the D_2O sample, we performed XPS analysis. It should be noted that the Pd NPs/RNTs samples deposited on the TEM grid or Si wafer, were analyzed without further washing with water. The spectra showed the presence of Pd^0 as well as PdO_x (X = 1 and 2) in the samples (Figure 2.14). The spectrum of the TEM grid sample showed a binding energy (E_b) peak at 335.1 eV ($Pd3d_{5/2}$), which corresponds to the elemental Pd.[54] On the other hand, the peaks at higher binding energies at 335.7 and 337.9 eV ($Pd3d_{5/2}$) correspond to PdO and PdO_2, respectively (Figure 2.14a).[55-57]
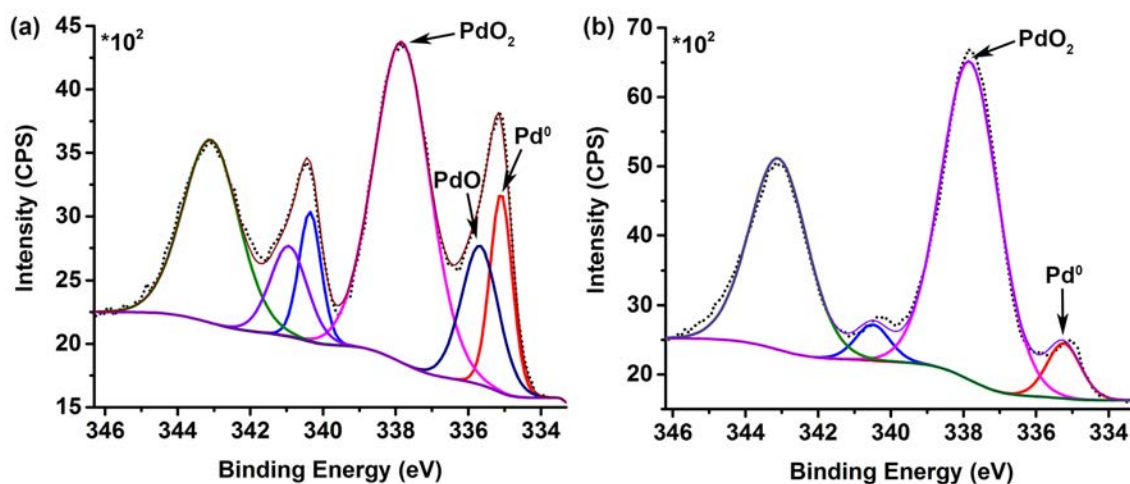
Figure 2.14: XPS analysis of Pd NPs/RNTs on the TEM grid (a), and on the Si wafer (b) in D_2O (E_b was calibrated with respect to the C1*s* peak at 284.8 eV).

In the case of the Si wafer sample, though there were no significant shifts in E_b for

Pd^0 ($Pd3d_{5/2}$ = 335.2) and PdO_2 ($Pd3d_{5/2}$ = 337.9), the E_b for PdO was not isolable due to

overlapping (Figure 2.14b). The ratio of the % concentration of Pd^0, PdO and PdO_2 was

1:1:4 in TEM grid sample. As expected, the hydrophobic nature of the TEM grid, which

was made of carbon mesh, would prefer the deposition of Pd (Pd^0) NPs/RNTs on the

surface of the grid instead of PdO_x species after drop casting the solution. On the other

hand, the ratio of the % concentration of Pd^0 and PdO_2 was increased to 1:10 in the Si

wafer sample, which perhaps due to the higher affinity of Si for oxygen. Because of this

affinity, PdO_x species were expected to bind strongly on the surface of the Si wafer after

drop casting. The presence of oxide in the sample could also be assigned from the O1s

spectrum. The binding energy peak appeared at 531.6 eV due to water or oxygen

chemisorbed on the surface of the samples (Figure 2.15).[57,58]
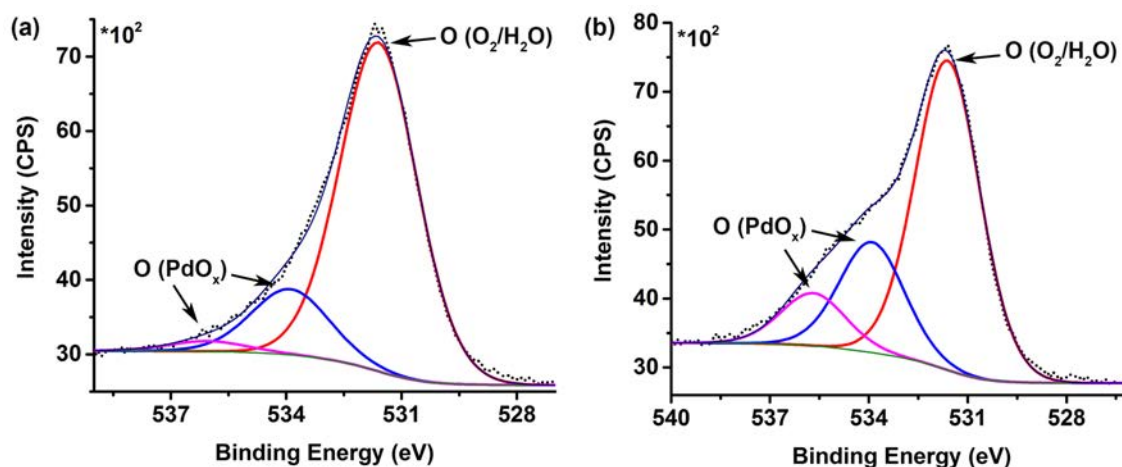
Figure 2.15: The O1s spectra of Pd NPs/RNTs on the TEM grid (a), and on the Si wafer

(b) in D_2O (E_b was calibrated with respect to the C1s peak at 284.8 eV).

The E_b of the O1s peak for PdO_2 is unknown and considering that the E_b of

oxygen for both PdO and PdO_2 would be closely lying,[58] we speculate that the additional

peak at higher E_b could be attributed to the PdO_x species.[58] As observed earlier, the %

concentration of the PdO_x species was higher in the Si wafer than in the TEM grid sample. The ratio of the % concentration of Pd and PdO_x species was 1:0.4:0.2 in the Si wafer sample (Figure 2.15 (b)), while it was 1:0.2:0.03 in TEM grid sample (Figure 2.15 (a)). To further understand the process of the Pd NP formation we carried out a detailed XPS analysis. Earlier we investigated the nature of Pd present in Pd NPs/RNTs sample synthesized in water by XPS analysis. Initially, the XPS samples were prepared by depositing 5-6 drops of Pd NPs/RNTs solution followed by washing the surface using fresh deionized water. The reason for washing the Pd NPs/RNTs sample surface was to obtain nice and clean binding energy peaks of Pd^0. However, cleaning the surface actually wipes off the evidence of counter side product formation. Hence, this leads to missing the detail picture of the NP formation, which could provide vital information on the mechanism of NP formation especially in the absence of a reducing agent. Indeed the XPS analysis of the sample deposited on TEM grid, washed with water, showed very nice binding energy peaks, which correspond to the elemental Pd ($Pd3d_{5/2}$ = 335.2) as well as the presence PdO ($Pd3d_{5/2}$ = 335.8) and PdO_2 ($Pd3d_{5/2}$ = 337.9) peaks (Figure 2.16a).[54-57] As expected, the oxygen spectrum showed the E_b of the O1s peaks at 531.6 and 533.9 eV, which correspond to the chemisorbed O_2 or water, and PdO_x, respectively. The unwashed sample also showed the $Pd3d_{5/2}$ peaks at 335.2, 335.9 and 338.1 eV for Pd^0, PdO and PdO_2, respectively (Figure 2.16c).
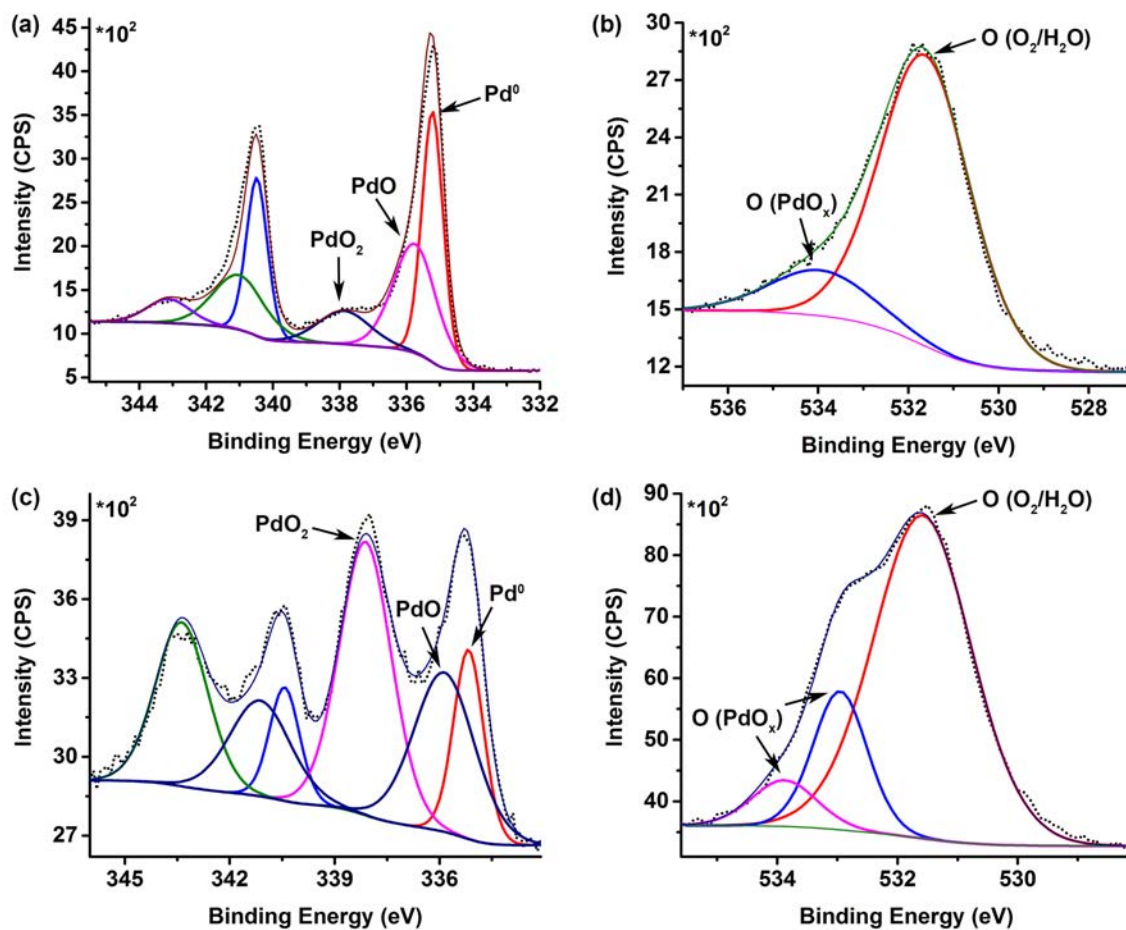
Figure 2.16: XPS analysis of Pd NPs/RNTs on a TEM grid in H_2O. The samples were washed with H_2O (a, b), and unwashed (c, d). The E_b of Pd3$d_{5/2}$ (a, c) and O1s (b, d) spectra was calibrated with respect to the C1s peak at 284.8 eV.

As the sample surface was not washed with water, it is expected that the spectrum should provide a detailed status of the reaction medium after the NP formation deposited on the TEM grid. Therefore, the XPS analysis should afford information about all the Pd species formed as side products. Similar to that of the washed sample, the unwashed sample also showed the presence of PdO_x species. However, the ratio of the % concentration of Pd^0, PdO and PdO_2 was higher in the unwashed sample (1:0.3:0.1) than in the washed sample (1:0.2). As the third peak in the washed sample was not present, we

surmised that it could be an artifact caused by the charging effect in the sample or a true peak, which belonged to potassium. As Si has higher binding affinity for oxygen, we repeated the analysis of the unwashed sample on the Si wafer (Figure 2.17). The $Pd3d_{5/2}$ spectrum showed the E_b peaks at 336.1 and 337.9 eV for PdO and PdO_2, respectively. In addition, the O1s spectrum contained peaks, which could be attributed to the PdO_x species. Though the analysis confirmed the formation of PdO and PdO_2 as the side products, it did not prove how the PdO_x species were formed.
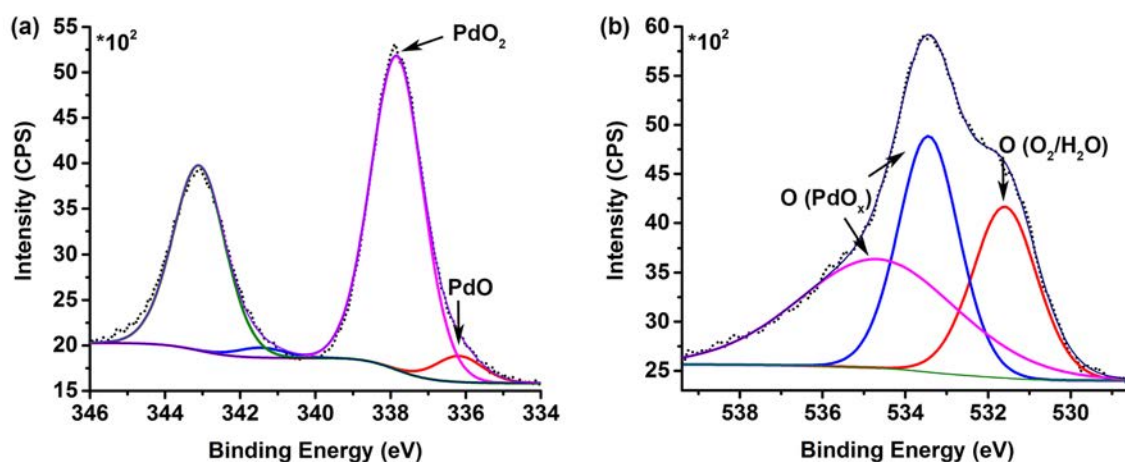
Figure 2.17: XPS analysis of Pd NPs/RNTs on a Si wafer in H_2O. The E_b of $Pd3d_{5/2}$ (a) and O1s (b) spectra was calibrated with respect to the C1s peak at 284.8 eV.

There are several possibilities (i) the oxides were formed by the water oxidation reaction as suspected; (ii) they could form upon exposure of the sample to the air during sample preparation and (iii) the oxides could also be in the K_2PdCl_4 solid or formed *in situ* when dissolved in water. It is well known that prolonged exposure of metal salt to the air could facilitate the corresponding oxide formation. Also as the solids of K_2PdCl_4 were dissolved in deionized water, perhaps it might be converted to the PdO_x species upon reacting with the dissolved oxygen already present in water. To rule out the third possibility of pre-formed PdO_x species in the sample, we carried out the XPS analysis of

K$_2$PdCl$_4$ in both water and in the crystalline form. The Pd spectra showed an E_b peak at 338.1 eV, which could be attributed to the Pd^{2+} peak in K$_2$PdCl$_4$ (Figure 2.18).[59] The spectra also displayed an E_b peak at 336.9 eV, which is higher than the PdO peak observed in the Pd NPs/RNTs samples. Previously, Bertolini *et al.* demonstrated the XPS analysis of bulk PdO where the E_b peak appeared at 336.8 eV.[60] Therefore, we suspected that the peak at 336.9 was due to the PdO in the K$_2$PdCl$_4$ sample. Beside these peaks associated with the Pd compounds, there was an additional peak at ~345 eV. We believed that this peak could be associated with the K satellite. In K$_2$PdCl$_4$ sample, as the Pd3$d_{5/2}$ peak at 338.1 was close to the PdO$_2$ peak (337.9 eV) observed in Pd NPs/RNTs samples, we performed mass spectroscopic analysis to detect the identity of the Pd species.
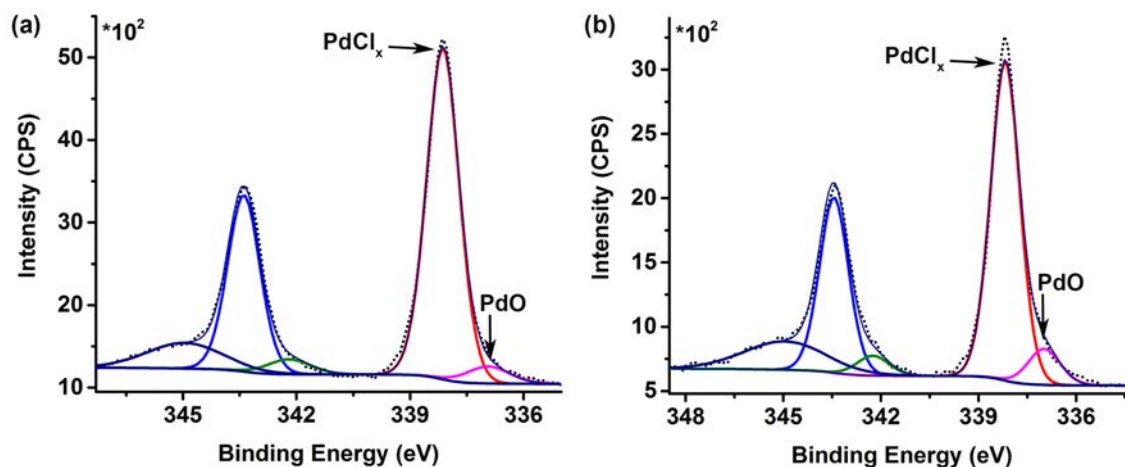
Figure 2.18: The Pd3$d_{5/2}$ spectra of K$_2$PdCl$_4$ in water (a) and crystals (b). The E_b was calibrated with respect to the C1s peak at 284.8 eV.

The ES mass of K$_2$PdCl$_4$ showed a fragment ion (PdCl$_3^-$) peak at m/z 210.8104 (calc. m/z 210.8106) due to the loss of one Cl$^-$ ion. Hence, the mass spectrometry confirmed that the E_b peak at 338.1 eV belonged to K$_2$PdCl$_4$. However, the mass spectrum did not show any m/z peak associated with PdO. This indicates that PdO,

observed in the XPS spectrum, was formed *in situ* inside the XPS analyzer chamber during the XPS analysis. Alternately, the Pd3$d_{5/2}$ peak at 336.9 eV could be associated with any unknown palladium chloro compound. To further rule out the possibility of air interruption in forming the PdO$_x$ species and prove the concept of water oxidation, we carried out the Pd NP synthesis under anaerobic condition. To minimize air exposure we prepared the solutions of RNT and K$_2$PdCl$_4$ in water properly degassed by bubbling with ultra pure Ar for 1h.[61] The resulting two solutions were then mixed under Ar environment in a glove bag. The glove bag was initially degassed to create an anaerobic environment by applying the purge and refill technique with Ar. The XPS analysis was performed on the Pd NPs/RNTs following the previous protocol. The samples were prepared on both the TEM grid and Si wafer for a detailed comparison with the previous results and applied for analysis without further washing with water. Interestingly, the analysis showed similar results to that of the previous observation. The Pd3$d_{5/2}$ spectrum of the TEM grid sample displayed the E_b peaks at 335.1, 335.9 and 338.1 eV attributed to the Pd^0, PdO and PdO$_2$, respectively (Figure 2.19a). In addition, the Pd3$d_{5/2}$ spectrum of the Si wafer sample also showed E_b peaks at 336.2 and 337.9 eV for the PdO and PdO$_2$, respectively (Figure 2.19b). In agreement with the previous observation, the Si wafer sample also contained the E_b peak (~345 eV) associated with the K satellite. The data obtained from the glove bag experiment are in good agreement with the aerobic condition experiments. Hence, this anaerobic experiment strongly suggests that the formation of PdO and PdO$_2$ was not because of the air interruption. Indeed the water oxidation led to the formation of PdO$_x$ species as well as Pd NPs as suspected. To further validate and support this observation we carried out the isotopic experiment by using H$_2$^{18}O as a

solvent instead to water. If water splitting caused the formation of the PdO_x species, then $H_2^{18}O$ would lead to the formation of the corresponding isotopic compounds ($Pd^{18}O_x$) upon oxidation.
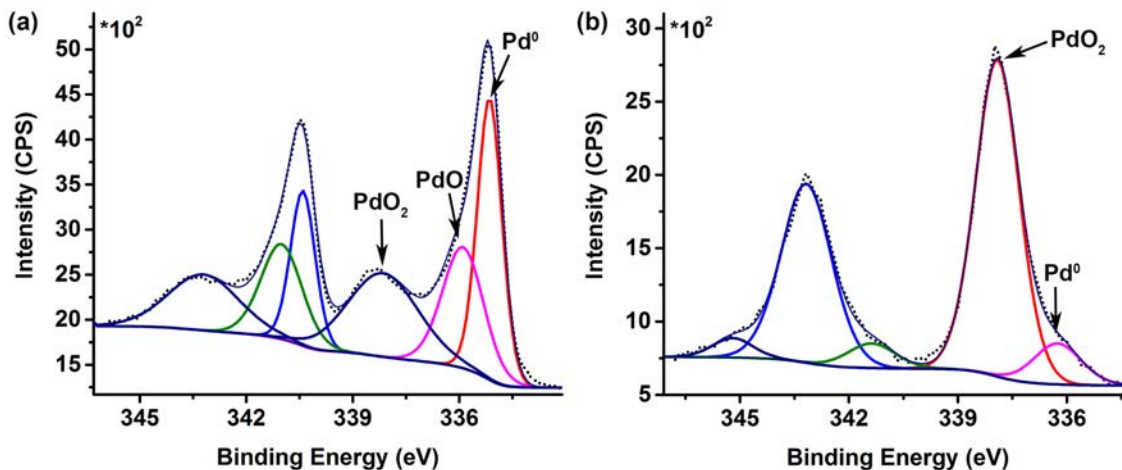
Figure 2.19: The Pd3$d_{5/2}$ spectra of Pd NPs/RNTs on the TEM grid (a), and Si wafer (b) in H_2O under anaerobic condition. The E_b was calibrated with respect to the C1s peak at 284.8 eV.

The XPS analysis was performed on the sample deposited on the Si wafer (Figure 2.20). As expected, the Pd3$d_{5/2}$ spectrum showed an E_b peak at 337.7 eV associated with PdO_2 (Figure 2.20a). However, the peak was shifted by 0.2 eV to the lower binding energy compared to that of the E_b peak previously observed for PdO_2 (337.9 eV). The Pd3$d_{5/2}$ spectrum also showed an E_b peak at 335.2 eV, which could be assigned to elemental Pd (Figure 2.20a). As the sample surface was not washed with water, the Pd3$d_{5/2}$ spectrum also contained an additional peak at ~345 eV due to the K satellite. Similarly, the O1s spectrum also showed a shift in the PdO_x binding energy peak by 0.3 eV from 533.9 eV to 533.6 eV (Figure 2.20b). Other than the shift in the binding energy peak, there was no discernible change in the Pd3$d_{5/2}$ and O1s peak shapes.[62] This

indicates that the presence of heavier isotope (^{18}O) does not affect the peak shapes. However, it is unclear whether the isotopic effect is responsible for the shift of the PdO$_x$ E_b peaks in both the Pd3$d_{5/2}$ and O1s spectra.
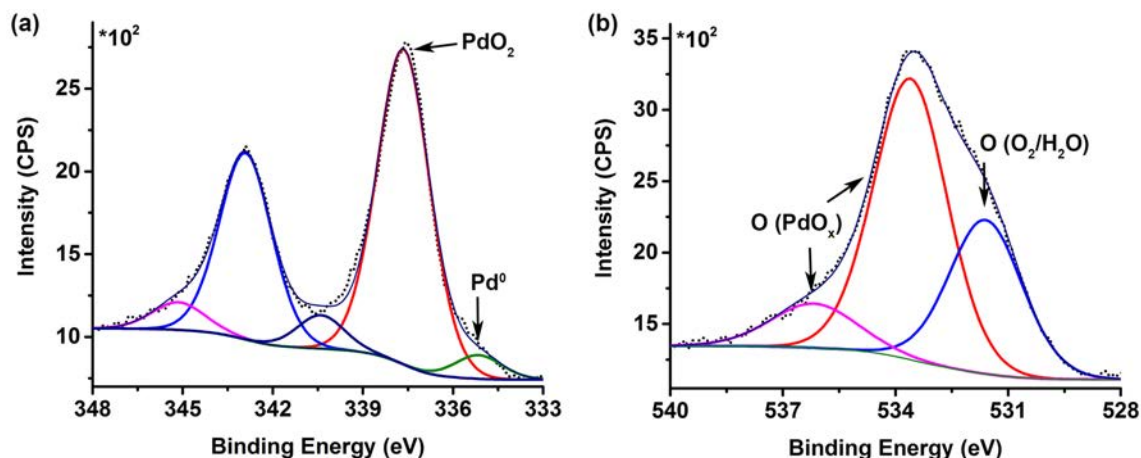
Figure 2.20: The Pd3$d_{5/2}$ (a), and O1s (b) spectra of Pd NPs/RNTs on a Si wafer in H$_2$^{18}O (E_b was calibrated with respect to the C1s peak at 284.8 eV).

The XPS analysis confirmed the formation of PdO$_x$ (X = 1, 2) along with Pd NPs. In addition, both the anaerobic (glove bag) experiment and the isotopic analysis (H$_2$^{18}O) showed that the PdO$_x$ species were formed by the water oxidation reaction, where the oxygen came from water. Also we found that the NP formation was a very rapid process indicating that the counter water oxidation reaction must be fast. The water oxidation reaction usually produces oxygen and proton, if the electron is being consumed by the counter species in the system. Hence the oxygen could further react to give oxides or evolve as molecular oxygen. The XPS analysis already confirmed the formation of oxides. To further investigate the possibility of molecular oxygen evolution we performed the dissolved oxygen (DO) content measurement of the system. If the oxygen evolution reaction takes place, this will lead to the increase in DO of the system and could be monitored by a DO meter. Under aerobic condition, the DO content of distilled

or deionized water at ambient temperature is ~8.5 ppm measured with oxygen electrode where the pH of the solution is close to neutral.[61] Therefore, to rule out the possibility of air oxygen interruption to the system the whole experiment was carried out in a glove bag under ultra pure Ar (oxygen content <0.5 ppm). The individual solutions of RNT and K_2PdCl_4 were purged with Ar for 1 h before mixing to remove the dissolved oxygen.[61] The DO of the RNT and K_2PdCl_4 solutions were measured in a glove bag pre-purged with Ar, and the values were found to be ~0.29 and ~0.93 ppm respectively. The residual oxygen contents of the two solutions were stable up to 5 min at 20.9 °C without any significant change. In a separate blank experiment, the DO content inside the glove bag was measured as ~0.10 ppm at 20.3 °C after purging with Ar for 1 h and was found to be stable for 5 min. When the two solutions of RNT and K_2PdCl_4 were mixed together, the immediate measurement showed a rapid increase in the dissolved oxygen content of the mixture solution to above 9.0 ppm and fluctuating between 10 to 14 ppm. The value then dropped to around 5 ppm within few minutes and continued to fluctuate. As the surface reaction on the electrode provides the DO measurement, the interaction between the electrode surface and the oxygen in solution is very important. Hence, we believe that perhaps the initial rapid production and inhomogeneous mixing of oxygen to the solution caused the fluctuation. The DO value continued to drop and fluctuate between 0.7 to 2.0 ppm within 30 min and then further dropped to ~0.58 ppm after 60 min. The DO measurement experiment suggested that the water oxidation reaction was a very fast process as it leads to an increase in dissolved oxygen content.

Finally, all the experimental data together with the theoretical analysis suggests that water could act as a reducing agent. While the XPS analysis confirmed the presence

of Pd^0 as well as PdO_x (x = 1 and 2) in the sample, the DO experiment provided the evidence of O_2 evolution. In addition, the pH measurement indicated the generation of H+ in solution. Therefore, all the experimental evidences agreed to the hypothesis of facile water oxidation reaction. The formation of Pd NP was followed by the production of both PdO_x and the evolution of O_2 in solution. Certainly, RNT played a vital role influencing the overall reaction as no Pd NP formation was observed in the absence of RNT or in the presence of L-LAA. It was difficult to propose an exact mechanism of the Pd NP formation on the surface of the RNT due to the complicated nature of the reaction. However, a number of potential factors that influenced the overall reaction could be highlighted. The reaction could be facilitated by the auto-catalysis of Pd, where the bond cleavage in water took place upon coordination to the Pd center. I hypothesize that the positively charged lysine nucleation pockets on the RNT surface provide a unique reaction environment where the oxidation potential of water and the corresponding reduction potential of Pd^{2+} shifted to a value, which favors spontaneous and facile reaction. Furthermore, the reduction potential of water is reduced from 1.229 V to ~0.82 V at pH = 7 ($E° = 1.229 − 0.059pH$), thus increasing the driving force for oxidation.[52c] Previously, it was reported that the rate of the water dissociation reaction was enhanced by the presence of Li^+ in alkaline environment.[64] In the case of our system, we believe that water onto the surface of RNT and inside the nucleation pocket will interact with the ammonium ions of lysine. Due to this interaction (NR_4^+----OH_2), water might undergo an interfacial structural change leading to facile O–H bond cleavage and the presence of KCl and CF_3COOK in solution could also accelerate the process.

Previously, we have observed the *in-situ* nucleation and growth of metal NPs on the surface of the RNTs without employing any external reducing agents. The stable NPs were formed by simply mixing the RNTs and metal salts in water at ambient temperature. In the previous section, I discussed in detail the experimental and theoretical analysis on the quest to understand the origin of the Pd NP formation. Both the experimental and theoretical analysis suggested that the Pd NPs were formed by the water oxidation reaction. As the Pd NPs were formed *in-situ* upon mixing of the two components, it was obvious for us to study the kinetics of the NP formation. The simplicity of our system was an advantage for the kinetics studies. Earlier, I hypothesized that upon mixing of RNT and $PdCl_4^{2-}$ solutions they would initially undergo complexation through electrostatic interaction. This interaction maintains the flow of fresh supply of $PdCl_4^{2-}$ on the surface of RNT and facilitates the Pd NP formation. The theoretical model studies demonstrated that this initial complexation is a very rapid process and indeed supports the concept of continuous fresh supply of $PdCl_4^{2-}$ on the surface of the RNT. To further confirm this concept and theoretical observation, I performed the XPS analysis of Pd NPs/RNTs by depositing the sample aged for 1 min. As RNT contains positively charged L-lysine side chains on the surface and counter balanced with CF_3COO^-, addition of $PdCl_4^{2-}$ would immediately replace CF_3COO^- to form the complex with RNT.
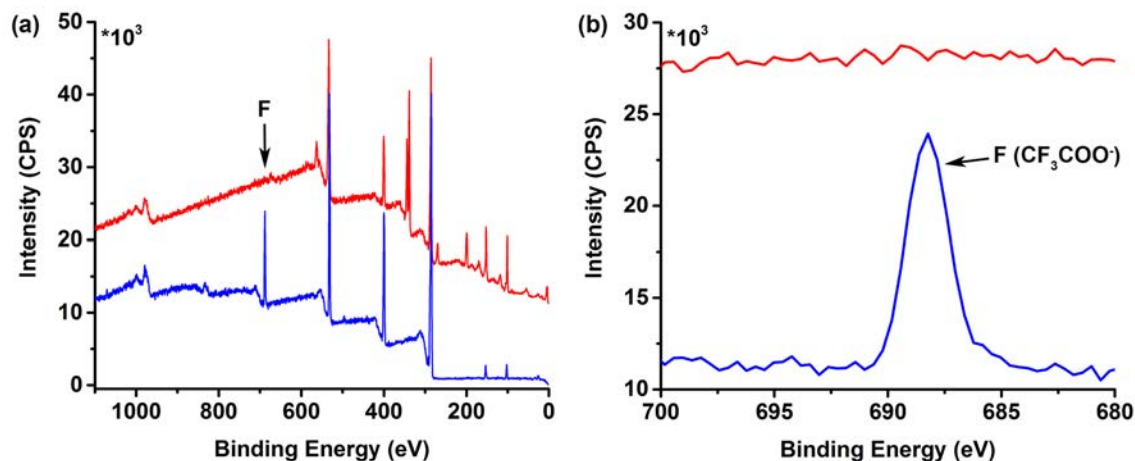
Figure 2.21: Comparison of the F1s E_b peak in RNT (blue) and Pd NPs/RNTs (red). The E_b was calibrated with respect to the C1s peak at 284.8 eV.

Hence, the analysis of the fluorine E_b peak by XPS could further support this rapid anion exchange reaction. I also carried out the XPS analysis of RNTs as a blank experiment. The XPS analysis of Pd NPs/RNTs in the region of fluorine binding energy (688.3 eV) showed no peak associated with F1s (Figure 2.21).[65] On the other hand, the spectrum of RNT contained an E_b peak at 688.2 eV, which could be attributed to F1s peak (688.3 eV) in CF_3COO^-.[65] This proves the concept of rapid complexation of $PdCl_4^{2-}$ and RNT in solution. In order to further investigate the nucleation and growth mechanism of the NP formation, both spectroscopic and microscopic studies were performed. The formation of the Pd NP was followed by time dependent studies. To gain further insight into the NP formation, three different ratios of $PdCl_4^{2-}$/RNTs were investigated including 10:1, 5:1 and 1:1. As the concentration of $PdCl_4^{2-}$ could play a vital role in the nucleation and subsequent NP growth process, I varied the loading concentration of $PdCl_4^{2-}$ with respect to the RNTs concentration. Previously, I have established that the 10:1 fold was the optimum condition to obtain the maximum loading of the RNTs with highly uniform sized NPs. Hence, I followed the kinetics of the NP formation starting with 10:1 fold

$PdCl_4^{2-}$/RNTs by UV-Vis and circular dichroism (CD). As the RNT shows supramolecular chirality and the NP forms onto the RNT surface, I carried out the time dependent CD studies to understand the RNT surface interaction with the NPs.

Upon addition of K_2PdCl_4 (10 fold excess) to an aqueous solution of RNT, the typical absorption maxima of the RNT at 236 nm and 287 nm showed an initial hyperchromic shift (1 min), and then a gradual decrease in absorbance up to 60 min (Figure 2.22a).[66,67] The drop in absorbance was very rapid within the first 10 min and then continued to drop slowly and temporarily leveled off within 60 min. Beyond 60 min, the drop in absorbance was very slow up to 2 h and then finally no significant decrease till 17 h (Figure 2.22a). The formation of Pd NPs on the surface of RNTs might be associated with this hypochromic effect. Also I suspect that the initial fast drop in absorbance could be due to rapid nucleation and growth of the NPs, while the hyperchromic effect (1 min) is perhaps responsible for the rapid complexation of the $PdCl_4^{2-}$ and the RNTs. As the absorption maxima temporarily leveled off around 60 min, I believe that most of the NP formation takes place within this 60 min leaving few nucleation pockets to be occupied. Finally after 60 min, the unoccupied nucleation pockets get filled up with the NPs as suggested by a very slow drop in absorbance. In addition, the formation of the Pd NPs was also evident by the gradual increase in absorbance from 500 nm to 325 nm, which was not seen with the RNT alone. This effect may be attributed to the electron scattering at the boundaries of the NPs.[68-70] This phenomenon was observed even after 1 min, suggesting rapid NP formation followed by nucleation (Figure 2.22a). The UV spectrum of Pd NPs/RNTs also showed a shoulder peak at 208 nm which could be assigned to $Pd(H_2O)Cl_3^-$.[71,72]
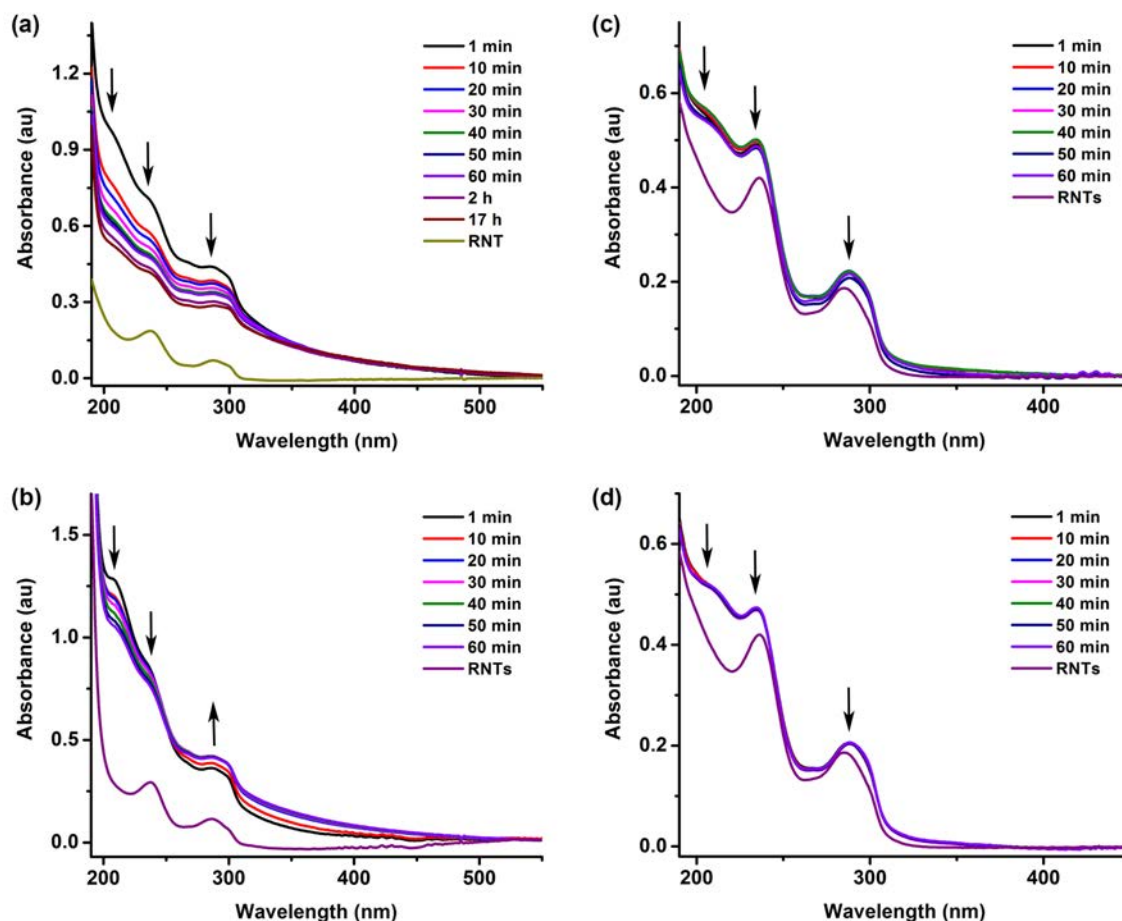
Figure 2.22: Kinetics of the Pd NPs/RNTs formation studied by UV-Vis spectroscopy. 10:1 fold in H_2O (a), and in H_2O/MeOH (b), 1:5 fold in H_2O (c), and 1:1 fold in H_2O (d).

Often alcohols are used to reduce metal salts to form the corresponding NPs.[50] As methanol could undergo facile oxidation to formaldehyde, it is expected that the addition of methanol to the aqueous solution of $PdCl_4^{2-}$ and RNTs would speed up the kinetics of the NP formation.[73] Hence, we repeated the UV studies of Pd NPs/RNTs (10:1 fold) in a mixture solvent containing 3:1 fold of water and methanol (Figure 2.22b). As expected, the spectrum showed very fast kinetics for the NP formation and reached the equilibrium within 30 min followed by slow drop in absorbance up to 60 min. The noticeable difference in the mixture solvent is the hyperchromic effect of the absorbance at 289 nm

where the isosbestic point at 248 nm (Figure 2.22b). On the other hand, the similar absorption band at 289 nm showed a hypochromic effect in water. Earlier I found that the deuterium isotopic effect slowed down the kinetics of the NP formation when water was replaced by D_2O (Figure 2.13a). This observation once again supports the concept of water oxidation leading to the formation of Pd NPs. Previously, I demonstrated that 10 fold excess of the metal salt ($PdCl_4^{2-}$) is essential for the maximum loading onto the surface of RNT. Hence, the variation of the salt concentration below 10-fold excess could provide vital information on the RNT-salt complexation as well as nucleation. The UV spectra of the Pd NPs/RNTs (5:1 and 1:1 fold) showed an immediate hyperchromic effect on the RNT absorption bands at 236 and 289 nm (Figure 2.22 (c, d)). Though there was a little drop in absorbance in 5:1 fold sample (Figure 2.22 (c)), the 1:1 fold sample showed no drop in absorbance within 60 min (Figure 2.22 (d)). This observation suggests the formation of fewer smaller sized NPs upon complexation in 5:1 fold sample. However, the loading onto the surface of RNT would be significantly incomplete.
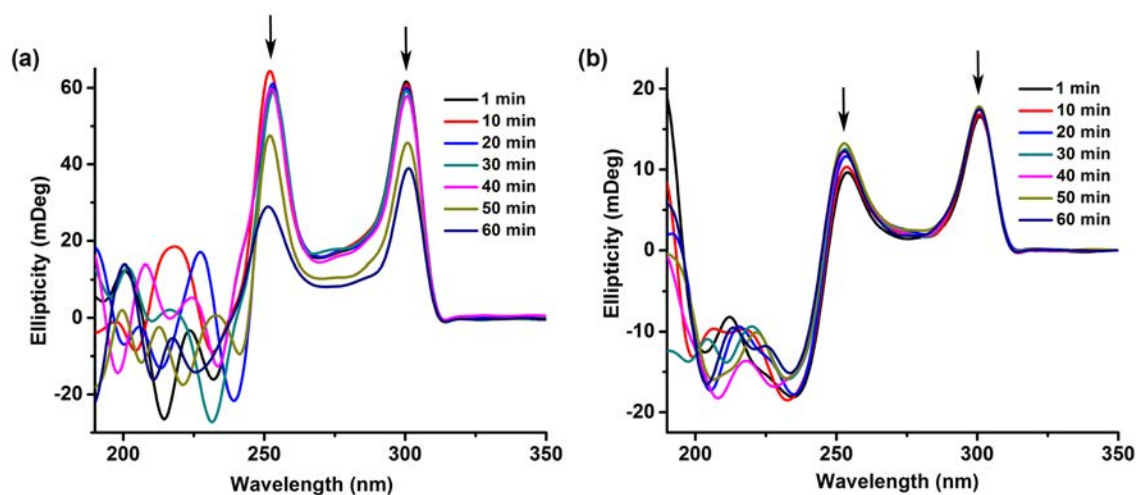
Figure 2.23: Kinetics of the Pd NPs/RNTs (10:1 (a), and 1:5 (b) fold) formation studied by CD spectroscopy in H_2O.

69

On the other hand, in the case of a 1:1 sample, the NP formation would be impossible due the lack of a fresh supply of excess $PdCl_4^{2-}$ to be deposited upon reduction. As the NP formation takes place on the surface of the RNT, the kinetics studies by CD could reveal the effect of the nucleation and growth on the supramolecular chirality. As shown in the corresponding time-dependent CD spectra of the 10:1 fold sample in Figure 2.23a, a decrease in the intensity of the molar ellipticity at 257 nm and 302 nm was observed during the course of the NP formation, although the exciton-coupled bisignate cotton effect typical of the RNTs was still maintained.[66] The change in the CD pattern below 250 nm may be rationalized by conformational changes of the lysine side-chains during the growth of the NPs on the RNT surface. The 1:1 fold sample showed no significant change in the intensity of the molar ellipticity in good agreement with the corresponding UV-Vis studies (Figure 2.23b). The perturbation of the molar ellipticity at the lower wavelength was found to be minimum in the 1:1 fold sample as $PdCl_4^{2-}$ interacts with the positively charged lysine onto the surface of RNT as a counter ion. To further understand the surface interactions between the RNTs and $PdCl_4^{2-}$, and the subsequent change in the surface properties upon NP formation, the time dependent zeta potential (ζ) measurement was carried out. Initially, the zeta potentials of aqueous solutions of RNTs (0.01 mM) and $PdCl_4^{2-}$ (0.1 mM) were measured as a blank experiment. The zeta potential values of RNT (25.0±4.2 mV, pH 6.72) and $PdCl_4^{2-}$ (−23.5±3.9 mV and pH 4.67) solutions suggested that both species have incipient instability.[74,75] When $PdCl_4^{2-}$ was added to the solution of RNTs, the initial ζ value dropped from 25.0±4.2 mV to 10.8±3.8 mV within 1 min. This rapid drop of ζ value suggests the formation of Pd NP, which attracts Cl^- ions to be adsorbed on the surface.

Table 2.5: Time dependent zeta potential measurement of PdNPs/RNTs in water (Dip cell)[a]

Time (min)	Zeta potential (mV)	Zeta deviation ($\pm$mV)	pH
1	10.8	3.8	4.31
10	5.04	4.9	4.27
20	6.77	3.6	4.25
30	−11.1	5.7	4.23
40	−11.2	5.5	4.20
50	−12.8	3.7	4.19
60	−14.5	5.1	4.18
70	−19.3	4.9	4.18
80	−21.1	6.1	4.16
90	−19.9	3.9	4.16
120	−22.4	3.9	4.15

[a] Conditions: RNTs = 0.01 mM; K_2PdCl_4 = 0.1 mM; Ambient temperature.

Hence this effect would considerably lower the net positive charges generated by the lysine side chains. Either the formation of new Pd NPs on the surface of the RNTs or the growth of the nucleated Pd NPs, both would prefer adsorbing more Cl^- ions and finally would replace the positively charged surface to negative one. The time dependent studies completely supported this hypothesis as we saw the ζ value switch to negative charge and reach equilibrium within 70 min (Table 2.5). This ζ measurement is also in good agreement with the previously discussed UV-Vis and CD studies. Finally, all of the solution based characterization methods (UV-Vis, CD and ζ measurement) suggest that

the NP formation is a very rapid process with both nucleation and growth of the NP taking place very quickly. Therefore, the kinetic studies could not isolate the nucleation and the NP growth steps. Instead it showed the growth of the NP upon rapid nucleation. To further prove this concept of rapid NP formation we performed the time dependent UV-Vis and ζ measurement of a mixture of $PdCl_4^{2-}$ and G∧C base. As expected, the addition of $PdCl_4^{2-}$ caused a hyperchromic effect of the absorption bands of the G∧C base at 237 and 289 nm (Figure 2.25a). This hyperchromic effect is due to the complexation between $PdCl_4^{2-}$ and the G∧C base. Although the intensity of the absorption bands then decreased with time up to 3 h as recorded, I believe that the hypochromic effect would continue because of further deposition. This trend of hypochromic effect is totally different from the trend observed for Pd NPs/RNTs (Figure 2.22a). Though the spectrum also showed an increase in the absorption with decreasing wavelength between 500 to 330 nm, I believe this is due to the scattering effect from the surface of the deposited $PdCl_4^{2-}$. The time dependent SEM images of the $PdCl_4^{2-}$/G∧C base were also in good agreement with the UV-Vis studies (Figure 2.24b,c). Interestingly, the kinetic studies of the $PdCl_4^{2-}$/G∧C base showed no significant change in the zeta potentials within 3 h and always possess positive zeta potentials. While the zeta potential of the G∧C base (28.3±4.4 mV) initially dropped to 23.6±4.3 mV upon addition of $PdCl_4^{2-}$ (Table 2.6), this was due to the complexation of $PdCl_4^{2-}$ and the G∧C base, and subsequent deposition of $PdCl_4^{2-}$. However, the time dependent zeta potential measurement of $PdCl_4^{2-}$/G∧C base is totally different from what we observed for Pd NPs/RNTs. The positive zeta potential of $PdCl_4^{2-}$/G∧C base suggests no Pd NP formation. Hence, this indicates that supramolecular organization of RNT is crucial for the Pd NP formation.

72
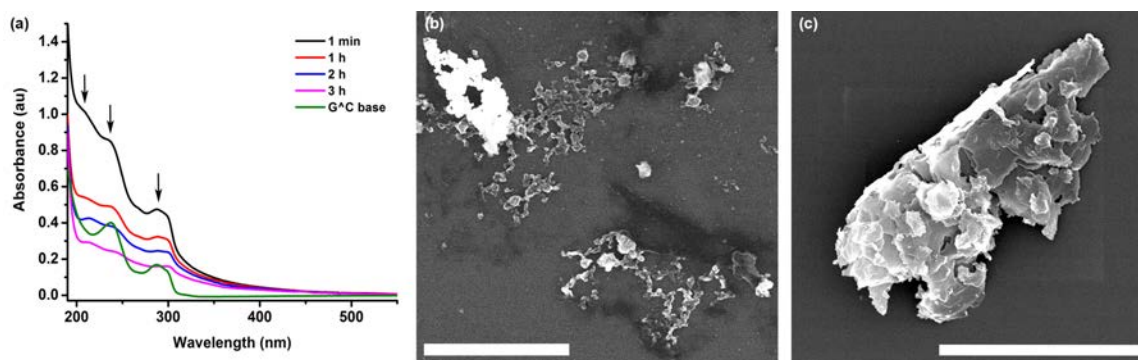
Figure 2.24: Time dependent UV-Vis (a) and SEM (1 min (b), 3 h (c)) studies of $PdCl_4^{2-}$/G∧C base in H_2O. Scale bar – 1 μm (b), and 2 μm (c).

Table 2.6: Time dependent zeta potential measurement of $PdCl_4^{2-}$/G^C base in water (Dip cell)[a]

Time	Zeta potential (mV)	Zeta deviation (±mV)	pH
1 min	23.6	4.3	6.21
1 h	22.3	4.0	6.18
2 h	21.2	3.6	6.20
3 h	18.7	4.0	6.19

[a] Conditions: G^C base = 0.01 mM; K_2PdCl_4 = 0.1 mM; Ambient temperature.

Finally, to obtain visual evidence of the kinetics of NP formation, time-dependent SEM and TEM studies were performed. These studies suggest that once the nucleation takes place in a few pockets, there is a tendency for the NPs to grow to a given size, rather than for additional pockets to be nucleated. The growth of the nucleated NPs may occur through the diffusion of palladium atoms according to the Ostwald ripening process.[76] This indicates that the nucleation and the subsequent NP formation is a stepwise process. Careful analysis of the SEM and TEM images of the Pd NPs/RNTs

supports this observation showing the presence of unoccupied RNTs in different areas. Overall, the Pd NP formation was found to be very rapid and in agreement with the UV-Vis and CD studies. Importantly, the lysine-side chains, forming the nucleation pockets, on the surface of the RNTs were able to stabilize and prevent the aggregation of the NPs over time, and finally dictate the size of the NPs.
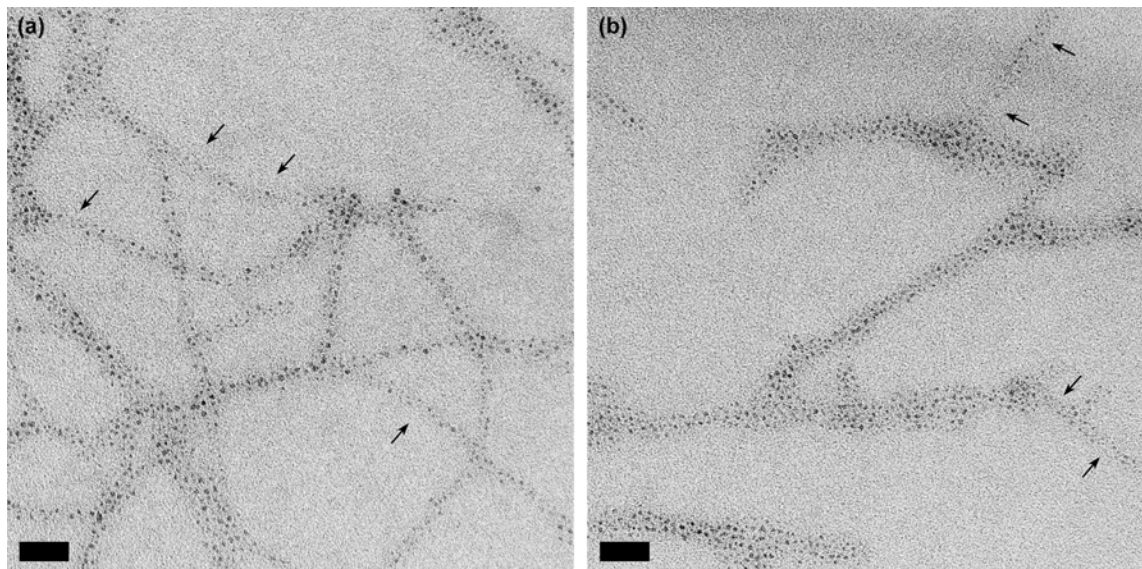
Figure 2.25: TEM images of the Pd NPs/RNTs (0 min (a) and 60 min (b)). The arrows indicate the incomplete loading and the growth of the Pd NPs on RNTs. Scale bar – 20 nm.

Time-dependent TEM studies showed that the size selective synthesis of the NPs could be achieved by varying the aging time of the solution (Figure 2.12a-c, 1 min – 1.5±0.1 nm; 30 min – 1.5±0.1 nm and 60 min – 1.6±0.1 nm). However when compared, the images show that the NP could be nucleated and grown to 1.5±0.1 nm within 1 min and are consistent with the rapid drop of absorbance in UV (Figure 2.22a). As the formation of the NP is a stepwise process, more loading of the NPs on the surface of RNT could be a fast process as well as the Ostwald ripening of the already nucleated NPs

74

to the maximum size of 1.6±0.1 nm (Figure 2.25). Also the TEM images of the deuterated sample showed that the kinetics of the NP formation was slowed down due to the deuterium isotopic effect as the O−H/D bond activation leads to the reduction of metal salt.

2.2.5 Size Tuning of NPs on the Surface of RNT by Surface Modification

Previously I have demonstrated that tunable sized NPs could be synthesized by varying the aging time of the Pd NPs/RNTs. However, the kinetic studies suggest that the nucleation and the subsequent growth of the Pd NPs is a very fast process in water. The growth of the NP could be accelerated either by adding methanol or slowed down by using D_2O. The important finding of this kinetic study is that even though the NP formation is a faster process, the size of the NP is finally dictated by the nucleation pocket affording highly monodispersed quantum dots. Hence this observation encouraged us to investigate the effect of the surface modification of the RNT on the size of the NP. As the dangling side chains such as lysines form the nucleation pockets, the surface modification with different functionalities could offer further opportunity to tune the NP size. Considering this, we modified the surface of RNT with a different number of lysines on the side chain (note: the surface modifications were performed by two of our former group members – Mounir E. Bakkari and Alaaeddin Alsbaiee). Initially we attached the lysine through different functional groups and then increased the chain length with three or five additional lysine units. Then we applied the resulting RNTs for synthesizing the NPs and investigated the effects of the increased chain length on the size of the NPs. We found that the NP size could be tuned by varying the length of the lysine side-chain on the surface of the RNTs (Figure 2.26). For example, the sizes of the Pd NPs formed after

60 min for RNTs (called twin K_1, K_3 and K_5) **1**, **2** and **3** (Figure 2.26) were 1.4±0.3 nm, 1.8±0.3 nm and 1.8±0.2 nm, respectively. Interestingly, we found that the size of the NP increases with increasing chain length up to three lysines. This suggests that the presence of three lysines could offer the optimum condition to obtain maximum size NP. We believe that when the chains possess more lysines, they tend to constrain the growth of the NP as they have less space into the nucleation pockets.
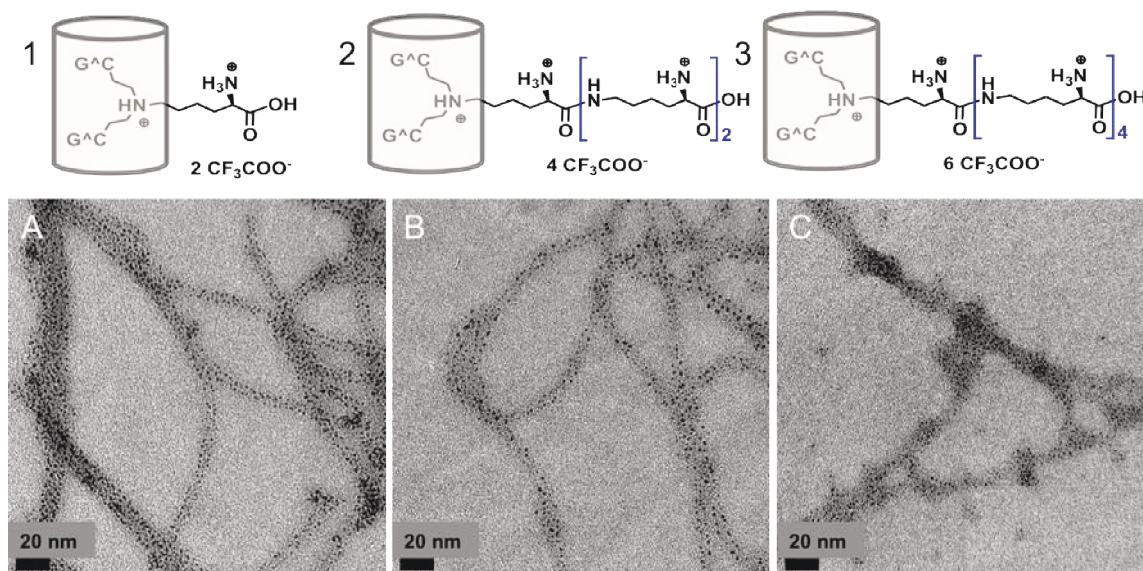
Figure 2.26. (A-C) TEM analysis of Pd NPs/RNTs aged for 60 minutes, in which the RNTs express lysine residues of different lengths on their outer surface.

Chapter 2 summarized that RNT could be successfully applied as a versatile template for synthesizing M NPs (M = Au, Pd and Pt). The nucleation pocket formed by the lysine side chains controlled the growth of the NP followed by the nucleation. The water soluble RNT improved the solubility and stability of the resulting NPs. While the kinetic studies suggested faster NP formation, the studies on the origin of the NP formation suggested that they were formed by water oxidation.

Experimental

Materials.

K_2PdCl_4 and $H_2{}^{18}O$ (enriched with 97% ^{18}O) were purchased from Aldrich Chemical Co. Inc. and used without further purification. D_2O was purchased from Cambridge Isotope Laboratories, Inc. Ultra dry argon (oxygen content <0.5 ppm) was purchased from Praxair, Canada. Twin G∧C bases were synthesized by Dr. Andrew J. Myles (G0), Dr. Mounir E. Bakkari (K3 and K5) and Dr. Alaaeddin Alsbaiee (K1). All the solutions were prepared by using deionized (DI) water. The experiments were carried out at ambient temperature and atmospheric condition without purging the solutions with nitrogen unless otherwise noted.

Instrumentation.

Spectroscopic studies. UV-Vis spectra were recorded on an Agilent 8453 and CD spectra were recorded on a JASCO J-810 spectropolarimeter. Samples for CD studies were scanned from 400-200 nm at a rate of 100 nm/min. The XPS measurements were performed on an AXIS ULTRA spectrometer (Kratos Analytical) at the Alberta Centre for Surface Engineering and Science (ACSES), University of Alberta. The base pressure in the sample analytical chamber (SAC) was lower than 1×10^{-9} torr. A monochromatized Al Kα source (hv=1486.6 ev) was used at 210 W. Survey scans spanned from binding energy of 1100 to 0 eV, collecting with analyzer pass energy of 160 eV and a step of 0.3 eV. For high resolution spectra, the pass energy was 20 eV and the step was 0.1 eV, with a dwell time of 200 ms. The number of scans for high resolution spectra were determined according to the spectrum intensities of the elements to be analyzed. Charge neutralization was applied to stabilize the spectra during collection, as the sample was an

insulator. The high-resolution ES mass spectra were obtained on an orthogonal acceleration TOF (oaTOF) spectrometer.

CV was obtained on a CHI420A Time-Resolved Electrochemical Quartz Crystal Microbalance potentiostat at 21±1 °C in DI water containing 0.1 M KCl as a supporting electrolyte. Solutions of RNT (1 mM) and K_2PdCl_4 (1 mM) were purged with dry argon (Ar) for 10 min directly before use, and were kept under a blanket of Ar during all experiments. The CV was obtained over a scan rate of 0.1 Vs^{-1} and a 3.0 mm BASi glassy carbon (GC) electrode was used as a working electrode. The GC electrode was polished by using a BAS polishing kit and aqueous slurries of alumina powder (0.05 μm) followed by ultra sonication for 20 sec in water before use.

Microscopy. All samples were deposited on carbon-coated 400-mesh copper grids for SEM/TEM characterizations. 5 μL of the sample was dropped on a grid and left to adsorb for 1 minute. Excess sample was removed by filter paper and the grid was then dried in vacuum for 30 minutes at 110 °C. The samples for SEM images were obtained by using a Hitachi S-4800 (with a field-emission gun) instrument working at 10 kV at NINT. TEM images were obtained with a JEOL 2200 FS TEM Schottky field emission instrument equipped with an in-column omega filter working at 200 kV (by Dr. Jae-Young Cho). The electron diffraction data were collected using a JEOL 3000F transmission electron microscope working at 300 kV, equipped with a post column energy filter. The electron diffraction patterns were collected using a 1024 x 1024 pixel slow scan camera with 14 bit dynamic range, mounted directly below the viewing screen of the microscope. For the AFM measurements, samples were prepared by placing 5 μL of the RNTs on freshly cleaved mica surfaces and left to adsorb for 2 minutes. The excess

sample was removed using a clean piece of filter paper. The nanotubes were then imaged using a Digital Instruments/Veeco Instruments MultiMode Nanoscope IV AFM equipped with an E scanner. Silicon cantilevers (MikroMasch USA, Inc.) with low spring constants of 4.5 N/m were used in tapping mode (TM-AFM). To obtain a clear image with high resolution, a low scan rate (0.5-1 Hz) and amplitude set point (1 V) were chosen during the measurement.

Glove bag experiments. To investigate the origin of the NP formation some of the experiments (XPS and DO measurement) were conducted in a glove bag under anaerobic condition. The glove bag was purged with ultra dry Ar to create the anaerobic condition. In brief, initially the glove bag was purged with slow Ar flow for 45 min. Finally, the glove bag was filled with Ar and then pushed all the way to remove Ar, and then refilled with Ar. This step was repeated 10 times to confirm the proper inert gas condition. All of the samples were properly degassed by bubbling with Ar and then placed into the glove bag for further analysis.

Synthetic methods.

Synthesis of RNTs. RNTs were synthesized following the same protocol as described previously.[41] In brief, the RNTs were self-assembled by dissolving the corresponding twin G∧C base (2 mg) in DI water (1 mL) and heated to 90 °C for 10 minutes in an oil bath. The solution was then allowed to cool at ambient temperature and aged for 24 hours. The formation of the RNTs (10 μM) was confirmed by scanning electron microscopy (SEM) before using them for the synthesis of the NP.

Preparation of a solution of K_2PdCl_4. The stock solution of K_2PdCl_4 was prepared by dissolving 3.26 mg of K_2PdCl_4 in 1 mL of DI water to afford the final solution concentration of 10 mM.

Synthesis of Pd NPs/RNTs. RNT supported Pd NPs were synthesized by mixing 1:10 fold of RNTs and K_2PdCl_4 in DI water in a small glass vial [Stock solution: RNTs = 50 μM (28.6 μL; 1.75 μM); K_2PdCl_4 = 500 μM (50 μL; 10 mM); Total volume of H_2O = 1 mL]. The reaction mixture was sonicated for 1 min for uniform distribution of the RNTs and K_2PdCl_4 in solution. The resulting mixture solution was then left undisturbed and aged for 1 h at ambient temperature under aerobic condition to complete the Pd NPs formation. The formation of the Pd NPs on the surface of the RNTs was confirmed by high res. SEM and TEM analysis. The samples of Pd NPs/RNTs (500:50 μM) were used for CD, XPS and DO measurements. On the other hand, for UV-Vis and microscopic analyses, the samples of Pd NPs/RNTs with a concentration of 100:10 μM were used.

Preparation of a solution of twin G∧C base. The stock solution of twin G∧C base was prepared by dissolving 2 mg in 1 mL of DI water at ambient temperature affording the final solution concentration of 1.75 mM.

2.3 References

(1)   Astruc, D. In *Nanoparticles and Catalysis*, Weinheim: Wiley-VCH, 2008.

(2)   Deraedt, C.; Astruc, D. *Acc. Chem. Res.* **2014**, *47*, 494–503.

(3)   Li, G.; Tang, Z. *Nanoscale* **2014**, *6*, 3995–4011.

(4)   Takale, B. S.; Bao, M.; Yamamoto, Y. *Org. Biomol. Chem.* **2014**, *12*, 2005–2027.

(5)   Na, K.; Zhang, Q.; Somorjai, G. A. *J. Clust. Sci.* **2014**, *25*, 83–114.

(6)   Sevonkaev, I.; Privman, V.; Goia, D. *J. Solid State Electrochem.* **2013**, *17*, 279–297.

(7)   Lu, Z.; Yin, Y. Chem. Soc. Rev. **2012**, *41*, 6874–6887.

(8)   Yan, N.; Xiao, C.; Kou, Y. *Coord. Chem. Rev.* **2010**, *254*, 1179–1218.

(9)   Bhandari, R.; Knecht, M. R. *ACS Catal.* **2011**, *1*, 89–98.

(10)   Manocchi, A. K.; Horelik, N. E.; Lee, B.; Yi, H. *Langmuir* **2010**, *26*, 3670–3677.

(11)   Lee, Y. J.; Lee, Y.; Oh, D.; Chen, T.; Ceder, G.; Belcher, A. M. *Nano Lett.* **2010**, *10*, 2433–2440.

(12)   Lee, Y. J.; Yi, H.; Kim, W. -J.; Kang, K.; Yun, D. S.; Strano, M. S.; Ceder, G.; Belcher, A. M. *Science* **2009**, *324*, 1051–1055.

(13)   Varghese, O. K.; Paulose, M.; LaTempa, T. J.; Grimes, C. A. *Nano Lett.* **2009**, *9*, 731–737.

(14)   Wang, L.; Yang, R. T. *Energy Environ. Sci.* **2008**, *1*, 268–279.

(15)   Nam, K. T.; Kim, D. -W.; Yoo, P. J.; Chiang, C. -Y.; Meethong, N.; Hammond, P. T.; Chiang, Y. -M.; Belcher, A. M. *Science* **2006**, *312*, 885–888.

(16)   Coppage, R.; Slocik, J. M.; Briggs, B. D.; Frenkel, A. I.; Heinz, H.; Naik, R. R.; Knecht, M. R. *J. Am. Chem. Soc.* **2011**, *133*, 12346–12349.

(17)   Wu, H.; Wu, C.; He, Q.; Liao, X.; Shi, B. *Mat. Sci. Eng. C* **2010**, *30*, 770–776.

(18)   Murphy, C. J.; San, T. K.; Gole, A. M.; Orendorff, C. J.; Gao, J. X.; Gou, L.; Hunyadi, S. E.; Li, T. *J. Phys. Chem. B* **2005**, *109*, 13857–138570.

(19)   Jain, P. K.; Huang, X.; El-Sayed, I. H.; El-Sayed, M. A. *Acc. Chem. Res.* **2008**, *41*, 1578–1586.

(20)   Seferos, D. S.; Giljohann, D. A.; Hill, H. D.; Prigodich, A. E.; Mirkin, C. A. *J. Am. Chem. Soc.* **2007**, *129*, 15477–15479.

(21)   Rosi, N. L.; Mirkin, C. A. *Chem. Rev.* **2005**, *105*, 1547–1562.

(22)   Rosi, N. L.; Giljohann, D. A.; Thaxton, C. S.; Lytton-Jean, A. K. R.; Han, M. S.; Mirkin, C. A. *Science* **2006**, *312*, 1027–1030.

(23)   Jain, P. K.; Lee, K. S.; El-Sayed, I. H.; El-Sayed, M. A. *J. Phys. Chem. B* **2006**, *110*, 7238–7248.

(24)   He, L.; Musick, M. D.; Nicewarner, S. R.; Salinas, F. G.; Benkovic, S. J.; Natan, M. J.; Keating, C. D. *J. Am. Chem. Soc.* **2000**, *122*, 9071–9077.

(25)   Coronado, E.; Ridera, A.; García-Martinez, J.; Linares, N.; Liz-Marzán, L. M. *J. Mater. Chem.* **2008**, *18*, 5682–5688.

(26)   Cui, H.; Feng, Y.; Ren, W.; Zeng, T.; Lv, H.; Pan, Y. *Rec. Pat. Nanotech.* **2009**, *3*, 32–41.

(27)   Bennett, J. A.; Creamer, N. J.; Deplanche, K.; Macaskie, L. E.; Shannon, I. J.; Wood, J. *Chem. Eng. Sci.* **2010**, *65*, 282–290.

(28)   Sethi, M.; Pacardo, D. B.; Knecht, M. R. *Langmuir* **2010**, *26*, 15121–15134.

(29)   Senra, J. D.; Malta, L. F. B.; Michel, R. C.; Cordeiro, Y.; Simão, R. A.; Simas, A. B. C.; Aguiar, L. C. S. *J. Mater. Chem.* **2011**, *21*, 13516–13523.

(30)   Søbjerg, L. S.; Lindhardt, A. T.; Skrydstrup, T.; Finster, K.; Meyer, R. L. *Colloids Surf., B* **2011**, *85*, 373–378.

(31)   Ogi, T.; Honda, R.; Tamaoki, K.; Saitoh, N.; Konishi, Y. *Powder Technol.* **2011**, *205*, 143–148.

(32)   Chiu, C. -Y.; Li. Y.; Huang, Y. *Chem. Commun.* **2010**, *2*, 927–930.

(33)   Pacardo, D. B.; Sethi, M.; Jones, S. E.; Naik, R. R.; Knecht, M. R. *ACS Nano* **2009**, *3*, 1288–1296.

(34)   Ohara, S.; Hatakeyama, Y.; Umetsu, M.; Tan, Z.; Adschiri, T. *Adv. Powder Technol.* **2011**, *22*, 559–565.

(35)   Mao, C.; Solis, D. J.; Reiss, B. D.; Kottmann, S. T.; Sweeney, R. Y.; Hayhurst, A.; Georgiou, G.; Iverson, B.; Belcher, A. M. *Science* **2004**, *303*, 213–217.

(36)   Lee, S. -W.; Mao, C.; Flynn, C. E.; Belcher, A. M. *Science* **2002**, *296*, 892–895.

(37)   Jakhmola, A.; Bhandari, R.; Pacardo, D. B.; Knecht, M. R. *J. Mater. Chem.* **2010**, *20*, 1522–1531.

(38)   Søbjerg, L. S.; Gauthier, D.; Lindhardt, A. T.; Bunge, M.; Finster, K.; Meyer, R. L. Skrydstrup, T. *Green Chem.* **2009**, *11*, 2041–2046.

(39)   Pietsch, T.; Appelhans, D.; Gindy, N.; Voit, B.; Fahmi, A. *Colloids Surf. A* **2009**, *341*, 93–102.

(40)   Chhabra, R.; Moralez, J. G.; Raez, J.; Yamazaki, T.; Cho, J. -Y.; Myles, A. J.; Kovalenko, A. Fenniri, H. *J. Am. Chem. Soc.* **2010**, *132*, 32–33.

(41)   Sylvestre, J. -P.; Poulin, S.; Kabashin, A. V.; Sacher, E.; Meunier, M.; Luong, J. H. T. *J. Phys. Chem. B* **2004**, *108,* 16864–16869.

(42)   Chen, R.; Jiang, Y.; Xing, W.; Jin, W. *Ind. Eng. Chem. Res.* **2013**, *52*, 5002−5008.

(43)   Yen, M. -Y.; Teng, C. -C.; Hsiao, M. -C.; Liu, P. -I.; Chuang, W. -P.; Ma, C. -C. M.; Hsieh, C. -K.; Tsai, M. -C.; Tsai, C. -H. *J. Mater. Chem.* **2011**, *21*, 12880–12888.

(44)   Kanvah, S.; Joseph, J.; Schuster, G. B.; Barnett, R. N.; Cleveland, C. L.; Landman, U. *Acc. Chem. Res.* **2010**, *43*, 280–287.

(45)   Duarte, V.; Gasparutto, D.; Jaquinod, M.; Cadet, J. *Nucleic Acids Res.* **2000**, *28*, 1555–1563.

(46)   Newman, J. D. S.; Blanchard, G. J. *Langmuir* **2006,** *22,* 5882–5887.

(47)   Newman, J. D. S.; Blanchard, G. J. *J. Nanopart. Res.* **2007**, *9*, 861–868.

(48)   Clukay, C. J.; Grabill, C. N.; Hettinger, M. A.; Dutta, A.; Freppon, D. J.; Robledo, A.; Heinrich, H.; Bhattacharya, A.; Kuebler, S. M. *Appl. Surf. Sci.* **2014**, *292*, 128–136.

(49)   Subramaniam, C.; Tom, R. T.; Pradeep, T. *J. Nanopart. Res.* **2005**, *7*, 209–217.

(50)   Redón, R.; Rendón-Lara, S. K.; Fernández-Osorio, A. L.; Ugalde-Saldivar, V. M. *Rev. Adv. Mater. Sci.* **2011**, *27*, 31–42.

(51)   Lim, J. -S.; Kim, S. -M.; Lee, S. -Y.; Stach, E. A.; Culver, J. N.; Harris, M. T. *Nano Lett.* **2010**, *10*, 3863–3867.

(52)   (a) Thiagarajan, S.; Yang, R. -F.; Chen, S. -M. *Bioelectrochemistry* **2009**, *75*, 163–169. (b) Haynes, W. M. Ed. *CRC Handbook of Chemistry and Physics*, 95th ed., 2014–2015. (c) Okouchi, S.; Suzuki, M.; Sugano, K.; Kagamimori, S.; Ikeda, S. J. Food Sci. **2002**, *67*, 1594–1598.

(53)   Steenken, S.; Jovanovic, S. V. *J. Am. Chem. Soc.* **1997**, *119*, 617–618.

(54)   Fischer, A. Krozer, A. Schlapbach, L. *Surf. Sci.* **1992**, *269*, 737–742.

(55)   Tura J. M.; Regull P.; Victori L.; Dolors D. C. M. *Surf. Interface Anal.* **1988**, *11*, 447–449.

(56)   Shafeev G. A.; Themlin J. -M.; Bellard L.; Marine W.; Cros A. *J. Vac. Sci. Technol. A* **1996**, *14*, 319–326.

(57)   Kim, K. S.; Gossmann, A. F.; Winograd, N. *Anal. Chem.* **1974**, *46*, 197–200.

(58)   Kibis, L. S.; Stadnichenko, A. I.; Koscheev, S. V.; Zaikovskii, V. I.; Boronin, A. I. *J. Phys. Chem. C* **2012**, *116*, 19342–19348.

(59)   Kumar G.; Blackburn, J. R.; Albridge R. G.; Moddeman W. E.; Jones M. M. *Inorg. Chem.* **1972**, *11*, 296–300.

(60)   Brun, M.; Berthet, A.; Bertolini, J. C. *J. Electron Spectrosc. Relat. Phenom.* **1999**, 104, 55–60.

(61)   Butler, I. B.; Schoonen, M. A. A.; Rickard, D. T. *Talanta* **1994**, *41*, 211–215.

(62)   Hamerton, I.; Hay, J. N.; Howlin, B. J.; Jones, J. R.; Lu, S. -Y.; Webb, G. A. *Chem. Mater.* **1997**, *9,* 1972–1977.

(63)   Souza, R. A. D.; Zehnpfenning, J.; Martin, M.; Maier, J. *Solid State Ionics* **2005**, *176*, 1465–1471.

(64)   Subbaraman, R.; Tripkovic, D.; Strmcnik, D.; Chang, K. -C.; Uchimura, M.; Paulikas, A. P.; Stamenkovic, V.; Markovic, N. M. *Science* **2011**, *334*, 1256–1260.

(65)   Yu, J. C.; Ho, W.; Yu, J.; Hark, S. K.; Iu K. *Langmuir* **2003,** *19,* 3889–3896.

(66) Moralez, J. G.; Raez, J.; Yamazaki, T.; Motkuri, R. K.; Kovalenko, A.; Fenniri, H. *J. Am. Chem. Soc.* **2005**, *127*, 8307–8309.

(67) Fenniri, H.; Deng, B. -L.; Ribbe, A. E.; Hallenga, K.; Jacob, J.; Thiyagarajan, P. *Proc. Natl. Acad. Sci. USA* **2002**, *99*, 6487–6492.

(68) Pacardo, D. B.; Sethi, M.; Jones, S. E.; Naik, R. R.; Knecht, M. R. *ACS Nano* **2009**, *3*, 1288–1296.

(69) Knecht, M. R.; Weir, M. G.; Frenkel, A. I.; Crooks, R. M. *Chem. Mater.* **2008**, *20*, 1019–1028.

(70) Creighton, J. A.; Eadon, D. G. *J. Chem. Soc., Faraday Trans.* **1991**, *87*, 3881–3891.

(71) Scott, R. W. J.; Ye, H.; Henriquez, R. R.; Crooks, R. M. *Chem. Mater.* **2003**, *15*, 3873–3878.

(72) Scott, R. W. J.; Wilson, O. M.; Crooks, R. M. *J. Phys. Chem. B* **2005**, *109*, 692–704.

(73) Lamy, H.; Léger, J. -M.; Srinivasan, S. "Direct methanol fuel cells – from a 20th century electrochemists' dream to a 21st century emerging technology" In *Modern Aspects of Electrochemistry*, Bockris, J. Ó. M.; Conway, B. E. Eds., Plenum Press, New York, 2000, Chapter 3, page 53.

(74) Greenwood, R; Kendall, K *J. Eur. Ceram. Soc.* **1999**, *19*, 479–488.

(75) Hanaor, D. A. H.; Michelazzi, M.; Leonelli, C.; Sorrell, C. C. *J. Eur. Ceram. Soc.* **2012**, *32*, 235–244.

(76) Woehl, T. J.; Evans, J. E.; Arslan, I.; Ristenpart, W. D.; Browning, N. D. *ACS Nano* **2012**, *6*, 8599–8610.

Chapter 3

Hydrogenation Catalysis

3.1 Introduction

The catalytic hydrogenation of unsaturated hydrocarbons is one of the most important and valuable chemical processes applied for the production of commodity chemicals including for both industry and academia.[1,2] To perform such reactions, a wide variety of homogeneous transition metal catalysts, derived from Rh, Ir, Pd, Pt and Ru, have been intensively investigated and successfully employed.[2] In the 1960s, a rhodium based catalyst, known as Wilkinson's catalyst [RhCl(PPh$_3$)$_3$], was discovered and successfully employed for hydrogenation on a large scale because of its high activity and robust stability (Figure 3.1A).[2] Twenty years later, Noyori and co-workers developed a ruthenium-based catalyst for the enantioselective hydrogenation of polar unsaturated organic compunds including ketones, aldehydes and imines (Figure 3.1B).[2]
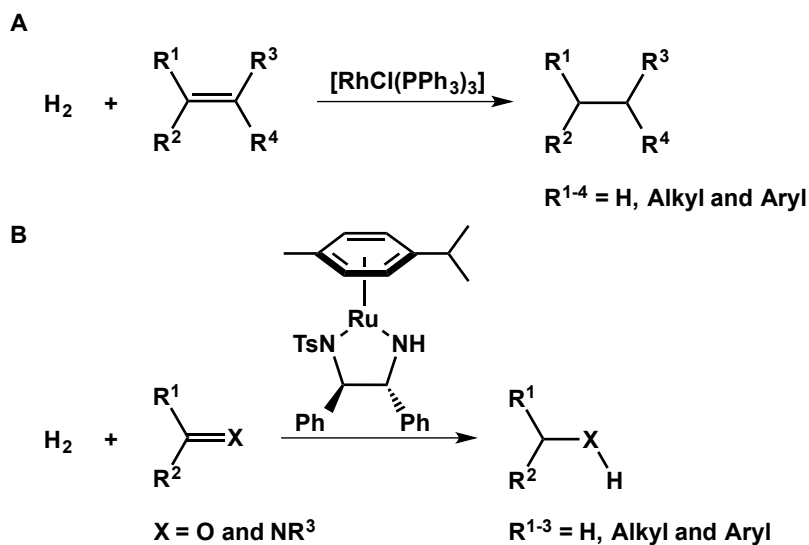
Figure 3.1: Examples of the catalytic hydrogenation of unsaturated hydrocarbons.

In addition to these traditional molecular catalysts, supported transition metal NPs for catalysis have received considerable interest in recent years and have been successfully employed in a variety of organic transformations.[3] This is because supported metal NPs possess several important and interesting features such as: (i) high surface-to-volume ratio, (ii) very reactive surface atoms, (iii) recyclability, and (iii) the potential for high turnover, which make them superior catalysts over molecular catalysts.[3] Though the homogeneous catalysts are very efficient and selective, they possess limited thermal stability and catalyst recyclability.[3] As heterogeneous catalysts are less reactive than their homogeneous counterparts and due to the inherent heterogeneity associated with metal NPs, it is crucial to develop new support nanomaterials. These supports should impart stability to the metal NPs in aqueous media and help catalyze the reaction at the interface between homogeneous and heterogeneous conditions. In addition, it should allow the synthesis of monodispersed metal NPs for uniform reactivity.

I designed water-soluble and biocompatible rosette nanotubes (RNTs) supported metal NPs composite nanomaterials for catalysis. As discussed in chapter 2, RNTs can be used for the *in-situ* formation and stabilization of metal NPs upon mixing with the corresponding metal salt at ambient temperature and without applying any reducing agent. Upon establishing the synthetic procedure for the preparation of the M NPs/RNTs (M = Au, Pd and Pt) catalysts, I decided to investigate their utility and the catalytic activity towards the hydrogenation of C=C double bonds under environmentally benign conditions. In this chapter, I will discuss the details of the hydrogenation using M NPs/RNTs (M = Au, Pd and Pt) catalysts and their characterization.

3.2 Results and Discussion

3.2.1 Optimization of the Catalytic Hydrogenation Reaction

For the catalysis studies, 3-methylstyrene (**3.1a**) was initially selected to optimize the conditions for the catalytic hydrogenation reaction (Table 3.1, scheme). Also, I employed Pd NPs for this initial study due to their known ability to act as a good hydrogenation catalyst.[3.4] As the dangling lysine side chains on the surface of the RNTs contain positively charged amines (in the form of ammonium ions), I envisioned that these chains could act as a source of H^+ ions. Therefore, an external hydrogen source would not be required. Considering this, I carried out a first control experiment by using 5 mol% of Pd NPs/RNTs catalyst loaded with **3.1a** in water under nitrogen atmosphere (Table 3.1, entry 2). Unfortunately, the hydrogenation reaction did not proceed and only starting material was observed after 18 h. In a second control experiment, I repeated the similar reaction by using only 5 mol% of the RNTs as a catalyst instead of the Pd NPs/RNTs catalyst under hydrogen. This reaction also did not result in the hydrogenated product (Table 3.1, entry 1). This indicated that I would need to explore the catalytic reaction in the presence of hydrogen. Indeed, when the reaction was repeated using 5 mol% of the Pd NPs/RNTs catalyst under hydrogen, the expected product 3-ethyltoluene (**3.2a**) was observed but with a % conversion of only 26% (Table 3.1, entry 3). Previously in chapter 2, I discussed that the nucleation pocket on the surface of the RNT formed by the four adjacent lysine side chains, passivate the nucleation and growth of the NP. Therefore, it is possible that most of the active surface of the NP is protected by the lysine side chains, which prevents the interactions between the catalyst and the reactants. Keeping this in mind, I synthesized the Pd NPs/RNTs catalyst by reducing $PdCl_4^{2-}$ with

hydrogen in the presence of the RNTs for 5 mins prior to the catalytic reaction. The new

catalyst was then employed in the similar hydrogenation reaction of **3.1a** in water under

hydrogen for 18 h. The reaction gave an improved conversion of 48%, indicating that the

NPs might have more available catalytically active surfaces (Table 3.1, entry 4).

Similarly, El-Sayed *et al.* also observed that when the surface of the NP is less protected

by the stabilizer, the NP catalyst possesses high catalytic activity.[5,6] I also carried out

another experiment by repeating the similar reaction by using 5 mol% of Pd NPs in the

absence of the RNTs (Table 3.1, entry 5). Interestingly, the reaction afforded only 22%

conversion of **3.1a**. Importantly, the Pd NPs underwent rapid agglomeration to form Pd

black, indicating their poor stability in the absence of the RNTs.[6]
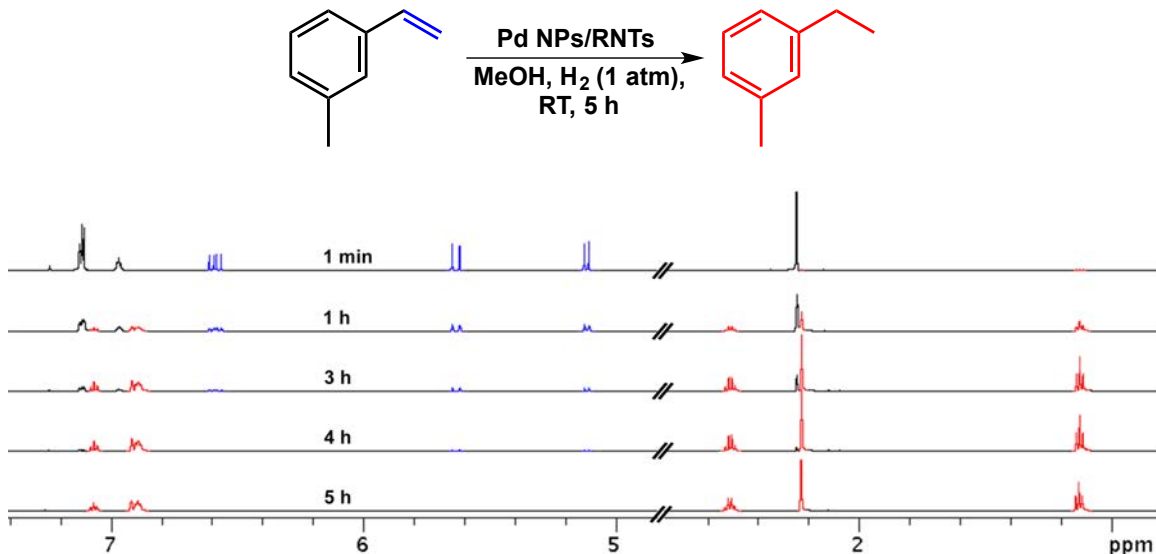
Figure 3.2: Stacked ^{1}H NMR spectra of the hydrogenation of **3.1a** in CDCl$_3$.

To further enhance the product conversion I chose methanol as a solvent instead

of water. I expected that **3.1a** would have higher solubility in methanol and give high

product conversion upon interaction with the Pd NPs/RNTs catalyst. This is also

supported by the Horiuti-Polanyi mechanism, where the hydrogenation occurs by

dissociative adsorption of H_2 onto the catalyst surface, followed by the stepwise hydrogenation of the C=C double bond.[7] This suggests that the interaction of the reactants on the surface of the catalyst is crucial for the product formation. When I performed the reaction in methanol using 5 mol% of the Pd NPs/RNTs catalyst, the reaction afforded 100% conversion of **3.1a** in 5 h (Table 3.1, entry 6; Figure 3.2). Other solvent experiments showed that the reaction in ethanol or in a mixture of solvents (water/methanol - 50:50 v/v) could lead to 100% conversion of **3.1a** in 5 and 9 h, respectively (Table 3.1, entry 10 and 11). However, the reaction in neat methanol or ethanol was found to be faster than in the solvent mixture, indicating that solubility plays an important role in the kinetic of the hydrogenation reaction by improving the interaction between **3.1a** and the catalyst. As the reaction in methanol gave 100% conversion of **3.1a** and to compare the reactivity with the Pd NPs/RNTs catalyst, I investigated the catalytic activity of naked Pd NPs and Pd NPs/L-LAA (L-lysine amino acid) in methanol. The Pd NPs and Pd NPs/L-LAA were synthesized by reducing with hydrogen before the catalytic reaction under the optimized condition of Pd NPs/RNTs catalyst. Under the optimized conditions, both the reactions gave very poor product conversion such as only 2 and 17% (Table 3.1, entry 6 and 8). These results again suggest that the stability of the Pd NPs is very important for high product conversion. Importantly, the LAA molecules did not act as a stabilizer of the Pd NPs in methanol. This supports the role of the supramolecular organization of the RNTs and the lysine side chains in stabilizing the Pd NPs in solution and providing high catalytic activity. This is because the presence of nucleation pockets could control the Pd NP size, which was not available in naked Pd NPs and Pd NPs/L-LAA catalysts.

Table 3.1: Optimization for the hydrogenation of 3-methylstyrene (**3.1a**).

H₂ +   [3-methylstyrene structure] $\xrightarrow[\text{Solvent (1 mL), RT}]{\text{Catalyst}}$ [3-ethyltoluene structure]

3.1a, 3-methylstyrene   **3.2a, 3-ethyltoluene**
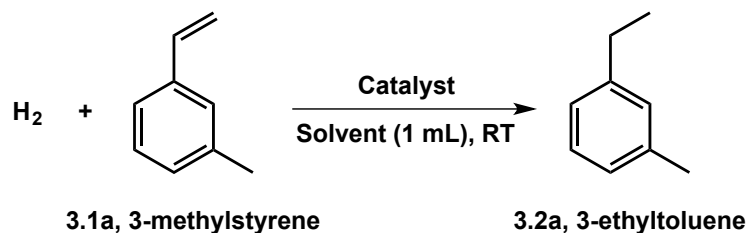
Entry	Catalyst	Pd loading (%)	Solvent	Reaction duration (h)	Convn.[a] (%)
1	RNTs	-	H_2O	18	0
2	Pd NPs/RNTs[b,c]	5	H_2O	18	0
3	Pd NPs/RNTs[b]	5	H_2O	18	26
4	Pd NPs/RNTs[d]	5	H_2O	18	48
5	Pd NPs[d]	5	H_2O	18	22
6	Pd NPs/RNTs[d]	5	MeOH	5	100
7	Pd NPs[d]	5	MeOH	5	6
8	Pd NPs/LAA[d,e]	5	MeOH	5	17
9	Pd NPs/RNTs[d]	3	MeOH	5	5
10	Pd NPs/RNTs[d]	5	EtOH	5	100
11	Pd NPs/RNTs[d]	5	H_2O:MeOH (50:50)	9	100

[a] Determined by ^1H NMR. [b] Catalyst was synthesized by overnight incubation as mentioned in chapter 2. [c] Under nitrogen. [d] Catalyst was synthesized by reducing with H_2 for 5 mins prior to the catalytic reaction. [e] LAA = Lysine amino acid. All reactions were carried out under hydrogen (1 atm) at ambient temperature unless otherwise noted.
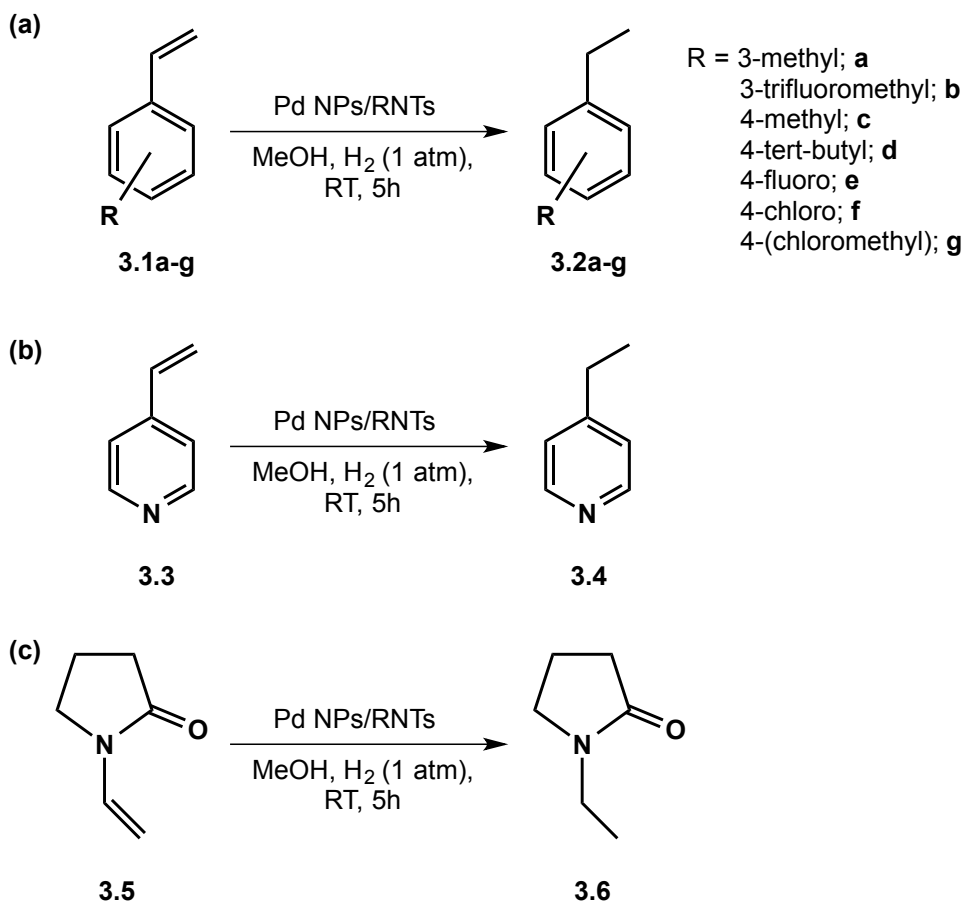
Finally, to investigate the effect of the catalyst loading on the product conversion, I performed a similar reaction with 3 mol% of the Pd NPs/RNTs catalyst loading. However, the decrease in catalyst loading resulted in a significant drop in reactivity affording only 5% product conversion in 5 h (Table 3.1, entry 9).[8] This finding suggests that 5 mol% of the catalyst loading is the optimal condition to obtain high product conversion.

In summary of the optimization process, the best condition was found when the reaction was carried out using 5 mol% of the palladium loading in methanol, where the Pd NPs/RNTs catalyst was synthesized by reducing with hydrogen before the catalytic reaction. It should be noted that the mol% of Pd loading refers to the concentration of the Pd atoms (equivalent to the $PdCl_4^{2-}$ ions) present in solution, and not the concentration of palladium nanoparticles in solution.

3.2.2 Exploration of the Catalytic Hydrogenation Reaction

Under the optimized condition, initially a variety of styrene derivatives containing both electron donating and withdrawing substituents at the 3- and 4-positions of the aromatic rings (Scheme 3.1a), 4-vinylpyridine (3.3, Scheme 3.1b), and 1-vinylpyrrolidin-2-one (3.5, Scheme 3.1c) were hydrogenated smoothly with full conversion except for 3-trifluoromethylstyrene (3.1b, 9%) due to the high electron withdrawing effect (Table 3.2). As the hydrogenation reaction proceeds through an initial coordination of the olefin double bond to the metal center, the ability of this coordination is highly influenced by the substituents present in the benzene ring of the styrenes. Therefore, an electron withdrawing substituent such as trifluromethyl group would decrease the coordination ability of 3-trifluoromethylstyrene to Pd center. Previously, Uozumi and co-workers

demonstrated the hydrogenation of styrene derivatives in water using polymer supported Pd NPs.[4] Although they obtained high yields of the hydrogenated products, the reaction duration was 24 h, which is longer than required in our system. Moreover, they used a special shaking instrument instead of stirring.[4]

(a)

R = 3-methyl; **a**
3-trifluoromethyl; **b**
4-methyl; **c**
4-tert-butyl; **d**
4-fluoro; **e**
4-chloro; **f**
4-(chloromethyl); **g**

Pd NPs/RNTs

MeOH, H$_2$ (1 atm), RT, 5h

3.1a-g → **3.2a-g**

(b)

Pd NPs/RNTs

MeOH, H$_2$ (1 atm), RT, 5h

3.3 → **3.4**

(c)

Pd NPs/RNTs

MeOH, H$_2$ (1 atm), RT, 5h

3.5 → **3.6**

Scheme 3.1: Catalytic hydrogenation of different olefins using Pd NPs/RNTs catalyst (5 mol% Pd loading).

To investigate the selectivity of our catalyst towards olefins, I performed the hydrogenation of **3.5** containing both olefin and carbonyl groups (Scheme 3.1c). Upon hydrogenation, **3.5** was selectively hydrogenated to give 1-ethylpyrrolidin-2-one (**3.6**) without accompanying any side products (1-ethylpyrrolidin-2-ol) as observed previously (Table 3.2, entry 9).[9] On the other hand, 4-(chloromethyl)styrene (**3.1g**) upon catalysis

afforded both the hydrogenated (4-(chloromethyl)ethylbenzene (**3.2g**), 85%), as well as the hydrogenated and hydrodechlorinated (4-ethyltoluene (**3.2c**), 15%) product (Table 3.2, entry 7).

**Table 3.2**: Hydrogenation of different styrene derivatives using the Pd NPs/RNTs catalyst.

Entry	Substrate	Product	Convn.[a] (%)
1	3-methylstyrene	3-Ethyltoluene	100
2	3-trifluoromethylstyrene	3-trifluoromethylethylbenzene	9
3	4-methylstyrene	4-ethyltoluene	100
4	4-*tert*-butylstyrene	4-tert-butylethylbenzene	100
5	4-fluorostyrene	4-fluoroethylbenzene	100
6	4-chlorostyrene	4-chloroethylbenzene	100
7	4-(Chloromethyl)styrene	4-(chloromethyl)ethylbenzene:4-ethyltoluene	85:15
8	4-vinylpyridine	4-ethylpyridine	100
9	1-vinylpyrrolidin-2-one	1-ethylpyrrolidin-2-one	100

[a] Determined by ^{1}H NMR. All reactions were carried out in the presence of 5 mol% of Pd NPs/RNTs catalyst (synthesized by reducing with hydrogen prior to the catalytic reaction) in MeOH (1 mL) under hydrogen (1 atm) at ambient temperature for 5 h.

3.2.3 Catalyst reactivity and recyclability

After screening the catalytic activity of Pd NPs/RNTs catalyst towards the hydrogenation of different styrene derivatives, I were interested in investigating the catalytic activity of different metal NPs such as Pt and Au NPs. Therefore, to compare the

catalytic activity of M NPs/RNTs (M = Pt and Au) with Pd NPs/RNTs, the hydrogenation of **3.1a** was carried out by using 5 mol% of M NPs/RNTs (M = Pt and Au) under the identical conditions to that of the Pd NPs/RNTs catalyzed reaction. Whereas the Pt NPs/RNTs catalyst resulted in 65% conversion of **3.1a** to **3.2a**, the Au NPs/RNTs catalyst had no catalytic activity (Scheme 3.2). Previously, Knecht *et al.* studied the catalytic hydrogenation of allyl alcohol by using peptide supported M NPs (M = Pd and Pt). They also reported the similar trend of poor reactivity of Pt NPs catalyst compared to the Pd NPs catalyst.[10] The different catalytic activity arises from the differences in the electronic density of the external *d* orbitals of the Pd (d^{10}) and the Pt (d^9) metals. As the Pt metal has less *d* electrons, they are less active towards interacting with the substrate through π backbonding, hence providing poor reactivity due to poor Pt and the olefin double bond interaction.[11,12] While the non-catalytic activity of the Au NPs/RNTs catalyst can be attributed to the weak adsorption and dissociation of H_2 molecule, which is the rate-limiting step in the hydrogenation reaction.[13]
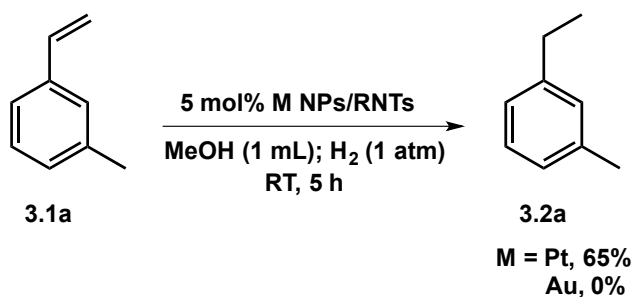
Scheme 3.2: Hydrogenation of **3.1a** using M NPs/RNTs (M = Pt and Au) catalyst.

Finally, I also compared the reactivity of our Pd NPs/RNTs catalyst with a commercially available catalyst. For comparison, I performed the catalytic hydrogenation of **3.1c** by using 5 mol% of the Pd/Al$_2$O$_3$ (1 wt % Pd) catalyst (courtesy by Dr. Natalia Semagina, Department of Chemical and Materials Engineering, University of Alberta)

under the identical condition to that of the Pd NPs/RNTs catalyst. The reaction afforded almost 100% product conversion after 5 h (Scheme 3.3).
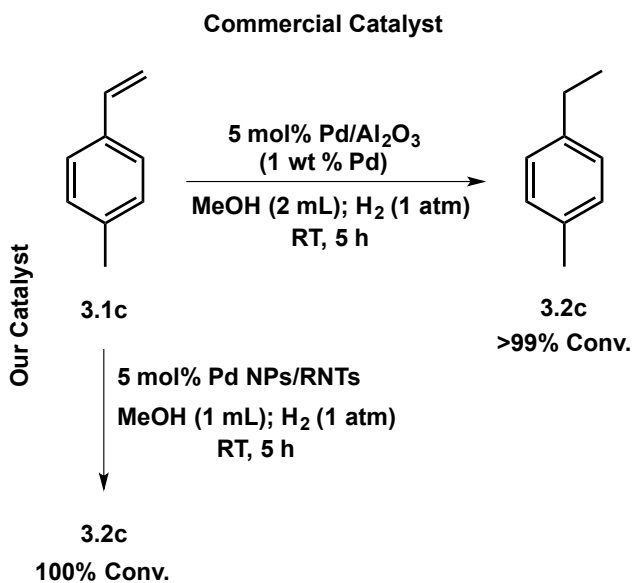
Scheme 3.3: Comparison of the catalytic activity between our Pd NPs/RNTs and Pd/Al$_2$O$_3$ (1 wt % Pd) catalyst.

Later, I also performed the catalyst recycling studies, which were examined for the hydrogenation of **3.1c**. As the hydrogenation reaction completes in 5 h, equal amounts (132 μL) of **3.1c** were charged each time using a syringe under hydrogen (1 atm) up to 10th cycle. The studies showed that the catalyst could be reused at least ten times without the loss of any significant catalytic activity. The high catalytic activity of the Pd NPs/RNTs catalyst was perhaps due to the high stability of the Pd NPs in solution. Hence, these experiments indicate that the RNTs are acting as an effective reservoir by improving the solubility and the stability of the NPs in solution.

3.2.4 Catalyst Characterization

3.2.4.1 Microscopic (SEM and TEM) Analysis

Earlier as discussed in Chapter 2, the microscopic images of the Pd NPs/RNTs catalyst, synthesized by overnight incubation, showed that the Pd NPs are evenly organized in a zigzag fashion into the nucleation pockets and most of the active surface of the NPs are protected by the lysine side chains. Because of this surface protection, the catalyst showed poor catalytic activity. However, when I employed the Pd NPs/RNTs catalyst for hydrogenation, synthesized by reducing with hydrogen prior to the catalytic reaction, I observed 100% product conversion. Hence, to gain more insight into these two very different catalytic activities of the Pd NPs/RNTs catalyst synthesized by over night incubation and by hydrogen reduction, I carried out SEM and TEM studies. As methanol is less polar than water and the mechanical stirring assists with mass transportation, I expected that the RNTs would form bundles in solution, which would result in the NPs having a bimodal distribution.[14] This means that the NPs can be located into the nucleation pocket on the surface of the RNT as observed earlier, and onto the surface of the bundle. To support this hypothesis, a methanol solution of the Pd NPs/RNTs catalyst, synthesized by reducing with hydrogen, was drop casted on a carbon grid before the catalytic reaction for the SEM and TEM analysis. The SEM image confirmed that the RNTs formed bundles in methanol (Figure 3.3a). Though the bimodal distribution of the NPs could not be conclusively determined from the SEM image, it showed the presence of some larger NPs on the surface of the RNTs bundle (Figure 3.3a).
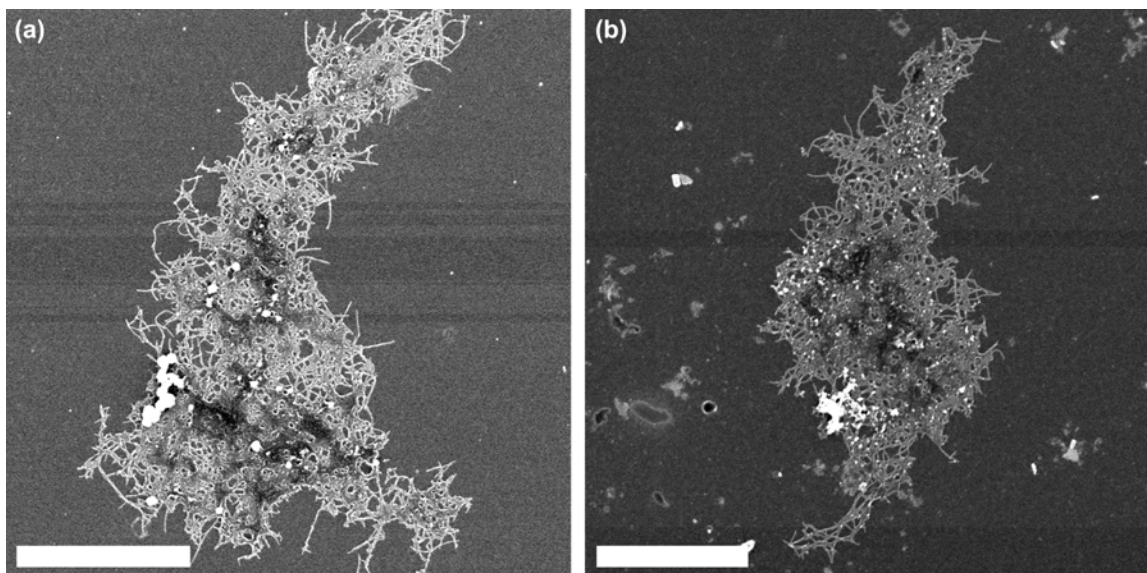
Figure 3.3: SEM images of the Pd NPs/RNTs before catalysis (a), and after catalysis (b). Scale bar 1 μm.

The SEM image of the Pd NPs/RNTs catalyst after the first cycle of the catalytic reaction also showed the formation of the RNTs bundle and the presence of some larger sized Pd NPs on the surface of the bundle (Figure 3.3b). It should be noted that most of the Pd NPs are located within a close vicinity of the RNTs bundle before and after the catalytic reaction. This indicates that the RNTs are effectively acting as a support as well as a reservoir for stabilizing the Pd NPs. Perhaps the high recyclability of our catalyst up to the 10th cycle could be rationalized from this affinity between the RNTs and the Pd NPs, which facilitates the initial formation of Pd NPs on the surface of the RNTs and their re-deposition after catalysis. To understand the nature of the Pd NPs distribution on the surface of the RNT and onto the bundle, I performed TEM analysis of the Pd NPs/RNTs catalyst before and after the catalytic reaction.
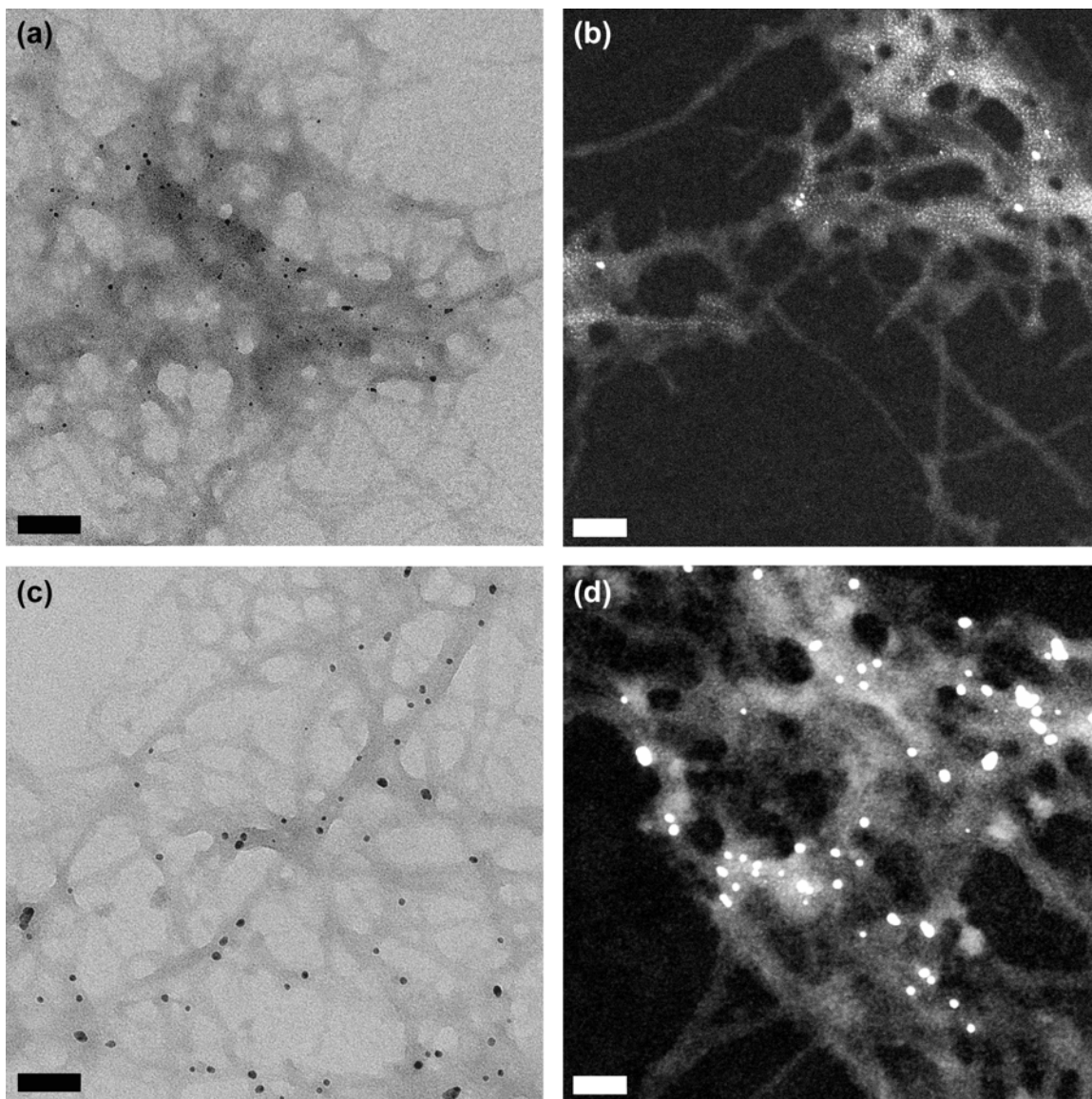
Figure 3.4: TEM images of the Pd NPs/RNTs before catalysis (a, b), and after catalysis (c, d). Scale bar – 50 nm.

Analysis of the TEM images of the Pd NPs/RNTs catalyst before and after the catalytic reaction, also confirmed the presence of the Pd NPs on the surface of the RNT and onto its bundle. Before the catalytic reaction, the average size of the Pd NPs, located into the nucleation pocket, is 1.3±0.2 nm. On the other hand, the Pd NPs on the surface of the RNTs bundle have an average particle size of 3.9±0.7 nm. The average size of the Pd

NP was calculated by averaging the size of 20 individual Pd NPs, where the Pd NP size was measured visually by using imageJ software from the TEM images. In contrast, the TEM analysis of the catalyst revealed an increase in the Pd NPs size after the catalytic reaction. The average Pd NPs sizes, positioned into the nucleation pocket and on the surface of the RNTs bundle, are 1.5±0.2 and 6.4±1.7 nm respectively. The higher standard deviations suggest the polydispersity of the Pd NPs on the surface of the RNTs bundle. This indicates that though the Pd NPs exist on the surface of the bundle, the size of the Pd NPs is poorly controlled by the RNTs outside the nucleation pocket. However, the cause of the increase in the Pd NPs size is still unclear, which could be either because of the leaching and the re-deposition of the Pd atoms after catalysis or the influence of the mechanical stirring during catalysis.[14] As the Pd NPs, located into the nucleation pocket show poor catalytic activity, I believe that most of the high catalytic activity resulted from the Pd NPs located on the surface of the bundle.[6]

3.2.4.2 Spectroscopic (UV, CD and XPS) Analysis

To understand the properties and the behavior of the M NPs/RNTs (M = Pd, Pt and Au) catalyst in solution I carried out detailed characterization by UV-Vis and CD spectroscopy. As the catalytic reaction was performed in water and methanol, I initially studied the properties of the RNTs in these two solvents. The UV spectrum of the RNT showed a hyperchromic shift of the typical absorption bands (237 and 288 nm) of the RNT by switching the solvent from water to methanol (Figure 3.5a).[15] This hyperchromicity of the absorption bands could be attributed to the shorter tube formation, which is significantly affected by the solution aging time. Usually, the prolonged incubation of the RNTs solution results in longer nanotube formation, which cause

hypochromic shift of the absorption bands compared to the shorter nanotubes. Similarly, it has been reported previously that the stacking of the base pairs in a double helical strand in DNAs showed hypochromicity of the absorption bands.[16-18] When compared, the RNTs displayed a typical strong exciton-coupled bisignate CD spectrum with a couplet centered at ~247 nm in both water and methanol (Figure 3.5b).[15] This strong CD effect is associated with the $\pi-\pi^*$ transition of the stacked G^C bases,[19] and attributed to the supramolecular helical organization of the RNTs.[15,20,21] The resulting helicity of the RNTs occurs in two steps - (i) hierarchical assembly of the G^C bases through H-bonding (hexameric rosette formation) and the stacking of the rosettes to form a tubular architecture,[20,21] and (ii) the enhanced crystallinity (well-defined organization) of the chiral lysine side chains, which induce the supramolecular helicity of the RNTs.[21-23]
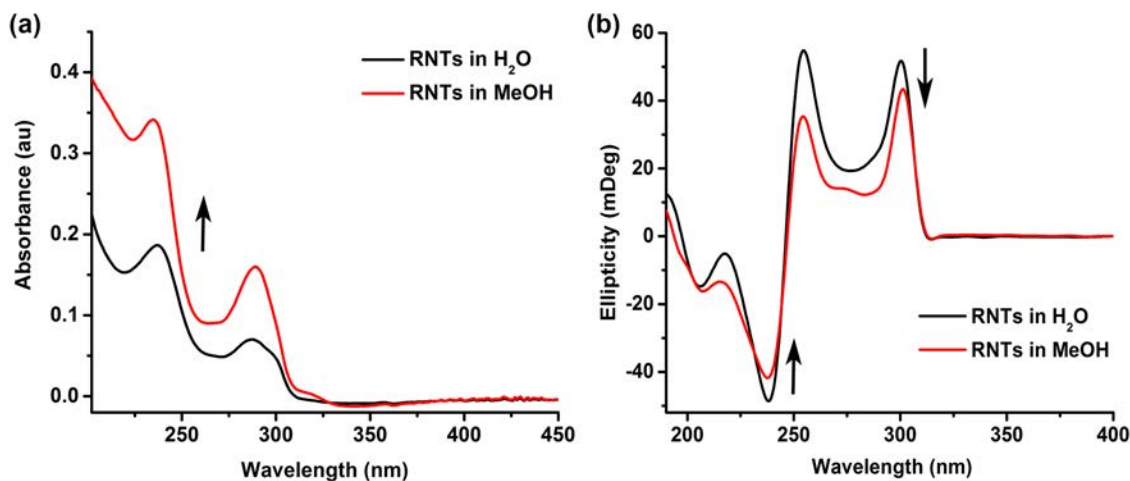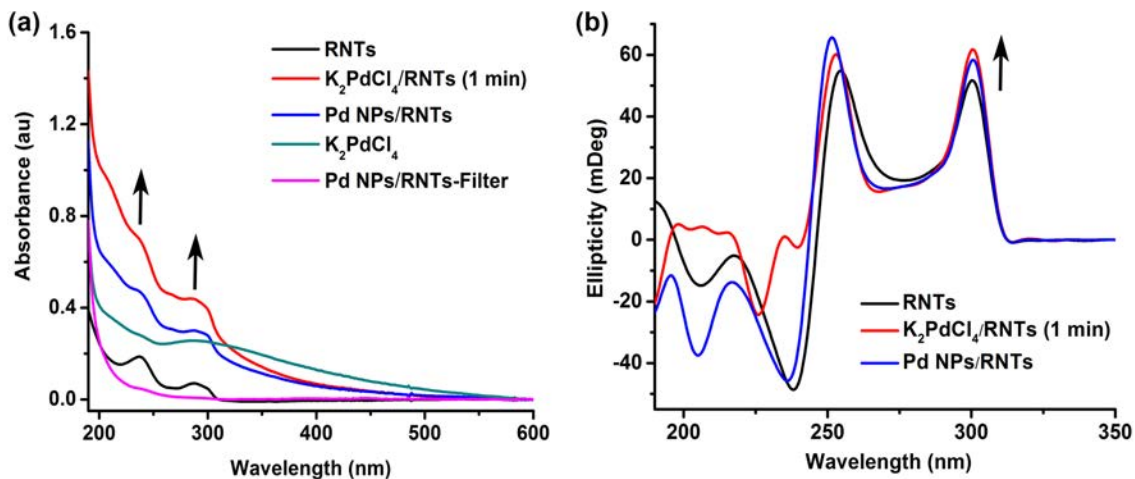

Figure 3.5: UV-Vis (a) and CD (b) spectra of the RNTs in H_2O and MeOH.

Previously, Fenniri and co-workers reported that the RNTs became CD silent in the absence of the crystallinity of the side chains. On the other hand, the induction of the helicity amplified the chirality of the RNTs when the chiral side chains were introduced showing the crystallinity.[20,21] This is known as the sergeants and soldiers principle.[24] The

observed non-conservative nature of the spectrum could arise from the non-degenerate couplings of the $\pi-\pi^*$ transition of the stacked G^C bases with the other transitions involved in the G^C bases[23] or by the influence of the $\pi-\pi^*$ and/or $n-\pi^*$ transition in the lysine amide bond (Figure 3.5b).[25] The bisignate CD effect in the spectrum resulted from the exciton coupling of the stacked G^C bases in the helical superstructure. Typically, the bisignate CD effect originates from the two close-lying states $(\pi-\pi^*)$ resulting from aggregation. However, they should have identical rotational strengths of the opposite sign and their dipole strengths should vary with respect to their relative orientation.[19,26] The decrease in the molar ellipticity of the RNT in methanol could be attributed to the bundling effect.

The UV spectrum of the Pd NPs/RNTs catalyst in water also showed the absorption bands at 237 and 288 nm, which could be assigned to the G^C base chromophores (Figure 3.6a).[15] Interestingly, the formation of the Pd NPs did not cause any shift in the absorption maxima. The addition of $PdCl_4^{2-}$ to the solution of RNTs exhibited two immediate effects: (i) hyperchromic shift of the absorption bands, and (ii) an increase in the absorbance with decreasing wavelength between 330 to 600 nm (red spectrum, Figure 3.6 a). The hyperchromic effect of the absorption bands could be due to the Plasmon excitation in the Pd NPs on the surface of the RNTs. The chromophore (G^C base) experiences an enhanced electric field near the Pd NP due to this Plasmon excitation.[27] In general, the absorbance is proportional to the square of the dot product of the dipole transition moment and the field. Therefore, if the field is enhanced, then the absorbance is also enhanced. This enhancement factor varies with the distance from the NPs to the chromophore. In the Pd NPs/RNTs catalyst, the Pd NPs are located into the

nucleation pocket as well as on the surface of the RNTs bundle, as confirmed by the TEM

analysis (Figure 3.4). Therefore, the distance between the NP and the G^C base is close

enough to contribute to the electric field enhancement causing the hyperchromic shift.

Figure 3.6: Detailed characterization of the Pd NPs/RNTs in H_2O by UV-Vis (a) and CD

(b) spectroscopy.

On the other hand, the gradual increase in absorbance with decreasing wavelength could

be attributed to the rapid Pd NP formation and the electrostatic interaction between the

$PdCl_4^{2-}$ and the RNTs (red and blue spectra, Figure 3.6a).[27] As discussed in chapter 2, the

kinetic studies suggest that the Pd NP formation is a very rapid process, which takes

place within 1 min upon mixing of the $PdCl_4^{2-}$ and the RNT solution. The presence of the

Pd NPs in solution causes electron scattering at the boundaries of the NPs leading to the

gradual increase in the absorbance with decreasing wavelength. This result is in

agreement with the literature reported UV analysis, which corresponds to the solution

containing M NPs.[28-30] The reduction of the $PdCl_4^{2-}$ ions by hydrogen resulted in

hypochromic shift of the absorption bands with respect to that of the initial $PdCl_4^{2-}$/RNTs

complex. This is because the complete Pd NP formation eliminates the hyperchromic

effect due to the initial $PdCl_4^{2-}$ and RNTs complexation (blue spectrum, Figure 3.6 a). To evaluate the interaction between the Pd NPs and the RNTs, and the formation of any Pd NPs outside the RNT surface, I filtered a solution of Pd NPs/RNTs catalyst after reduction with H_2. The filtration was carried out on a 20 nm pore size inorganic membrane filter. The UV spectrum of the filtered solution did not display an increase in the absorbance with decreasing wavelength between 330 to 600 nm (pink spectrum, Figure 3.6a). The UV spectrum of the Pd NPs/RNTs catalyst in methanol also showed similar features as observed in water such as (i) hyperchromic shift of the absorption bands upon addition of $PdCl_4^{2-}$ to the RNTs solution, (ii) increase in the absorbance with decreasing wavelength between 330 to 600 nm, and (iii) hypochromic shift of the absorption bands upon complete conversion of the $PdCl_4^{2-}$ to Pd NPs (Figure 3.7a).

The CD spectra of the Pd NPs/RNTs catalyst in both water and methanol exhibited a similar CD profile as the RNTs alone (blue spectrum, Figure 3.6b and Figure 3.7b). This indicates that the formation of the Pd NPs onto the surface of the RNTs has no observable effect on the supramolecular helicity of the RNTs. However, the intensity of the molar ellipticity of the Pd NPs/RNTs catalyst in methanol was very low compared to that of the RNTs. This is perhaps due to the bundling of the Pd NPs/RNTs catalyst in methanol. Although the CD spectra of the initial $PdCl_4^{2-}$/RNTs mixture displayed a similar CD pattern at a higher wavelength as the RNTs and the Pd NPs/RNTs catalyst, the spectra showed a different pattern at lower wavelength. This is perhaps due to the conformational bias of the lysine side chains influenced by the nucleation and growth of the Pd NPs.[19,31] The UV and CD spectra of M NPs/RNTs (M = Pt and Au) catalysts also showed similar features as observed for the Pd NPs/RNTs catalyst.
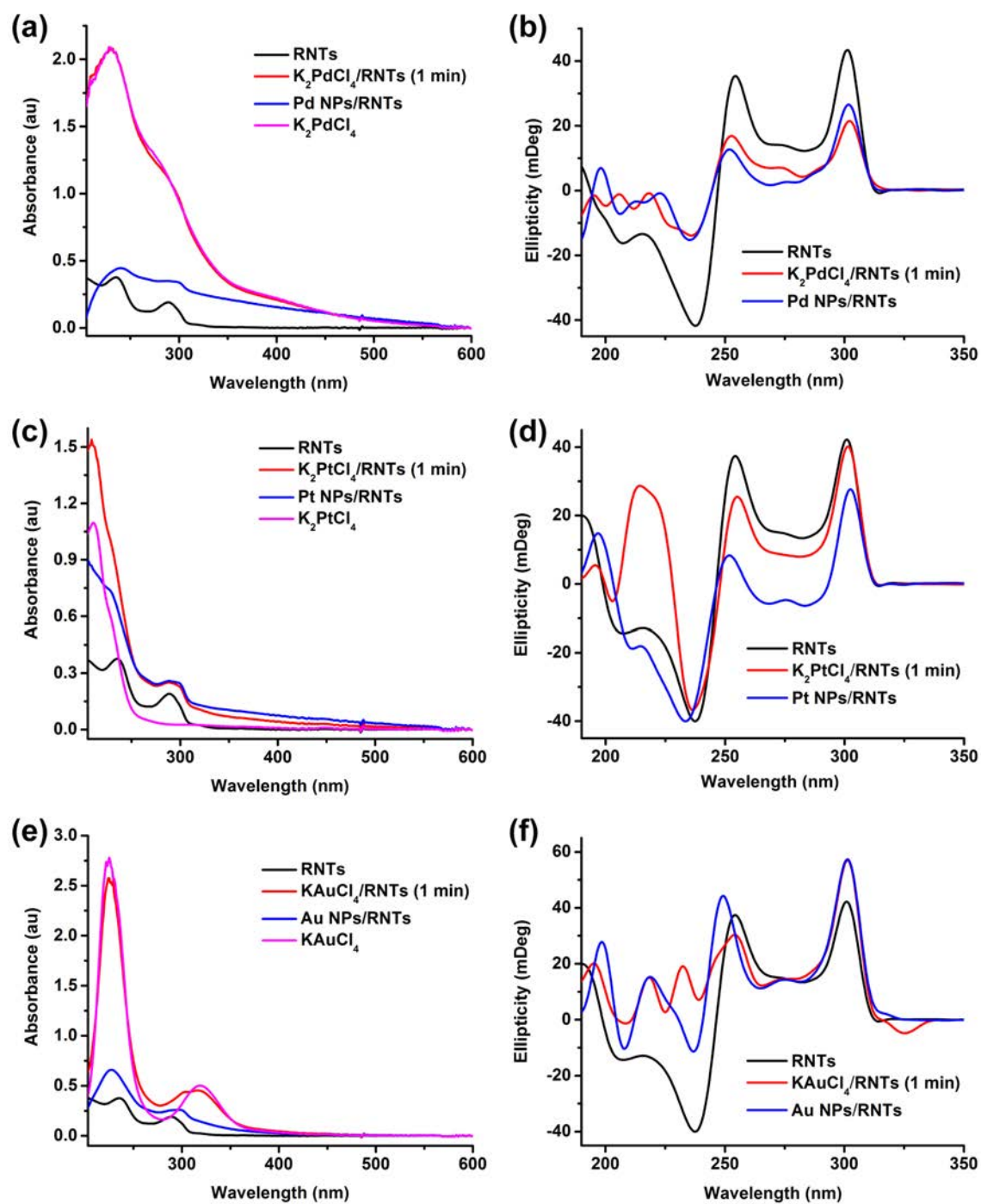
Figure 3.7: UV-Vis and CD spectra of M NPs/RNTs in MeOH (M = Pd (a, b); Pt (c, d) and Au (e, f)).

To gain further insight into the nature of the Pd NPs/RNTs catalyst in water and methanol, I performed XPS analysis on a TEM grid. The spectra showed the presence of

Pd^0 as well as PdO$_x$ (X = 1 and 2) species in the sample (Figure 3.8). In general, both the water and methanol samples exhibited E_b peaks associated with the elemental Pd^0 (Pd3$d_{5/2}$ = 335.2 eV), PdO (Pd3$d_{5/2}$ = 336.0 eV), and PdO$_2$ (Pd3$d_{5/2}$ = 337.9 eV) (Figure 3.8a,c).[32-35] The Pd NPs/RNTs catalyst was synthesized by reducing with hydrogen, which confirms the complete reduction of the PdCl$_4$$^{2-}$ ions. The presence of the PdO$_x$ species in the samples could be perhaps due to the surface oxidation upon air exposure or solvent (water and methanol) during the sample preparation. The ratio of the % concentration of Pd^0, PdO and PdO$_2$ was 1:1.5:6, which indicated that the Pd NPs were highly reactive and were oxidized rapidly upon exposure to oxygen. The O1s spectrum of the water sample showed two E_b peaks at 531.6 and 534.1 eV, which could be attributed to the chemisorbed oxygen on the surface of the sample and the PdO$_x$ species (Figure 3.8b).[35,36]

I also investigated the stability of the Pd NPs/RNTs catalyst in solution. To address this issue, I aged a methanol solution of the Pd NPs/RNTs catalyst for 7 days, and then carried out the XPS analysis. The Pd3$d_{5/2}$ spectrum of the 7 days aged catalyst displayed similar E_b peaks at 335.2, 336.0 and 338.1 eV, which could be assigned to the Pd^0, PdO and PdO$_2$, respectively (Figure 3.8d).[32-35] This result indicates that the Pd NPs/RNTs catalyst is stable in solution for as least 7 days. Interestingly, the Pd3$d_{5/2}$ spectrum also showed an E_b peak at 345.7 eV for the K satellite (Figure 3.8d). This is perhaps due to the deposition of the K$^+$ salt on the surface of the Pd NPs/RNTs catalyst caused by the solution aging for 7 days (Chapter 2). The ratio of the % concentration of Pd^0, PdO and PdO$_2$ in methanol was found to be higher (1:0.8:5) for the 7 days stored sample than for the freshly prepared catalyst (1:0.4:4). It is expected that the prolonged

107

storage of the catalyst can facilitate the formation of more PdO_x species by the reaction of the Pd NPs and dissolved oxygen.
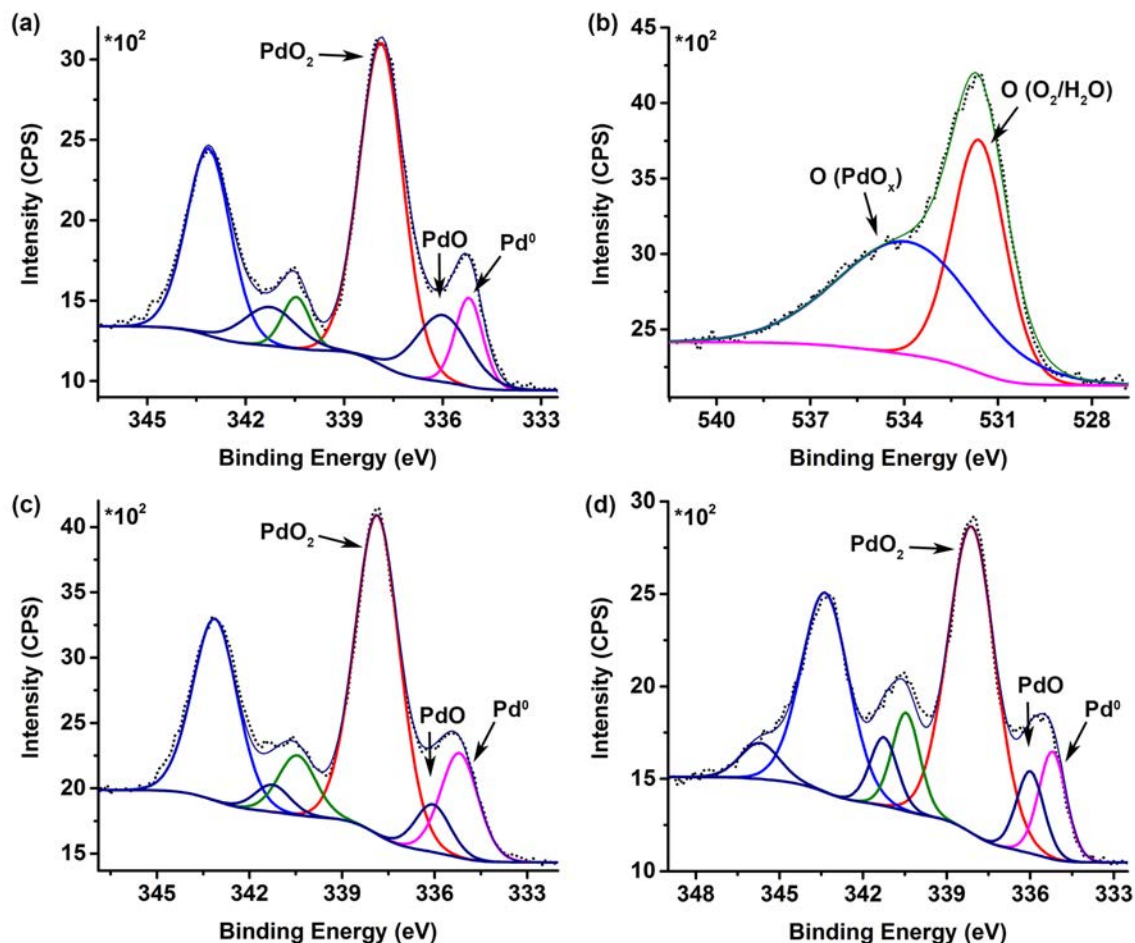

Figure 3.8: The Pd3$d_{5/2}$ (a, c and d), and O1s (b) spectra of the Pd NPs/RNTs in H_2O (a, b), and in MeOH (c, d). The catalyst was aged for 7 days (d). The E_b was calibrated with respect to the C1s peak at 284.8 eV.

3.2.5 Reaction Mechanism and Turnover Frequency (TOF) Calculation

It is widely accepted that the alkene hydrogenation occurs via the Horiuti-Polanyi mechanism on the surface of a heterogeneous catalyst.[10,37-39] This involves the dissociative adsorption of H_2 on to the catalyst surface (Figure 3.9). The hydrogenation of the C=C double bond then takes place in a stepwise fashion. Therefore, it is crucial that

both the H_2 and the C=C double bond co-adsorb on the surface of the NP. However, there is still debate on the nature of the catalysis whether it proceeds via the heterogeneous surface mechanism, or the homogeneous mechanism following the leaching of the metal atoms upon oxidative addition.[39] Earlier, I found that the TEM analysis of the Pd NPs/RNTs catalyst displayed the formation of larger sized NPs after catalysis (Figure 3.4c, d). The increase in the NP size could be due to the aggregation of the smaller sized NPs, influenced by the mechanical stirring during the catalysis. Alternately, the re-deposition of the leached Pd atoms could lead to the increase in the size of the NPs. However, I speculate that it is also possible that both the processes cooperatively influence in the NP size increase after the catalytic event.
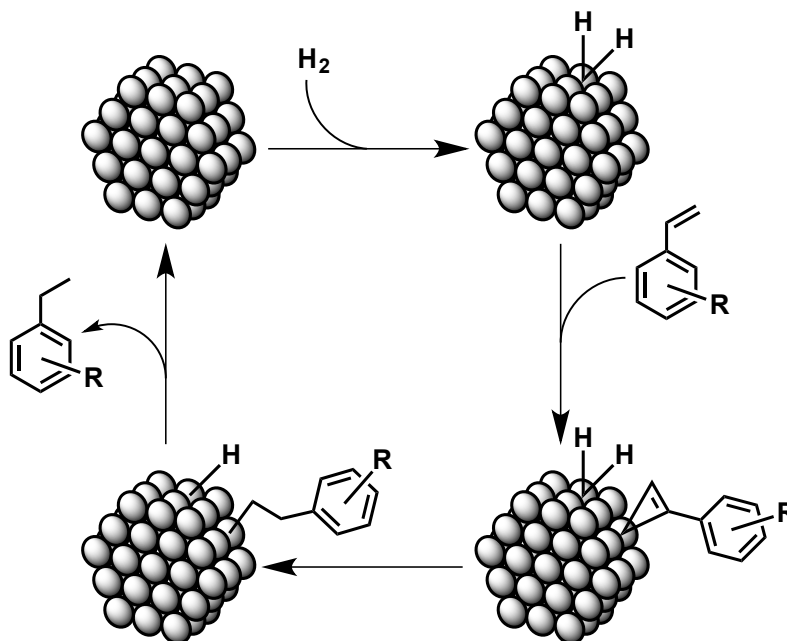
Figure 3.9: Schematic representation of the hydrogenation reaction mechanism driven by the Pd NPs/RNTs.

The attempt to calculate the TOF of the reaction was unsuccessful as the bundling of the Pd NPs/RNTs catalyst caused an unavoidable complication in determining the distribution of the NPs. Because of the bundling effect it is impossible to count the number of NPs present in the system, where a large number of the NPs could be buried under the envelop of the thick layers of the RNTs. In addition, the bimodal distribution of the NPs creates complication in determining the percent contribution of each type of the NPs towards catalysis. However, as discussed in section 3.2.3, I compared the reactivity of our catalyst with a commercially available catalyst, and concluded that our catalyst is as active as the commercial catalyst.

In conclusion, I have demonstrated that Pd NPs/RNTs catalyst could be applied for smooth hydrogenation of styrenes in methanol, methanol/water (50:50 v/v) and ethanol at ambient temperature with a very high conversion. The use of RNT as a support has several advantages: (i) solubility and stability of the Pd NPs in water, therefore allows catalysis in environmentally benign and aqueous solvents, (ii) affords smaller Pd NPs, and (iii) high catalyst recyclability. However, the use of water soluble RNT limits the catalytic application of the Pd NPs/RNTs catalyst in organic solvent. In addition, the stability of the RNT up to 70 °C also limits the reaction temperature below 70 °C.

Experimental

Materials.

3-Methylstyrene, 3-trifluoromethylstyrene, 4-methylstyrene, 4-*tert*-butylstyrene, 4-fluorostyrene, 4-chlorostyrene, 4-benzylchlorostyrene, 4-vinylpyridine and 1-vinylpyrrolidin-2-one were purchased from Sigma-Aldrich.

Instrumentation.

The ^{1}H NMR spectra were measured on a Varian Direct Drive 600 MHz NMR spectrometer in the specified deuterated solvents. The NMR data are presented as follows: chemical shift, peak assignment, multiplicity, coupling constant and integration. The following abbreviations were used to explain the multiplicities (s = singlet, d = doublet, t = triplet, m = multiplet) referenced to the protonated NMR solvent peaks that occur as impurities.

Methods.

Stock solutions of RNTs and K$_2$PdCl$_4$. The stock solutions of the RNTs and the K$_2$PdCl$_4$ were prepared following to the similar procedure under the optimized condition as mentioned in chapter 2.

Catalyst synthesis: Procedure 1. The M NPs/RNTs catalyst (M = Pd, Pt and Au) was prepared prior to the catalytic reaction following the similar procedure as discussed in chapter 2. **Procedure 2.** A mixture of the RNTs (5.0 μmol) and the K$_2$PdCl$_4$ (50.0 μmol) in methanol (1 mL) was stirred at ambient temperature. The resulting solution was then degassed under vacuum and purged with hydrogen (1 atm) for 5 mins to reduce the PdCl$_4^{2-}$ ions. The Pd NPs/RNTs catalyst was characterized by microscopy (SEM and TEM) as well as spectroscopy (UV, CD and XPS) techniques.

Catalytic reaction: General Procedure. To a methanol solution (1 mL) of the Pd

NPs/RNTs catalyst (5 mol%, based on Pd concentration) was added 3-methylstyrene

(132.0 µL, 1.0 mmol) with a syringe. The reaction mixture was then continued to stir at

ambient temperature under hydrogen (1 atm) for 5 h. The hydrogenated products were in

the liquid form and had a very low solubility in methanol. Therefore, upon completion of

the reaction an aliquot (top product layer) was carefully collected by a syringe and

analyzed by ^{1}H NMR spectroscopy in CDCl$_3$, which showed 100% product conversion.

All the reactions were carried out following the similar procedure as mentioned above.

Spectroscopic data.
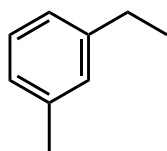
3-Ethyltoluene[40] (**3.2a**) from the catalytic hydrogenation of 3-methylstyrene

(132.0 µL, 1.0 mmol): 100% conversion; ^{1}H NMR (600 MHz, CDCl$_3$): δ 7.28 (m, 1H),

7.11 (m, 3H), 2.72 (q, J = 7.8 Hz, 2H), 2.44 (s, 3H), 1.34 (t, J = 7.8 Hz, 3H).
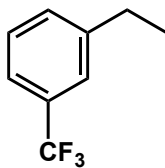

3-(Trifluoromethyl)ethylbenzene[41] (**3.2b**) from the catalytic hydrogenation of 3-

trifluoromethylstyrene (148.0 µL, 1.0 mmol): 9% conversion; ^{1}H NMR (600 MHz,

CDCl$_3$): δ 7.32 (m, 1H), 7.28 (m, 3H), 2.60 (q, J = 7.8 Hz, 2H), 1.15 (t, J = 7.8 Hz, 3H).
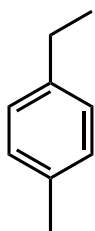
4-Ethyltoluene[4,40] (**3.2c**) from the Catalytic hydrogenation of 4-methylstyrene (132.0 μL, 1.0 mmol): 100% conversion; ^{1}H NMR (600 MHz, CDCl$_3$): δ 7.01 (s, 5H), 2.53 (q, J = 7.8 Hz, 2H), 2.24 (s, 3H), 1.14 (t, J = 7.8 Hz, 3H).
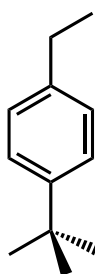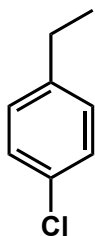

4-*Tert*-butylethylbenzene[41,42] (**3.2d**) from the catalytic hydrogenation of 4-*tert*-butylstyrene (105.0 μL, 1.0 mmol): 100% conversion; ^{1}H NMR (600 MHz, CDCl$_3$): δ 7.18 (d, J = 7.8 Hz, 2H), 7.01 (d, J = 7.8 Hz, 2H), 2.50 (q, J = 7.8 Hz, 2H), 1.18 (s, 9H), 1.10 (t, J = 7.8 Hz, 3H).
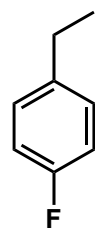
4-Fluoroethylbenzene[43] (**3.2e**) from the catalytic hydrogenation of 4-fluorostyrene (120.0 μL, 1.0 mmol): 100% conversion; ^{1}H NMR (600 MHz, CDCl$_3$): δ 7.03 (dd, J = 6 Hz, 2H), 6.84 (dd, J = 8.4 Hz, 2H), 2.50 (q, J = 7.8 Hz, 2H), 1.10 (t, J = 7.8 Hz, 3H).
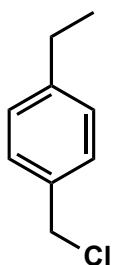
4-Chloroethylbenzene[41] (**3.2f**) from the catalytic hydrogenation of 4-chlorostyrene (128.0 μL, 1.0 mmol): 100% conversion; ^{1}H NMR (600 MHz, CDCl$_3$): δ 7.10 (d, J = 8.4 Hz, 2H), 2.50 (q, J = 7.8 Hz, 2H), 1.10 (t, J = 7.8 Hz, 3H).

4-(Chloromethyl)ethylbenzene[44] (**3.2g**) from the catalytic hydrogenation of 4-(Chloromethyl)styrene (141.0 μL, 1.0 mmol): 85% conversion; ^{1}H NMR (600 MHz, CDCl$_3$): δ 7.20 (d, J = 7.2 Hz, 2H), 7.09 (d, J = 7.2 Hz, 2H), 2.54 (q, J = 7.8 Hz, 2H), 1.13 (t, J = 7.8 Hz, 3H); (3.2c): 15% conversion.
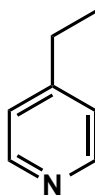
4-Ethylpyridine[45] (**3.4**) from the catalytic hydrogenation of 4-vinylpyridine (106.0 μL, 1.0 mmol): 100% conversion; ^{1}H NMR (600 MHz, CDCl$_3$): δ 8.26 (d, J = 5.4 Hz, 2H), 7.05 (d, J = 5.4 Hz, 2H), 2.54 (q, J = 7.8 Hz, 2H), 1.12 (t, J = 7.8 Hz, 3H).
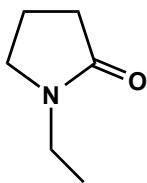
1-Ethylpyrrolidin-2-one[46] (**3.6**) from the catalytic hydrogenation of 1-vinylpyrrolidin-2-one (110.0 μL, 1.0 mmol): 100% conversion; ^{1}H NMR (600 MHz, CDCl$_3$): δ 3.29 (q, J = 7.8 Hz, 2H), 3.18 (quintet, 2H), 2.26 (t, J = 7.8 Hz, 2H), 1.91 (quintet, 2H), 1.00 (t, J = 7.8 Hz, 2H).

3.3 References

(1)   Paradies, J. *Angew. Chem. Int. Ed.* **2014**, *53*, 3552–3557.

(2)   Hounjet, L. J.; Stephan, D. W. *Org. Process Res. Dev.* **2014**, *18*, 385–391.

(3)   Astruc, D. *Nanoparticles and Catalysis*; Weinheim: Wiley-VCH, 2008.

(4)   Nakao, R.; Rhee, H.; Uozumi, Y. *Org. Lett.* **2005**, *7*, 163–165.

(5)   Narayanan, R.; Tabor, C.; El-Sayed, M. A. *Top Catal.* **2008**, *48*, 60–74.

(6)   Pérez-Lorenzo, M. *J. Phys. Chem. Lett.* **2012**, *3*, 167–174.

(7)   Horiuti, I.; Polanyi, M. *Trans. Faraday Soc.* **1934**, *30*, 1164–1172.

(8)   Wang, Z. -J.; Zhou, H. -F.; Wang, T. -L.; He, Y. -M.; Fan, Q. -H. *Green Chem.* **2009**, *11*, 767–769.

(9)   Simakova, I. L.; Semikolenov, V. A. *Kinet. Catal.* **2000**, *41*, 421–425.

(10)   Bhandari, R.; Pacardo, D. B.; Bedford, N. M.; Naik, R. R.; Knecht, M. R. *J. Phys. Chem. C* **2013**, *117*, 18053−18062.

(11)   Karhu, H.; Kalantar, A.; Väyrynen, I. J.; Salmi, T.; Murzin, D. Yu. *Appl. Catal. A* **2003**, *247*, 283−294.

(12)   Badano, J.; Lederhos, C.; L'Argentière, M. Q. P.; Coloma-Pascual, F. *Quim. Nova* **2010**, *33*,48−51.

(13)   Hugon, A.; Delannoy, L.; Louis, C. *Gold Bulletin* **2008**, *41*, 127−138.

(14)   Li; D.; Kaner, R. B. *J. Am. Chem. Soc.* **2006**, *128*, 968−975.

(15)   Moralez, J. G.; Raez, J.; Yamazaki, T.; Motkuri, R. K.; Kovalenko, A.; Fenniri, H. *J. Am. Chem. Soc.* **2005**, *127*, 8307–8309.

(16)   Nakano, T. *Polym. J.* **2010**, *42*, 103–123.

(17)   Tinoco, I. *J. Am. Chem. Soc.* **1960**, *82*, 4785–4790.

(18)   Rohdes, W. *J. Am. Chem. Soc.* **1961**, *83*, 3609–3617.

(19)   Langeveld-Voss, B. M. W.; Janssen, R. A. J.; Meijer, E. W. *J. Mol. Struct.* **2000**, *521*, 285–301.

(20)   Fenniri, H.; Mathivanan, P.; Vidale, K. L.; Sherman, D. M.; Hallenga, K.; Wood, K. V.; Stowell, J. G. *J. Am. Chem. Soc.* **2001**, *123*, 3854–3855.

(21)   Fenniri, H.; Deng, B. -L.; Ribbe, A. E. *J. Am. Chem. Soc.* **2002**, *124*, 11064–11072.

(22)   Hoeben, F. J. M.; Jonkheijm, P.; Meijer, E. W.; Schenning, A. P. H. J. *Chem. Rev.* **2005**, *105*, 1491–1546.

(23)   Gottarelli, G.; Lena, S.; Masiero, S.; Pieraccini, S.; Spada, G. P. *Chirality* **2008**, *20*, 471–485.

(24)   Mateos-Timoneda, M. A.; Crego-Calama, M.; Reinhoudt, D. N. *Chem. Soc. Rev.* **2004**, *33*, 363–372.

(25)   Song, S.; Asher, S. A. *J. Am. Chem. Soc.* **1989**, *111*, 4295–4305.

(26)   Lermo, E. R.; Langeveld-Voss, B. M. W.; Janssen, R. A. J.; Meijer, E. W. *Chem. Commun.* **1999**, 791–792.

(27)   Ma, H.; Lin, D., Liu, H.; Yang, L.; Zhang, L.; Liu, J. Mater. Chem. Phys. 2013, 138, 573–580.

(28)   Pacardo, D. B.; Sethi, M.; Jones, S. E.; Naik, R. R.; Knecht, M. R. *ACS Nano.* **2009**, *3*, 1288–1296.

(29)   Knecht, M. R.; Weir, M. G.; Frenkel, A. I.; Crooks, R. M. *Chem. Mater.* **2008**, *20*, 1019–1028.

(30)   Creighton, J. A.; Eadon, D. G. *J. Chem. Soc., Faraday Trans.* **1991**, *87*, 3881–
        3891.

(31)   Lacaze, E.; Urdal, K.; Bodö, P.; Garbarz, J.; Salaneck, W. R.; Schott, M. *J.
        Polym. Sci., Part B: Polym. Phys.* **1993**, *31*, 111–114.

(32)   Fischer, A. Krozer, A. Schlapbach, L. *Surf. Sci.* **1992**, *269*, 737–742.

(33)   Tura J. M.; Regull P.; Victori L.; Dolors D. C. M. *Surf. Interface Anal.* **1988**, *11*,
        447–449.

(34)   Shafeev G. A.; Themlin J. -M.; Bellard L.; Marine W.; Cros A. *J. Vac. Sci.
        Technol. A* **1996**, *14*, 319–326.

(35)   Kim, K. S.; Gossmann, A. F.; Winograd, N. *Anal. Chem.* **1974**, *46*, 197–200.

(36)   Kibis, L. S.; Stadnichenko, A. I.; Koscheev, S. V.; Zaikovskii, V. I.; Boronin, A.
        I. *J. Phys. Chem. C* **2012**, *116*, 19342–19348.

(37)   Wilson, O. M.; Knecht, M. R.; Garcia-Martinez, J. C.; Crooks, R. M *J. Am. Chem.
        Soc.* **2006**, *128*, 4510–4511.

(38)   Cremer, P. S.; Somorjai, G. A. *J. Chem. Soc., Faraday Trans.* **1995**, *91*,
        3671−3677.

(39)   Astruc, D. *Organometallic Chemistry and Catalysis: Heterogeneous Catalysis*;
        Springer, 2007, Chapter 20.

(40)   Krüger, T.; Vorndran, K.; Linker, T. *Chem. Eur. J.* **2009**, *15*, 12082–12091.

(41)   MacNair, A. J.; Tran, M. -M.; Nelson, J. E.; Sloan, G. U.; Ironmonger, A.;
        Thomas, S. P. *Org. Biomol. Chem.* **2014**, *12*, 5082–5088.

(42)   Imada, Y.; Iida, H.; Kitagawa, T.; Naota, T. *Chem. Eur. J.* **2011**, *17*, 5908–5920.

(43) Verho, O.; Nagendiran, A.; Johnston, E. V.; Tai, C. -W.; Bäckvall, J. -E. *ChemCatChem* **2013**, *5*, 612–618.

(44) Hu, Y. L.; Ge, Q.; He, Y.; Lu, M. *ChemCatChem* **2010**, *2*, 392–396.

(45) Brunel, J. M. *Tetrahedron* **2007**, *63*, 3899–3906.

(46) Martín, C.; Belderraín, T. R.; Pérez, P. J. *Org. Biomol. Chem.* **2009**, *7*, 4777–4781.

Chapter 4

## Cross-coupling Catalysis

4.1 Introduction

In recent years, the NPs emerged as an attractive alternative to the molecular catalysts for a wide variety of organic reactions because of their high surface-to-volume ratio and very reactive surface atoms.[1-5] In particular, compared to other transition metal nanoparticles, Pd NPs have been extensively studied in catalysis. Therefore, the catalytic activity of the Pd NPs towards the hydrogenation and the C–C bond formation reactions is well documented.[1-17] Though a variety of different cross-coupling reactions are available in the literature, the Suzuki-Miyaura cross-coupling reaction is one of the most effective methods for synthesizing biaryl precursors suitable for the production of drugs, agrochemicals, fine chemicals, ionic liquids and polymers.[12,18-23]

R$_1$ = R$_2$ = Functional groups
X = I, Br and Cl
Y = Boronic acid and acid esters
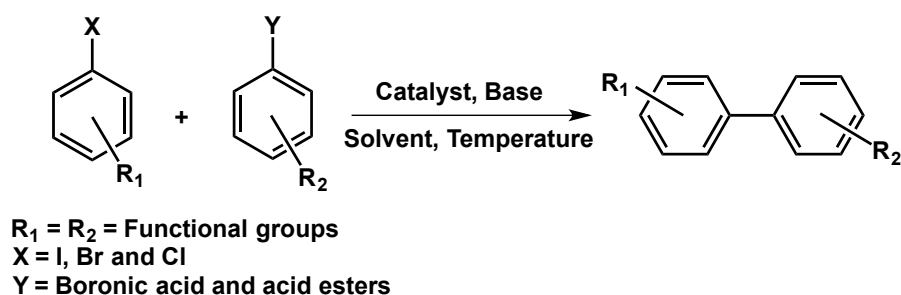
Figure 4.1: An example of a Suzuki-Miyaura cross-coupling reaction.

Recently, numerous techniques have been demonstrated for the synthesis of catalytic Pd NPs supported on oxides such as silicas, aluminas and other metal oxides, or in the forms of carbon supports including carbon nanotubes.[1-17] However, the reaction was either carried out in organic solvents[16] or aqueous solutions at high temperature[6-17]

and suffered from high catalytic recyclability.[6-17] In contrast, only a few examples of the biosupported Pd NPs for catalysis have been documented, which further provides a medium for phosphine free catalysis in the aspects of the *Green Chemistry*.[7,8] Very recently, Knecht and coworkers demonstrated an aqueous Stille cross-coupling reaction by using peptide-functionalized Pd NPs and could obtain a very good turnover frequency (TOF) for the reaction.[7,8]

R = OH and COOH
X = I, Br and Cl
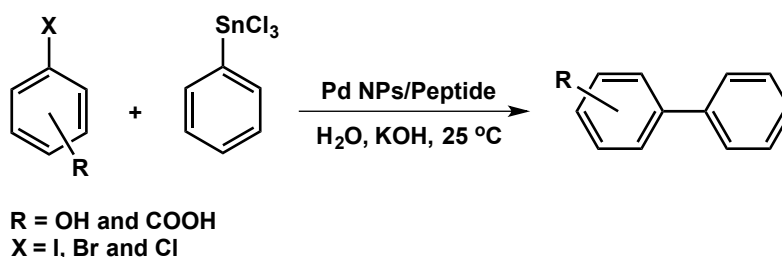
Figure 4.2: Stille cross-coupling reactions demonstrated by Knecht and coworkers.[7,8]

Detailed reaction mechanism studies suggested that the coupling reaction occurred via the Pd atom leaching upon oxidative addition of the aryl halides.[8] In addition, they also found that the modification of the peptide chains had significant impact on the size and the catalytic activity of the Pd NPs catalysts.[24-27] Later, Knecht and coworkers also investigated the reactivity of their catalyst towards the Suzuki-Miyaura cross-coupling reaction.[28] They found that the nature of the base and their concentration plays a vital role in the product yield.[28]

To this end, I developed RNT supported M NPs (M = Au, Pd and Pt), which are water-soluble.[29] Because of their stability and solubility in water, they could catalyze the reaction at the interface between homogeneous and heterogeneous condition. As discussed in chapter 3, I successfully employed our M NPs/RNTs (M = Au, Pd and Pt) catalyst towards olefin hydrogenation. The results suggest that our catalyst is very active for olefin hydrogenation and their catalytic activity is comparable with the leading

commercial catalysts. Following our previous success on the hydrogenation catalysis, herein this chapter, I report the scope of our M NPs/RNTs (M = Au, Pd and Pt) catalyst for the Suzuki-Miyaura cross-coupling reaction of different halide and boronic acid substrates. In addition, the utility of this catalyst for producing drug and agrochemical intermediates as well as organic materials (solar cell, OLED and sensor) by the cross-coupling reaction is also investigated.
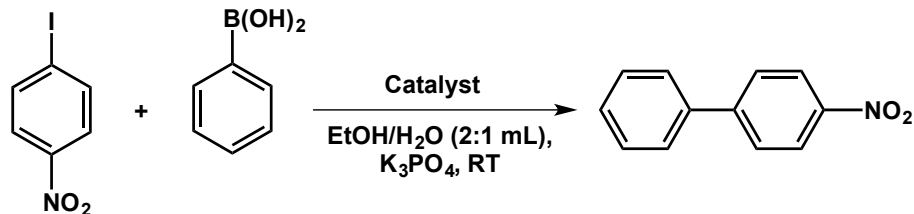
4.2 Results and Discussion

4.2.1 Optimization of the Suzuki Coupling Reaction

Initially for the reaction optimization, I employed 1 mol% of the Pd NPs/RNTs catalyst for the coupling reaction of 1-iodo-4-nitrobenzene and phenylboronic acid (Table 4.1, scheme). Previously, it was observed that the catalytic activity of a catalyst for the Suzuki coupling reaction was strongly dependent on the nature of the base and the substrate ratio.[28,30,31] Though the most commonly used bases include K_2CO_3, K_3PO_4, KOH and KF, the choice of the base is still empirical and no specific selection is established to date.[31] The key role of the base is to facilitate the slow transmetalation step either by – forming a more reactive boronate species, which can interact with the Pd center, or replacing the halide in the coordination sphere of the palladium complex prior to the intramolecular transmetalation.[31] Therefore, to probe the reactivity of the Pd NPs/RNTs catalyst for the Suzuki coupling, three different bases such as KOH, K_2CO_3 and K_3PO_4 were selected, and the concentration of phenylboronic acid was varied with respect to the concentration of 1-iodo-4-nitrobenzene. The Pd NPs/RNTs catalyst was synthesized by following the same protocol as discussed in chapter 3. In brief, the Pd NPs/RNTs catalyst was prepared either by the reduction of the $PdCl_4^{2-}$ ions with H_2 in the

presence of the RNTs prior to the catalytic reaction, or by the overnight incubation of the RNTs and the $PdCl_4^{2-}$ solutions. Although the use of KOH led to the formation of the desired coupling products for other catalytic systems, the reaction did not occur for the RNTs/Pd-NPs catalyst (Table 4.1, entry 1 and 2).[7,8,32] On the other hand, the reaction was found to be very efficient leading to the quantitative conversion of the coupling product in the presence of both K_2CO_3 and K_3PO_4 (Table 4.1, entry 3 and 4). Very recently, Knecht *et al.* also reported that the Suzuki coupling reaction did not occur at higher KOH concentrations (>0.75 M) in presence of the Pd NPs/Peptide catalyst. They suggested that perhaps KOH was significantly influencing the overall reaction especially at the transmetalation step.[28] Though the reaction gave quantitative conversion of the coupling product in the presence of both K_2CO_3 and K_3PO_4, I decided to use K_3PO_4 to further optimize the reaction condition. Later, I investigated the effect of the phenylboronic acid concentration on the coupling product yield. The studies suggested that the conversion of the corresponding biaryl product increased with increasing the substrate ratio and a minimum substrate ratio of 1:2 was required to obtain 100% coupling product conversion in 4 h at ambient temperature (Table 4.1, entries 4-7).[30] I also observed that the coupling reaction was faster for a substrate ratio of 1:2.5, which completed in 2 h (Table 4.1, entry 7). It is well documented that often excess arylboronic acid is required in the Suzuki coupling reaction because of protodeboronation under hydroxylic conditions such as in aqueous solutions. However, I did not observe any protodeboronation of the phenylboronic acid in our system. Therefore, I hypothesize that the excess amount of the phenylboronic acid perhaps facilitates the transmetalation step.

To compare the reactivity with the Pd NPs/RNTs catalyst, I investigated the catalytic activity of the Pd NPs in the absence of the RNTs. Under optimized conditions, the Pd NPs (1 mol%) catalyzed reaction afforded less than 5% coupling product conversion (Table 4.1, entry 8). This result indicates that the stability of the Pd NPs in solution is crucial for high product conversion, and agrees well with the earlier observation regarding the hydrogenation reaction discussed in chapter 3. Interestingly, the Pd NPs/RNTs catalyst, synthesized by overnight incubation- was determined to be as active as the catalyst prepared by the hydrogen reduction prior to the catalytic reaction (Table 4.1, entry 9). This observation is contrary to the hydrogenation reaction as discussed in chapter 3. I hypothesize that the presence of K_3PO_4 in the solution could enhance the leaching of the Pd species from the surface of the RNTs. The TEM images of the Pd NPs/RNTs catalyst discussed in section 4.3.3, which was synthesized by the hydrogen reduction showed bimodal distribution of the Pd NPs (Figure 4.8d). Because of this bimodal distribution, it is hard to predict the reactivity of the Pd NPs located into the nucleation pockets with respect to the Pd NPs formed on the surface of the RNTs bundle. Previously, the model studies of the Au NPs/RNTs composite suggested that a maximum of 30% loading of the Au NPs is possible on the surface of the RNTs.[29] However, I use 10-fold excess of the $PdCl_4^{2-}$ ions with respect to the RNTs concentration to synthesize the Pd NPs/RNTs catalyst. Therefore upon reduction with hydrogen, the excess $PdCl_4^{2-}$ ions form larger sized Pd NPs on the surface of the RNTs bundle after completion of the 30% loading. Considering this, I carried out a reaction by using the Pd NPs/RNTs catalyst, where the ratio of the RNTs and the $PdCl_4^{2-}$ ions was adjusted based on the 30% loading of the Pd NPs (Table 4.1, entry 10).

Table 4.1: Optimization of the Suzuki-Miyaura cross coupling reaction[a]

Reaction scheme: 4-iodonitrobenzene (NO_2 substituent) + phenylboronic acid $B(OH)_2$ → with Catalyst, EtOH/H_2O (2:1 mL), K_3PO_4, RT → 4-nitrobiphenyl (NO_2).

Entry	Catalyst	Substrate ratio	Base	Reaction duration (h)	Convn.[b] (%)
1	Pd NPs/RNTs	1:1.5	KOH	24	0
2	Pd NPs/RNTs	1:2	KOH	4	0
3	Pd NPs/RNTs	1:3	K_2CO_3	24	100
4	Pd NPs/RNTs	1:3	K_3PO_4	24	100
5	Pd NPs/RNTs	1:2	K_3PO_4	4	100
6	Pd NPs/RNTs	1:1.5	K_3PO_4	4	56
7	Pd NPs/RNTs	1:2.5	K_3PO_4	2	100
8	Pd NPs	1:2	K_3PO_4	4	<5
9	Pd NPs/RNTs[c]	1:2	K_3PO_4	4	100
10	Pd NPs/RNTs[c,d]	1:2	K_3PO_4	4	100
11[g]	Pd NPs/RNTs[e]	1:2	K_3PO_4	14	100
12[h]	Pd NPs/RNTs[f]	1:2	K_3PO_4	24	68

[a] Reaction conditions: 1 mol% of catalyst (prepared by H_2 reduction) in ethanol/H_2O (2:1 mL), Base (KOH = 112 mg; K_2CO_3 = 276 mg; and K_3PO_4 = 425 mg) under N_2 unless otherwise noted. [b] Determined by ^1H NMR. [c] Prepared by overnight incubation. [d] Based on the 30% loading of the Pd NPs onto the RNTs. [e] 0.1 mol% of catalyst. [f] 0.01 mol% of catalyst.

The ratio adjustment greatly reduced the possibility of the Pd NPs formation on the surface of the RNTs bundle. Though I increased the concentration of the RNTs, the Pd loading was maintained 1 mol% with respect to the substrate. Finally, the Pd NPs/RNTs catalyst was reduced by hydrogen prior to the catalytic reaction after the overnight incubation. The reaction resulted in quantitative biaryl product conversion. This suggested that the Pd NPs located into the nucleation pockets on the surface of the RNTs are equally active as the Pd NPs present on the surface of the RNTs bundle. As speculated earlier, perhaps the K_3PO_4 plays a vital role in unloading and/or leaching of the Pd species from the nucleation pocket of the RNTs. In addition, I also investigated the effect of the Pd NPs/RNTs catalyst loading on the coupling reaction. Under the optimized conditions, the coupling reaction of 1-iodo-4-nitrobenzene and phenylboronic acid gave quantitative product conversion in 14 h for a catalyst loading of 0.1 mol% (Table 4.1, entry 11). The result suggested that though I could achieve quantitative conversion, the reaction took longer time for completion. Later, I further reduced the catalyst loading to 0.01 mol% for the same reaction, which gave 68% of the coupling product conversion in 24 h (Table 4.1, entry 12). The studies concluded that our catalyst is very active where the loading could be reduced to as low as 0.01 mol% with increased reaction time.

4.2.2 Exploration of the Suzuki Coupling Reaction

4.2.2.1 Reactivity of the Aryl Iodides

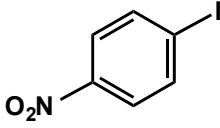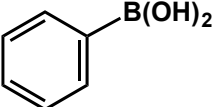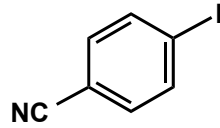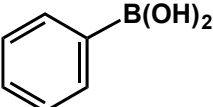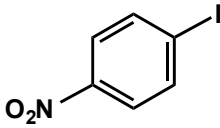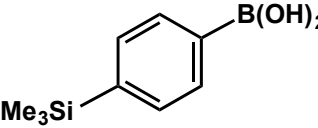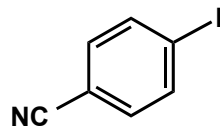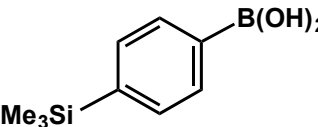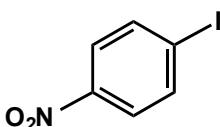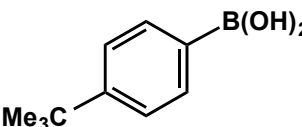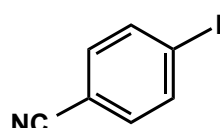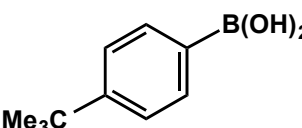Under the optimized reaction conditions, a variety of different aryl iodides containing electron withdrawing groups- and arylboronic acids were employed for the cross-coupling reaction using 1 mol% Pd NPs/RNTs catalyst in a EtOH/H_2O (2:1 mL) solvent mixture at ambient temperature under N_2 (Scheme 4.1). In general, the aryl iodide

substrates readily underwent the coupling reaction leading to high product conversion (87-100%). Though 2-iodobenzonitrile gave quantitative coupling product conversion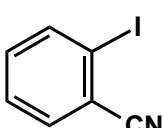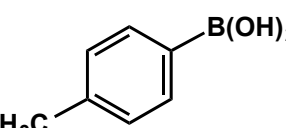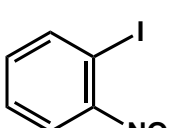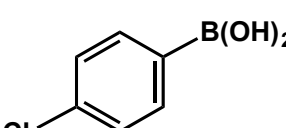, 1-iodo-2-nitrobenzene did not react with the corresponding arylboronic acid at ambient temperature. However, the same reaction of 1-iodo-2-nitrobenzene was found to be very efficient at 40 °C. leading to 100% product conversion in 24 h. I investigated the electron withdrawing inductive effect of the 4-NO$_2$ and 4-CN groups on the reactivity of the aryl iodides with arylboronic acids containing 4-H, 4-SiMe$_3$ and 4-CMe$_3$ groups. Interestingly, though it is well accepted that the NO$_2$ group is more electron withdrawing than the CN group, I found quantitative coupling product conversion in all cases for 4-iodobenzonitrile. Whereas for 1-iodo-4-nitrobenzene, the coupling product conversion varied with different arylboronic acids (4-H, 100%; 4-SiMe$_3$, 87%; and 4-CMe$_3$, 92%).

R$_1$ = 2/4-NO$_2$ and 2/4-CN
R$_2$ = H, CH$_3$, CMe$_3$, SiMe$_3$ and Cl
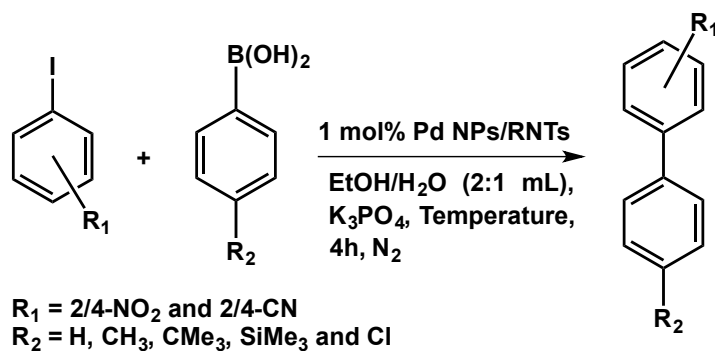
Scheme 4.1: The Suzuki-Miyaura cross coupling reactions of aryl iodides and arylboronic acids at ambient temperature in 4 h (except the reaction of 1-iodo-2-nitrobenzene and 4-chloro benzene boronic acid at 40 °C in 24 h). The % conversions are listed in Table 4.2.
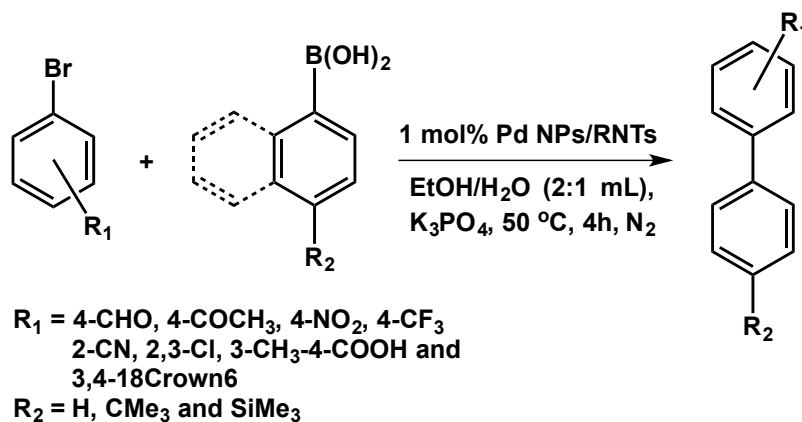
Table 4.2: The Suzuki-Miyaura cross coupling of aryl iodides and arylboronic acids[a,b]

Entry	Aryl iodides	Arylboronic acids	Convn.[c] (%)
1	O_2N—C$_6$H$_4$—I	C$_6$H$_5$—B(OH)$_2$	100
2	NC—C$_6$H$_4$—I	C$_6$H$_5$—B(OH)$_2$	100
3	O_2N—C$_6$H$_4$—I	Me_3Si—C$_6$H$_4$—B(OH)$_2$	87
4	NC—C$_6$H$_4$—I	Me_3Si—C$_6$H$_4$—B(OH)$_2$	100
5	O_2N—C$_6$H$_4$—I	Me_3C—C$_6$H$_4$—B(OH)$_2$	92
6	NC—C$_6$H$_4$—I	Me_3C—C$_6$H$_4$—B(OH)$_2$	100
8	2-iodo-benzonitrile (CN)	H_3C—C$_6$H$_4$—B(OH)$_2$	100
9[d]	2-iodo-nitrobenzene (NO_2)	Cl—C$_6$H$_4$—B(OH)$_2$	100

[a] Reaction conditions: Aryl iodides (0.5 mmol), arylboronic acids (1.0 mmol), 1 mol% of Pd NPs/RNTs catalyst in EtOH/H$_2$O (2:1 mL), K$_3$PO$_4$ (425 mg), 4 h, ambient temperature and under N$_2$. [b] Catalyst was prepared by H$_2$ reduction prior to the reaction. [c] Determined by ^{1}H NMR. [d] 24 h and 40 °C.

Later, I explored the scope of the Suzuki coupling reaction for a wide variety of aryl bromides and arylboronic acids (Scheme 4.2 and Table 4.3). Under the optimized conditions for aryl iodides, an initial reaction of 4-bromobenzaldehyde and phenylboronic acid did not afford any coupled product (not listed in Table 4.3). Therefore, as aryl bromides are less reactive than aryl iodides, I raised the reaction temperature to 50 °C to facilitate the reaction.[33] Fortunately, this modification resulted in quantitative coupling product conversion in 24 h. Following this newly optimized condition, I continued performing coupling reactions of different aryl bromides and arylboronic acids (Scheme 4.2 and Table 4.3). In general, the reactions showed a wide tolerance of the functional groups on the reactivity of both the aryl bromides and arylboronic acids.
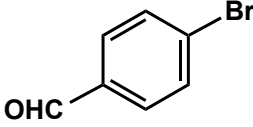

R_1 = 4-CHO, 4-COCH$_3$, 4-NO$_2$, 4-CF$_3$
2-CN, 2,3-Cl, 3-CH$_3$-4-COOH and
3,4-18Crown6
R_2 = H, CMe$_3$ and SiMe$_3$
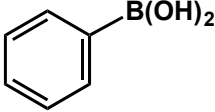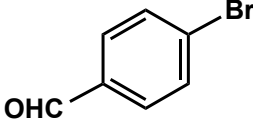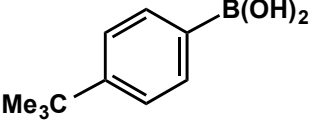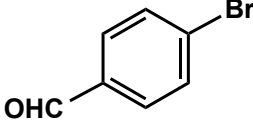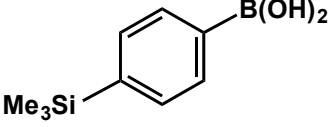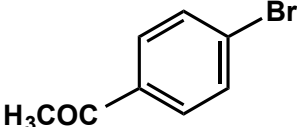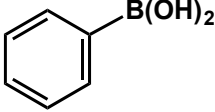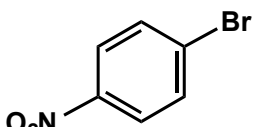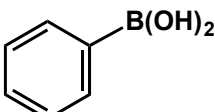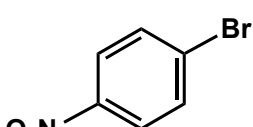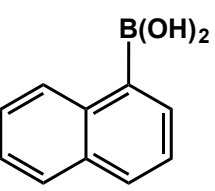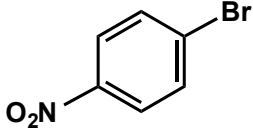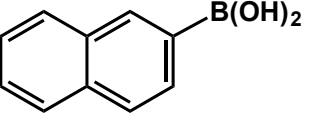
Scheme 4.2: The Suzuki-Miyaura cross coupling reactions of aryl bromides and arylboronic acids at 50 °C in 24 h. The % conversions are listed in Table 4.3.

The reactions of 4-bromobenzaldehyde with different arylboronic acids containing 4-H, 4-SiMe$_3$ and 4-CMe$_3$ groups, revealed that the reactivity of the arylboronic acid decreased in the order of 4-H>4-SiMe$_3$>4-C(Me)$_3$ (Table 4.3, entries 1-3). To study the effect of the steric hindrance of the naphthalene ring, I performed the
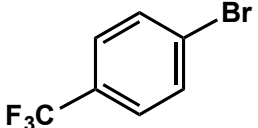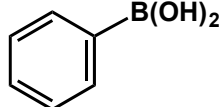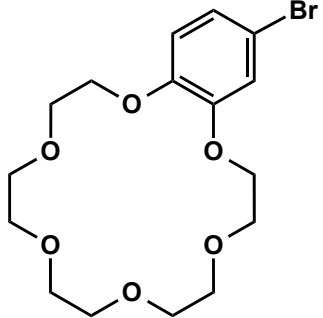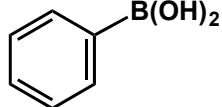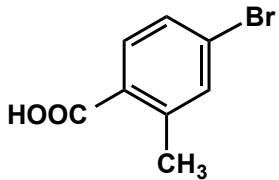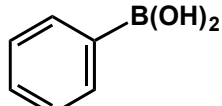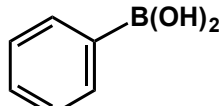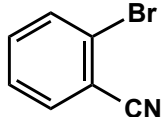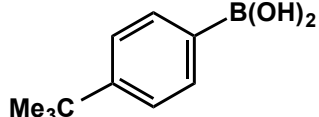
reactions of 1-bromo-4-nitrobenzene with 1-naphthylboronic acid and 2-naphthylboronic acid. Interestingly, both the reactions gave 100% coupling product conversion in 24 h (Table 4.3, entry 6 and 7). This result suggested that the reactivity is independent of the position of the boronic acid in the naphthalene ring. It should be noted that the aryl bromides were equally active in the presence of both 4-CHO and 4-COCH$_3$ groups, which afforded quantitative coupling product conversion (Table 4.3, entries 1-4). In addition, the *ortho* substituted aryl bromides smoothly underwent coupling reaction with the corresponding arylboronic acids leading to 100% product conversion (Table 4.3, entry 11 and 12). To achieve chemoselective Suzuki cross-coupling of bromochloro-benzene, a reaction of 1-bromo-2,3-dichlorobenzene and phenylboronic acid was carried out. The reaction resulted in only the mono-coupling product through the selective C-Br bond activation under the optimized conditions at 50 °C (Table 4.3, entry 11).[34,35]

Table 4.3: The Suzuki-Miyaura cross coupling of aryl bromides and arylboronic acids[a,b]

Entry	Aryl bromides	Arylboronic acids	Convn.[c] (%)
1	4-Br-C$_6$H$_4$-CHO (OHC)	C$_6$H$_5$-B(OH)$_2$	96
2	4-Br-C$_6$H$_4$-CHO (OHC)	4-Me$_3$C-C$_6$H$_4$-B(OH)$_2$	36
3	4-Br-C$_6$H$_4$-CHO (OHC)	4-Me$_3$Si-C$_6$H$_4$-B(OH)$_2$	77
4	4-Br-C$_6$H$_4$-COCH$_3$ (H$_3$COC)	C$_6$H$_5$-B(OH)$_2$	100
5	4-Br-C$_6$H$_4$-NO$_2$ (O$_2$N)	C$_6$H$_5$-B(OH)$_2$	100
6	4-Br-C$_6$H$_4$-NO$_2$ (O$_2$N)	1-naphthyl-B(OH)$_2$	100
7	4-Br-C$_6$H$_4$-NO$_2$ (O$_2$N)	2-naphthyl-B(OH)$_2$	100

[a] Reaction conditions: Aryl bromides (0.5 mmol), arylboronic acids (1.0 mmol), 1 mol% of Pd NPs/RNTs catalyst in EtOH/H$_2$O (2:1 mL), K$_3$PO$_4$ (425 mg), 24 h, 50 °C and under N$_2$. [b] Catalyst was prepared by H$_2$ reduction prior to the reaction. [c] Determined by ^{1}H NMR.

Table 4.3: Continued[a,b]

Entry	Aryl bromides	Arylboronic acids	Convn.[c] (%)
8			100
9			56
10			84
11			100
12			100

[a] Reaction conditions: Aryl bromides (0.5 mmol), arylboronic acids (1.0 mmol), 1 mol% of Pd NPs/RNTs catalyst in EtOH/H_2O (2:1 mL), K_3PO_4 (425 mg), 24 h, 50 °C and under N_2. [b] Catalyst was prepared by H_2 reduction prior to the reaction. [c] Determined by ^{1}H NMR.

4.2.2.3 Reactivity of the Aryl Dihalides

In recent years, a sequential double C-C cross-coupling of aryl dihalides attracted much attention for the synthesis of unsymmetrically substituted arenes due to their potential applications in the pharmaceutical, fungicide and materials industries.[34-45] Achieving selectivity in mono-coupling over bis-coupling product formation is important for many of its applications.[41] Considering this, I performed the reactions of 1-bromo-4-iodobenzene with phenylboronic acid at ambient temperature and 50 °C for 4 h (Scheme 4.3a, Table 4.4, entry 1). Previously, several authors reported that the coupling reactions of bromoiodoarenes took place in a stepwise fashion because of the two very different reactivities of the C-I and C-Br bonds tow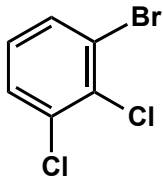ards the oxidative addition reaction.[36-38] Hence, as the mechanism of the reaction was realized, our focus was to investigate the temperature effect on the mono- vs bis-coupling product distribution. While the reaction at ambient temperature gave a mono- vs bis-coupling product distribution of 58:42, the reaction at 50 °C afforded a product distribution of 18:82 (Table 4.4, entry 1). These results suggested that the temperature increase favoured the bis-coupling over the mono-coupling product formation.

Later, I studied the reactivity of different arylboronic acids with 2,6-dibromonaphthalene (Scheme 4.3b, Table 4.4, entries 2-6).[39,40,43] Towards the bis-coupling product formation, the reactivity of different arylboronic acid decreased in the order of 4-H>4-SiMe$_3$>4-C(Me)$_3$ leading to 100%, 86% and 67% conversion, respectively (Table 4.4, entries 2-4). These findings are in good agreement with our previous observations (Table 4.3, entries 1-3). However, I only investigated the bis-coupling product formation for those reactions.
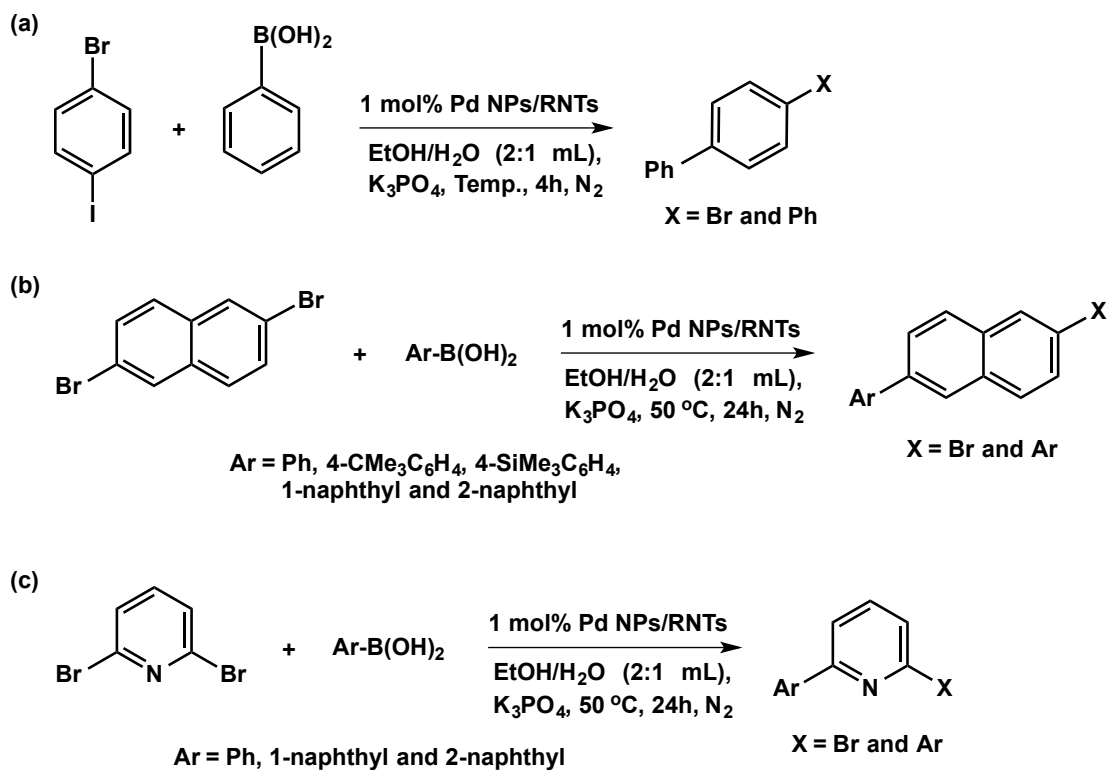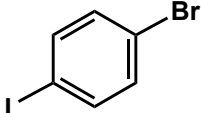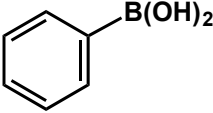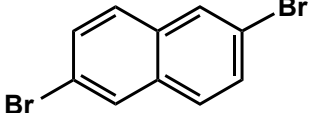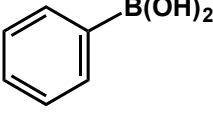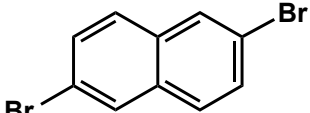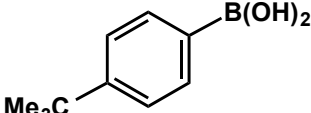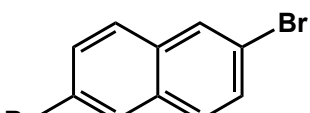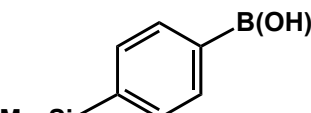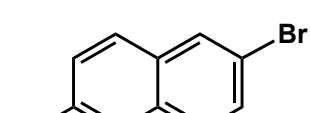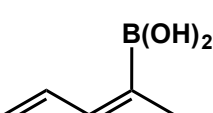
Scheme 4.3: The Suzuki-Miyaura cross coupling reactions of aryl dihalides and arylboronic acids (a-c) at ambient temperature and 50 °C (a). The % conversions are listed in Table 4.4.

Another study showed that the position of the boronic acid in the naphthalene ring played a vital role in dictating the mono- vs bis-coupling product distribution with 2,6-dibromonaphthalene. Therefore, the reaction of 1-naphthalene boronic acid and 2,6-dibromonaphthalene gave a product distribution of 57:43 (Table 4.4, entry 5). On the other hand, the reaction of 2-naphthalene boronic acid and 2,6-dibromonaphthalene afforded the mono-coupling product in almost quantitative conversion (Table 4.4, entry 6). As pyridine is found at the core of many industrially important compounds including pharmaceuticals and materials, I also investigated the reactivity of 2,6-dibromopyridine with different arylboronic acids (Scheme 4.3c, Table 4.4, entries 7-9).[45] While the reaction of 2,6-dibromopyridine and phenylboronic acid gave quantitative bis-coupling
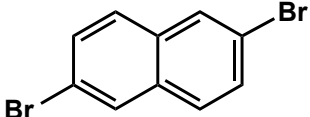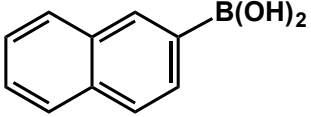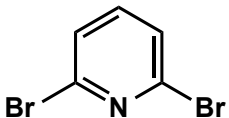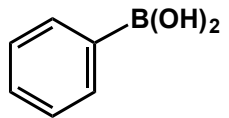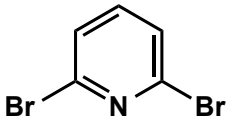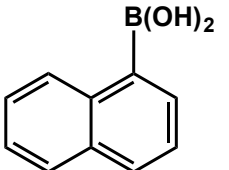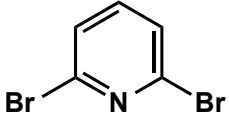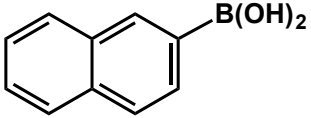
product conversion, the reactions with 1-naphthalene boronic acid and 2-naphthalene boronic acid yielded a product distributions of 33:5 and 86:14, respectively (Table 4.4, entries 7-9).

Table 4.4: The Suzuki-Miyaura cross coupling of aryl dihalides and arylboronic acids[a,b]

Entry	Aryl dihalides	Arylboronic acids	convn.[c] (%)	
			MC	BC
1	(4-bromo-iodobenzene) Br, I	$B(OH)_2$	58^d / 18^e	42^d / 82^e
2	(2,6-dibromonaphthalene) Br, Br	$B(OH)_2$	-	100
3	(2,6-dibromonaphthalene) Br, Br	Me_3C—$B(OH)_2$	-	67
4	(2,6-dibromonaphthalene) Br, Br	Me_3Si—$B(OH)_2$	-	86
5	(2,6-dibromonaphthalene) Br, Br	(1-naphthalene) $B(OH)_2$	57	43

[a] Reaction conditions: Aryl dihalides (0.5 mmol), arylboronic acids (1.5 mmol), 1 mol% of Pd NPs/RNTs catalyst in EtOH/H_2O (2:1 mL), K_3PO_4 (425 mg), 24 h, 50 ^{o}C and under N_2. [b] Catalyst was prepared by H_2 reduction prior to the reaction. [c] Determined by ^1H NMR. [d] At ambient temperature. [e] At 50 °C. MC = mono coupled, BC = bis coupled.

Table 4.4: Continued[a,b]

Entry	Aryl dihalides	Arylboronic acids	convn.[c] (%)	
			MC	BC
6	Br, Br (dibromonaphthalene)	B(OH)$_2$ (naphthylboronic acid)	>98	Trace
7	Br, N, Br (2,6-dibromopyridine)	B(OH)$_2$ (phenylboronic acid)	-	100
8	Br, N, Br (2,6-dibromopyridine)	B(OH)$_2$ (1-naphthylboronic acid)	33	5
9	Br, N, Br (2,6-dibromopyridine)	B(OH)$_2$ (2-naphthylboronic acid)	86	14

[a] Reaction conditions: Aryl dihalides (0.5 mmol), arylboronic acids (1.5 mmol), 1 mol% of Pd NPs/RNTs catalyst in EtOH/H$_2$O (2:1 mL), K$_3$PO$_4$ (425 mg), 24 h, 50 °C and under N$_2$. [b] Catalyst was prepared by H$_2$ reduction prior to the reaction. [c] Determined by ^{1}H NMR. MC = mono coupled, BC = bis coupled.

4.2.2.4 Catalyst Recycling, Scale up Reaction and Reactivity Comparison

The feasibility of recycling the Pd NPs/RNTs catalyst was examined on the model reaction of 1-iodo-4-nitrobenzene and phenylboronic acid. To accomplish that, after each cycle of the completed reaction, the product was extracted with diethylether. Then the next cycle was loaded with the original aqueous layer containing the catalyst and the base, fresh ethanol and the reactants under the optimized conditions. The recycling experiments were repeated up to the 10th cycle, and interestingly, each cycle showed

quantitative coupling product conversion. These results suggested that our catalyst could be reused at least ten times without apparent loss of any catalytic activity. The high activity of the Pd NPs/RNTs catalyst could be rationalized from the fact of efficient re-deposition of the leached Pd species onto the surface of RNTs after the event of catalysis (Figure 4.3).[46] This indicates that the RNTs play a vital role in stabilizing the Pd NPs in solution and preventing the precipitation of the leached Pd species as Pd black after the catalytic event.[46]

ArX

Leaching

Ar

X

ArX

Pd^0

Redeposition

Pd NPs/RNTs

Ar-Ar'
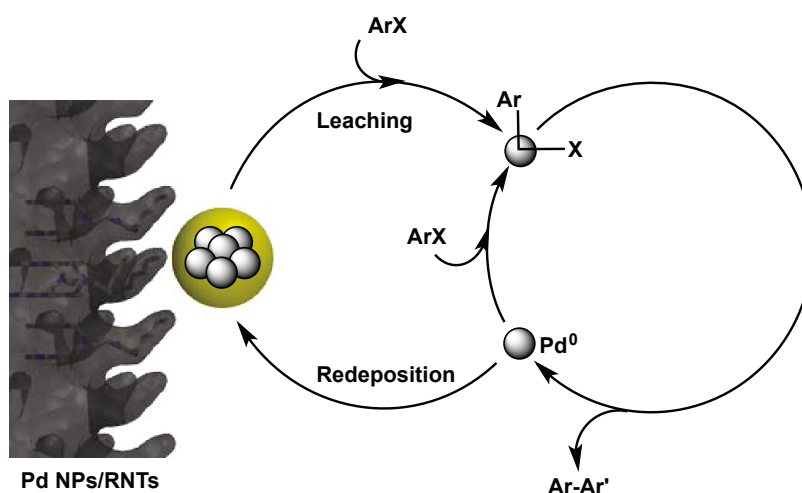
Figure 4.3: Schematic representation of the leaching and re-deposition of Pd species on the surface of the RNTs.

I also evaluated the compatibility of our catalyst for the large-scale production of the coupling product. For the scale-up reaction, again I loaded the reaction with 1-iodo-4-nitrobenzene and phenylboronic acid. Initially, I scaled up the reaction by 5 times and performed the reaction under the optimized conditions. Unfortunately, the reaction gave the coupling product in 17% isolated yield. As the reactivity of a catalyst could vary from the laboratory scale to the mass production, I modified the conditions by (i) increasing the reaction temperature to 40 °C, and (ii) reducing the ratio of the ethanol/water mixture to

1:1 (v/v). Fortunately, the modification led to quantitative coupling product conversion with an isolated product yield of 96%. Under the modified conditions, the reaction was further scaled up to 50 times, which afforded the expected coupling product in 95% yield.

For comparative studies, I also investigated the reactivity of the Pt NPs/RNTs and Au NPs/RNTs catalysts for the cross-coupling reaction under the optimized conditions to that of the Pd NPs/RNTs catalyst. In both cases, the Pt NPs/RNTs and Au NPs/RNTs catalysts remained catalytically inactive towards the coupling reaction.

4.3 Applied Suzuki Coupling Reaction

4.3.1 Drug and Agrochemical Intermediates

The utility of the Pd NPs/RNTs catalyst was also investigated for the synthesis of the drug intermediates of sartan (Scheme 4.4a) and NPY-5 (Scheme 4.4c) receptor antagonist, and an agrochemical intermediate of boscalid fungicide (Scheme 4.4b).[47] Initial attempts to synthesize the sartan intermediate from the reaction of 2-bromobenzonitrile and p-tolylboronic acid at ambient temperature as well as prolonged heating at 50 ^{o}C were unsuccessful. When 2-iodobenzonitrile was used for the similar reaction, it gave 100% coupling product conversion at ambient temperature and the isolated yield was 82% (Scheme 4.4a; Table 4.2, entry 8). Previously, the same sartan intermediate was synthesized from high temperature catalytic reaction either by microwave or conventional heating method. [20,21,23] On the other hand, in attempt to synthesize the boscalid intermediate, 2-chloronitrobenzene did not undergo the coupling reaction with 4-chlorophenylboronic acid because of the steric effect and less reactivity. Even 2-iodonitrobenzene, which should be the most reactive, did not afford the coupling product at ambient temperature due to the steric effect of the nitro group at the 2-position.

138

Fortunately the coupling reaction of 2-iodonitrobenzene and 4-chlorophenylboronic acid occurred smoothly when the temperature was increased to 40 °C in 24 h, with an isolated yield of 86% (Scheme 4.4b; Table 4.2, entry 9).[18,19] However, attempts to synthesize the NPY-5 receptor antagonist intermediate from the coupling of 2-amino-5-bromopyrazine and phenylboronic acid were unsuccessful even at 50 °C (Scheme 4.4c).[47]
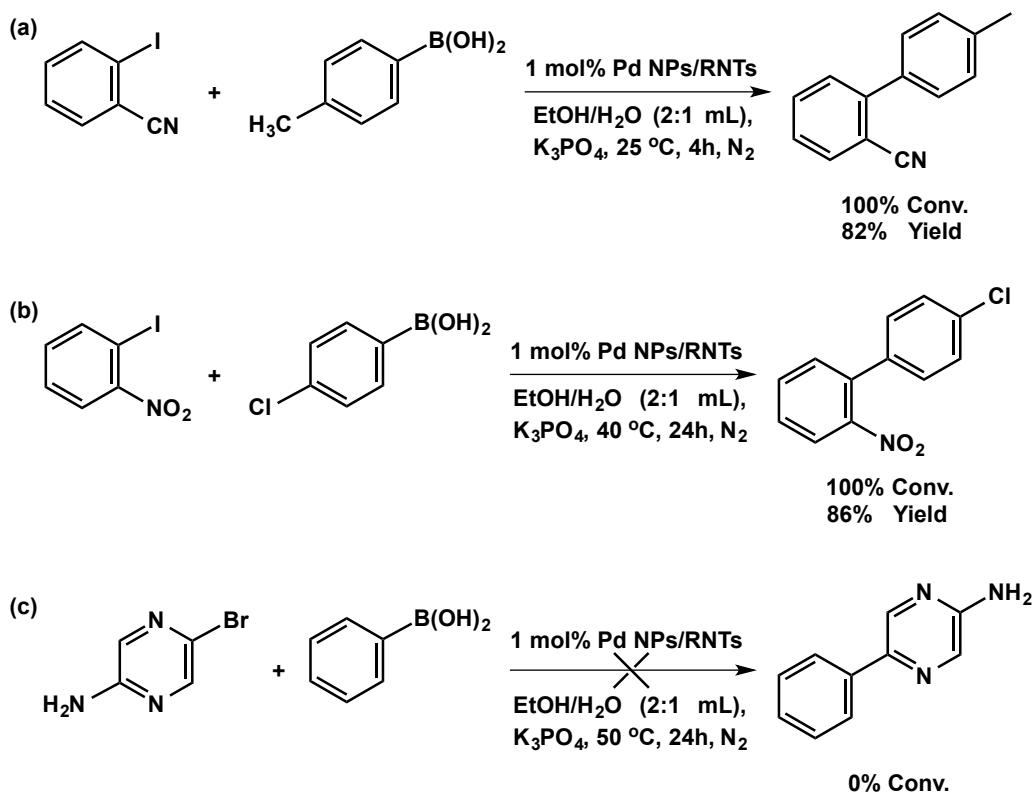
Scheme 4.4: Attempts to synthesize (a) the sartan intermediate, (b) the boscalid fungicide intermediate, and (c) the NPY-5 receptor antagonist intermediate.

4.3.2 Benzothiadiazole Based Materials

4.3.2.1 Reaction Optimization and Exploration
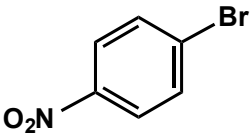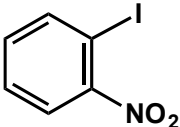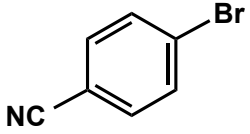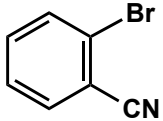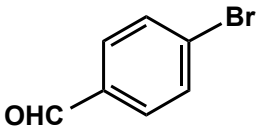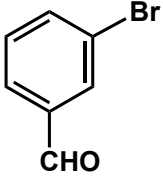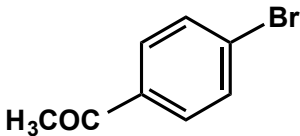
In recent years, 2,1,3-benzothiadiazole based π-conjugated systems showing redox-active and luminescent properties have attracted much attention due to their electronic, optical and optoelectronic function.[48-72] The 2,1,3-benzothiadiazole core has

tunable high reduction potential and electron affinity. More importantly the 2,1,3-benzothiadiazole derivatives are efficient fluorophores and form well-defined crystal structures, which are necessary for organic light emitting diode (OLED) applications.[50,51] However, the synthesis of such materials is limited to high temperature reactions using toxic organic reactants and solvents.[48-72] Unfortunately, the authors mainly paid attention to obtain the customized molecules rather than exploring the scope of the reaction in the aspects of catalysis such as solvent, temperature and environmentally benign conditions. Therefore, because of the increasing demand for the 2,1,3-benzothiadiazole based organic materials, I explored the scope of the reaction using our catalyst under environmentally benign optimized conditions for the first time.

Under the optimized conditions for the aryl bromides, the initial reaction of 4,7-dibromobenzothiadiazole and phenylboronic acid pinacol ester did not afford the expected bis-coupling product (Scheme 4.5). Similarly, another reaction of 4,7-dibromo-benzothiadiazole and 4-(N-Boc-amino)phenylboronic acid pinacol ester was also found to be unreactive. Although the results were unfortunate, the reason was unclear and not further investigated. Later, I replaced the bromo and **boronic acid pinacol ester** functional groups between the two reactants. Fortunately, this functional group exchange worked perfectly for the Suzuki double cross-coupling reaction. Hence, the reaction of bromobenzene and 2,1,3-benzothiadiazole-4,7-bis(boronic acid pinacol ester) (**4.1**) gave the expected bis-coupling product in 75% yield in 5 h (Scheme 4.5). The newly optimized protocol enabled for the synthesis of a series of 2,1,3-benzothiadiazole derivatives incorporating both electron withdrawing and electron donating substituents under environmentally benign conditions (Scheme 4.6). In general, the reactions of the

aryl bromides containing electron withdrawing substituents were found to be faster than electron donating substituents (Table 4.5).

Scheme 4.5: Attempts to synthesize 4,7-diphenyl-2,1,3-benzothiadiazole under the previously optimized conditions.

Scheme 4.6: The catalytic reactions of **4.1** with a variety of aryl bromides containing both electron withdrawing and donating substituents except 1-iodo-2-nitrobenzene. The yields (%) are listed in Table 4.5.

Table 4.5: The Suzuki-Miyaura double cross-coupling of aryl bromides and **4.1**[a,b]

Entry	Aryl halides	Reaction duration (h)	Yield. (%)	
			MC	BC
1	4-bromo-nitrobenzene (O$_2$N–C$_6$H$_4$–Br)	0.5	-	81
2	2-iodo-nitrobenzene (I, NO$_2$)	1.0	35[c]	38
3	4-bromo-benzonitrile (NC–C$_6$H$_4$–Br)	0.5	-	84
4	2-bromo-benzonitrile (Br, CN)	1.0	-	48
5	4-bromo-benzaldehyde (OHC–C$_6$H$_4$–Br)	0.5	-	84
6	3-bromo-benzaldehyde (CHO)	0.5	-	86
7	4-bromo-acetophenone (H$_3$COC–C$_6$H$_4$–Br)	0.5	-	86
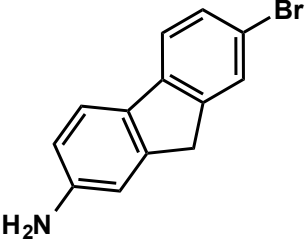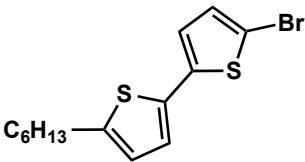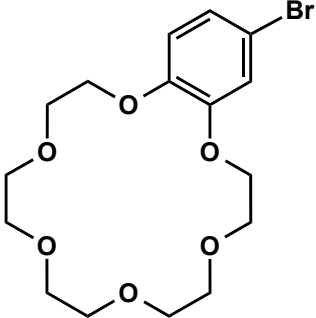
[a] Reaction conditions: Aryl halides (0.5 mmol), **4.1** (0.25 mmol), 1 mol% of Pd NPs/RNTs catalyst in EtOH/H$_2$O (2:1 mL), K$_3$PO$_4$ (425 mg), 50 $^\circ$C and under N$_2$. [b] Catalyst was prepared by H$_2$ reduction prior to the reaction. [c] Deboronated product. MC = mono coupled, BC = bis coupled.

Table 4.5: Continued[a,b]

Entry	Aryl halides	Reaction duration (h)	Yield. (%) MC	Yield. (%) BC
			MC	BC
8		0.5	-	90
9		1.0	-	92
10		0.5	-	76
11		1.0	-	89
12		1.0	-	84
13		4		30
14		1.0	-	88

[a] Reaction conditions: Aryl halides (0.5 mmol), **4.1** (0.25 mmol), 1 mol% of Pd NPs/RNTs catalyst in EtOH/H_2O (2:1 mL), K_3PO_4 (425 mg), 50 ^{o}C and under N_2. [b] Catalyst was prepared by H_2 reduction prior to the reaction. MC = mono coupled, BC = bis coupled.

Table 4.5: Continued[a,b]

Entry	Aryl halides	Reaction duration (h)	Yield. (%)	
			MC	BC
15		23	-	19
16		2.0	-	63
17		2.0	-	14
18		2.0	-	58

[a] Reaction conditions: Aryl halides (0.5 mmol), **4.1** (0.25 mmol), 1 mol% of Pd NPs/RNTs catalyst in EtOH/H$_2$O (2:1 mL), K$_3$PO$_4$ (425 mg), 50 °C and under N$_2$. [b] Catalyst was prepared by H$_2$ reduction prior to the reaction. MC = mono coupled, BC = bis coupled.

The poor yields from the reactions of 1-iodo-2-nitrobenzene and 2-bromobenzonitrile with **4.1** can be rationalized from the steric effect of the *ortho* substituents (Table 4.5, entry 2 and 4). Interestingly, the reaction of 1-iodo-2-

nitrobenzene with **4.1** resulted in the expected bis-coupling product as well as the mono-coupling and deboronated products in 38% and 35% yields, respectively (Scheme 4.7; Table 4.5, entry 2). Similar products were formed from the reaction of 2-bromobenzothiazole and **4.1**. However, though the product yields were very low (<5%), only a few miligrams were obtained (not listed in Table 4.5), I were able to fully characterize the compounds by spectroscopy and mass spectrometry (Scheme 4.7).
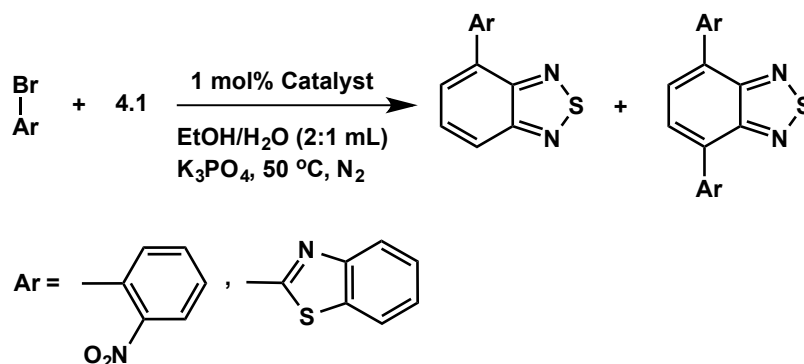
Scheme 4.7: The mono-coupling and deboronated product formation along with the expected bis-coupling product.

Other reactions of 2-bromopyridine and 2-bromopyrimidine with **4.1** were unsuccessful (not listed in Table 4.5).[49,50] In addition, the reaction of 5-bromo-5′-hexyl-2,2′-bithiophene and **4.1** gave the bis-coupling product in only 14% yield (Table 4.5, entry 17). Hence, this general trend of the poor reactivity of the heterocyclic bromides could be due to the catalyst poisoning by the surface capping and/or chelation of the initial coupling product under aqueous condition. Previously, it was reported that even the use of toluene as a solvent for such reactions led to <50% product yield.[49,50] Poor reactivity was also observed when 1-bromo-3,4,5-trimethoxybenzene was replaced by 1-bromo-2,3,4-trimethoxybenzene (Table 4.5, entry 14 and 15).

4.3.2.2 Unsymmetrical Bis-coupling Product Synthesis

After successfully exploring the bis-coupling reactions of **4.1**, I planned to study the scope for preparing unsymmetrically substituted 2,1,3-benzothiadiazole derivatives.[34-45] Incorporation of the two different functionalities allows for the opportunity for further modification, which can be beneficial for device fabrication.[36] Considering this, I set up a one-pot reaction employing **4.1** (0.25 mmol) together with 1-bromo-4-nitrobenzene (0.25 mmol) and 4-bromobenzaldehyde (0.25 mmol). Under the optimized conditions, the reaction gave 4,7-(*bis*-4-nitrophenyl)-2,1,3-benzothiadiazole, 4,7-(*bis*-4-formylphenyl)-2,1,3-benzothiadiazole and the expected 4-(4-nitrophenyl)-7-(4-formylphenyl)-2,1,3-benzothiadiazole in 30%, 17% and 49%, respectively (Scheme 4.8). The lower yield of 4,7-(*bis*-4-formylphenyl)-2,1,3-benzothiadiazole compared to the corresponding bis-nitro compound was because of the poor reactivity of 4-bromobenzaldehyde. This result suggested that our catalyst could be successfully applied for the synthesis of unsymmetrically substituted arenes.
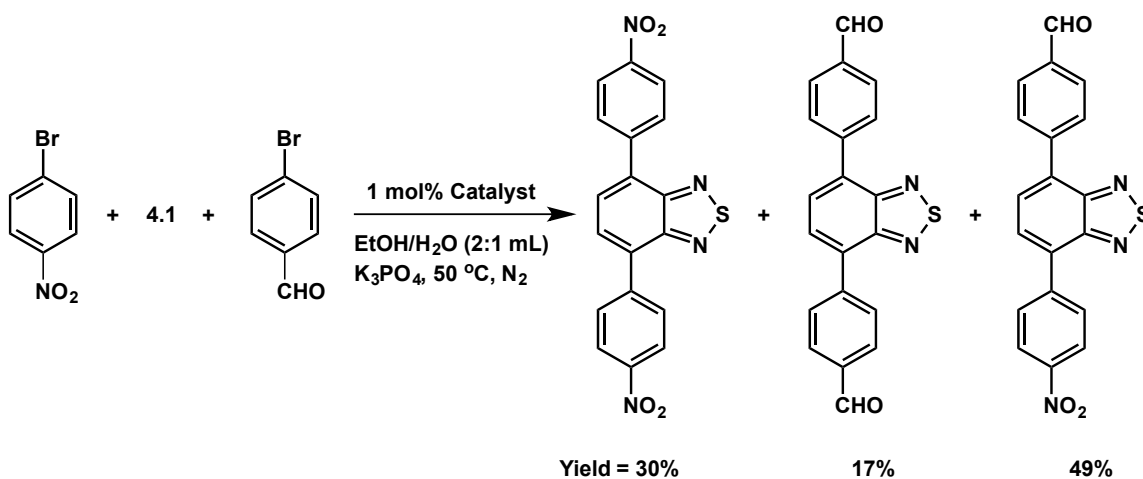
Scheme 4.8: The synthesis of 4-(4-nitrophenyl)-7-(4-formylphenyl)-2,1,3-benzothiadiazole.

146

4.3.2.3 Oligomer Synthesis

Finally, I also explored the utility of our catalyst for the synthesis of 2,1,3-benzothiadiazole based polymeric materials for their potential optoelectronic application.[70-75] Our goals were to demonstrate and establish an effective and industrially viable green synthetic protocol. Towards these efforts, I initially performed a reaction containing **4.1** and 9,9-dioctyl-2,7-dibromofluorene under the optimized conditions. The reaction resulted in an oligomer with an average M_n of 700-2000 in 20 h (Table 4.6, entry 1). The observed precipitation of the coupling product from the solution due to poor solubility and/or capping of the active Pd species could be rationalized by the low M_n oligomer formation. Therefore, to improve the solubility and to increase the oligomer average M_n, I replaced the ethanol/water mixture with THF/water. I hypothesized that the introduction of THF would increase the solubility of the initial coupling product and enhance the subsequent coupling with the monomers. In addition, the improved solubility would increase the dispersion of the active Pd species in solution. Indeed, the modification helped to improve the average M_n of the oligomer to 1300-5000 in 9 h (Table 4.6, entry 2). Unfortunately, another reaction with prolonged reaction duration of 18 h did not further increase the average M_n of the oligomer (Table 4.6, entry 2). Later, to further escalate the average M_n, I increased the catalyst loading to 5 and 10 mol% leading to the average M_n of 1300-7000 and 1300-9300, respectively in 18 h (Table 4.6, entry 3 and 4). To evaluate the thermal stability of the oligomer (M_n 1300-5000), I performed the TGA analysis (Figure 4.4). The TGA results showed that the oligomer underwent thermal degradation beginning at 409 °C and with a mass loss of 58.3%. The decomposed material was then further burned off at 660 °C (Figure 4.4).

Table 4.6: The synthesis of 2,1,3-benzothiadiazole based oligomer[a,b]

n = 1.3-18

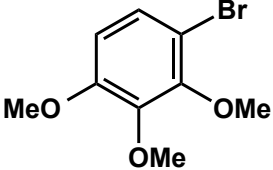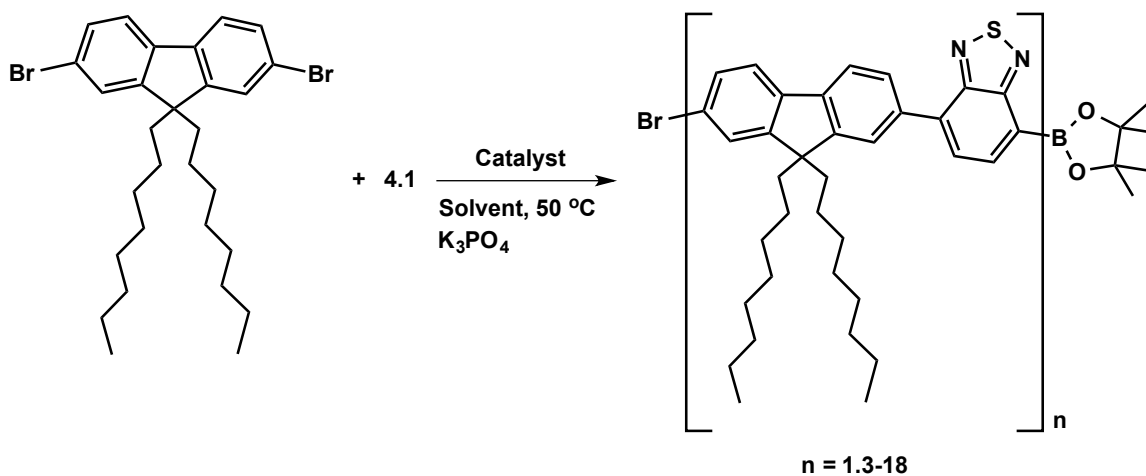| Entry	Catalyst loading (%)	Solvent (2:1 mL, v/v)	Reaction duration (h)	Av. M_n[c]
1	1	EtOH/H$_2$O	20	700-2000
2	1	THF/H$_2$O	9	1300-5000
			18	
3	5	THF/H$_2$O	18	1300-7000
4	10	THF/H$_2$O	18	1300-9300

[a] Reaction conditions: Aryl dibromide (0.5 mmol), **4.1** (0.5 mmol), Pd NPs/RNTs catalyst, K$_3$PO$_4$ (425 mg), 50 $^\circ$C and under N$_2$. [b] Catalyst was prepared by H$_2$ reduction prior to the reaction. [c] Determined by GPC analysis.

148
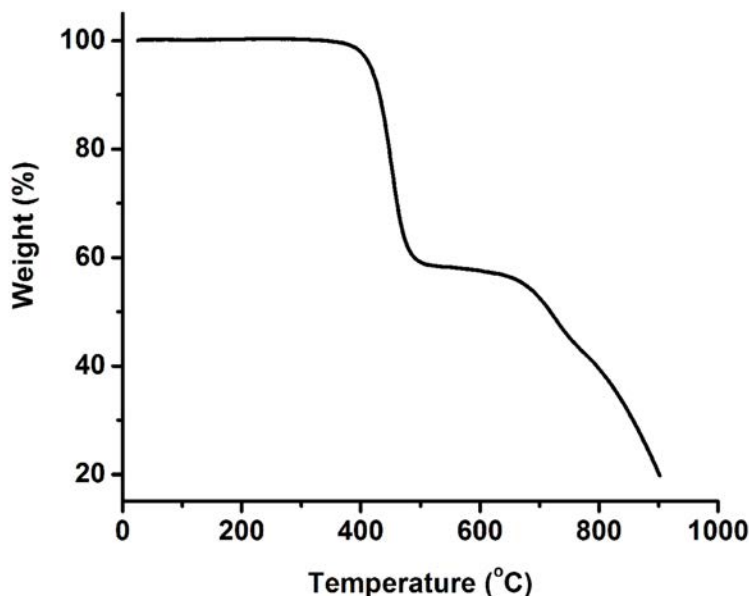
Figure 4.4: TGA analysis of the oligomer (M_n 1300-5000) under N_2.

4.3.3 Suzuki Coupling Catalyst Characterization

To gain more insight into the properties and the behavior of the Pd NPs/RNTs catalyst, I carried out detailed characterization by spectroscopy and microscopy. The spectrum (black solid line) in the UV-Vis representing the RNTs in ethanol/water (50:50 v/v), displayed a profile typical of the DNA bases with two maxima at 237 nm and 287 nm, respectively (Figure 4.5a).[76] Similarly to that of the hydrogenation catalyst, the formation of the Pd NPs did not cause any shift in the absorption maxima. The presence of Pd NPs in solution could be assigned from the gradual increase in the absorbance with decreasing wavelength phenomenon, which is characteristic to the presence of NP in solution and was consistent with the previous observation in chapter 3 (Figure 4.5, red and blue solid lines). The CD spectra also were in good agreement with the previous findings. As observed earlier in chapter 3, the formation of Pd NPs on the surface of the RNTs did not alter the CD profile (Figure 4.5a).
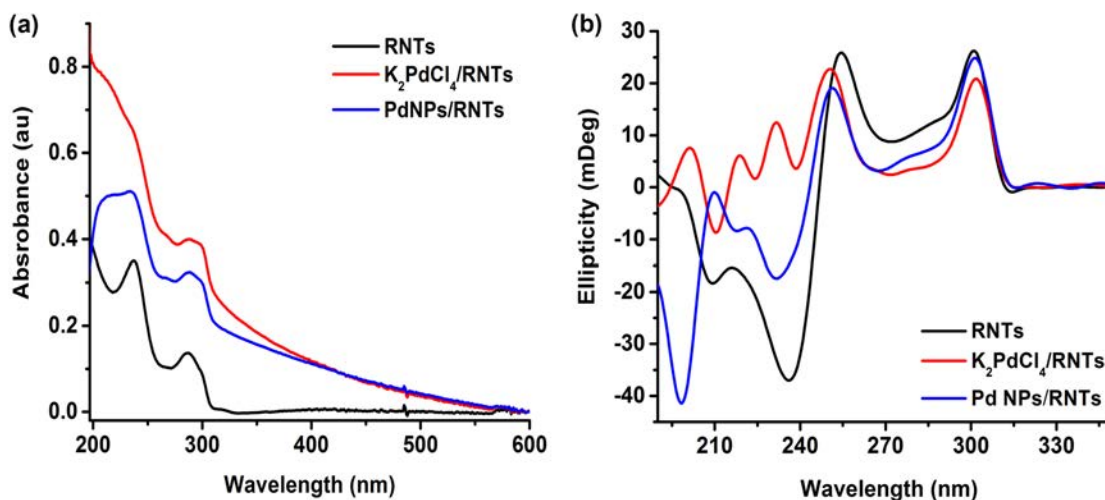
Figure 4.5: Detailed characterization of the Pd NPs/RNTs by UV-Vis (a) and CD (b) spectroscopy.

As the Suzuki coupling reaction uses base, I also studied the effect of the base on the Pd NPs/RNTs catalyst. For detail comparison, I investigated the properties of the RNTs and the Pd NPs/RNTs catalyst by UV and CD in the presence of different concentrations of the K_3PO_4. In general, the addition of K_3PO_4 to the RNTs and Pd NPs/RNTs catalyst did not cause any significant shift in the absorption maxima. However, the presence of 1 M K_3PO_4 (212.5 mg), based on 1 mL of water, caused a hyperchromic shift of the RNTs absorption bands. On the other hand, for the Pd NPs/RNTs catalyst, there was a hypochromic shift of the absorption bands. The effect of the K_3PO_4 concentration on the CD profile of the RNTs was very large. Only 10-fold excess of K_3PO_4 led to a dramatic drop in the molar ellipticity of the RNTs causing them to be almost CD silent. Previously, it was observed that the tubular architecture of the RNTs with or without the presence of chiral side chains did not lead to the CD effect.[77,78] This is due to the (i) racemic nanotube formation upon stacking of the hierarchically self-assembled rosettes and, (ii) the lack of induced helicity resulted from the crystallinity of

150

the side chains.[77-79] Hence, I hypothesize that the complexation of the RNTs and K_3PO_4 greatly reduced the induced helicity of the lysine side chains, which resulted in racemic RNTs in solution. The increase in the K_3PO_4 concentration to 1 M gave completely different CD profile.
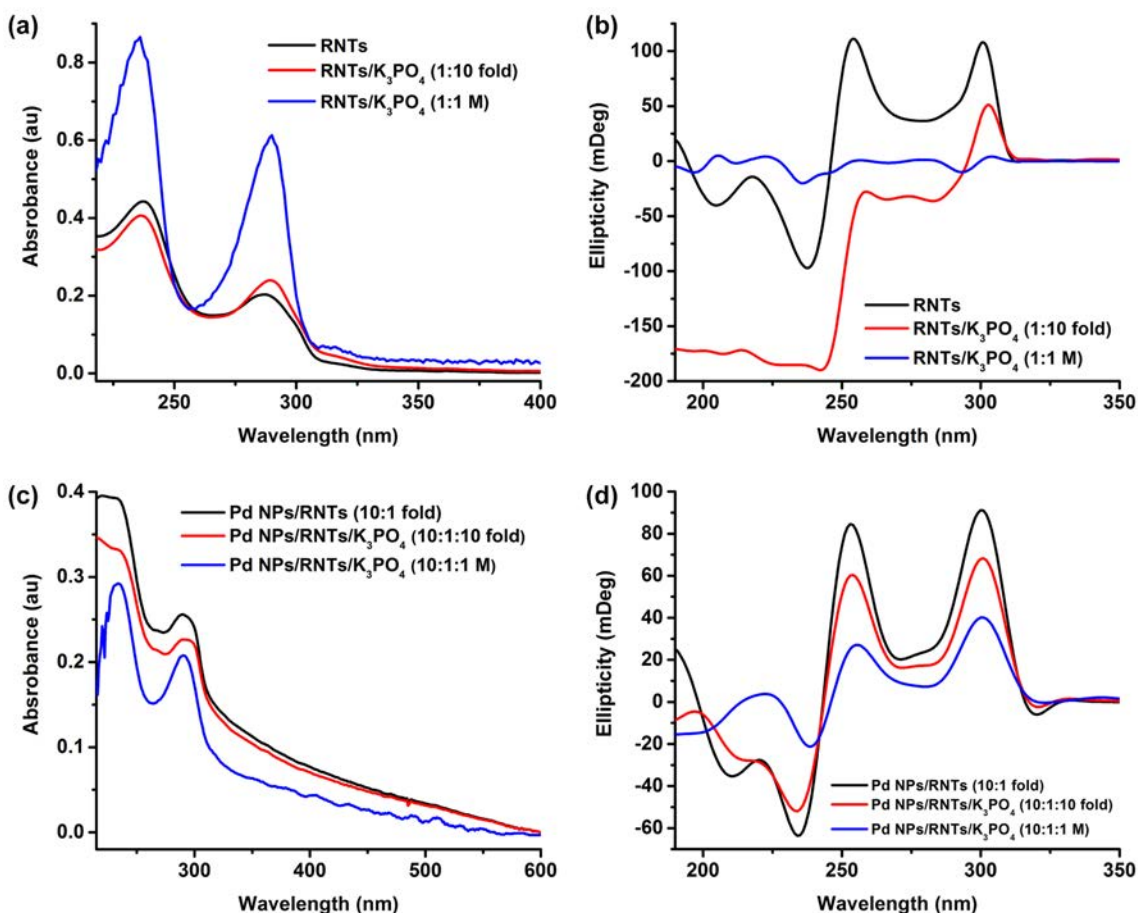
Figure 4.6: UV-Vis and CD spectra of the RNTs (a, b), and Pd NPs/RNTs (c, d) in the presence of K_3PO_4.

Interestingly, though the molar ellipticity of the Pd NPs/RNTs catalyst dropped in the presence of K_3PO_4, the catalyst maintained the similar CD profile. Perhaps, the formation of the Pd NPs on the surface of the RNTs preserved the induced crystallinity of the lysine side chains. As I studied the Suzuki coupling reaction at 50 °C, I investigated

the effect of the temperature on the CD profile of both the RNTs and the Pd NPs/RNTs catalyst. The intensity of the molar ellipticity of the RNTs dropped gradually with increasing the temperature, which became almost CD silent. Alternatively, in the presence of the Pd NPs, the intensity dropped slightly up to 45 °C and then by almost 50% at 55 °C. Finally, the intensity almost became zero at 95 °C similar to the RNTs. Usually, RNTs have a reversible CD profile, where the intensity of the molar ellipticity decreases with increasing temperature and retains to its original state after cooling back to ambient temperature.[77,78]
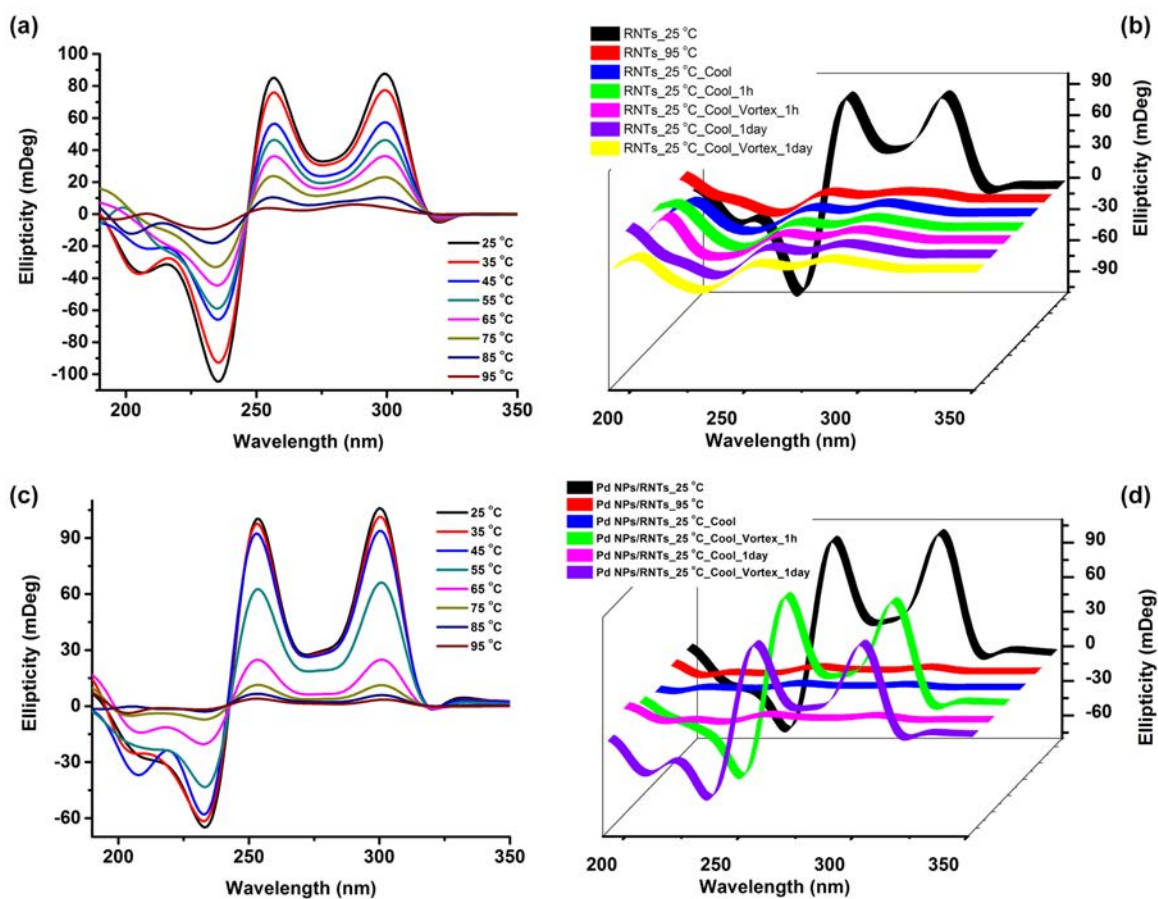
Figure 4.7: VT-CD spectra and vortex effect on the ellipticity of the RNTs (a, b) and Pd NPs/RNTs catalyst (c, d).

This is because of the reversible assembly and disassembly of the RNTs at ambient temperature and higher temperature, respectively.[77,78] Unfortunately, the RNTs did not retain its original molar ellipticity intensity in ethanol/water as observed in pure water.[77] I also homogenized the RNTs solution by using a vortex but it did not help regaining the intensity. Interestingly, though the catalyst initially had almost zero intensity, upon vortex the CD intensity reverted back to the original state. This result suggested that the Pd NPs somehow helped preserving the nano-tubular structure of the RNTs in solution. I hypothesize that the drop in CD intensity with increasing temperature resulted form the bundling of the Pd NPs/RNTs, which separates upon vortex. To prove this hypothesis I performed the time-dependent vortex studies. As expected, I found zero CD intensity for the undisturbed Pd NPs/RNTs solution, while the intensity reverted back to the original state upon vortex. As I performed the Suzuki coupling reactions at the maximum temperature of 50 °C, the CD studies suggested that the catalyst should preserve its original supramolecular chirality under the reaction conditions.

The SEM and TEM images displayed that the Pd NPs/RNTs catalyst also formed bundles in ethanol/water (2:1 mL, v/v) similar to that in methanol (Figure 4.8a, b). The TEM images of the Pd NPs/RNTs catalyst reduced with hydrogen, showed the presence of random and polydispersed Pd NPs on the surface of the RNTs bundles (Figure 4.8, d). The average size of the Pd NPs on the surface of the RNTs bundles was found to be 2.1 ± 0.7 nm (Figure 4.8, d). I hypothesize that the stirring facilitated the random distribution of the Pd NPs on the surface of the RNTs bundle. However, several attempts to locate the Pd NPs on the surface of the RNTs bundle after the addition of K_3PO_4 was unsuccessful because of the high K_3PO_4 concentration.
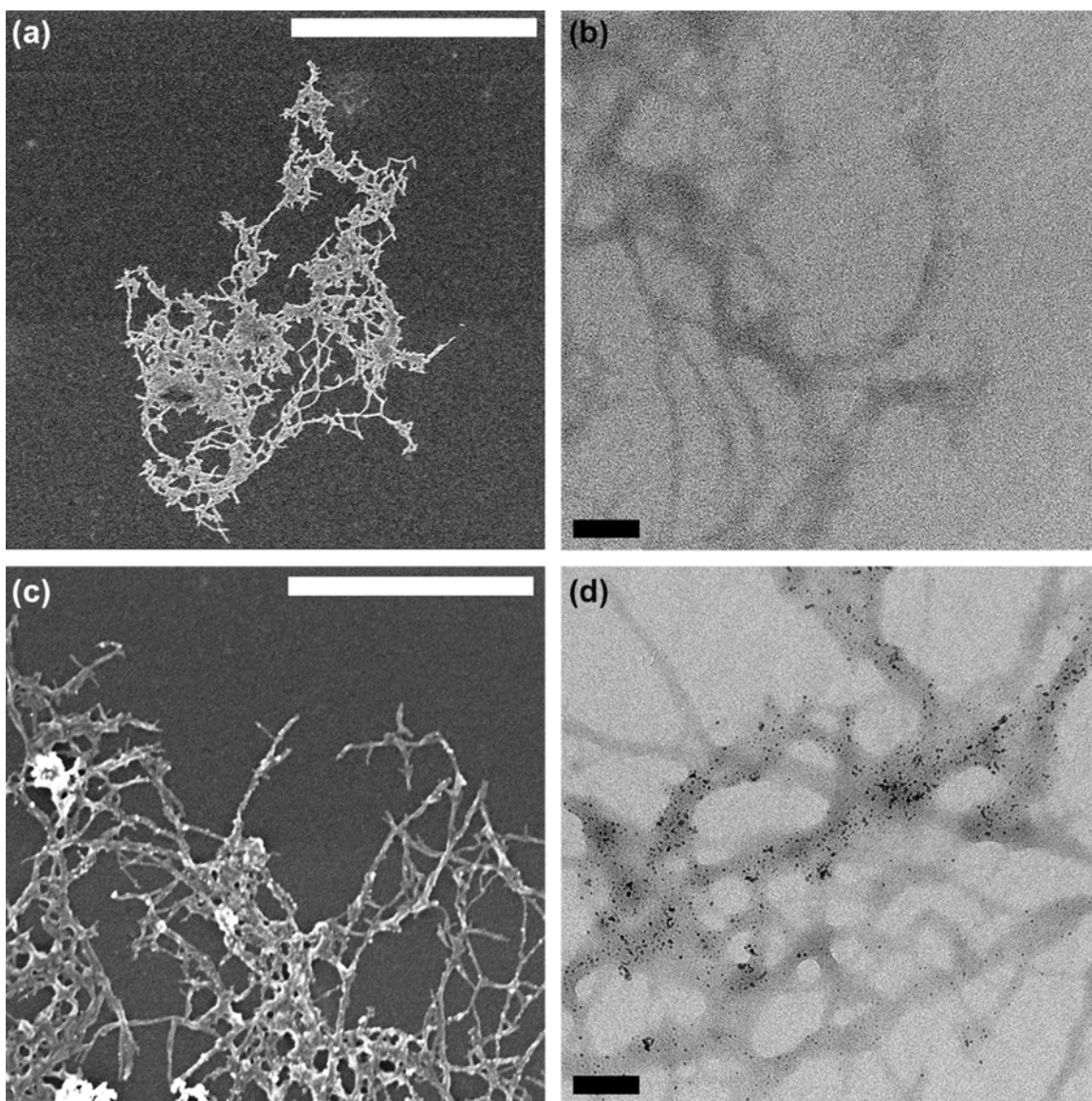
Figure 4.8: SEM (a, c) and TEM (b, d) images of the Pd NPs/RNTs before (a, d) and after (c, d) reducing with H_2. Scale bar – 1 μm (a), 500 nm (c) and 50 nm (b, d).

In conclusion, I have demonstrated that Pd NPs/RNTs catalyst can be successfully applied to the Suzuki-Miyaura cross-coupling reaction. The results showed that aryl iodides and bromides could readily be coupled to aryl boronic acids with a wide tolerance of functional groups on the aryl groups. However, the solubility of the catalyst in water limits the catalysis in organic solvents.

Experimental

Materials.

All chemicals were purchased from Sigma-Aldrich and TCI America. They were used for catalysis as received without further purification. Ethanol and THF were used as mixture solvents with water without further drying.

Instrumentation.

The ^{13}C NMR spectra were measured on a Varian Direct Drive 600 MHz NMR spectrometer in the specified deuterated solvents. All mass spectrometric analyses were performed by the staff at the University of Alberta Mass Spectrometry Facility. Samples requiring high-resolution electron impact (EI) mass spectrometry were obtained on a Kratos MS50G spectrometer. Samples requiring low-resolution MALDI-TOF mass spectrometry were obtained on a Bruker Ultraflextreme MALDI TOF/TOF spectrometer. The high-resolution MALDI-TOF mass spectra were obtained on a Bruker 9.4T Apex-Qe FTICR spectrometer. The GPC analysis was performed using a Agilent 1100 HPLC instrument with phenogel column (particle size 10 μm and diameter 300×7.8 mm) with Sedex 75 ELSD detection. THF was used a solvent and the flow rate was 1 mL/min.

Methods.

Stock solutions of RNTs and K$_2$PdCl$_4$. The stock solutions of the RNTs and the K$_2$PdCl$_4$ were prepared following the similar procedure under the optimized condition as mentioned in chapter 2.

Catalyst synthesis: The Pd NPs/RNTs catalyst was synthesized either by following the incubation protocol or by reducing with hydrogen in water prior to the catalytic reaction as mentioned in chapter 3.

Catalytic reaction: General Procedure. Though a variety of different halides and boronic acids were employed for the Suzuki cross-coupling reaction, the coupling reaction of 1-iodo-4-nitrobenzene and phenyl boronic acid was presented as the model procedure for this studies. An ethanol/water solution (2:1 mL, v/v) of the Pd NPs/RNTs (5.0/0.5 μmol, 1 mol% based on Pd concentration) catalyst was treated with 1-iodo-4-nitrobenzene (124.5 mg; 0.5 mmol) and phenyl boronic acid (121.9 mg; 1.0 mmol), and K_3PO_4 (425 mg; 2.0 mmol) under nitrogen atmosphere. The reaction mixture was degassed under vacuum for 2 min and then back filled with N_2 and stirred at ambient temperature for 4 h under N_2. An aliquot of the reaction mixture was taken into a glass vial and the product was extracted with diethylether (2 mL) and dried over anhydrous $MgSO_4$ and filtered. The solvent was then removed under reduced pressure and the residue was analyzed by ^{1}H NMR to determine the product conversion. When necessary, the resulting mixture was extracted with diethylether (4 × 5 mL) followed by quenching with brine after completion of the reaction. The extract was dried over anhydrous $MgSO_4$ and filtered. The solvent was removed under reduced pressure and the residue was chromatographed on a silica column by using appropriate solvent mixtures as an eluent.

Catalyst recycling. The experiment was performed by following the above-mentioned procedure using 1-iodo-4-nitrobenzene and phenyl nicnic acid as the coupling partners. However, the experiment was repeated up to the tenth successive cycle. In each cycle, after completion of the reaction, the product was extracted with diethylether (4 × 5 mL) and the catalyst was reloaded followed by the addition of ethanol (2 mL) and the reactants.

Scale up reaction. The scale up reaction was conducted by increasing the loading of the catalyst (1 mol%, based on Pd concentration), base (21.3 g, 100.0 mmol) and reactants (1-iodo-4-nitrobenzene (6.2 g, 25.0 mmol) and phenyl boronic acid (6.1 g, 50.0 mmol)) by 50 times under the newly modified conditions (EtOH/H$_2$O (50:50 mL, v/v) and 40 ^{o}C) in 4 h. The reaction resulted in 100% conversion of the coupling product with 95% isolated yield.

Spectroscopic data.
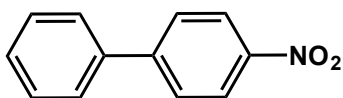
4-Nitrobiphenyl[80] from 1-iodo-4-nitrobenzene (124.5 mg, 0.5 mmol) and phenyl boronic acid (121.9 mg; 1.0 mmol): 100% conversion; ^{1}H NMR (600 MHz, CDCl$_3$) δ 8.30 (d, J = 9.0 Hz, 2H), 7.74 (d, J = 9.0 Hz, 2H), 7.63 (d, J = 7.2 Hz, 2H), 7.50 (t, J = 7.2 Hz, 2H), 7.45 (t, J = 7.2 Hz, 1H).

4-Nitrobiphenyl[80] from 1-bromo-4-nitrobenzene (101.0 mg, 0.5 mmol) and phenyl boronic acid (121.9 mg; 1.0 mmol): 100% conversion.
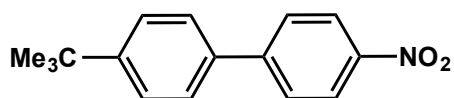
4-Nitro-4'-*tert*-butylbiphenyl[81] from 1-iodo-4-nitrobenzene (124.5 mg, 0.5 mmol) and 4-*tert*-butylphenyl boronic acid (178.0 mg; 1.0 mmol): 92% conversion; ^{1}H NMR (600 MHz, CDCl$_3$) δ 8.29 (d, J = 9.0 Hz, 2H), 7.73 (d, J = 9.0 Hz, 2H), 7.58 (d, J = 7.8 Hz, 2H), 7.52 (d, J = 9.0 Hz, 2H), 1.38 (s, 9 H).
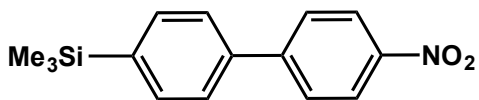
4-Nitro-4'-*tri*-methylsilylbiphenyl[82] from 1-iodo-4-nitrobenzene (124.5 mg, 0.5 mmol) and 4-*tri*-methylsilylphenyl boronic acid (194.0 mg; 1.0 mmol): 87% conversion; ^{1}H NMR (600 MHz, CDCl$_3$) δ 8.30 (d, J = 8.4 Hz, 2H), 7.74 (d, J = 9.0 Hz, 2H), 7.65 (d, J = 7.2 Hz, 2H), 7.61 (d, J = 7.8 Hz, 2H), 0.31 (s, 9H).
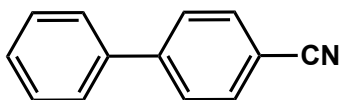
4-Cyanobiphenyl[83] from 4-Iodobenzonitrile (114.5 mg, 0.5 mmol) and phenyl boronic acid (121.9 mg; 1.0 mmol): 100% conversion; ^{1}H NMR (600 MHz, CDCl$_3$) δ 7.66 (d, J = 8.4 Hz, 2H), 7.62 (d, J = 7.8 Hz, 2H), 7.52 (d, J = 7.8 Hz, 2H), 7.40 (t, J = 7.8 Hz, 2H), 7.35 (t, J = 7.8 Hz, 1H).

4-Cyano-4'-*tert*-butylbiphenyl[84] from 4-Iodobenzonitrile (114.5 mg, 0.5 mmol) and 4-*tert*-butylphenyl boronic acid (178.0 mg; 1.0 mmol): 100% conversion; ^{1}H NMR (600 MHz, CDCl$_3$) δ 7.71 (d, J = 8.4 Hz, 2H), 7.68 (d, J = 9.0 Hz, 2H), 7.54 (d, J = 8.4 Hz, 2H), 7.51 (d, J = 9.0 Hz, 2H), 1.37 (s, 9H).
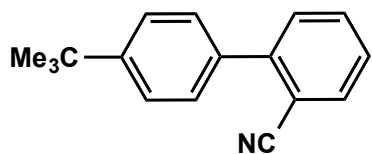
2-Cyano-4'-*tert*-butylbiphenyl from 2-bromobenzonitrile (91.0 mg, 0.5 mmol) and 4-*tert*-butylphenyl boronic acid (178.0 mg; 1.0 mmol): 100% conversion; ^{1}H NMR (600 MHz, CDCl$_3$) δ 7.76 (d, J = 9.0 Hz, 1H), 7.63 (dt, J = 1.2, 7.8 Hz, 1H), 7.53-7.52 (m,

5H), 7.42 (dt, J = 1.2, 7.8 Hz, 1H). ^{13}C NMR (150 MHz, CDCl$_3$): δ 151.9, 145.5, 135.3, 133.9, 132.9, 130.2, 128.6, 127.4, 125.8, 119.1, 111.3, 34.8, 31.4. EI-MS (m/z): M$^+$ 235.13624, Calcd. 235.13609 for C$_{17}$H$_{17}$N; [M – CH$_3$]$^+$ 220.11291, Calcd. 220.11263 for C$_{16}$H$_{14}$N.
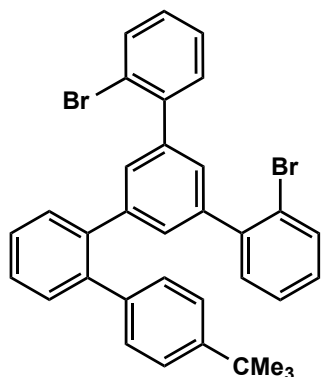
2,4-*Bis*-(2-bromophenyl)-6-(4'-*tert*-butyl-2-biphenyl)triazine from 2-bromo-benzonitrile (91.0 mg, 0.5 mmol) and 4-*tert*-butylphenyl boronic acid (178.0 mg; 1.0 mmol): 5% yield; ^{1}H NMR (600 MHz, CDCl$_3$) δ 7.74 (d, J = 6.6 Hz, 1H), 7.69-7.61 (m, 5H), 7.52-7.51 (m, 5H), 7.47-7.40 (m, 5H). ^{13}C NMR (150 MHz, CDCl$_3$): δ 151.9, 145.5, 135.3, 134.5, 134.1, 133.9, 133.3, 132.9, 130.2, 128.6, 127.8, 127.4, 125.8, 125.4, 119.1, 117.3, 116.0, 111.2. ESI-MS (m/z): [C$_{17}$H$_{17}$N + Na]$^+$ 258.1.
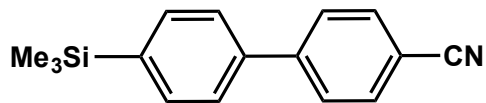
4-Cyano-4'-*tri*-methylsilylbiphenyl from 4-Iodobenzonitrile (114.5 mg, 0.5 mmol) and 4-*tri*-methylsilylphenyl boronic acid (194.0 mg; 1.0 mmol): 100% conversion; ^{1}H NMR (600 MHz, CDCl$_3$) δ 7.72 (d, J = 8.4 Hz, 2H), 7.68 (d, J = 8.4 Hz, 2H), 7.64 (d, J = 8.4 Hz, 2H), 7.57 (d, J = 8.4 Hz, 2H). ^{13}C NMR (150 MHz, CDCl$_3$): δ 145.7, 141.4, 139.5, 134.2, 132.7, 127.8, 126.6, 119.0, 111.1, – 1.1. EI-MS (m/z): M$^+$ 251.11251,

Calcd. 251.11302 for $C_{16}H_{17}NSi$; $[M - CH_3]^+$ 236.08916, Calcd. 236.08955 for $C_{15}H_{14}NSi$.
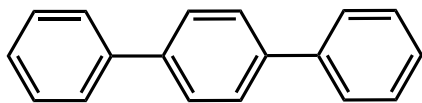
4-Phenylbiphenyl[85] from 1-bromo-4-iodobenzene (142.0 mg; 0.5 mmol) and phenyl boronic acid (121.9 mg; 1.0 mmol): 42 and 82% conversions at ambient and 50 °C, respectively; ^{1}H NMR (600 MHz, CDCl$_3$) δ 7.70 (s, 4H), 7.67 (d, J = 7.2 Hz, 4H), 7.48 (t, J = 7.8 Hz, 4H), 7.38 (t, J = 7.8 Hz, 2H). ^{13}C NMR (150 MHz, CDCl$_3$): δ 140.8, 140.2, 128.9, 127.6, 127.4, 127.2.
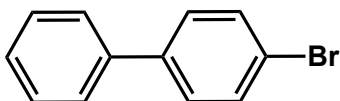
4-Bromobiphenyl[86] from 1-bromo-4-iodobenzene (142.0 mg; 0.5 mmol) and phenyl boronic acid (121.9 mg; 1.0 mmol): 58 and 18% conversions at ambient and 50 °C, respectively; 7.57-7.55 (m, 4H), 7.47-7.43 (m, 4H), 7.37 (t, J = 7.8 Hz, 1H).
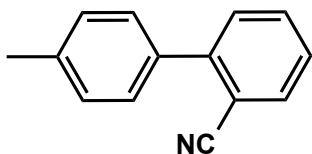
2-Tolylbenzonitrile[87,88] from 2-Iodobenzonitrile (114.5 mg, 0.5 mmol) and p-tolyl boronic acid (135.0 mg; 1.0 mmol): 100% conversion; ^{1}H NMR (600 MHz, CDCl$_3$) δ 7.75 (d, J = 7.8 Hz, 1H), 7.63 (t, J = 7.8 Hz, 1H), 7.51 (d, J = 8.4 Hz, 1H), 7.47 (d, J = 7.8 Hz, 2H), 7.42 (t, J = 7.8 Hz, 1H), 7.31 (d, J = 7.8 Hz, 2H), 2.43 (s, 3H). ^{13}C NMR (150 MHz, CDCl$_3$): δ 145.5, 138.7, 135.3, 133.7, 132.8, 123.0, 129.4, 128.6, 127.3, 118.9, 111.2, 21.3. EI-MS (m/z): M$^+$ 193.08868, Calcd. 193.08914 for $C_{14}H_{11}N$; $[M - CH_2N]^+$ 165.07028, Calcd. 165.07042 for $C_{13}H_9$.
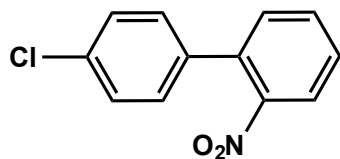
2-(4-Chlorophenyl)nitrobenzene[89] from 2-iodonitrobenzene (124.5 mg, 0.5 mmol) and 4-chlorophenyl boronic acid (156.0 mg; 1.0 mmol): 100% conversion and 86% yield; ^{1}H NMR (600 MHz, CDCl$_3$) δ 7.88 (d, J = 8.4 Hz, 1H), 7.63 (t, J = 7.8 Hz, 1H), 7.51 (t, J = 7.8 Hz, 1H), 7.42-7.39 (m, 3H), 7.25 (d, J = 8.4 Hz, 2H). ^{13}C NMR (150 MHz, CDCl$_3$): δ 149.1, 135.9, 135.2, 134.5, 132.5, 131.8, 129.3, 128.9, 128.6, 124.3. EI-MS (m/z): M$^+$ 235.02101, Calcd. 235.02141 for C$_{12}$H$_8$NO$_2$^{37}Cl; 233.02388, Calcd. 233.02435 for C$_{12}$H$_8$NO$_2$^{35}Cl.
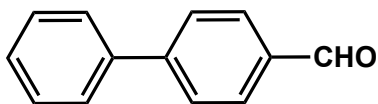
4-Phenylbenzaldehyde[85] from 4-bromobenzaldehyde (92.5 mg; 0.5 mmol) and phenyl boronic acid (121.9 mg; 1.0 mmol): 96% conversion; ^{1}H NMR (600 MHz, CDCl$_3$): δ 10.06 (s, 1H), 7.95 (d, J = 8.4 Hz, 2H), 7.75 (d, J = 8.4 Hz, 2H), 7.63 (d, J = 7.8 Hz, 2H), 7.48 (t, J = 7.8 Hz, 2H), 7.41 (t, J = 7.2 Hz, 1H).
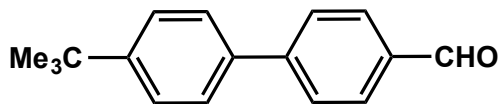
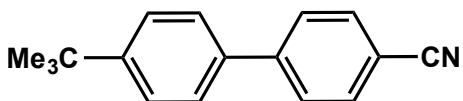4-Carbaldehyde-4'-*tert*-butylbiphenyl from 4-bromobenzaldehyde (92.5 mg; 0.5 mmol) and 4-*tert*-butylphenyl boronic acid (178.0 mg; 1.0 mmol): 36% conversion; ^{1}H NMR (600 MHz, CDCl$_3$): δ 10.05 (s, 1H), 7.94 (d, J = 8.4 Hz, 2H), 7.75 (d, J = 7.8 Hz, 2H), 7.59 (d, J = 9.0 Hz, 2H), 7.51 (d, J = 7.8 Hz, 2H), 1.38 (s, 9H). ^{13}C NMR (150 MHz, CDCl$_3$): δ 191.9, 151.8, 147.0, 136.8, 135.0, 130.3, 127.4, 127.0, 126.0, 31.3. EI-MS

(m/z): M$^+$ 238.13537, Calcd. 238.13577 for C$_{17}$H$_{18}$O; [M – CH$_3$]$^+$ 223.11227, Calcd. 223.11229 for C$_{16}$H$_{15}$O.

Me$_3$Si———⟨benzene ring⟩———⟨benzene ring⟩———CHO
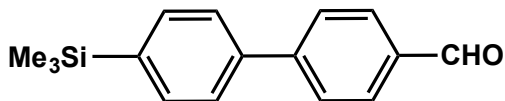
4-Carbaldehyde-4'-trimethylsilylbiphenyl from 4-bromobenzaldehyde (92.5 mg; 0.5 mmol) and 4-*tri*-methylsilylphenyl boronic acid (194.0 mg; 1.0 mmol): 77% conversion; ^{1}H NMR (600 MHz, CDCl$_3$): δ 10.05 (s, 1H), 7.95 (d, J = 8.4 Hz, 2H), 7.76 (d, J = 8.4 Hz, 2H), 7.63 (m, 4H), 0.31 (s, 9H). ^{13}C NMR (150 MHz, CDCl$_3$): δ 193.0, 148.3, 142.2, 141.2, 136.4, 135.2, 131.4, 128.8, 127.8, 0.0. EI-MS (m/z): M$^+$ 254.11279, Calcd. 254.11269 for C$_{16}$H$_{18}$OSi; [M – CH$_3$]$^+$ 239.08853, Calcd. 239.08922 for C$_{15}$H$_{15}$OSi.

⟨biphenyl structure⟩———COCH$_3$
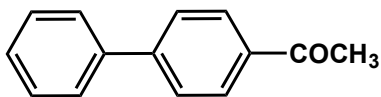
4'-Acetylbiphenyl[90] from 4'-bromoacetophenone (99.5 mg; 0.5 mmol) and phenyl boronic acid (121.9 mg; 1.0 mmol): 100% conversion; ^{1}H NMR (600 MHz, CDCl$_3$): δ 8.03 (d, J = 9.0 Hz, 2H), 7.68 (d, J = 8.4 Hz, 2H), 7.63 (d, J = 7.8 Hz, 2H), 7.47 (t, J = 7.8 Hz, 2H), 7.41 (t, J = 7.8 Hz, 1H). ^{13}C NMR (150 MHz, CDCl$_3$): δ 197.8, 145.9, 140.0, 136.0, 129.1, 129.0, 128.4, 127.4, 127.3, 26.8.

⟨biphenyl structure⟩———CF$_3$
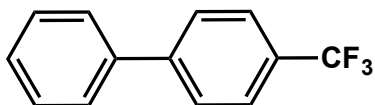
4-Trifluoromethylbiphenyl[91] from 4-bromobenzotrifluoride (114.1 mg; 0.5 mmol) and phenyl boronic acid (121.9 mg; 1.0 mmol): 100% conversion; ^{1}H NMR (600 MHz, CDCl$_3$): δ 7.70 (s, 4H), 7.61 (d, J = 8.4 Hz, 2H), 7.49 (t, J = 8.4 Hz, 2H), 7.42 (t, J = 6.0, 7.8 Hz, 1H).
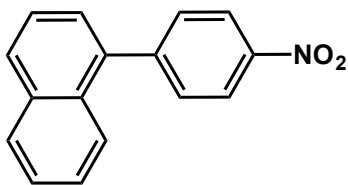
1-(4-Nitrophenyl)naphthalene[81] from 1-bromo-4-nitrobenzene (101.0 mg, 0.5 mmol) and 1-naphthalene boronic acid (172.0 mg; 1.0 mmol): 100% conversion; ^{1}H NMR (600 MHz, CDCl$_3$): δ 8.35 (d, J = 9.0 Hz, 2H), 7.95 (m, 2H), 7.78 (d, J = 9.0 Hz, 1H), 7.67 (d, J = 9.0 Hz, 2H), 7.583-7.537 (m, 2H), 7.49 (t, J = 7.8 Hz, 1H), 7.44 (d, J = 6.6 Hz, 1H). ^{13}C NMR (150 MHz, CDCl$_3$): δ 147.7, 147.2, 137.8, 133.8, 130.9, 129.0, 128.6, 127.1, 126.8, 126.2, 125.3, 125, 1, 123.6. LC-MS (m/z): [M + H]$^+$ 250.2.
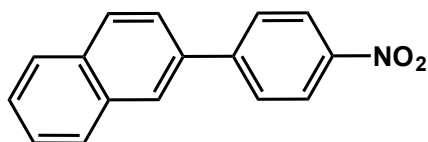
2-(4-Nitrophenyl)naphthalene[81] from 1-bromo-4-nitrobenzene (101.0 mg, 0.5 mmol) and 2-naphthalene boronic acid (172.0 mg; 1.0 mmol): 100% conversion; ^{1}H NMR (600 MHz, CDCl$_3$): δ 8.33 (d, J = 9.0 Hz, 2H), 8.09 (d, J = 1.2 Hz, 1H), 7.97 (d, J = 8.4 Hz, 1H), 7.94 (t, J = 5.4 Hz, 1H), 7.90 (t, J = 5.4 Hz, 1H), 7.85 (d, J = 9.0 Hz, 1H), 7.74 (dd, J = 2.4, 9.0 Hz, 1H), 7.57-7.54 (m, 2H). ^{13}C NMR (150 MHz, CDCl$_3$): δ 147.5, 147.1, 136.0, 133.5, 133.3, 129.0, 128.4, 128.0, 127.7, 126.9, 126.8, 124.9, 124.2.
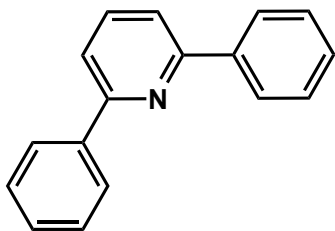
2,6-Diphenylpyridine[92] from 2,6-dibromopyridine (118.5 mg; 0.5 mmol) and phenyl boronic acid (181.5 mg; 1.5 mmol): 100% conversion; ^{1}H NMR (600 MHz,

CDCl$_3$): δ 8.18 (d, J = 9.0 Hz, 4H), 7.81 (t, J = 7.8 Hz, 1H), 7.70 (d, J = 7.8 Hz, 2H), 7.52 (dd, J = 7.2, 7.8 Hz, 4H), 7.45 (t, J = 7.2 Hz, 2H). ^{13}C NMR (150 MHz, CDCl$_3$): δ 156.8, 139.5, 137.5, 129.0, 128.7, 127.0, 118.6. LC-MS (m/z): [M + H]$^+$ 232.1.
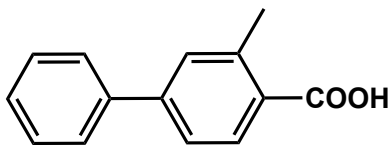
Biphenyl-3-methyl-4-carboxylic acid from 4-bromo-2-methylbenzoic acid (107.5 mg; 0.5 mmol) and phenyl boronic acid (121.9 mg; 1.0 mmol): 84% conversion; ^{1}H NMR (600 MHz, CDCl$_3$): δ 8.17 (d, J = 9.0 Hz, 1H), 7.64 (d, J = 7.2 Hz, 2H), 7.53-7.51 (m, 2H), 7.47 (t, J = 7.2 Hz, 2H), 7.40 (t, J = 7.2 Hz, 1H), 2.76 (s, 3H). ^{13}C NMR (150 MHz, CDCl$_3$): δ 173.2, 145.7, 142.1, 140.0, 132.4, 130.7, 129.0, 128.3, 127.4, 127.0, 124.6, 22.5. ESI-MS (m/z): [M − H]$^-$ 211.0762, Calcd. 211.0765 for [C$_{14}$H$_{11}$O$_2$]$^-$.
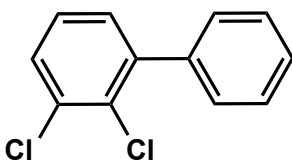
2,3-Dichlorobiphenyl[80] from 1-bromo-2,3-dichlorobenzene (113.0 mg; 0.5 mmol) and phenyl boronic acid (121.9 mg; 1.0 mmol): 100% conversion; ^{1}H NMR (600 MHz, CDCl$_3$): δ 7.48-7.44 (m, 3H), 7.42-7.40 (m, 3H), 7.27-7.24 (m, 2H). ^{13}C NMR (150 MHz, CDCl$_3$): δ 142.9, 139.3, 133.6, 131.2, 129.5, 129.4, 129.3, 128.1, 127.9, 127.1.
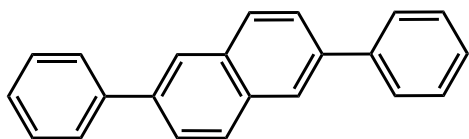
2,6-Diphenylnaphthalene[82] from 2,6-dibromonaphthalene (143 mg; 0.5 mmol) and phenyl boronic acid (181.5 mg; 1.5 mmol): 100% conversion; ^{1}H NMR (600 MHz,

CDCl$_3$): δ 8.07 (d, J = 2.4 Hz, 2H), 7.98 (d, J = 8.4 Hz, 2H), 7.79 (dd, J = 1.8, 8.4 Hz, 2H), 7.75 (d, J = 8.4 Hz, 4H), 7.50 (t, J = 7.8 Hz, 4H), 7.39 (t, J = 7.2 Hz, 2H).
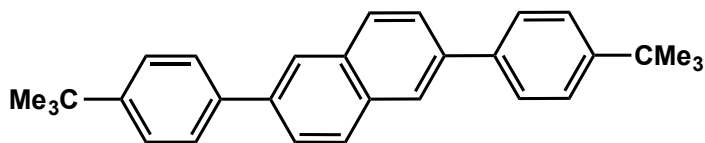
2,6-*Bis*(4-*tert*-butylphenyl)naphthalene from 2,6-dibromonaphthalene (143 mg; 0.5 mmol) and 4-*tert*-butylphenyl boronic acid (267.0 mg; 1.5 mmol): 67% conversion; ^{1}H NMR (600 MHz, CDCl$_3$): δ 8.05 (d, J = 1.2 Hz, 2H), 7.94 (d, J = 8.4 Hz, 2H), 7.77 (dd, J = 1.8, 9.0 Hz, 2H), 7.69 (d, J = 8.4 Hz, 4H), 7.52 (d, J = 7.8 Hz, 4H). ^{13}C NMR (150 MHz, CDCl$_3$): δ 150.7, 138.6, 138.5, 133.1, 128.9, 127.3, 126.2, 126.1, 125.5, 31.7. EI-MS (m/z): M$^+$ 392.24999, Calcd. 292.25040 for C$_{30}$H$_{32}$; [M − CH$_3$]$^+$ 377.22700, Calcd. 377.22693 for C$_{19}$H$_{29}$.
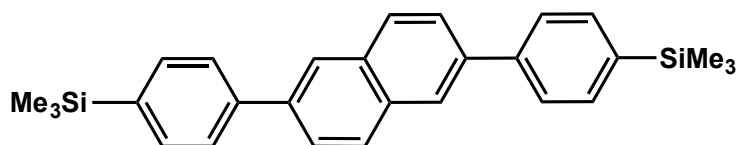
2,6-*Bis*(4-*tri*-methylsilylphenyl)naphthalene from 2,6-dibromonaphthalene (143 mg; 0.5 mmol) and 4-*tri*-methylsilylphenyl boronic acid (291.0 mg; 1.5 mmol): 86% conversion; ^{1}H NMR (600 MHz, CDCl$_3$): δ 8.08 (d, J = 1.2 Hz, 2H), 7.97 (d, J = 8.4 Hz, 2H), 7.79 (dd, J = 1.8, 9.0 Hz, 2H), 7.74 (d, J = 7.8 Hz, 4H), 7.66 (d, J = 7.8 Hz, 4H). ^{13}C NMR (150 MHz, CDCl$_3$): δ 141.6, 139.7, 138.8, 134.1, 133.1, 128.9, 126.9, 126.2, 125.7, − 0.9. EI-MS (m/z): M$^+$ 424.20360, Calcd. 424.20425 for C$_{28}$H$_{32}$Si$_2$; [M − CH$_3$]$^+$ 409.18077, Calcd. 409.18079 for C$_{27}$H$_{29}$Si.
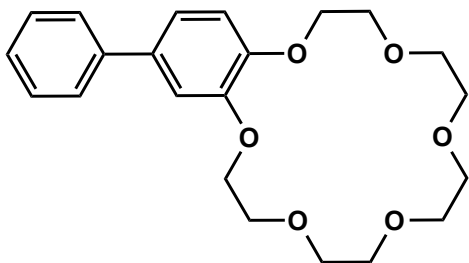
4-Phenylbenzo-18-crown-6 from 4-bromobenzo-18-crown-6 (195.6 mg; 0.5 mmol) and phenyl boronic acid (121.9 mg; 1.0 mmol): 56% conversion; ^{1}H NMR (600 MHz, CDCl$_3$): δ 7.53 (d, J = 8.4 Hz, 2H), 7.41 (t, J = 8.4 Hz, 2H), 7.30 (t, J = 7.8 Hz, 1H), 7.14-7.12 (m, 2H), 6.94 (d, d, J = 8.4 Hz, 1H), 4.25 (m, 4H), 3.96-3.95 (m, 4H), 3.79-3.78 (m, 4H), 3.73-3.72 (m, 4H), 3.69 (s, 4H). ^{13}C NMR (150 MHz, CDCl$_3$): δ 141.0, 134.8, 128.8, 126.9, 120.1, 114.2, 113.2, 70.8, 69.7, 69.1. ESI-MS (m/z): [M + NH$_4$]$^+$ 406.2225, Calcd. 406.2224 for C$_{22}$H$_{32}$NO$_6$; [M + Na]$^+$ 411.1771, Calcd. 411.1778 for C$_{22}$H$_{28}$NaO$_6$; [M + K]$^+$ 427.1513, Calcd. 427.1517 for C$_{22}$H$_{28}$KO$_6$.
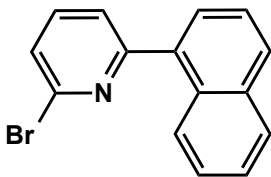
2-Bromo-6-(1-naphthyl)pyridine[93] from 2,6-dibromopyridine (118.5 mg; 0.5 mmol) and 1-naphthalene boronic acid (258.0 mg; 1.5 mmol): 33% conversion; ^{1}H NMR (600 MHz, CDCl$_3$): δ 8.08-8.06 (m, 1H), 7.93-7.90 (m, 2H), 7.68 (t, = 7.8 Hz, 1H), 7.62-7.60 (m, 1H), 7.55-7.49 (m, 5H). ^{13}C NMR (150 MHz, CDCl$_3$): δ 160.5, 142.0, 138.8, 137.0, 134.1, 131.1, 129.7, 128.6, 128.0, 127.0, 126.6, 126.2, 125.4, 125.4, 124.1. EI-MS (m/z): M$^+$ 284.99685, Calcd. 284.99762 for C$_{15}$H$_{10}$^{81}BrN; 283.99083, Calcd. 283.98978 for C$_{15}$H$_{10}$^{79}BrN; [M – Br]$^+$ 204.08093, Calcd. 204.08133 for C$_{15}$H$_{10}$N.
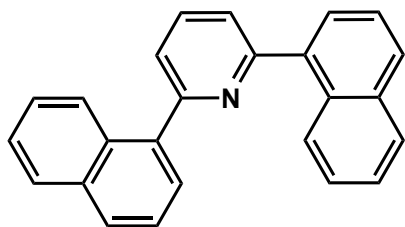
2,6-*Bis*-(1-naphthyl)pyridine[94] from 2,6-dibromopyridine (118.5 mg; 0.5 mmol) and 1-naphthalene boronic acid (258.0 mg; 1.5 mmol): 5% conversion; ^{1}H NMR (600 MHz, CDCl$_3$): δ 8.24-8.22 (m, 2H), 7.97 (t, *J* = 7.2 Hz, 1H), 7.91 (d, *J* = 9.0 Hz, 4H), 7.72 (dd, *J* = 1.2, 7.2 Hz, 2H), 7.64 (d, *J* = 7.2 Hz, 2H), 7.57 (dd, *J* = 7.2, 8.4 Hz, 2H), 7.52-7.49 (m, 4H). ^{13}C NMR (150 MHz, CDCl$_3$): δ 159.3, 138.9, 136.8, 134.2, 131.5, 129.0, 128.6, 127.9, 126.6, 126.0, 125.9, 125.6, 123.6. ESI-MS (m/z): [M + H]$^+$ 332.1425, Calcd. 332.1434 for C$_{25}$H$_{18}$N; [M + Na]$^+$ 354.1248, Calcd. 354.1253 for C$_{25}$H$_{17}$NNa.
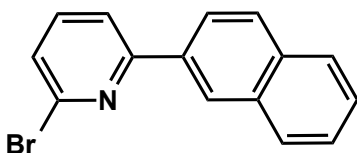
2-Bromo-6-(2-naphthyl)pyridine from 2,6-dibromopyridine (118.5 mg; 0.5 mmol) and 2-naphthalene boronic acid (258.0 mg; 1.5 mmol): 86% conversion; ^{1}H NMR (600 MHz, CDCl$_3$): δ 8.50 (s, 1H), 8.11 (dd, *J* = 1.8, 9.0 Hz, 1H), 7.96-7.92 (m, 2H), 7.88-7.86 (m, 1H), 7.82 (d, *J* = 7.2 Hz, 1H), 7.63 (t, *J* = 7.8 Hz, 1H), 7.53-7.51 (m, 2H), 7.44 (d, *J* = 8.4 Hz, 1H). ^{13}C NMR (150 MHz, CDCl$_3$): δ 158.7, 142.5, 139.2, 135.1, 134.1, 133.6, 129.0, 128.8, 127.9, 127.1, 126.9, 126.6 (2C), 124.5, 119.4. ESI-MS (m/z): [M + H]$^+$ 284.0068, Calcd. 284.0069 for C$_{15}$H$_{11}$BrN; [M + Na]$^+$ 305.9885, Calcd. 305.9889 for C$_{15}$H$_{10}$BrNNa.
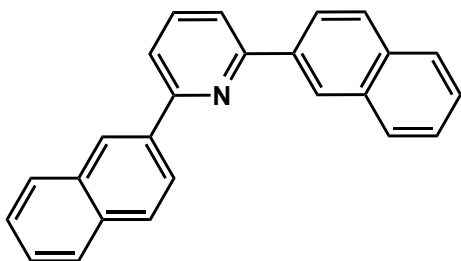
2,6-*Bis*-(2-naphthyl)pyridine[95] from 2,6-dibromopyridine (118.5 mg; 0.5 mmol) and 2-naphthalene boronic acid (258.0 mg; 1.5 mmol): 14% conversion; ^{1}H NMR (600 MHz, CDCl$_3$): δ 8.65 (s, 2H), 8.38 (dd, J = 1.8, 9.0 Hz, 2H), 8.02-7.99 (m, 4H), 7.93-7.87 (m, 5H), 7.55-7.52 (m, 4H). ^{13}C NMR (150 MHz, CDCl$_3$): δ 157.1, 137.8, 137.1, 134.0, 133.7, 129.0, 128.6, 127.9, 126.7, 126.6, 126.4, 125.0, 119.2. ESI-MS (m/z): [M + H]$^+$ 332.1426, Calcd. 332.1434 for C$_{25}$H$_{18}$N; [M + Na]$^+$ 354.1246, Calcd. 354.1253 for C$_{25}$H$_{17}$NNa.
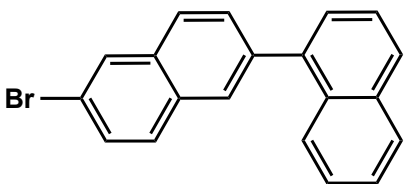
2-Bromo-6-(1-naphthyl)naphthalene from 2,6-dibromonaphthalene (143 mg; 0.5 mmol) and 1-naphthalene boronic acid (258.0 mg; 1.5 mmol): 57% conversion; ^{1}H NMR (600 MHz, CDCl$_3$): δ 8.11 (d, J = 1.8 Hz, 1H), 7.96-7.90 (m, 4H), 7.87 (d, J = 7.8 Hz, 1H), 7.76 (d, J = 8.4 Hz, 1H), 7.67 (dd, J = 1.8, 8.4 Hz, 1H), 7.62 (dd, J = 1.8, 9.0 Hz, 1H), 7.58 (t, J = 7.8 Hz, 1H), 7.54-7.51 (m, 2H), 7.47-7.44 (m, 1H). ^{13}C NMR (150 MHz, CDCl$_3$): δ 139.9, 139.0, 134.0, 133.8, 132.0, 131.8, 130.0, 129.9, 129.7, 128.9, 128.6, 128.2, 127.4, 127.0, 126.4, 126.1(2C), 125.6, 120.2. EI-MS (m/z): M$^+$ 334.01946, Calcd. 334.01801 for C$_{20}$H$_{13}$^{81}Br; 332.02027, Calcd. 332.02005 for C$_{20}$H$_{13}$^{79}Br; [M − Br]$^+$ 253.09874, Calcd. 253.10173 for C$_{20}$H$_{13}$.
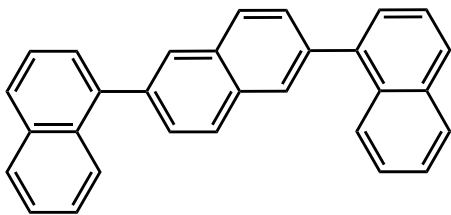
2,6-*Bis*-(1-naphthyl)naphthalene from 2,6-dibromonaphthalene (143 mg; 0.5 mmol) and 1-naphthalene boronic acid (258.0 mg; 1.5 mmol): 43% conversion; ^{1}H NMR (600 MHz, CDCl$_3$): δ 8.08 (s, 2H), 8.04-8.02 (m, 4H), 7.98 (d, J = 8.4 Hz, 2H), 7.94 (d, J = 7.8 Hz, 2H), 7.73 (d, J = 7.8 Hz, 2H), 7.63-7.59 (m, 4H), 7.55 (t, J = 7.2 Hz, 2H), 7.55 (t, J = 7.2 Hz, 2H) ^{13}C NMR (150 MHz, CDCl$_3$): δ 140.4, 138.8, 134.1, 132.8, 132.0, 129.2, 128.8, 128.6, 128.1, 128.0, 127.5, 126.4, 126.3, 126.1, 125.7. EI-MS (m/z): M$^+$ 380.15724, Calcd. 380.15649 for C$_{30}$H$_{20}$.
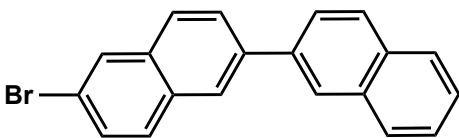
2-Bromo-6-(2-naphthyl)naphthalene from 2,6-dibromonaphthalene (143 mg; 0.5 mmol) and 2-naphthalene boronic acid (258.0 mg; 1.5 mmol): >98% conversion; ^{1}H NMR (600 MHz, CDCl$_3$): δ 8.16 (s, 1H), 8.13 (s, 1H), 8.05 (d, J = 1.2 Hz, 1H), 7.97-7.81 (m, 6H), 7.80 (d, J = 9.0 Hz, 1H), 7.60 (dd, J = 1.8, 8.4 Hz, 1H), 7.55-7.50 (m, 2H). ^{13}C NMR (150 MHz, CDCl$_3$): δ 139.11, 138.13, 133.9 (2C), 132.9, 132.4, 130.1, 129.9, 128.8, 128.4, 127.9, 127.8, 127.0, 126.6, 126.4, 126.2, 125.7, 120.1. EI-MS (m/z): M$^+$ 334.01862, Calcd. 334.01801 for C$_{20}$H$_{13}$^{81}Br; 332.02038, Calcd. 332.02005 for C$_{20}$H$_{13}$^{79}Br; [M – HBr]$^+$ 252.09392, Calcd. 252.09390 for C$_{20}$H$_{12}$.
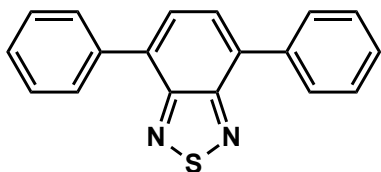
4,7-Biphenyl-2,1,3-benzothiadiazole[51] from bromobenzene (78.5 mg, 0.5 mmol) and 2,1,3-benzothiadiazole-4,7-bis(boronic acid pinacol ester) (**4.1**; 97.0 mg; 0.25 mmol): 75% yield; ^{1}H NMR (600 MHz, CDCl$_3$): δ 7.97 (d, J = 7.2 Hz, 4H), 7.80 (s, 2H), 7.57-7.55 (m, 4H), 7.48-7.46 (m, 4H). ^{13}C NMR (150 MHz, CDCl$_3$): δ 154.3, 137.7, 133.6, 129.5, 128.9, 128.6, 128.4. High res. MALDI-MS (m/z): 288.07131 (Calcd. 288.07211 for C$_{18}$H$_{12}$N$_2$S (M$^+$)).
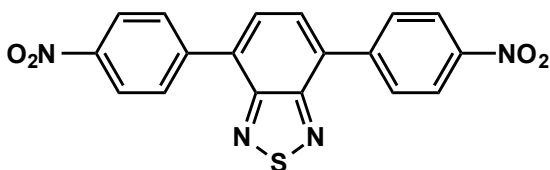
4,7-*Bis*-(4-nitrophenyl)-2,1,3-benzothiadiazole from 1-bromo-4-nitrobenzene (101.0 mg, 0.5 mmol) and **4.1** (97.0 mg; 0.25 mmol): 81% yield; ^{1}H NMR (600 MHz, CDCl$_3$): δ 8.43 (d, J = 8.4 Hz, 4H), 8.19 (d, J = 8.4 Hz, 4H), 7.93 (s, 2H). ^{13}C NMR (150 MHz, CDCl$_3$): δ 153.8, 148.0, 143.3, 132.6, 130.4, 129.0, 124.1. High res. MALDI-MS (m/z): 378.04189 (Calcd. 378.04227 for C$_{18}$H$_{10}$O$_4$N$_4$S (M$^+$)).
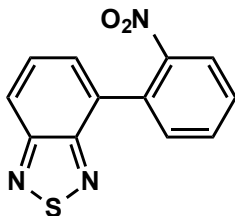
4-(2-Nitrophenyl)-2,1,3-benzothiadiazole from 2-iodonitrobenzene (124.5 mg, 0.5 mmol) and **4.1** (97.0 mg; 0.25 mmol): 35% yield; ^{1}H NMR (600 MHz, CDCl$_3$): δ 8.16 (d, J = 7.8 Hz, 1H), 8.06 (d, J = 8.4 Hz, 1H), 7.76-7.69 (m, 2H), 7.65-7.58 (m, 3H). ^{13}C

NMR (150 MHz, CDCl$_3$): δ 154.8, 153.4, 149.5, 133.4, 132.8, 132.7, 132.0, 129.7, 129.6, 128.1, 125.1, 121.9. High res. MALDI-MS (m/z): 257.02573 (Calcd. 257.02591 for C$_{12}$H$_7$O$_2$N$_3$S (M$^+$)).
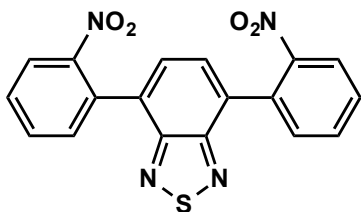
4,7-*Bis*-(2-nitrophenyl)-2,1,3-benzothiadiazole[48] from 2-iodonitrobenzene (124.5 mg, 0.5 mmol) and **4.1** (97.0 mg; 0.25 mmol): 38% yield; ^{1}H NMR (600 MHz, CDCl$_3$): δ 8.18 (d, *J* = 9.0 Hz, 2H), 7.79-7.77 (m, 2H), 7.71 (s, 2H), 7.67-7.65 (m, 4H). ^{13}C NMR (150 MHz, CDCl$_3$): δ 153.2, 149.5, 133.5, 132.9, 132.4, 132.0, 129.8, 128.3, 125.1. High res. MALDI-MS (m/z): 378.04239 (Calcd. 378.04227 for C$_{18}$H$_{10}$O$_4$N$_4$S (M$^+$)).

4,7-*Bis*-(4-cyanophenyl)-2,1,3-benzothiadiazole[57,58] from 4-bromobenzonitrile (91.0 mg, 0.5 mmol) and **4.1** (97.0 mg; 0.25 mmol): 84% yield; ^{1}H NMR (600 MHz, CDCl$_3$): δ 8.12 (d, *J* = 8.4 Hz, 4H), 7.88 (s, 2H), 7.85 (d, *J* = 8.4 Hz, 4H). ^{13}C NMR (150 MHz, CDCl$_3$): δ 153.8, 141.5, 132.8, 132.7, 130.1, 128.8, 118.9, 112.5.
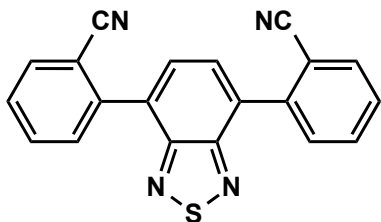
4,7-*Bis*-(2-cyanophenyl)-2,1,3-benzothiadiazole from 2-bromobenzonitrile (91.0 mg, 0.5 mmol) and **4.1** (97.0 mg; 0.25 mmol): 48% yield; ^{1}H NMR (600 MHz, CDCl$_3$): δ

7.90-7.89 (m, 4H), 7.86 (d, J = 7.2 Hz, 2H), 7.81-7.78 (m, 2H), 7.62-7.59 (m, 2H). [13]C

NMR (150 MHz, CDCl$_3$): δ 153.7, 140.8, 133.9, 133.0, 131.9, 131.7, 130.0, 129.1, 118.5,

112.8. Low res. MALDI-MS (m/z): 339.0 (M+H)$^+$. High res. MALDI-MS (m/z):

339.06989 (Calcd. 339.06971 for C$_{20}$H$_{11}$N$_4$S (M+H)$^+$; 356.09644 (Calcd. 356.09653 for

C$_{20}$H$_{14}$N$_5$S (M+NH$_4$)$^+$; 361.05184 (Calcd. 361.05170 for C$_{20}$H$_{10}$N$_4$NaS (M+Na)$^+$).
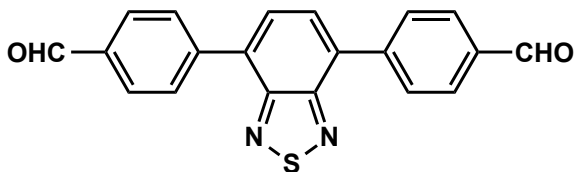
2,1,3-Benzothiadiazolyl-4,7-*bis*-(phenyl-4-carbaldehyde)[53,54] from 4-bromobenz-

aldehyde (92.5 mg, 0.5 mmol) and **4.1** (97.0 mg; 0.25 mmol): 84% yield; ^{1}H NMR (600

MHz, CDCl$_3$): δ 10.13 (s, 2H), 8.17 (d, J = 8.4 Hz, 4H), 8.07 (d, J = 8.4 Hz, 4H), 7.91 (s,

2H). ^{13}C NMR (150 MHz, CDCl$_3$): δ 192.0, 154.0, 143.1, 136.3, 133.2, 130.2, 130.1,

128.9.
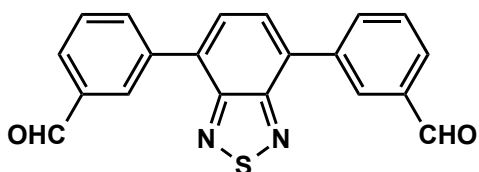
2,1,3-Benzothiadiazolyl-4,7-*bis*-(phenyl-3-carbaldehyde) from 3-bromobenz-

aldehyde (92.5 mg, 0.5 mmol) and **4.1** (97.0 mg; 0.25 mmol): 86% yield; ^{1}H NMR (600

MHz, CDCl$_3$): δ 10.16 (s, 2H), 8.51 (s, 2H), 8.30 (d, J = 7.8 Hz, 2H), 8.00 (d, J = 7.8 Hz,

2H), 7.90 (s, 2H), 7.75 (t, J = 7.8 Hz, 2H). ^{13}C NMR (150 MHz, CDCl$_3$): δ 192.3, 154.0,

138.3, 137.1, 135.3, 132.8, 130.6, 129.9, 129.6, 128.6. Low res. MALDI-MS (m/z): 345.0

(M+H)$^+$. High res. MALDI-MS (m/z): 345.06922 (Calcd. 345.06914 for C$_{20}$H$_{13}$O$_2$N$_2$S

(M+H)$^+$).
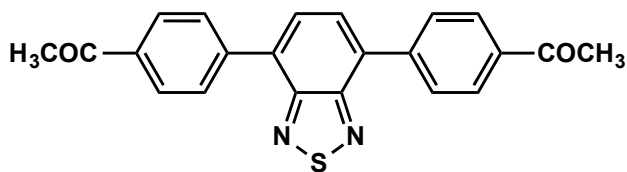
4,7-*Bis*-(4′-acetylphenyl)-2,1,3-benzothiadiazole from 4′-bromoacetophenone (99.5 mg; 0.5 mmol) and **4.1** (97.0 mg; 0.25 mmol): 86% yield; ^{1}H NMR (600 MHz, CDCl$_3$): δ 8.15 (d, J = 8.4 Hz, 4H), 8.09 (d, J = 8.4 Hz, 4H), 7.88 (s, 2H), 2.69 (s, 6H). ^{13}C NMR (150 MHz, CDCl$_3$): δ 197.9, 154.0, 141.9, 137.0, 133.2, 129.7, 128.9, 128.7, 27.0. Low res. MALDI-MS (m/z): 372.0 (M$^+$). High res. MALDI-MS (m/z): 372.09267 (Calcd. 372.09275 for C$_{22}$H$_{16}$O$_2$N$_2$S (M$^+$)).

4,7-*Bis*-(4-trifluoromethylphenyl)-2,1,3-benzothiadiazole[51] from 4-bromobenzo-trifluoride (114.1 mg; 0.5 mmol) and **4.1** (97.0 mg; 0.25 mmol): 90% yield; ^{1}H NMR (600 MHz, CDCl$_3$): δ 8.10 (d, J = 7.8 Hz, 4H), 7.86 (s, 2H), 7.82 (d, J = 7.8 Hz, 4H). ^{13}C NMR (150 MHz, CDCl$_3$): δ 154.0, 140.8, 133.0, 130.7 (q, J = 32.3 Hz), 129.9, 128.7, 125.8 (q, J = 3.5 Hz), 124.4 (q, J = 271.4 Hz). ^{19}F NMR (564 MHz, CDCl$_3$): δ −62.6 (s, 6F). High res. MALDI-MS (m/z): 425.05428 (Calcd. 425.05440 for C$_{20}$H$_{11}$F$_6$N$_2$S (M+H)$^+$).
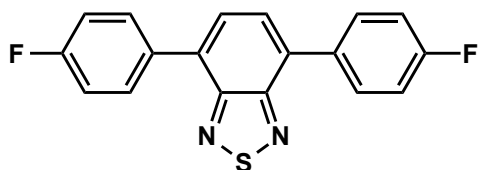
4,7-*Bis*-(4-fluorophenyl)-2,1,3-benzothiadiazole[58] from 4-bromofluorobenzene (87.5 mg; 0.5 mmol) and **4.1** (97.0 mg; 0.25 mmol): 92% yield; ^{1}H NMR (600 MHz,

CDCl$_3$): δ 7.97-7.94 (m, 4H), 7.75 (s, 2H), 7.26-7.23 (m, 4H). ^{13}C NMR (150 MHz, CDCl$_3$): δ 163.2 (d, J = 247.2 Hz), 154.2, 133.6 (d, J = 2.3 Hz), 132.6, 131.2 (d, J = 8.1 Hz), 128.1, 115.9 (d, J = 21.8 Hz). ^{19}F NMR (564 MHz, CDCl$_3$): δ −113.3-113.4 (m, 2F).
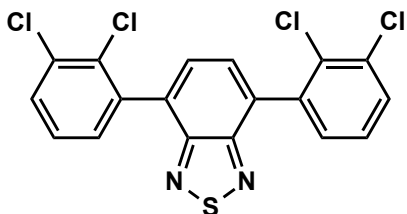
4,7-*Bis*-(2,3-dichlorophenyl)-2,1,3-benzothiadiazole from 1-bromo-2,3-dichloro-benzene (113.0 mg; 0.5 mmol) and **4.1** (97.0 mg; 0.25 mmol): 76% yield; ^{1}H NMR (600 MHz, CDCl$_3$): δ 7.68 (s, 2H), 7.61 (dd, J = 1.2, 7.8 Hz, 2H), 7.46 (dd, J = 1.2, 7.8 Hz, 2H), 7.38 (t, J = 7.2, 7.8 Hz, 2H). ^{13}C NMR (150 MHz, CDCl$_3$): δ 153.7, 138.5, 134.1, 132.6, 132.3, 130.9, 130.2, 129.7, 127.5. Low res. MALDI-MS (m/z): 424.9 (M+H)$^{+}$. High res. MALDI-MS (m/z): 424.92346 (Calcd. 424.92351 for C$_{18}$H$_9$Cl$_4$N$_2$S (M+H)$^{+}$).

4,7-*Bis*-(4-tolyl)-2,1,3-benzothiadiazole[52] from 4-bromotoluene (85.5 mg; 0.5 mmol) and **4.1** (97.0 mg; 0.25 mmol): 89% yield; ^{1}H NMR (600 MHz, CDCl$_3$): δ 7.87 (d, J = 8.4 Hz, 4H), 7.76 (s, 2H), 7.37 (d, J = 8.4 Hz, 4H), 2.46 (s, 6H). ^{13}C NMR (150 MHz, CDCl$_3$): δ 154.4, 138.5, 134.9, 133.3, 129.6, 129.3, 128.0, 21.5.
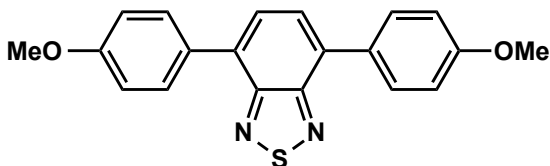
4,7-*Bis*-(4-methoxyphenyl)-2,1,3-benzothiadiazole[59-62] from 4-bromoanisole (93.5 mg; 0.5 mmol) and **4.1** (97.0 mg; 0.25 mmol): 84% yield; ^{1}H NMR (600 MHz, CDCl$_3$): δ

7.93 (d, J = 8.4 Hz, 4H), 7.72 (s, 2H), 7.09 (d, J = 8.4 Hz, 4H), 3.90 (s, 6H). ^{13}C NMR

(150 MHz, CDCl$_3$): δ 160.0, 154.4, 132.6, 130.6, 130.2, 127.6, 114.3, 55.6.
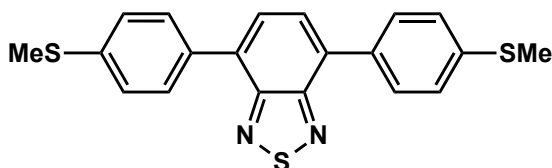
4,7-*Bis*-(4-(mercaptomethyl)phenyl)-2,1,3-benzothiadiazole[59-62] from 4-bromo-

thioanisole (101.6 mg; 0.5 mmol) and **4.1** (97.0 mg; 0.25 mmol): 30% yield; ^{1}H NMR

(600 MHz, CDCl$_3$): δ 7.92 (d, J = 8.4 Hz, 4H), 7.76 (s, 2H), 7.43 (d, J = 8.4 Hz, 4H),

2.57 (s, 6H). ^{13}C NMR (150 MHz, CDCl$_3$): δ 154.3, 139.4, 134.3, 132.8, 129.7, 127.9,

126.7, 15.9. Low res. MALDI-MS (m/z): 379.9 (M$^+$). High res. MALDI-MS (m/z):

380.04673 (Calcd. 380.04681 for $C_{20}H_{16}N_2S_3$ (M$^+$)).
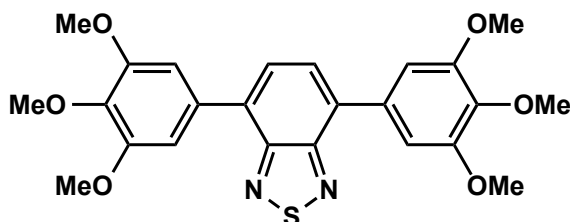
4,7-*Bis*-(3,4,5-trimethoxyphenyl)-2,1,3-benzothiadiazole from 1-bromo-3,4,5-

trimethoxybenzene (123.5 mg; 0.5 mmol) and **4.1** (97.0 mg; 0.25 mmol): 88% yield; [1]H

NMR (600 MHz, CDCl$_3$): δ 7.77 (s, 2H), 7.21 (s, 4H), 3.97 (s, 12H), 3.95 (s, 6H). [13]C

NMR (150 MHz, CDCl$_3$): δ 154.3, 153.6, 138.8, 133.4, 133.1, 128.0, 106.9, 61.2, 56.5.

Low res. MALDI-MS (m/z): 468.0 (M$^+$). High res. MALDI-MS (m/z): 468.13496 (Calcd.

468.13503 for $C_{24}H_{24}O_6N_2S$ (M$^+$)).
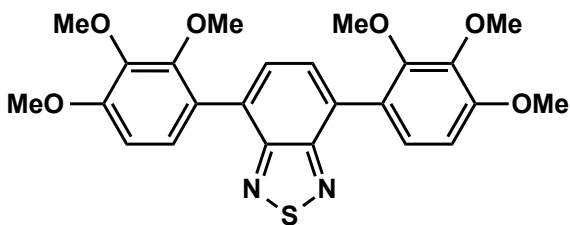
4,7-*Bis*-(2,3,4-trimethoxyphenyl)-2,1,3-benzothiadiazole from 1-bromo-2,3,4-trimethoxybenzene (123.5 mg; 0.5 mmol) and **4.1** (97.0 mg; 0.25 mmol): 19% yield; ^{1}H NMR (600 MHz, CDCl$_3$): δ 7.69 (s, 2H), 7.31 (d, J = 9.0 Hz, 2H), 6.85 (d, J = 9.0 Hz, 2H), 3.96 (s, 6H), 3.95 (s, 6H) 3.78 (s, 6H). ^{13}C NMR (150 MHz, CDCl$_3$): δ 154.8, 154.2, 152.2, 142.6, 130.3, 129.9, 126.2, 124.4, 107.4, 61.5, 61.1, 56.3. High res. MALDI-MS (m/z): 468.13613 (Calcd. 468.13550 for C$_{24}$H$_{24}$O$_6$N$_2$S (M$^+$)).
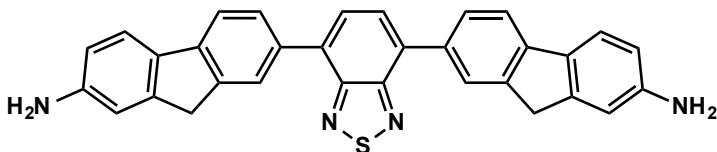
4,7-*Bis*-(2-amino-7-fluoryl)-2,1,3-benzothiadiazole from 2-Amino-7-bromo-fluorene (130.1 mg; 0.5 mmol) and **4.1** (97.0 mg; 0.25 mmol): 63% yield; ^{1}H NMR (600 MHz, DMSO): δ 8.14 (s, 2H), 7.97-7.96 (m, 4H), 7.76 (d, J = 7.8 Hz, 2H), 7.76 (d, J = 8.4 Hz, 2H), 6.81 (s, 2H), 6.64-6.63 (m, 2H), 5.31 (s, 4H), 3.87 (s, 4H). ^{13}C NMR (150 MHz, DMSO): δ 153.6, 148.8, 145.3, 142.5, 141.8, 132.9, 132.2, 129.1, 127.8, 127.7, 125.3, 120.9, 117.9, 112.9, 110.3, 36.3. Low res. MALDI-MS (m/z): 494.0 (M$^+$). High res. MALDI-MS (m/z): 494.15590 (Calcd. 494.15599 for C$_{32}$H$_{22}$N$_4$S (M$^+$)).
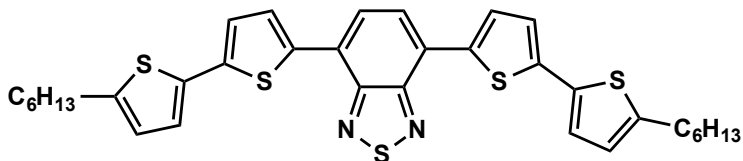
4,7-*Bis*-(5-(5′-hexyl-2,2′-bithienyl))-2,1,3-benzothiadiazole from 5-Bromo-5′-hexyl-2,2′-bithiophene (164.7 mg; 0.5 mmol) and **4.1** (97.0 mg; 0.25 mmol): 14% yield;

^{1}H NMR (600 MHz, CDCl$_3$): δ 8.03 (d, J = 3.6 Hz, 2H), 7.83 (s, 2H), 7.19 (d, J = 3.6 Hz, 2H), 7.11 (d, J = 3.6 Hz, 2H), 6.73 (d, J = 3.6 Hz, 2H), 2.82 (t, J = 7.2 Hz, 4H), 1.73-1.68 (m, 4H), 1.42-1.38 (m, 4H), 1.34-1.32 (m, 8H), 0.91 (m, 6H). ^{13}C NMR (150 MHz, CDCl$_3$): δ 152.8, 146.3, 139.6, 137.7, 134.9, 128.5, 125.8, 125.3, 125.2, 124.1, 124.0, 31.8, 30.5, 29.0, 22.8, 14.3. Low res. MALDI-MS (m/z): 631.9 (M$^+$). High res. MALDI-MS (m/z): 632.14764 (Calcd. 632.14773 for C$_{34}$H$_{36}$N$_2$S$_5$ (M$^+$)).
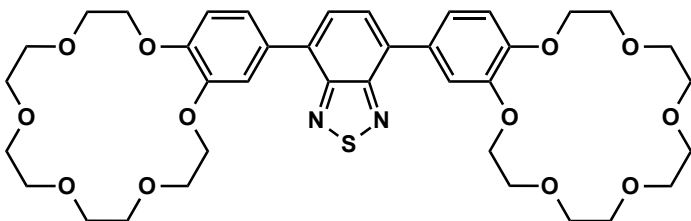
4,7-*Bis*-(4'-(benzo-18-crown-6))-2,1,3-benzothiadiazole from 4-bromobenzo-18-crown-6 (195.6 mg; 0.5 mmol) and **4.1** (97.0 mg; 0.25 mmol): 58% yield; ^{1}H NMR (600 MHz, CDCl$_3$): δ 7.72 (s, 2H), 7.58 (d, J = 1.8 Hz, 2H), 7.55 (dd, J = 1.8, 8.4 Hz, 2H), 7.04 (d, J = 8.4 Hz, 2H), 4.30-4.25 (m, 8H), 3.99 (s, 8H), 3.82-3.80 (m, 8H), 3.75-3.71 (m, 16H). ^{13}C NMR (150 MHz, CDCl$_3$): δ 154.4, 149.4, 149.0, 132.6, 130.9, 127.7, 122.6, 115.6, 114.2, 70.9, 69.8, 69.7, 69.4, 54.0, 31.9, 29.9, 29.5, 22.9, 14.3. Low res. MALDI-MS (m/z): 756.0 (M$^+$); 779.0 (M+Na)$^+$; 795.0 (M+K)$^+$. ESI-MS (m/z): [M + NH$_4$]$^+$ 774.3252, Calcd. 774.3266 for C$_{38}$H$_{52}$N$_3$O$_{12}$S; [M + Na]$^+$ 779.2809, Calcd. 779.2820 for C$_{38}$H$_{48}$N$_2$NaO$_{12}$S; [M + K]$^+$ 795.2570, Calcd. 795.2583 for C$_{38}$H$_{48}$N$_2$KO$_{12}$S.
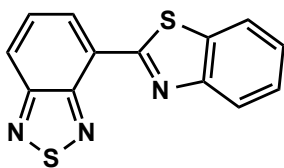
4-(2-Benzothiazolyl)-2,1,3-benzothiadiazole from 2-bromobenzothiazole (107.0 mg; 0.5 mmol) and **4.1** (97.0 mg; 0.25 mmol): <5% yield; ^{1}H NMR (600 MHz, CDCl$_3$): δ

8.79 (d, J = 7.2 Hz, 1H), 8.17 (t, J = 8.4 Hz, 2H), 8.02 (d, J = 7.8 Hz, 1H), 7.79 (dd, J = 7.2, 9.0 Hz, 1H), 7.55 (t, J = 7.2 Hz, 1H), 7.45 (t, J = 7.2 Hz, 1H). ^{13}C NMR (150 MHz, CDCl$_3$): δ 162.8, 155.5, 153.0, 152.3, 137.0, 129.7, 129.1, 126.7, 126.5, 125.6, 123.8, 123.6, 121.9. High res. MALDI-MS (m/z): 269.00753 (Calcd. 269.00815 for C$_{13}$H$_7$N$_3$S$_2$ (M$^+$)).
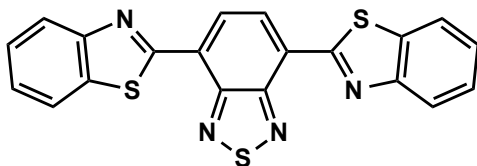
4,7-*Bis*-(2-benzothiazolyl)-2,1,3-benzothiadiazole from 2-bromobenzothiazole (107.0 mg; 0.5 mmol) and **4.1** (97.0 mg; 0.25 mmol): <5% yield; ^{1}H NMR (600 MHz, CDCl$_3$): δ 8.99 (s, 2H), 8.21 (d, J = 7.8 Hz, 2H), 8.04 (d, J = 7.8 Hz, 2H), 7.58 (t, J = 7.8 Hz, 2H), 7.47 (t, J = 7.8 Hz, 2H). ^{13}C NMR (150 MHz, CDCl$_3$): δ 162.2, 153.1, 152.8, 137.3, 129.1, 127.8, 126.9, 126.0, 123.9, 122.0. High res. MALDI-MS (m/z): 402.00647 (Calcd. 402.00677 for C$_{20}$H$_{10}$N$_4$S$_3$ (M$^+$)).
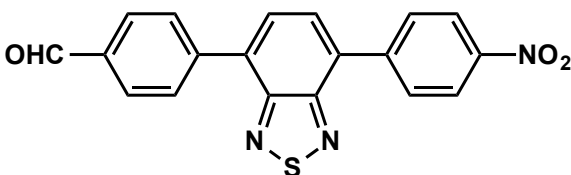
4-(4-Nitrophenyl)-7-(phenyl-4-carbaldehyde)-2,1,3-benzothiadiazole from 1-bromo-4-nitrobenzene (50.5 mg, 0.25 mmol), 4-bromobenzaldehyde (46.3 mg, 0.25 mmol) and **4.1** (97.0 mg; 0.25 mmol): 49% yield; ^{1}H NMR (600 MHz, CDCl$_3$): δ 10.13 (s, 1H), 8.41 (d, J = 9.0 Hz, 2H), 8.20-8.17 (m, 4H), 8.08 (d, J = 8.4 Hz, 2H), 7.92 (s, 2H). ^{13}C NMR (150 MHz, CDCl$_3$): δ 192.0, 154.0, 153.8, 147.9, 143.5, 142.9, 136.4, 133.7, 132.1, 130.3, 130.2, 130.1, 129.1, 128.8, 124.1. Low res. MALDI-MS (m/z): 361.9

(M+H)$^{+}$. High res. MALDI-MS (m/z): 362.05939 (Calcd. 362.05967 for C$_{19}$H$_{12}$O$_{3}$N$_{3}$S (M+H)$^{+}$).

n = 2.4-9.1
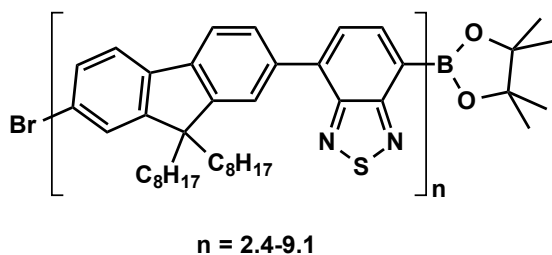
Poly[(9,9-di-n-octylfluorenyl-2,7-diyl)-alt-(benzo[2,1,3]thiadiazol-4,8-diyl)] from 2,7-Dibromo-9,9-di-n-octylfluorene (274.2 mg; 0.5 mmol) and **4.1** (194.1 mg; 0.5 mmol): 51% yield; ^{1}H NMR (600 MHz, CDCl$_{3}$): δ 8.09-7.80 (m, 6H), 7.52-7.49 (m, 1H), 2.14-1.96 (m, 4H), 1.22-1.11 (m, 24H), 0.95 (s, 2H), 0.83-0.77 (m, 9H). Average M$_{n}$ 1300-5000 (GPC).

4.4 References

(1)   Astruc, D. *Nanoparticles and Catalysis*; Weinheim: Wiley-VCH, 2008.

(2)   Astruc, D. *Inorg. Chem.* **2007**, *46*, 1884–1894.

(3)   Narayanan, R. *Molecules* **2010**, *15*, 2124–2138 and references therein.

(4)   Ogasawara, S.; Kato, S. *J. Am. Chem. Soc.*, **2010**, *132*, 4608–4613.

(5)   Piao, Y.; Jang, Y.; Shokouhimehr, M.; Lee, I. S.; Hyeon, T. *Small* **2007**, *3*, 255–260.

(6)   Zhou, S.; Johnson, M; Veinot, J. G. C. *Chem. Commun* **2010**, *46*, 2411–2413.

(7)   Pacardo, D. B.; Sethi, M.; Jones, S. E.; Naik, R. R.; Knecht, M. R. *ACS Nano* **2009**, *3*, 1288–1296.

(8)   Pacardo, D. B.; Slocik, J. M.; Kirk, K. C.; Naik, R. R.; Knecht, M. R. *Nanoscale* **2011**, *3*, 2194–2201.

(10)   Chen, Y. -H.; Hung, H. -H.; Huong, M. H. *J. Am. Chem. Soc.*, **2009**, *131*, 9114–9121.

(11)   Kovala-Demertzi, D.; Kourkoumelis, N.; Derlat, K.; Michalak, J.; Andreadaki, F. J.; Kostas, I. D. *Inorg. Chim. Acta* **2008**, *361*, 1562–1565.

(12)   Meng, L. J.; Ren, L. Z. *eXPRESS Polym. Lett.* **2008**, *2*, 251–255.

(13)   Proch, S.; Mei, Y.; Villanueva, J. M. R.; Lu, Y.; Karpov, A.; Ballauff, M. Kempe, R. *Adv. Synth. Catal.* **2008**, *350*, 493–500.

(14)   Zhang, Z.; Wang, Z. *J. Org. Chem.* **2006**, *71*, 7485–7487.

(15)   Lu, F.; Ruiz, J.; Astruc, D. *Tetrahedron Lett.* **2004**, *45*, 9443–9445.

(16)   Gopidas, K. R.; Whitesell, J. K.; Fox, M. A. *Nano Lett.* **2003**, *3*, 1757–1760.

(17)   Fihri, A.; Bouhrara, M.; Nekoueishahraki, B.; Basset, J. -M.; Polshettiwar V. *Chem. Soc. Rev.* **2011**, *40*, 5181–5203.

(18)   Torborga, C.; Beller, M. *Adv. Synth. Catal.* **2009**, *351*, 3027–3043.

(19)   Glasnova, T. N.; Kappe, C. O. *Adv. Synth. Catal.* **2010**, *352*, 3089–3097.

(20)   Nowothnick, H.; Blum, J.; Schomäcker, R. *Angew. Chem. Int. Ed.* **2011**, *50*, 1918–1921.

(21)   Alonso, D. A.; Cívicos, J. F.; Nájera, C. *Synlett.* **2009**, *18*, 3011–3015.

(22)   Itoh, T.; Kato, S.; Nonoyama, N.; Wada, T.; Maeda, K.; Mase, T. *Org. Process Res. Dev.* **2006**, *10*, 822–828.

(23)   Dey, R.; Sreedhar, B.; Ranu, B. C. *Tetrahedron* **2010**, *66*, 2301–2305.

(24)   Coppage, R.; Slocik, J. M.; Sethi, M.; Pacardo, D. B.; Naik, R. R.; Knecht, M. R. *Angew. Chem., Int. Ed.* **2010**, *49*, 3767−3770.

(25)   Coppage, R.; Slocik, J. M.; Briggs, B. D.; Frenkel, A. I.; Heinz, H.; Naik, R. R.; Knecht, M. R. *J. Am. Chem. Soc.* **2011**, *133*, 12346−12349.

(26)   Coppage, R.; Slocik, J. M.; Briggs, B. D.; Frenkel, A. I.; Naik, R. R.; Knecht, M. R. *ACS Nano* **2012**, *6*, 1625−1636.

(27)   Coppage, R.; Slocik, J. M.; Ramezani-Dakhel, H.; Bedford, N. M.; Heinz, H.; Naik, R. R.; Knecht, M. R. *J. Am. Chem. Soc.* **2013**, *135*, 11048−11054.

(28)   Briggs, B. D.; Pekarek, R. T.; Knecht, M. R. *J. Phys. Chem. C* **2014**, *118*, 18543−18553.

(29)   Chhabra, R.; Moralez, J. G.; Raez, J.; Yamazaki, T.; Cho, J. -Y.; Myles, A. J.; Kovalenko, A.; Fenniri, H. *J. Am. Chem. Soc.* **2010**, *132*, 32−33.

(30)   Nan, G.; Ren, F.; Luo, M. *Beilstein J. Org. Chem.* **2010**, *6,* No. 70.

(31)   Martin, R.; Buchwald, S. L. *Acc. Chem. Res.* **2008**, *41*, 1461−1473.

(32)   Wang, J. -W.; Meng, F. -H.; Zhang, L. -F. *Organometallics* **2009**, *28*, 2334-2337.

(33)   Barnard, C. *Platinum Metals Rev.* **2008**, *52*, 38–45.

(34)   Miguez, J. M. A.; Adrio, L. A.; Sousa-Pedrares, A.; Vila, J. M.; Hii, K. K. *J. Org. Chem.* **2007**, *72*, 7771–7774.

(35)   Borhade, S. R.; Waghmode, S. B. *Beilstein J. Org. Chem.* **2011**, *7*, 310–319.

(36)   Zhang, X.; Liu, A.; Chen, W. *Org. Lett.* **2008**, *10*, 3849–3852.

(37)   Chen, M.; Zhang, Z.; Li, L.; Liu, Y.; Wang, W.; Gao, J. *RSC Adv.* **2014**, *4*, 30914–30922.

(38)   Suzuki, A. *J. Organomet. Chem.* **1999**, *576*. 147–168.

(39)   Jang, S. H.; Tai, T. B.; Kim, M. K.; Han, J. W.; Kim, Y. -H.; Shin, S. C.; Yoon, Y. J.; Kwon, S. K.; Lee, S. -G. *Bull. Korean Chem. Soc.* **2009**, *30*, 618–622.

(40)   Zhao, H.; Xu, C.; Wang, B.; Zhao, J.; Cui, C.; Zhang, X. *Int. J. Electrochem. Sci.* **2012**, *7*, 10685–10697.

(41)   Habashneh, A. Y.; Dakhil, O. O.; Zein, A.; Georghiou, P. E. *Synth. Commun.* **2009**, *39*, 4221–4229.

(42)   Urbaneja, X.; Mercier, A.; Besnard, C.; Kündig, E. P. *Chem. Commun.* **2011**, *47*, 3739–3741.

(43)   Sato, M.; Maruyama, G.; Tanemura, A. *J. Organomet. Chem.* **2002**, *655*, 23–30.

(44)   Ikeda, S.; Aratani, N.; Osuka, A. *Chem. Commun.* **2012**, *48*, 4317–4319.

(45)   Handy, S. T.; Wilson, T.; Muth, A. *J. Org. Chem.* **2007**, *72*, 8496–8500.

(46)   Pérez-Lorenzo, M. *J. Phys. Chem. Lett.* **2012**, *3*, 167–174.

(47)   Magano, J.; Dunetz, J. R. *Chem. Rev.* **2011**, *111*, 2177–2250.

182

(48)   Balaji, G.; Shim, W. L.; Parameswaran, M.; Valiyaveettil, S. Org. Lett. **2009**, *11*, 4450–4453.

(49)   Akhtaruzzaman, M.; Kamata, N.; Nishida, J. -I.; Ando, S.; Tada, H.; Tomura, M.; Yamashita, Y. *Chem. Commun.* **2005**, 3183–3185.

(50)   Akhtaruzzaman, M.; Tomura, M.; Nishida, J. -I.; Yamashita, Y. J. Org. Chem. **2004**, *69*, 2953–2958.

(51)   Neto, B. A. D.; Lopes, A. S.; Ebeling, G.; Gonçalves, R. S.; Costa, V. E. U.; Quina, F. H.; Dupont, J. *Tetrahedron* **2005**, *61*, 10975–10982.

(52)   Sandanayaka, A. S. D.; Taguri, Y.; Araki, Y.; Ishi-i, T.; Mataka, S.; Ito, O. *J. Phys. Chem. B* **2005**, *109*, 22502–22512.

(53)   Dou, C.; Chen, D.; Iqbal, J.; Yuan, Y.; Zhang, H.; Wang, Y. *Langmuir* **2011**, *27*, 6323–6329.

(54)   Zhang, X.; Yamaguchi, R.; Moriyama, K.; Kadowaki, M.; Kobayashi, T.; Ishi-i, T.; Thiemann, T.; Mataka, S. *J. Mater. Chem.* **2006**, *16*, 736–740.

(55)   Omer, K. M.; Ku, S. -Y.; Wong, K. -T.; Bard, A. J. *J. Am. Chem. Soc.* **2009**, *131*, 10733–10741.

(56)   Thomas, K. R. J.; Lin, J. T.; Velusamy, M.; Tao, Y. -T.; Chuen, C. -H. *Adv. Funct. Mater.* **2004**, *14*, 83–90.

(57)   Neto, B. A. D.; Lopes, A. S.; Wüst, M.; Costa, V. E. U.; Ebeling, G.; Dupont, J. *Tetrahedron Lett.* **2005**, *46*, 6843–6846.

(58)   Mancilha, F. S.; Neto, B. A. D.; Lopes, A. S.; Moreira Jr., P. F.; Quina, F. H.; Gonçalves, R. S.; Dupont, J. *Eur. J. Org. Chem.* **2006**, 4924–4933.

(59)   Ku, S. -Y.; Wong, K. -T.; Bard, A. J. *J. Am. Chem. Soc.* **2008**, *130*, 2392–2393.

(60) Neto, B. A. D.; Lapis, A. A. M.; Mancilha, F. S.; Vasconcelos, I. B.; Thum. C.; Basso, L. A.; Santos, D. S.; Dupont, J. *Org. Lett.* **2007**, *9*, 4001–4004.

(61) Aldakov, D.; Palacios, M. A.; Anzenbacher, Jr., P. *Chem. Mater.* **2005**, *17*, 5238–5241.

(62) Zhang, X.; Gorohmaru, H.; Kadowaki, M.; Kobayashi, T.; Ishi-i, T.; Thiemann, T.; Mataka, S. *J. Mater. Chem.* **2004**, *14*, 1901–1904.

(63) Fang, Y.; Pandey, A. K.; Nardes, A. M.; Kopidakis, N.; Burn, P. L.; Meredith, P. *Adv. Energy Mater.* **2013**, *3*, 54–59.

(64) Chiu, S. -W.; Lin, L. -Y.; Lin, H. -W.; Chen, Y. -H.; Huang, Z. -Y.; Lin, Y. -T.; Lin, F.; Liu, Y. -H.; Wong, K. -T. *Chem. Commun.* **2012**, *48*, 1857–1859.

(65) Anthony, J. E. *Chem. Mater.* **2011**, *23*, 583–590.

(66) Lin, L. -Y.; Chen, Y. -H.; Huang, Z. -Y.; Lin, H. -W.; Chou, S. -H.; Lin, F.; Chen, C. -W.; Liu, Y. -H.; Wong, K. -T. *J. Am. Chem. Soc.* **2011**, *133*, 15822–15825.

(67) Chen, Y. -H.; Lin, L. -Y.; Lu, C. -W.; Lin, F.; Huang, Z. -Y.; Lin, H. -W.; Wang, P. -H.; Liu, Y. -H.; Wong, K. -T.; Wen, J.; Miller, D. J.; Darling, S. B. *J. Am. Chem. Soc.* **2012**, *134*, 13616−13623.

(68) Sun, Y.; Welch, G. C.; Leong, W. L.; Takacs, C. J.; Bazan, G. C.; Heeger, A. J. *Nature Mater.* **2012**, *11*, 44−48.

(69) Lin, L. -Y.; Lu, C. -W.; Huang, W. -C.; Chen, Y. -H.; Lin, H. -W.; Wong, K. -T. *Org. Lett.* **2011**, *13*, 4962–4965.

(70) Bernius, M.; Inbasekaran, M.; Woo, E.; Wu, W.; Wujkowski, L. *J. Mater. Sci.: mater. Electronics* **2002**, *11*, 111–116.

(71) Grey, J. K.; Kim, D. Y.; Donley, C. L.; Miller, W. L.; Kim, J. S.; Silva, C.; Friend, R. H.; Barbara, P. F. *J. Phys. Chem. B* **2006**, *110*, 18898–18903.

(72) Bernius, M. T.; Inbasekaran, M.; O'Brien, J.; Wu, W. *Adv. Mater.* **2000**, *12*, 1737–1750.

(73) Benedetto, F. D.; Camposeo, A.; Pagliara, S.; Mele, E.; Persano, L.; Stabile, R.; Cingolani, R.; Pisignano, D. *Nature Nanotech.* **2008**, *3*, 614–619.

(74) Edder, C.; Armstrong, P. B.; Prado, K. B.; Fréchet, J. M. J. *Chem. Commun.* **2006**, 1965–1967.

(75) Herguth, P.; Jiang, X.; Liu, M. S.; Jen, A. K. -Y. *Macromolecules* **2002**, *35*, 6094–6100.

(76) Moralez, J. G.; Raez, J.; Yamazaki, T.; Motkuri, R. K.; Kovalenko, A.; Fenniri, H. *J. Am. Chem. Soc.* **2005**, *127*, 8307–8309.

(77) Fenniri, H.; Mathivanan, P.; Vidale, K. L.; Sherman, D. M.; Hallenga, K.; Wood, K. V.; Stowell, J. G. *J. Am. Chem. Soc.* **2001**, *123*, 3854–3855.

(78) Fenniri, H.; Deng, B. -L.; Ribbe, A. E. *J. Am. Chem. Soc.* **2002**, *124*, 11064–11072.

(79) Mateos-Timoneda, M. A.; Crego-Calama, M.; Reinhoudt, D. N. *Chem. Soc. Rev.* **2004**, *33*, 363–372.

(80) Kylmälä, T.; Kuuloja, N.; Xu, Y.; Rissanen, K.; Franzén, R. *Eur. J. Org. Chem.* **2008**, 4019–4024.

(81) Qin, C.; Lu, W. *J. Org. Chem.* **2008**, *73*, 7424–7427.

(82) Rottländer, M.; Palmer, N.; Knochel, P. *Synlett* **1996**, *6*, 573–575.

(83) Chen, H.; Huang, Z.; Hu, X.; Tang, G.; Xu, P.; Zhao, Y.; Cheng, C. -H. *J. Org. Chem.* **2011**, *76*, 2338–2344.

(84)   Qiu, J.; Wang, L.; Liu, M.; Shen, Q.; Tang, J. *Tetrahedron Lett.* **2011**, *52*, 6489–
         6491.

(85)   Li, P.; Wang, L.; Zhang, L.; Wang, G. -W. *Adv. Synth. Catal.* **2012**, *354*, 1307–
         1318.

(86)   Felpin, F. -X.; Fouquet, E. *Adv. Synth. Catal.* **2008**, *350*, 863–868.

(87)   Liu, N.; Liu, C.; Jin, Z. *Green Chem.* **2012**, *14*, 592–597.

(88)   Seechurn, C. C. C. J.; Parisel, S. L.; Colacot, T. J. *J. Org. Chem.* **2011**, *76*, 7918–
         7932.

(89)   Felpin, F. -X.; Fouquet, E.; Zakri, C. *Adv. Synth. Catal.* **2009**, *351*, 649–655.

(90)   Alacid, E.; Nájera, C. *Org. Lett.* **2008**, *10*, 5011–5014.

(91)   Hong, M. C.; Choi, M. C.; Chang, Y. W.; Lee, Y.; Kim, J.; Rhee, H. *Adv. Synth.
         Catal.* **2012**, *354*, 1257–1263.

(92)   Sindhuja, E.; Ramesh, R.; Liu, Y. *Dalton Trans.* **2012**, *41*, 5351–5361.

(93)   Jin, R.; Bian, Z.; Kang, C.; Guo, H.; Gao, L. *Synth. Commun.* **2005**, *35*, 1897–
         1902.

(94)   Bolliger, J. L.; Frech, C. M. *Chem. Eur. J.* **2010**, *16*, 11072–11081.

(95)   Bolliger, J. L.; Frech, C. M. *Adv. Synth. Catal.* **2010**, *352*, 1075–1080.

Chapter 5

Supramolecular Asymmetric Catalysis

5.1 Introduction

Asymmetric catalysis with transition metals is one of the most important and general strategies to produce chiral products, whereby achiral starting materials are directly converted to enantioenriched products.[1-4] Over the last few decades, intensive research in this area has broadened the scope of performing several asymmetric reactions routinely to produce chiral building blocks or fine chemicals used in pharmaceutical, agrochemical and perfume industries.[4,5] The catalyst used in asymmetric catalysis typically comprises a chiral ligand coordinated to a metal (Figure 5.1a). The structural and electronic properties of the chiral ligand play a vital role in the catalytic activity as well as chirality induction to the product formed.[6] Very recently, a new concept of using chiral ion pair catalysts has been explored where the catalyst consists of cationic transition metals with chiral anions (Figure 5.1b).[6-11]

(a)

M

M = Metal Centre

= Chelating Chiral Ligand

(b)

$[ML_1]^{n+}$ $[L_2]^{m-}$

M = Metal Cation
L_1 = Ligand
L_2 = Chiral Anion
n = m = No. of Charge
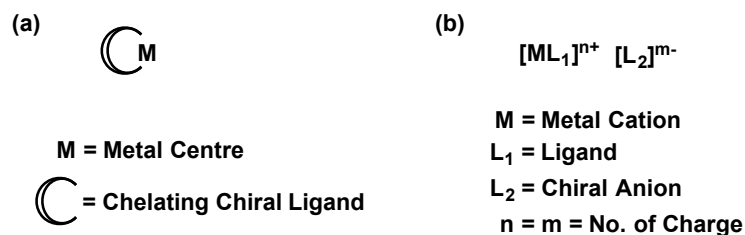
Figure 5.1: Design of the asymmetric catalysts using (a) chiral ligand-metal complex and (b) metal cation containing chiral anion.

In parallel to the impressive developments of small transition metal complex and organometallic catalysts for asymmetric catalysis, supramolecular chiral catalysis has

grown into a mature field.[12] The inspiration for these concepts is then derived from nature.[13-16] Nature selects a few number of building blocks to produce enzymes that catalyze asymmetric reactions a with very high reaction rate and exquisite selectivity beyond conventional synthetic methods.[14,16] For example, DNases catalyze the hydrolysis of phosphate diester bonds in DNA within a few seconds,[16-20] while it has been estimated that in absence of an enzyme the reaction half-life would be 200 million years.[21] The binding of a substrate molecule to the active site on the enzyme results in activation of the substrate molecule and thus enhances the rate of reaction (Figure 5.2).[15,22] On the other hand, the spatial factors such as specific interactions between the substrate molecule and amino-acid residues near the active site may induce exquisite selectivity (Figure 5.2).[23,24] Apart from the purely biological function of enzymes, they offer the catalysis under environmentally benign mild reaction conditions using fully biodegradable catalysts.[25,26]
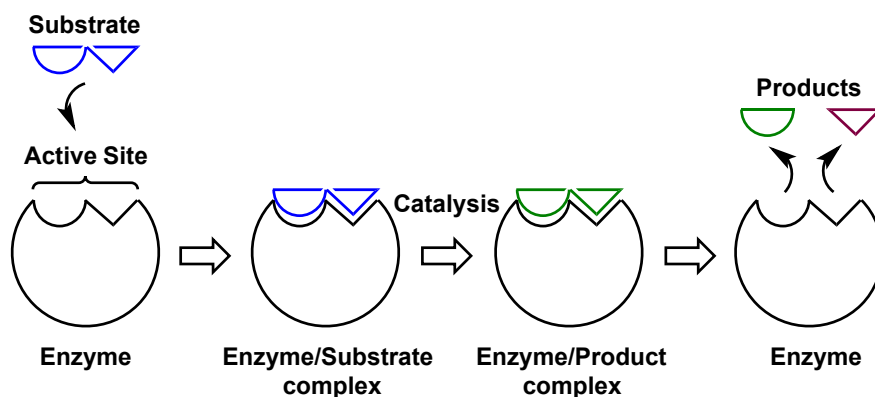
Figure 5.2: Schematic representation of the induced fit hypothesis of enzyme catalysis.

Inspired by enzyme catalysis, a large variety of artificial metalloenzymes have been synthesized, where proteins have been used as the scaffold.[27] The resulting metalloenzymes have been employed for asymmetric catalysis including hydrolyses,[28] hydrogenations,[29,30] transfer hydrogenations,[31,32] allylic alkylations,[33] sulfoxidations,[34-37]

epoxidations,[38,39] dihydroxylations,[40] Diels-Alder reactions,[41,42] and transaminations.[43] Besides this, oligonucleotides have also been employed for asymmetric catalysis.[27,44-51] Very recently, Feringa *et al.* demonstrated asymmetric catalysis using DNA-based catalysts.[16,27,52-58] The catalyst was constructed from a natural duplex DNA and a Cu complex of a nonchiral ligand attached to the DNA (Figure 5.3). They have found that the catalyst could catalyze the Diels-Alder reaction (Figure 5.3) and the Michael addition with very high enantioselectivity.[53-55] As the catalysis takes place at the Cu center attached to the DNA, the supramolecular chirality of DNA was induced to the product during catalysis.
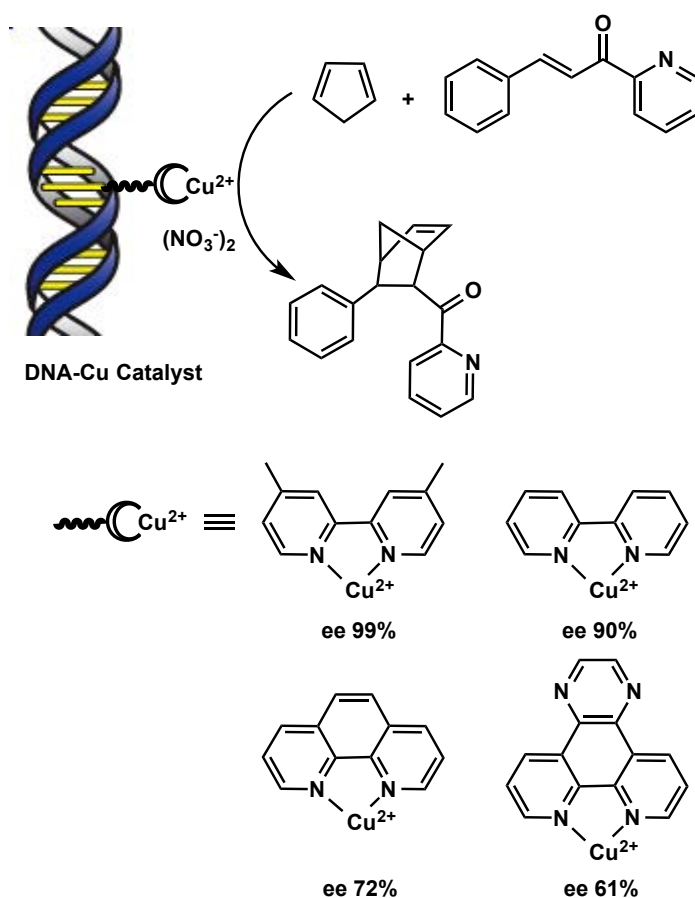
Figure 5.3: DNA-Cu catalyzed Diels–Alder cycloaddition reaction. Enanatioselectivity varies depending on different chelating ligand.

Taking inspiration from this DNA-based metal catalyst design, several groups have demonstrated different asymmetric catalysis using DNA-based hybrid catalysts.[59-67] In contrast to the rapid development of supramolecular chiral metal complex catalyst, only a few examples have been reported in the literature incorporating supramolecular chiral metal nanoparticle catalysts for asymmetric catalysis.[14,68-70] Very recently, Somorjai *et al.* demonstrated asymmetric cyclopropanation using a polyamidoamine (PAMAM) dendrimer encapsulated Au NP catalyst.[70] They employed a fixed-bed flow reactor where both the catalytic reactivity and the product diastereoselectivity depended on the flow rate. Later, they modifed the catalyst by replacing the dendrimer with a mesoporous silica (MCF-17) catalyst immobilized with a chiral self-assembled monolayer (SAM) containing Au NPs (Figure 5.4).[14] They found enhanced catalytic reactivity and selectivity when the amino acid SAM was substituted with the peptide SAM.
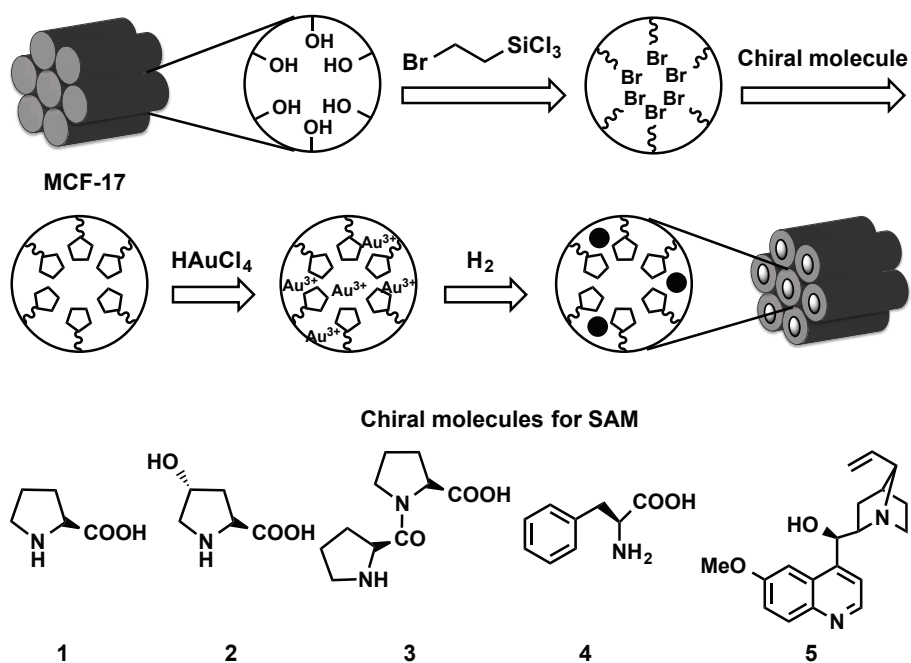
Figure 5.4: Synthesis of Au NPs encapsulated in chiral SAM/MCF-17 support.

As RNT (called "G0") shows supramolecular chirality and the presence of Pd NPs onto its surface preserves the chirality (Chapter 2), I decided to carry out the supramolecular asymmetric catalysis by using the Pd NPs/RNTs catalyst. I envisioned that the supramolecular chirality would induce to the product during the catalytic event.

5.2 Results and Discussion

5.2.1 Initial Attempts at the Asymmetric Suzuki-Miyaura Cross-Coupling Reaction

Earlier, I optimized the conditions and established an effective general procedure for the Suzuki-Miyaura cross-coupling reaction. The detailed spectroscopic characterization of the Pd NPs/RNTs catalyst under the catalytic condition (Chapter 4) suggested that the catalyst could be a suitable candidate for asymmetric catalysis. In addition, this study could allow us to understand the fundamentals of the event of chirality induction in nanoparticle catalysis either it is chiral center or global chiral matrix effect. Keeping this in mind and with the initial results in hand, I decided to carry out an atroposelective biaryl coupling reaction.[71] Generally, this is a type of Suzuki-Miyaura cross-coupling reaction, where two ortho-substituted aryl or naphthalene reactants are used to produce a coupling product.[72-75] Due to restricted rotation the coupling product could show *R*- or *S*- configuration depending on the nature of the chiral catalyst (Figure 5.5).[72-75]
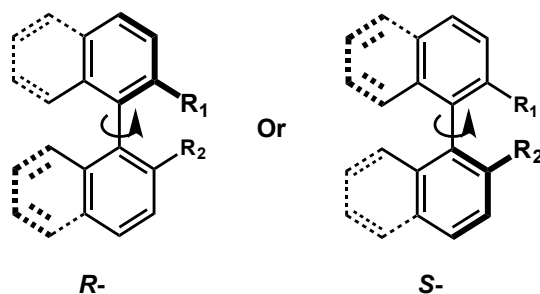
Figure 5.5: The possible *R*- or *S*- configuration of binaphthyl compounds.

For ease of chromatographic separation and analysis by ^{1}H NMR spectroscopy, I planned to synthesize a binaphthyl product, which is a diastereomer, and determine the diastereoselectivity for the catalytic reaction. In addition, as the RNT showed right handed helicity, it was expected that the reaction would afford the *R*-configured coupling product as the major product. With this in mind, I carried out a catalytic reaction of 1-bromo-2-naphthaldehyde and 2,1,3-benzothiadiazole-4,7-*bis*(boronic acid pinacol ester) following the previously optimized procedure (Chapter 4) using 1 mol% Pd NPs/RNTs catalyst in EtOH/H$_2$O mixture solution (Scheme 5.1).
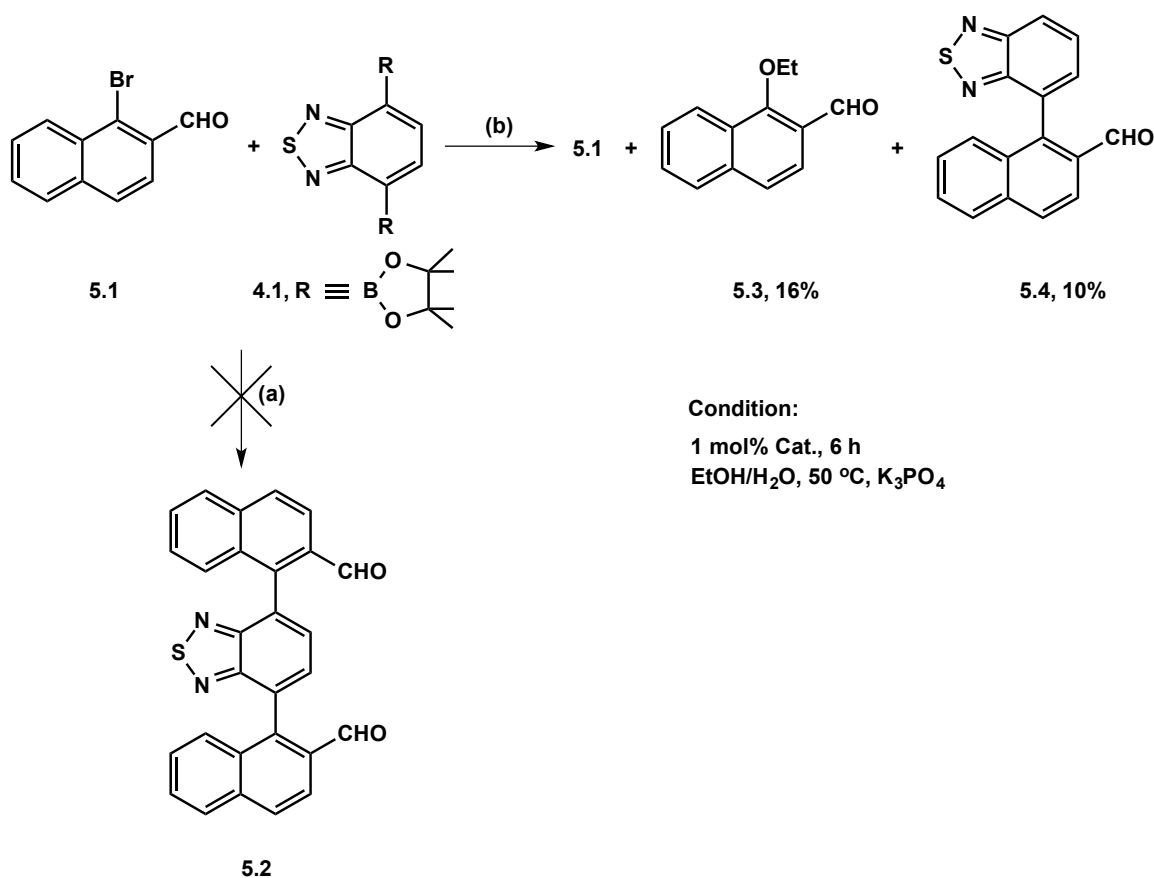
Scheme 5.1: Attempt to synthesize a benzothiadiazole-based diastereomer (**5.2**).

Unfortunately, instead of producing the expected *bis*-coupling product (**5.2**; Scheme 5.1, route a), the reaction afforded the mono-coupling and deboronation product

(**5.4**) in 10% yield (Scheme 5.1, route b). In addition, the reaction afforded bromine-exchanged product 1-ethoxy-2-naphthaldehyde (**5.3**) in 16% yield along with the recovered (26%) bromo starting material (Scheme 5.1, route b).
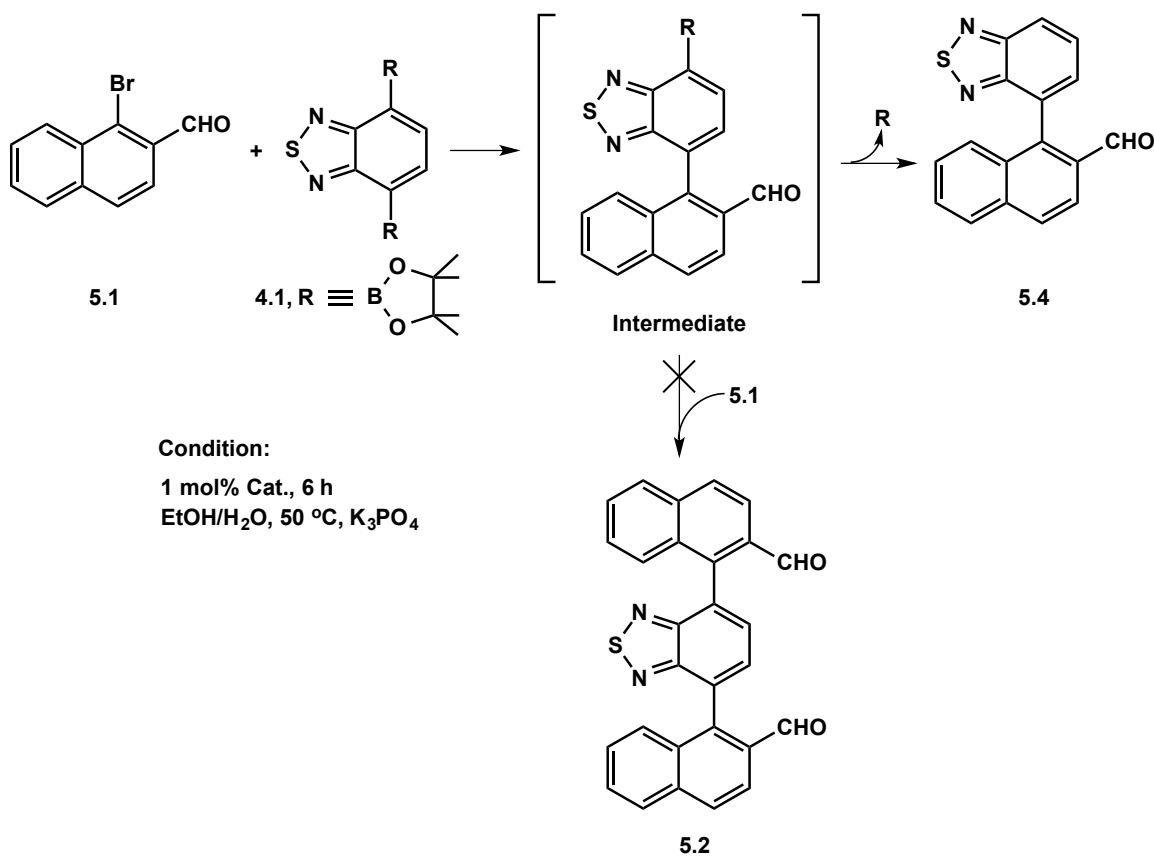
Scheme 5.2: The formation of **5.4** by the deboronation of the intermediate compound.

The formation of mono-coupling product was not surprising and was expected to form in the first catalytic cycle. Unfortunately, the deboronation of the intermediate compound leads to the formation of **5.4** and blocks the second coupling reaction affording the desired *bis*-coupling product **5.2** (Scheme 5.2). Previously, different groups observed similar deboronation reaction in Suzuki-Miyaura cross-coupling reaction.[76-78] Recently, Sankararaman *et al.* reported the deboronation of both 2-benzoxy-1-naphthalene boronic acid and 2-methoxy-1-naphthalene boronic acid when used for the

cross-coupling reaction.[76] It is well documented that deboronation tends to dominate over coupling reaction for sterically hindered aryl boronic acids containing ortho substituents.[76,77] In a sterically demanding compound, the boronic acid group possesses an out-of-plane conformation which makes it more prone to deboronation.[78] Despite a few example of coupling under rigorously anhydrous conditions, the deboronation was found to be more facile in aqueous solution and in the presence of an inorganic base.[76,77] As the initial reaction with 1 mol% catalyst loading was found to be incomplete in 6 h with low product yield, I repeated the reaction by varying the catalyst loading and reaction duration. The attempts to achieve complete reaction with high product yield were unsuccessful (Table 5.1).

Table 5.1: Product distribution in attempted coupling reaction (Scheme 5.1) under different conditions.

Entry	Catalyst loading (%)	Reaction duration (h)	Product yield (%)			ee (%)
			5.1 (recovered)	5.3	5.4	
1.	1	6	26	16	10	
2.	1	24	21	21	13	
3.	5	24	20	21	13	6[a]
4.	5	48	22	26	15	
5.	10	48	17	23	11	6[b]

[a] The ee determination performed on the isolated TLC band. [b] The ee determination performed on the crystalline solid.

Firstly, the same reaction (Scheme 5.1) with 1 mol% catalyst loading was repeated for a longer reaction time of 24 h. Though the yield of the product was slightly improved, still the reaction was incomplete. Secondly, the similar reaction was repeated with higher

catalyst loadings (5 and 10 mol%) and prolonged reaction time. However, there was very little influence of the increased catalyst loading as well as the reaction duration towards the reaction completion and the product yield (Table 5.1). The incomplete reaction could be explained by two reasons- (i) formation of 1-ethoxy-2-naphthaldehyde (**5.3**), and (ii) the deboronation reaction (Scheme 5.1). The formation of **5.3** blocks the possibility of coupling reaction, although the reaction was always encountered with recovering unreacted bromo substrate (**5.1**). Besides this, the deboronation reaction of the intermediate (Scheme 5.2) also greatly reduced the chances of further consumption of **5.1**. Hence, this investigation indicates that the increased catalyst loading or the prolonged reaction time has no significant impact on the completion of the reaction.

*5.2.2 Characterization of the Mono-coupling Product (**5.4**)*

The ^{1}H NMR spectrum of **5.4** shows a total of eight signals due to the nine aromatic protons of the naphthalene and the benzothiadiazole rings. The singlet at δ 9.76 ppm is distinguishable for the aldehyde proton on the naphthalene ring. The ^{13}C NMR spectrum has seventeen distinct signals attributed to the seventeen different carbon atoms in **5.4**. The high resolution MALDI mass spectrum of **5.4** consists of a cation peak at m/z 290.05189 due to the molecular ion and matches with the calculated value of 290.05139 for $C_{17}H_{10}ON_2S$ (M^+). Several attempts to grow single crystals of **5.4** in different solvent combinations were found to be unsuccessful. Those attempts only led to flower type twin crystalline solids. Hence to learn the detailed structural features of **5.4**, I carried out the geometry optimization and the energy calculation using macromodel software. The low energy model of **5.4** shows that the naphthalene ring is twisted with respect to the benzothiadiazole ring with a dihedral angle (θ) of 95° (Figure 5.6a). The θ value suggests

that the compound has a quasiorthogonal conformation in solution.[79,80] The potential

curve of **5.4** shows a flat-bottomed well located at $\theta \sim 95°$. The well is delimited at $\theta \sim 60°$

and $\sim115°$ by steep walls due to strong steric interactions between the two rings

approaching planarity (Figure 5.6b).[79] The high energy barrier indicates that compound

5.4 could exist as enantiomers due to the restricted rotation. Hence this suggests that the

induction of the supramolecular chirality is possible during the catalytic event. However,

it does not confirm the amount of chirality induction to the coupling product. This

calculation found to be very crucial at the initial stage, as I could not obtain

diastereomeric *bis*-coupling product **5.2**. This is because, if the rotation of the C−C bond

between the two rings is not restricted then there would be no asymmetry transformation

to **5.4**.
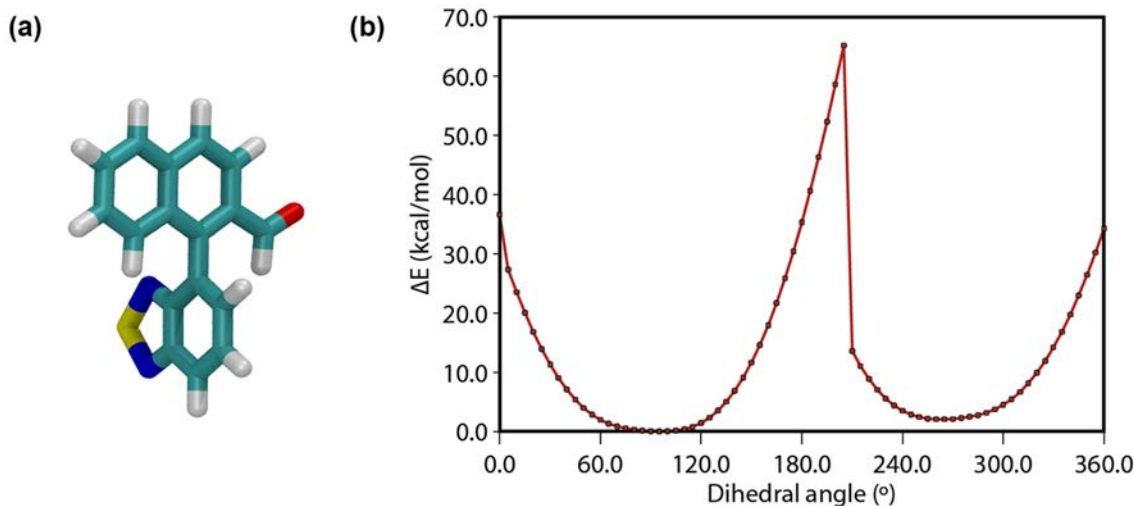
Figure 5.6: Energy optimized molecular model of **5.4** (a) and the potential curve of **5.4** (b).

The CD spectrum of **5.4** shows a negative exciton couplet, which is typical of (*R*)-configured binaphthyl compounds (Figure 5.7a).[79-82] The splitting of the CD couplet (the wavelength difference of the two extrema) $\Delta\lambda_{max}$ is 4.9 nm (<10 nm), which is consistent

with the θ calculation and the quasiorthogonal conformation of **5.4** in solution.[80,82] The couplet crossover point (where the ellipticity is zero) is shifted to 247 nm from the main absorption maximum at 253 nm (Figure 5.7b) due to two nonidentical chromophores. It has been well documented that for two identical chromophores the couplet crossover point coincides with the absorption maximum.[79] Although the CD spectrum of **5.4** shows the presence and dominance of (*R*)-isomer in solution, it does not confirm the exact percentage of the (*R*)-isomer. Hence, it is possible that the two isomers (*R* and *S*) are either in distribution where the (*R*)-isomer is the major product or the (*R*)-isomer exists in pure form.
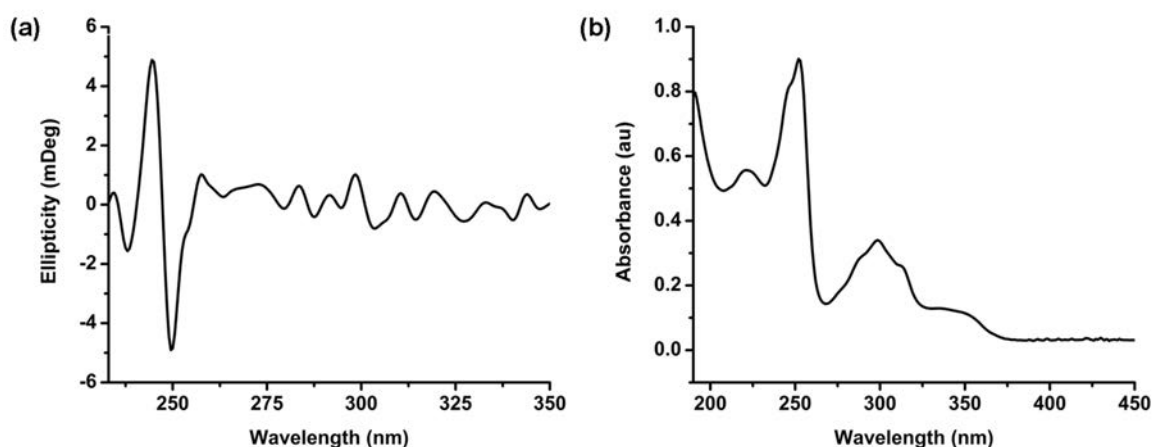
Figure 5.7: CD (a) and UV-Vis (b) spectra of **5.4**.

*5.2.3 Chiral HPLC Analysis of the Mono-coupling Product (**5.4**)*

To obtain further insight into the isomeric existence of **5.4** in solution I carried out chiral HPLC analysis on the crystalline solid obtained from a reaction with 10 mol% catalyst loading. The best separation of the enantiomers of **5.4** was obtained on the Chiralcel OD-RH column using water–acetonitrile (95:5 v/v) mixture solvent containing 0.1% acetic acid as the mobile phase (Figure 5.8). However, the complete baseline

separation of the two enantiomers of **5.4** was not possible due to very close retention time (Figure 5.8, Inset). The enantiomeric distribution of **5.4** was found to be 48:52 and the "ee" was calculated only 6%. Though the CD analysis of **5.4** showed the dominance of (*R*)-isomer in solution, the poor "ee" determination discouraged us to further investigate the identity and the order of the elution of the two enantiomers. As the chiral HPLC performed on the crystalline solid, it was possible that **5.4** crystallized in racemic mixture with 6% "ee" of the (*R*)-isomer.
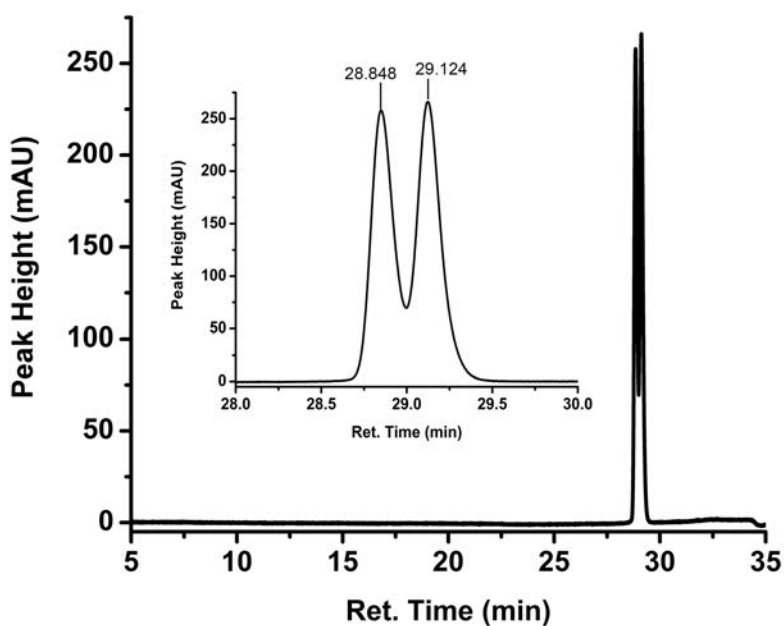
Figure 5.8: Chromatogram of **5.4** (crystalline solid) on a Chiralcel OD-RH column.

To rule out this possibility, I investigated the chiral HPLC of the purely isolated TLC band of **5.4** obtained from a reaction with 5 mol% catalyst loading. The analysis concluded with the same result to that of crystalline solid with 6% "ee" of the (*R*)-isomer (Figure 5.9). This indicates that there was a very poor supramolecular chirality induction to the coupling product during catalysis. The chiral HPLC analysis of **5.4** obtained from the reactions with 5 and 10 mol% catalyst loading, resulted in similar chirality induction

to the coupling product. Hence, this finding concludes that the increased catalyst loading has no effect on the improvement of the supramolecular chirality induction to the coupling product.
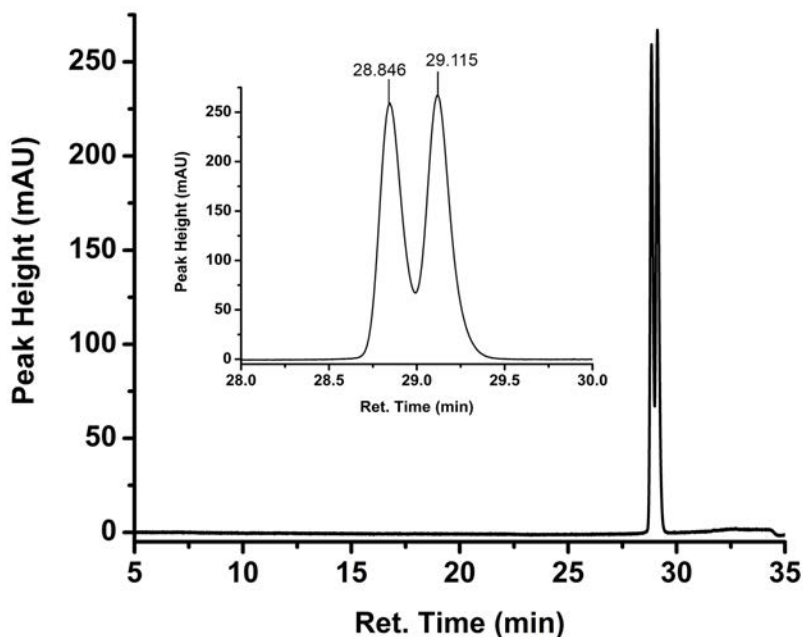
Figure 5.9: Chromatogram of **5.4** (isolated TLC band) on a Chiralcel OD-RH column.

5.2.4 Approach to Synthesize Known Binaphthyl Compound

To further confirm the observation of the supramolecular chirality induction using the Pd NPs/RNTs catalyst, I carried out the Suzuki-Miyaura cross-coupling reaction to synthesize known binaphthyl compounds. The initial coupling reaction of 1-bromo-2-naphthaldehyde (**5.1**) and 2-methoxy-1-naphthalene boronic acid (**5.5**) was unsuccessful (Scheme 5.3) affording only deboronation product 2-methoxynaphthalene (**5.7**) and compound **5.3** in 99 and 7% yield, respectively. Besides this, the bromo substrate (**5.1**) was recovered in 32% yield. Unfortunately, another approach by introducing 1-naphthalene boronic acid (**5.6**) also did not lead to the formation of coupling product

(Scheme 5.3). The reaction yielded naphthalene (**5.8**) and **5.3** in 24 and 11% yield, respectively along with the recovery of **5.1** in 48% yield.
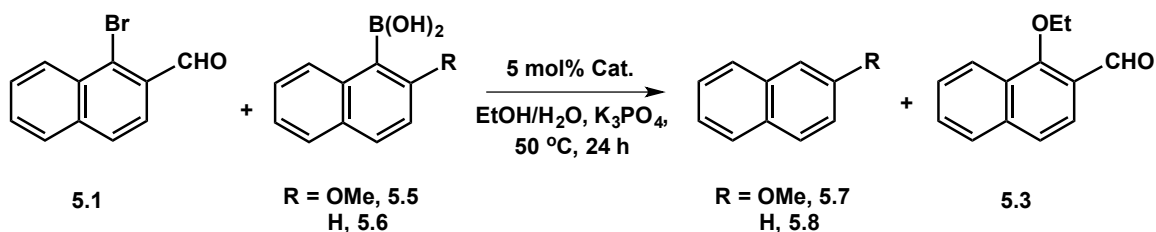
Scheme 5.3: Attempts to synthesize known binaphthyl coupling product.

Considering further reduction of the steric bulk of the naphthalene ring at the 2-position and poor reactivity of the bromosubstrate under mild conditions, 1-iodonaphthalene (**5.9**) was employed with 1-naphthalene boronic acid (**5.6**) for coupling reaction (Scheme 5.4). Finally, this reaction gave the desired coupling product 1,1'-binaphthyl (**5.10**) in 95% yield. The chiral HPLC analysis of the purely isolated TLC band of **5.10** was obtained on the Chiralcel OD column using normal phase. Fortunately, the complete baseline separation of the two enantiomers of **5.10** was possible under the optimized condition (Figure 5.10, Inset). However, the enantiomeric distribution of **5.10** was found to be 48:52 and the "ee" was calculated only 4%. This result complies with the previous observations and suggests that the reaction indeed has very poor supramolecular chirality induction to the coupling product.
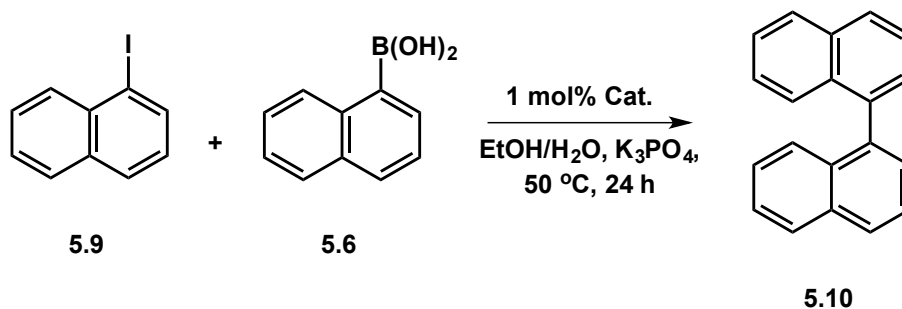
Scheme 5.4: Synthesis of 1,1'-binaphthyl (**5.10**).
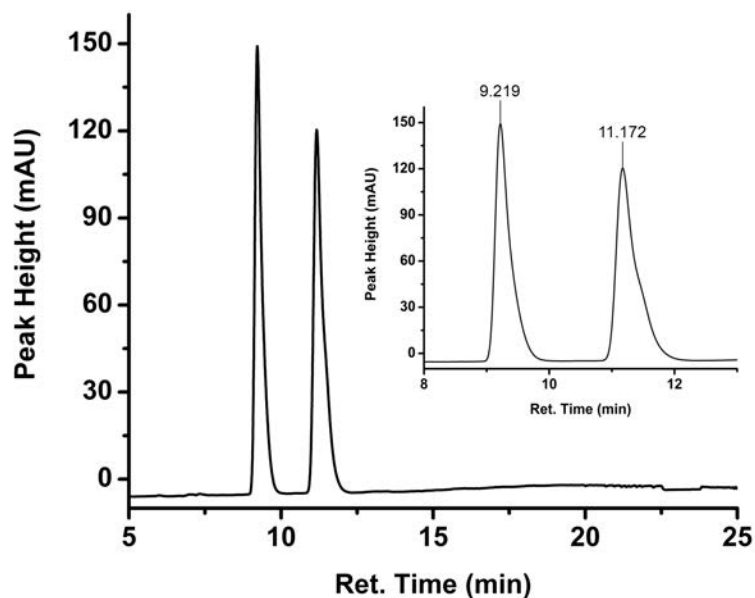
Figure 5.10: Chromatogram of **5.10** (isolated TLC band) on a Chiralcel OD column (normal phase).

5.2.5 Understanding the poor asymmetry induction

The poor chirality transformation during the catalytic event could be explained on the basis of the NP mediated cross-coupling reaction mechanism. It has been well documented and widely accepted that the Suzuki-Miyaura reaction takes place by leaching of the metal atoms from the surface of the NPs.[83-87] Hence the catalysis could take place in the bulk solution followed by subsequent redeposition of the leached Pd species onto the support.[83-87] Despite the detail of the asymmetry transformation mechanism in asymmetric catalysis, one of basic condition for the induction is that to have a local chiral environment.[88,89] This unique feature is created by designing a chiral catalyst where the substrate binds to the chiral center and/or stay in close proximity to the chiral environment. Hence, an enantiomerically pure compound is formed upon attack by a reagent at the less hindered face. Now considering this scenario and implicating these

201

concepts to our system, I can rationalize the poor asymmetry transformation into the coupling product. When the palladium atoms are leached into the bulk solution from the NPs located onto the surface of RNTs, the catalysis takes place far away from the RNTs (Figure 5.11). Under this circumstance, as RNTs possess supramolecular chirality the leaching of the palladium atoms fails to create a local chiral environment in the bulk solution essential for asymmetry transformation. Hence, the coupling reaction takes place to the palladium center within the chiral free environment where the supramolecular chirality of RNTs has less influence.
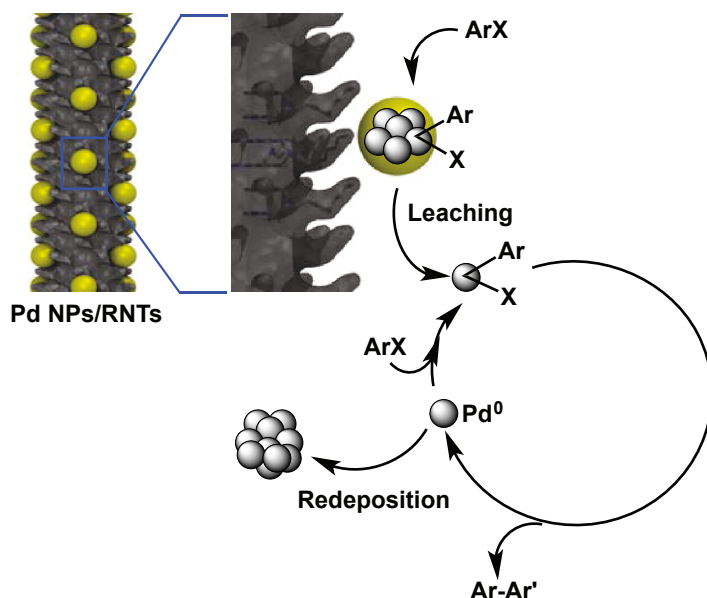
Figure 5.11: Proposed mechanism for the coupling reaction using Pd NPs/RNTs Catalyst.

In conclusion, I have investigated the supramolecular chiral catalysis using Pd NPs/RNTs catalyst. However, the reaction afforded poor chirality induction to the product. We believed that the leaching of the Pd atoms allowed the coupling reaction took place in the bulk solution far away from the RNT surface. Therefore provided poor chirality induction.

Experimental

Materials.

1-Bromo-2-naphthaldehyde, 2,1,3-benzothiadiazole-4,7-*bis*(boronic acid pinacol ester), 1-naphthalene boronic acid, and 1-iodonaphthalene were purchased from Sigma-Aldrich. 2-Methoxy-1-naphthalene boronic acid was purchased from TCI America. TLC glass plates (20×20 cm; 0.5 mm) were purchased from Macherey-Nagel.

Instrumentation.

The enantiomeric excesses (ee) for chiral compounds were determined using a HPLC Agilent instrument with DAICEL Chiralcel OD (normal phase) and DAICEL Chiralcel OD-RH (reverse phase) columns with UV detection at 250 and 220 nm, respectively. The chiralcel OD column was 250 mm in length and 4.6 mm in diameter. The chiralcel OD-RH column was 150 mm in length and 4.6 mm in diameter. The particle size for both columns was 5 μm. The temperatures of the chiralcel OD and chiralcel OD-RH columns were 20 and 30 $^{\circ}$C, respectively. The flow rates of the chiralcel OD and chiralcel OD-RH columns were 0.5 mL/min and 1.0 mL/min, respectively. For the normal phase, the mobile phase was composed of a mixture of two solvents (A: Hexanes, and B: Isopropyl alcohol). The gradient elution program was used consisting of 0-19 min, 2% B; 20-21 min, 10% B; 22 min, 40% and 23-28 min, 2% B. For the reverse phase, the mobile phase was composed of a mixture of two solvents containing 0.1% acetic acid (A: water + 0.1% acetic acid, and B: acetonitrile + 0.1% acetic acid). The gradient elution program was used consisting of 0-49 min, 5% B; 50-51 min, 50% B; 52 min, 90% B and 53-55 min, 5% B.

Methods.

Stock solutions of RNTs and K$_2$PdCl$_4$. The stock solutions of RNTs and K$_2$PdCl$_4$ were synthesized following to the similar procedure under the optimized condition as mentioned in chapter 2.

Catalyst synthesis. The catalyst was prepared prior to the catalytic reaction following the similar procedure as discussed in chapter 4.

Catalytic reaction.

Reaction of 5.1 and 4.1 using 1 mol% Catalyst. The cross-coupling reaction of 1-bromo-2-naphthaldehyde (**5.1**; 117.5 mg; 0.5 mmol) and 2,1,3-benzothiadiazole-4,7-*bis*(boronic acid pinacol ester) (**4.1**; 97.0 mg; 0.25 mmol) was carried out using 1 mol% Pd NPs/RNTs catalyst loading and applying the similar procedure under the optimized condition as mentioned in chapter 4. Upon completion, the reaction was worked up following the similar procedure as discussed in chapter 4 and the residue was chromatographed by TLC on silica gel. Elution with hexanes/CH$_2$Cl$_2$ (6:4 v/v; 2 times) resulted in three bands. The first band afforded the unreacted **5.1** (24.6 mg, 21% recovered). The second band afforded 1-ethoxy-2-naphthaldehyde (**5.3**; 20.7 mg, 25%). The third band gave the mono-coupled and deboronated product 1-(4-(2,1,3)-benzothiadiazolyl)-2-naphthaldehyde (**5.4**; 19.2 mg, 13%).

Spectroscopic data.
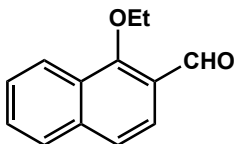
1-ethoxy-2-naphthaldehyde (**5.3**) from 1-bromo-2-naphthaldehyde (**5.1**) and 2,1,3-benzothiadiazole-4,7-*bis*(boronic acid pinacol ester) (**4.1**): 25% yield; ^{1}H NMR (600 MHz, CDCl$_3$): δ (ppm) 10.59 (s, 1H), 8.24 (d, J = 8.4 Hz, 1H), 7.86 (d, J = 9.0 Hz, 2H), 7.62 (t, J = 8.4 Hz, 2H), 7.57 (t, J = 8.4 Hz, 1H), 4.28 (q, J = 7.2 Hz, 2H) and 1.57 (t, J = 7.2 Hz, 3H). ^{13}C NMR (150 MHz, CDCl$_3$): δ (ppm) 190.0, 161.8, 138.3, 129.5, 128.5, 128.4, 126.9, 125.4, 124.7, 123.6, 122.8, 74.6 and 15.8. EI-MS (m/z): 200.08343 (Calcd. 200.08372 for C$_{13}$H$_{12}$O$_2$ (M$^+$)).
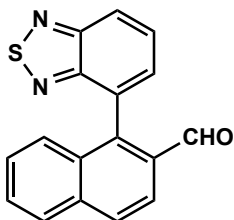
1-(4-(2,1,3)-benzothiadiazolyl)-2-naphthaldehyde (**5.4**) from 1-bromo-2-naphthaldehyde (**5.1**) and **4.1**: 13% yield; ^{1}H NMR (600 MHz, CDCl$_3$): δ (ppm) 9.76 (s, 1H), 8.22 (dd, J = 1.2, 9.0 Hz, 1H), 8.16 (d, J = 8.4 Hz, 1H), 8.07 (d, J = 8.4 Hz, 1H), 7.98 (d, J = 8.4 Hz, 1H), 7.81 (dd, J = 6.6, 9.0 Hz, 1H), 7.68 (dd, J = 1.2, 6.6 Hz, 1H), 7.61-7.64 (m, 1H) and 7.38-7.43 (m, 2H). ^{13}C NMR (150 MHz, CDCl$_3$): δ (ppm) 191.8, 155.3, 154.8, 141.3, 136.5, 132.5, 132.1, 132.0, 129.7, 129.3, 129.2, 129.1, 128.8, 127.4, 127.2, 122.7 and 122.4. Low res. MALDI-MS (m/z): 291.0 (M+H)$^+$. High res. MALDI-MS (m/z): 290.05189 (Calcd. 290.05139 for C$_{17}$H$_{10}$ON$_2$S (M$^+$)). HPLC (Chiralcel OD-RH, reverse phase): λ = 220 nm, ee = 6% (prior to recrystallization and crystals).

Repeat reaction of 5.1 and 4.1 using 1 mol% Catalyst. A similar catalytic reaction of 1-bromo-2-naphthaldehyde (**5.1**; 117.5 mg; 0.5 mmol) and 2,1,3-benzothiadiazole-4,7-*bis*(boronic acid pinacol ester) (**4.1**; 97.0 mg; 0.25 mmol) was repeated by using 1 mol% catalyst loading under the identical condition for a prolonged reaction time of 24 h and worked up applying the similar procedure as mentioned above. The reaction afforded **5.3** and **5.4** in 21 and 13% yield, respectively along with unreacted **5.1** recovered in 21% yield.

Reaction of 5.1 and 4.1 using 5 mol% Catalyst. A similar catalytic reaction of 1-bromo-2-naphthaldehyde (**5.1**; 117.5 mg; 0.5 mmol) and 2,1,3-benzothiadiazole-4,7-*bis*(boronic acid pinacol ester) (**4.1**; 97.0 mg; 0.25 mmol) was repeated with 5 mol% catalyst loading for the reaction durations of 24 and 48 h, respectively. The reactions were worked up applying the similar procedure as mentioned above. The 24 h reaction gave **5.3** and **5.4** in 21 and 13% yield, respectively along with unreacted **5.1** recovered in 20% yield. While the 48 h reaction gave **5.3** and **5.4** in 26 and 15% yield, respectively along with unreacted **5.1** recovered in 22% yield.

Reaction of 5.1 and 4.1 using 10 mol% Catalyst. A similar catalytic reaction of 1-bromo-2-naphthaldehyde (**5.1**; 117.5 mg; 0.5 mmol) and 2,1,3-benzothiadiazole-4,7-*bis*(boronic acid pinacol ester) (**4.1**; 97.0 mg; 0.25 mmol) was repeated with 10 mol% catalyst loading for a reaction duration of 48 h and worked up applying the similar procedure as mentioned above. The reaction afforded **5.3** and **5.4** in 23 and 11% yield, respectively along with unreacted **5.1** recovered in 17% yield.

Reaction of 5.1 and 5.5 using 5 mol% Catalyst. A similar catalytic reaction of 1-bromo-2-naphthaldehyde (**5.1**; 117.5 mg; 0.5 mmol) and 2-methoxy-1-naphthalene

boronic acid (**5.5**; 101.0 mg; 0.5 mmol) was carried out by using 5 mol% catalyst loading for 24 h. The reaction was worked up applying the similar procedure as mentioned above. The compounds were separated by TLC on silica gel. Elution with hexanes/CH$_2$Cl$_2$ (7:3 v/v; 2 times) developed three bands. The first band gave the deboronated compound 2-methoxynaphthalene (78.2 mg, 98%). The second band afforded the unreacted 1-bromo-2-naphthaldehyde (37.2 mg, 32% recovered). The third band gave 1-ethoxy-2-naphthaldehyde (6.9 mg, 7%).

Spectroscopic data:
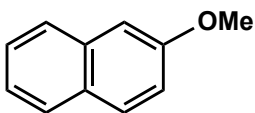
2-methoxynaphthalene[76,90] (**5.7**) from 1-bromo-2-naphthaldehyde (**5.1**) and 2-methoxy-1-naphthalene boronic acid (**5.5**): 98% yield; ^{1}H NMR (600 MHz, CDCl$_3$): δ (ppm) 7.80 (d, J = 8.4, 1H), 7.77 (d, J = 8.4 Hz, 2H), 7.48 (t, J = 8.4 Hz, 1H), 7.38 (t, J = 8.4 Hz, 1H), 7.20-7.17 (m, 2H) and 3.95 (s, 3H).

Reaction of 5.1 and 5.6 using 5 mol% Catalyst. A similar catalytic reaction of 1-bromo-2-naphthaldehyde (**5.1**; 117.5 mg; 0.5 mmol) and 1-naphthalene boronic acid (**5.6**; 105.0 mg; 0.6 mmol) was carried out by using 5 mol% catalyst loading for 24 h. The reaction was worked up applying the similar procedure as mentioned above. The compounds were isolated by TLC on silica gel. Elution with hexanes/CH$_2$Cl$_2$ (7:3 v/v; 2 times) developed three bands. The first band gave the deboronated compound naphthalene (18.6 mg, 24%). The second band afforded the unreacted 1-bromo-2-naphthaldehyde (56.6 mg, 48% recovered) and the third band gave 1-ethoxy-2-naphthaldehyde (11.1 mg, 11%).

Spectroscopic data:
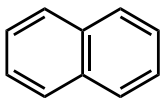
Naphthalene[91] (**5.8**) from 1-bromo-2-naphthaldehyde (**5.1**) and 1-naphthalene boronic acid (**5.6**): 24% yield; ^{1}H NMR (600 MHz, CDCl$_3$): δ (ppm) 7.86-7.84 (m, 4H) and 7.50-7.48 (m, 4H).

Reaction of 5.9 and 5.6 using 5 mol% Catalyst. A similar catalytic reaction of 1-iodonaphthalene (**5.9**; 127.0 mg; 0.5 mmol) and 1-naphthalene boronic acid (**5.6**; 105.0 mg; 0.6 mmol) was carried out by using 1 mol% catalyst loading for 24 h. The reaction was worked up applying the similar procedure as mentioned above. The product binaphthyl (**5.10**) was purified by TLC on silica gel (elution: hexanes/CH$_2$Cl$_2$ (8.5:1.5 v/v)). Yield: 95% (121 mg).

Spectroscopic data:
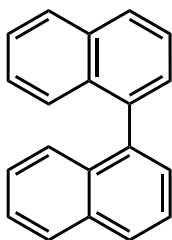
1,1'-binaphthyl[92] (**5.10**) from 1-iodonaphthalene (**5.9**) and 1-naphthalene boronic acid (**5.6**): 95% yield; ^{1}H NMR (600 MHz, CDCl$_3$): δ (ppm) 7.98-7.96 (m, 2H), 7.61 (t, J = 7.8 Hz, 1H), 7.53-7.48 (m, 2H), 7.42 (d, J = 7.8 Hz, 1H) and 7.32-7.29 (m, 1H). ^{13}C NMR (150 MHz, CDCl$_3$): δ (ppm) 138.7, 133.8, 133.1, 128.4, 128.1, 128.0, 126.8, 126.2, 126.0 and 125.6. HPLC (Chiralcel OD, normal phase): λ = 250 nm, ee = 4% (pure TLC isolated band).

5.3 References

(1)   Zhao, D; Ding, K. *ACS Catalysis* **2013**, *3*, 928–944.

(2)   Mikami, K.; Lautens, M. Eds. *New Frontiers in Asymmetric Catalysis*, John Wiley & Sons Inc.: New York, 2007.

(3)   Ojima, I. Ed. *Catalytic Asymmetric Synthesis,* 3rd ed., John Wiley & Sons Inc.: New York, 2010.

(4)   Lühr, S; Holz, J.; Börner, A. *ChemCatChem* **2011**, *3*, 1708–1730.

(5)   Blaser, H. -U.; Schmidt, S. Eds. *Asymmetric Catalysis on Industrial Scale,* Wiley-VCH: Weinheim, 2004.

(6)   Ohmatsu, K.; Ito, M.; Kunieda, T.; Ooi, T. *Nat. Chem.* **2012**, *4*, 473–477.

(7)   Hamilton, G. L.; Kang, E. J.; Mba, M.; Toste, F. D. *Science* **2007**, *317*, 496–499.

(8)   Mukherjee, S.; List, B. *J. Am. Chem. Soc.* **2007**, *129*, 11336–11337.

(9)   Liao, S.; List, B. *Angew. Chem. Int. Ed.* **2010**, *49*, 628–631.

(10)   Jiang, G.; List, B. *Angew. Chem. Int. Ed.* **2011**, *50*, 9471–9474.

(11)   Jiang, G.; Halder, R.; Fang, Y.; List, B. *Angew. Chem. Int. Ed.* **2011**, *50*, 9752–9755.

(12)   Meeuwissen, J.; Reek, J. N. H. *Nat. Chem.* **2010**, *2*, 615–621.

(13)   Ringe, D.; Petsko, G. A. *Science* **2008**, *320*, 1428–1429.

(14)   Gross, E.; Liu, J. H.; Alayoglu, S.; Marcus, M. A.; Fakra, S. C.; Toste, F. D. Somorjai, G. A. *J. Am. Chem. Soc.* **2013**, *135*, 3881–3886.

(15)   Raynal, M.; Ballester, P.; Vidal-Ferran, A.; Leeuwen, P. W. N. M. V *Chem. Soc. Rev.* **2014**, *43*, 1734–1787.

(16)   Park, S.; Sugiyama, H. *Molecules* **2012**, *17*, 12792–12803.

(17) Pluth, M. D.; Bergman, R. G.; Raymond, K. N. *Supramolecular Catalysis*, Chapter 8, Wiley-VCH: Weinheim, 2008, 165–191.

(18) Chin, J. *Acc. Chem. Res.* **1991**, *24*, 145–152.

(19) Uhlenbeck, O. C. *Nature* **1987**, *328*, 596–600.

(20) Zaug, A. J.; Michael, D. B.; Cech, T. R. *Nature* **1986**, *324*, 429–433.

(21) Chin, J.; Banaszczyk, M. *J. Am. Chem. Soc.* **1989**, *111*, 4103–4105.

(22) Benkovic, S. J.; Hammes-Schiffer, S. *Science* **2003**, *301*, 1196–1202.

(23) Marshall, S. T.; O'Brien, M.; Oetter, B.; Corpuz, A.; Richards, R. M.; Schwartz, D. K.; Medlin, J. W. *Nat. Mat.* **2010**, *9,* 853–858.

(24) Rod, T. H.; Norskov, J. K. *Surf. Sci.* **2002**, *500*, 678–698.

(25) Janssen, K. P. F.; Cremer, G. D.; Neely, R. K.; kubarev, A. V.; Loon, J. V.; Martens, J. A.; Vos, D. E. D.; Roeffaers, M. B. J.; Hofkens, J. *Chem. Soc. Rev.* **2014**, *43*, 990–1006.

(26) Sheldon, R. A. *Chem. Soc. Rev.* **2012**, *41*, 1437–1451.

(27) Boersma, A. J.; Klijn, J. E.; Feringa, B. L.; Roelfes, G. *J. Am. Chem. Soc.* **2008**, *130*, 11783–11790.

(28) Davies, R. R.; Distefano, M. D. *J. Am. Chem. Soc.* **1997**, *119*, 11643–11652.

(29) Collot, J.; Gradinaru, J.; Humbert, N.; Skander, M.; Zocchi, A.; Ward, T. R. *J. Am. Chem. Soc.* **2003**, *125*, 9030–9031.

(30) Wilson, M. E.; Whitesides, G. M. *J. Am. Chem. Soc.* **1978**, *100,* 306–307.

(31) Letondor, C.; Pordea, A.; Humbert, N.; Ivanova, A.; Mazurek, S.; Novic, M.; Ward, T. R. *J. Am. Chem. Soc.* **2006**, *128*, 8320–8328.

(32)   Letondor, C.; Humbert, N.; Ward, T. R. *Proc. Natl. Acad. Sci. U.S.A.* **2005**, *102*, 4683–4687.

(33)   Pierron, J.; Malan, C.; Creus, M.; Gradinaru, J.; Hafner, I.; Ivanova, A.; Sardo, A.; Ward, T. R. *Angew. Chem., Int. Ed.* **2008**, *47*, 701–705.

(34)   Mahammed, A.; Gross, Z. *J. Am. Chem. Soc.* **2005**, *127*, 2883–2887.

(35)   Carey, J. R.; Ma, S. K.; Pfister, T. D.; Garner, D. K.; Kim, H. K.; Abramite, J. A.; Wang, Z.; Guo, Z.; Lu, Y. *J. Am. Chem. Soc.* **2004**, *126*, 10812–10813.

(36)   Velde, F. V. D.; Könemann, L.; Rantwijk, F. V.; Sheldon, R. A. *Chem. Commun.* **1998**, 1891–1892.

(37)   Sugimoto, T.; Kokubo, T.; Miyazaki, J.; Tanimoto, S.; Okano, M. *J. Chem. Soc., Chem. Commun.* **1979**, 402–404.

(38)   Okrasa, K.; Kazlauskas, R. J. *Chem. Eur. J.* **2006**, *12*, 1587–1596.

(39)   Fernández-Gacio, A.; Codina, A.; Fastrez, J.; Riant, O.; Soumillion, P. *ChemBioChem* **2006**, *7*, 1013–1016.

(40)   Kokubo, T.; Sugimoto, T.; Uchida, T.; Tanimoto, S.; Okano, M. *J. Chem. Soc., Chem. Commun.* **1983**, 769–770.

(41)   Reetz, M. T.; Jiao, N. *Angew. Chem., Int. Ed.* **2006**, *45*, 2416–2419.

(42)   Colonna, S.; Manfredi, A.; Annunziata, R. *Tetrahedron Lett.* **1988**, *29*, 3347–3350.

(43)   Roy, R. S.; Imperiali, B. *Protein Eng.* **1997**, *10*, 691–698.

(44)   Roelfes, G. *Mol. Biosys.* **2007**, *3*, 126–135.

(45)   Stuhlmann, F.; Jäschke, A. *J. Am. Chem. Soc.* **2002**, *124*, 3238–3244.

(46)   Li, X.; Liu, D. R. *J. Am. Chem. Soc.* **2003**, *125*, 10188–10189.

(47)   Seelig, B.; Keiper, S.; Stuhlmann, F.; Jäschke, A. *Angew. Chem., Int. Ed.* **2000**, *39*, 4576–4579.

(48)   Kozlov, I. A.; Politis, P. K.; Pitsch, S.; Herdewijn, P.; Orgel, L. E. *J. Am. Chem. Soc.* **1999**, *121*, 1108–1109.

(49)   Schmidt, J. G.; Nielsen, P. E.; Orgel, L. E. *J. Am. Chem. Soc.* **1997**, *119*, 1494–1495.

(50)   Bolli, M.; Micura, R.; Eschenmoser, A. *Chem. Biol.* **1997**, *4*, 309–320.

(51)   Joyce, G. F.; Visser, G. M.; Boeckel, C. A. A. V.; Boom, J. H. V.; Orgel, L. E.; Westrenen, J. V. *Nature* **1984**, *310*, 602–604.

(52)   Roelfes, G.; Feringa, B. L. *Angew. Chem. Int. Ed.* **2005**, *44*, 3230–3232.

(53)   Roelfes, G.; Boersma, A. J.; Feringa, B. L. *Chem. Commun.* **2006**, 635–637.

(54)   Boersma, A. J.; Feringa, B. L.; Roelfes, G. *Org. Lett.* **2007**, *9*, 3647–3650.

(55)   Coquière, D.; Feringa, B. L.; Roelfes, G. *Angew. Chem. Int. Ed.* **2007**, *46*, 9308–9311.

(56)   Boersma, A. J.; Feringa, B. L.; Roelfes, G. *Angew. Chem. Int. Ed.* **2009**, *48*, 3346–3348.

(57)   Boersma, A. J.; Coquière, D.; Greerdink, D.; Rosati, F.; Feringa, B. L.; Roelfes, G. *Nat. Chem.* **2010**, *2*, 991–995.

(58)   Boersma, A. J.; Bruin, B.; Feringa, B. L.; Roelfes, G. *Chem. Commun.* **2012**, *48*, 2394–2396.

(59)   Oltra, N. S.; Roelfes, G. *Chem. Commun.* **2008**, 6039–6041.

(60)   Fournier, P.; Fiammengo, R.; Jäschke, A. *Angew. Chem. Int. Ed.* **2009**, *48*, 4426–4429.

(61) Shibata, N.; Yasui, H.; Nakamura, S.; Toru, T. *Synlett* **2007**, 1153–1157.

(62) Park, S.; Ikehata, K.; Watabe, R.; Hidaka, Y.; Rajendran, A.; Sugiyama, H. *Chem. Commun.* **2012**, 10398–10400.

(63) Roe, S.; Ritson, D. J.; Garner, T.; Searle, M.; Moses, J. E. *Chem. Commun.* **2010**, 4309–4311.

(64) Wang, C.; Li, Y.; Jia, G.; Liu, Y.; Lu, S.; Li, C. *Chem. Commun.* **2012**, 6232–6234.

(65) Wang, C.; Jia, G.; Zhou, J.; Li, Y.; Liu, Y.; Lu, S.; Li, C. *Angew. Chem. Int. Ed.* **2012**, *51*, 9352–9355.

(66) Megens, R. P.; Roelfes, G. *Org. Biomol. Chem.* **2010**, *8*, 1387–1393.

(67) Rozenman, M. M.; Liu, D. R. *ChemBioChem* **2006**, *7*, 253–256.

(68) Oila, M. J.; Koskinen, A. M. P. *ARKIVOC* **2006**, *xv*, 76–83.

(69) Huang, Y.; Xu, S.; Lin, V. S. -Y. *ChemCatChem* **2011**, *3*, 690–694.

(70) Gross, E.; Liu, J. H. -C.; Toste, F. D.; Somorjai, G. A. *Nat. Chem.* **2012**, *4*, 947–952.

(71) Bringmann, G.; Mortimer, A. J. P.; Keller, P. A.; Gresser, M. J.; Garner, J.; Breuning, M. *Angew. Chem. Int. Ed.* **2005**, *44*, 5384–5427.

(72) Mikami, K.; Miyamoto, T.; Hatano, M. *Chem. Commun.* **2004**, 2082–2083.

(73) Colobert, F.; Valdivia, V.; Choppin, S.; Leroux, F. R.; Fernández, I.; Alvarez, E.; Khiar, N. *Org. Lett.* **2009**, *11*, 5130–5133.

(74) Shen, X.; Jones, G. O.; Watson, D. A.; Bhayana, B.; Buchwald, S. L. *J. Am. Chem. Soc.* **2010**, *132*, 11278–11287.

(75)   Tang, W.; Patel, N. D.; Xu, G.; Xu, X.; Savoie, J.; Ma, S.; Hao, M. -H.; Keshipeddy, S.; Capacci, A. G.; Wei, X.; Zhang, Y.; Gao, J. J.; Li, W.; Rodriguez, S.; Lu, B. Z.; Yee, N. K.; Senanayake, C. H. *Org. Lett.* **2012**, *14*, 2258–2261.

(76)   Karthikeyan, T.; Sankararaman, S. *Tetrahedron Lett.* **2009**, *50*, 5834–5837.

(77)   Cammidge, A. N.; Crépy, K. V. L. *J. Org. Chem.* **2003**, *68*, 6832–6835.

(78)   Suau, R.; Rico, R.; Nájera, F.; Ortiz-López, F. J.; López-Romero, J. M.; Moreno-Mañas, M.; Roglans, A. *Tetrahedron* **2004**, *60*, 5725–5735.

(79)   Bari, L. D.; Pescitelli, G.; Salvadori, P. *J. Am. Chem. Soc.* **1999**, *121*, 7998–8004.

(80)   Kubinyi, M.; Pál, K.; Baranyai, P.; Grofcsik, A.; Bitter, I.; Grün, A. *Chirality* **2004**, *16*, 174–179.

(81)   Nishizaka, M.; Mori, T.; Inoue, Y. *J. Phys. Chem. A* **2011**, *115*, 5488–5495.

(82)   Nakai, Y.; Nishizaka, M.; Yang, C.; Fukuhara, G.; Mori, T.; Inoue, Y. *Chirality* **2011**, *23*, E22–E27.

(83)   Zhou, S.; Johnson, M.; Veinot, J. G. C. *Chem. Commun.* **2010**, *46*, 2411–2413.

(84)   Pérez-Lorenzo, M. *J. Phys. Chem. Lett.* **2012**, *3*, 167–174.

(85)   Astruc, D. *Inorg. Chem.* **2007**, *46*, 1884–1894.

(86)   Richardson, J. M.; Jones, C. W. *J. Catal.* **2007**, *251*, 80–93.

(87)   Balanta, A.; Godard, C.; Claver, C. *Chem. Soc. Rev.* **2011**, *40*, 4973–4985.

(88)   Trost, B. M.; Fandrick, D. R. *Aldrichimica Acta* **2007**, *40*, 59–72.

(89)   Walsh, P. J.; Kozlowski, M. C. *Fundamentals of Asymmetric Catalysis*, Chapter 4, University Science Books: Virginia, 2009.

(90)   Hsu, Y. -C.; Datta, S.; Ting, C. -M.; Liu, R. -S. *Org. Lett.* **2008**, *10*, 521–524.

(91)   Shen, H. -C.; Pal, S.; Lian, J. -J.; Liu, R. -S. *J. Am. Chem. Soc.* **2003**, *125*, 15762–15763.

(92)   Toummini, D.; Ouazzani, F.; Taillefer, M. *Org. Lett.* **2013**, *15*, 4690–4693.

Chapter 6

Conclusions

This thesis has discussed the development of a very simple one-pot synthesis of RNT supported M NPs followed by their application in "Green" catalysis under mild conditions. To conclude this thesis, this chapter summarizes the results of each chapter and addresses some key future research directions.

6.1 Summaries of Chapters

6.1.1 Chapter 1

Chapter 1 discussed the background of this thesis work inspired by the concepts of nanoparticles (NPs) and catalysis. This chapter described the initial notion of nanotechnology and the strategies used to synthesize NPs followed by their properties and applications in catalysis. A brief summary of the stability of the NPs in solution using different approaches was provided including the application of different support systems. I then introduced the concept of applying bio- and/or inspired supports for the synthesis of M NPs for catalysis and reviewed the relevant literature. Also discussed the potential of the RNTs as a bio-inspired support to prepare highly monodispersed and smaller sized M NPs (1-2± 0.1 nm). Finally, the chapter reported the demand and the rapid progression of NP catalysis within the nanotechnology scientific community.

The results reported in this thesis can be divided into two main sections (i) synthesis and characterization of the M NPs/RNTs composites followed by the origin and kinetics studies, and (ii) their application in catalysis including olefin hydrogenation and Suzuki-Miyaura cross-coupling reactions.

6.1.2 Chapter 2

In general, this chapter reported the development and characterization of a simple, efficient and green protocol for the synthesis M NPs using RNTs as a support. A detailed study on the NP origin and the kinetics was also presented. As the thesis work was a continuation of the initial results reported by Fenniri and coworkers, firstly I summarized the findings based on the contents published in JACS (2010) and obtained by a former group member. Followed by the summary, I discussed the further optimization and simplification of the methodology. I reported that the M NPs could be synthesized in the absence of any reducing agent by simply mixing the corresponding metal salt precursor and RNTs in water at ambient temperature. The detailed kinetic study suggested that the formation of M NPs onto the surface of the RNTs was a very rapid process, which took place within 1 min. The time-dependent spectroscopy studies showed that the system reached equilibrium within 60 min, which was supported by the time-dependent microscopy studies. A careful and detailed analysis of the time-dependent TEM images showed that the NPs could form within 1 min with an average particle size of 1.48±0.1 nm. However, the nucleation and growth of the NPs were incomplete. The maximum occupancy of the available nucleation pockets was improved and completed by aging the solution to 60 min. These results were further supported by spectroscopic analysis. The aging of the solution allowed for the growth of the nucleated NPs to reach a maximum average size of 1.55±0.1 nm, and then subsequent nucleation and growth of another NP into a new nucleation pocket occurred. As the TEM images of the 60 min aged sample showed the maximum loading of the NPs onto the surface of the RNTs, I believed that the total process of the step-wise formation of the NP completed in 60 min. The TEM

analysis of the 120 min aged samples showed neither any improvement of the loading or further growth of the NPs.

As I demonstrated that RNTs facilitated the M NP formation in the absence of any reducing agent, I performed spectroscopy and microscopy studies to detect the origin of the reduction of the metal ions. The initial pH studies showed a drop in pH of the solution within 60 min, which indicated the generation of protons (H^+) upon oxidation of the reducing agent. The XPS analysis confirmed the presence of Pd^0 and PdO_x (x = 1 and 2) in the samples under both aerobic and anaerobic conditions. In addition, the DO measurement of the mixture under anaerobic condition showed a random fluctuation in the DO content. Therefore, all these studies supported the hypothesis of water oxidation. I suspect that this oxidation process may be facilitated by the presence of well-defined nucleation pockets on the surface of the RNTs. Besides this, the auto-catalysis of Pd could also enhances the water oxidation.

6.1.3 Chapter 3, 4 and 5

Chapter 3 discussed the catalytic hydrogenation of olefins using the Pd NPs/RNTs catalyst. I demonstrated the utility and scope of our catalyst towards the hydrogenation of C=C bonds in the presence of aromatic and heteroaromatic ring systems. In addition, the studies suggested that the selectivity of the olefin hydrogenation could also be achieved by using our catalyst in the presence of other unsaturated functional groups. A comparative study of the catalytic activity revealed that the Pd NPs/RNTs catalyst is as active as a commercial catalyst. Besides this, the catalyst recycling experiment showed that the Pd NPs/RNTs catalyst could be recycled up to ten times with no significant loss of activity. The catalyst was characterized by spectroscopy as well as microscopy.

Chapter 4 discussed the application of our catalyst to the Suzuki-Miyaura cross-coupling reaction. Initially, I studied the scope and utility of our catalyst for the coupling of different aryl halides and arylboronic acids in the presence of a variety of functional groups. The chapter also reported the scale-up reaction using the Pd NPs/RNTs. Similarly to that of the hydrogenation catalysis, I were able to recycle our catalyst up to ten times with no apparent loss of activity. Later, I also successfully applied our catalyst to synthesize drug and agrochemical intermediates, and benzothiadiazole based organic materials for solar cells, OLEDs and sensors applications. A detailed characterization of the catalyst was performed using both spectroscopy and microscopy. Interestingly, the time-dependent and variable-temperature CD studies showed that the supramolecular chirality of RNT was preserved and restored under the coupling reaction condition in the presence of Pd NPs, while the RNT itself was unable to restore the supramolecular chirality after heat treatment.

Inspired by the VT-CD results, I then carried out the asymmetric Suzuki-Miyaura cross-coupling reaction using the Pd NPs/RNTs catalyst as reported in chapter 5. The results showed that under the optimized condition for the coupling reaction, there was poor chirality induction to the coupled products. I hypothesized that this could be due to the leaching of the Pd atoms from the Pd NPs on the surface of the RNTs. Therefore, the coupling of the two reactants took place in the bulk solution and thus too far away from the RNT surface to induce the chirality.

6.2 Proposed Research Directions

As the application of the Pd NPs/RNTs in catalysis is a new direction in our group, there are many other catalytic reactions that that could be investigated, including Heck

and Sonogashira coupling reactions. Though the main focus of this thesis was to explore catalysis using Pd NPs, other catalytic reactions could be explored by using Au NPs for example for catalytic oxidation reactions. Apart from the synthesis and catalytic applications of different M NPs, the detailed mechanistic studies of each catalytic reaction could be explored. This would give us the in-depth understanding of the catalytic event and the function of RNTs as a support providing high catalytic activity as reported in this thesis. To improve the chirality induction in the supramolecular chiral catalysis, a bulky tertiary amine can be introduced on the lysine of the G0 twin G∧C base (Figure 6.1). Because of the bulkiness, the tertiary amine will be pointed outwards more close to the Pd NPs and may improve the chirality induction in the Suzuki coupling reaction. Alternately, asymmetric hydrogenation reaction can also be explored. As it is well accepted that the catalytic hydrogenation reaction takes place on the surface of the NP, this will offer the catalysis occurring close to the RNT surface and may improve the chirality induction to the hydrogenated product.
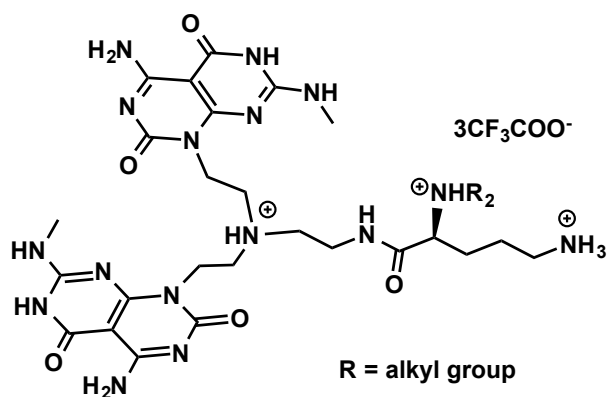
Figure 6.1: Derivatization of the amine at the chiral center of the L-lysine.

Bibliography

(1)   Siegel, R. W.; Hu, E; Roco, M. C. Eds. *Nanostructure Science and Technology-A Worldwide Study. Prepared under the guidance of the IWGN and NSTC*, WTEC: Loyola College, Maryland, 1999.

(2)   Mansoori, G. A. *Principles of Nanotechnology: Molecular Based Study of Condensed Matter in Small Systems*, World Scientific: New York, 2005.

(3)   Mansoori, G. A.; George, T. F.; Assoufid, L.; Zhang, G. *Molecular Building Blocks for Nanotechnology: from Diamondoids to Nanoscale Materials and Applications*, Springer: New York, 2007.

(4)   Ranu, B. C.; Chattopadhyay, K.; Adak, L.; Saha, A.; Bhadra, S.; Dey, R.; Saha, D. *Pure Appl. Chem.* **2009**, *81*, 2337−2354.

(5)   Astruc, D. In *Nanoparticles and Catalysis*; Weinheim: Wiley-VCH, 2008.

(6)   Schmid, G.; Fenske, D. *Phil. Trans. R. Soc. A* **2010**, *368*, 1207–1210.

(7)   Balanta, A.; Godard, C.; Claver, C. *Chem. Soc. Rev.* **2011**, *40*, 4973−4985.

(8)   Roduner E. In *Nanoscopic Materials: Size-dependent Phenomena*; Cambridge: The Royal Society of Chemistry, 2006.

(9)   Davies, P. R.; Roberts, M. W. In *Atom Resolved Surface Reactions: Nanocatalysis*; Cambridge: The Royal Society of Chemistry, 2008.

(10)   Johánek, V.; Laurin, M.; Grant, A. W.; Kasemo, B.; Henry, C. R.; Libuda, J. *Science* **2004**, *304*, 1639−1644.

(11)   Ertl, G. *J. Mol. Catal. A: Chem.* **2002**, *182*, 5−16.

(12)   Astruc, D.; Lu, F.; Aranzaes, J. R. *Angew. Chem. Int. Ed. Engl.* **2005**, *44*, 7852−7872.

(13)   Wieckowski, A.; Savinova, F. R.; Vayenas, C. G. In *Catalysis and Electrocatalysis at Nanoparticle Surfaces*; New York: Dekker, 2003.

(14)   Valentini, F.; Biagiotti, V.; Lete, C.; Palleschi, G.; Wang, J. *Sensor Actuat. B: Chem.* **2007**, *128*, 326−333.

(15)   Tsoukalas, D. *Int. J. Nanotechnol.* **2009**, *6*, 35−45.

(16)   Sevilla, M.; Sanchis, C.; Valdés-Solís T.; Morallón, E.; Fuertes, A. B. *Electrochim. Acta* **2009**, *54*, 2234−2238.

(17)   Gutiérrez, J. M.; González, C.; Mastr, A.; Solè, I.; Pey, C. M.; Nola, J. *Curr. Opin. Colloid Interface Sci.*, **2008**, *13*, 245−251.

(18)   Enoch, S.; Quidant, R.; Badenes, G. *Opt. Express* **2004**, *12*, 3422−3427.

(19)   Astruc, D. *Inorg. Chem.* **2007**, *46*, 1884−1894.

(20)   Jia, C. -J.; Schüth, F. *Phys. Chem. Chem. Phys.* **2011**, *13*, 2457−2487.

(21)   Roucoux, A.; Schulz, J.; Patin, H. *Chem. Rev.* **2002**, *102*, 3757−3778.

(22)   Redón, R.; Rendón-Lara, S. K.; Rernández-Osorio, A. L. Ugalde-Saldivar, V. M. *Rev. Adv. Mater. Sci.* **2011**, *27*, 31−42.

(23)   Finney, E. E.; Finke, R. G. *J. Colloid Interface Sci.* **2008**, *317*, 351−374.

(24)   Lim, J. -S.; Kim, S. -M.; Lee, S. -Y.; Stach, E. A.; Culver, J. N.; Harris, M. T. *Nano Lett.* **2010**, *10*, 3863–3867.

(25)   Faraday, M. *Phil. Trans. R. Soc. London* **1857**, *147*, 145–153.

(26)   Turkevich, J.; Stevenson, P. C.; Hillier, J. *Discuss. Faraday Soc.* **1951**, *11*, 55–75.

(27)   Turkevich, J.; Kim, G. *Science* **1970**, *169*, 873–879.

(28) Turkevich, J. *Gold Bull.* **1985**, *18*, 86–91.

(29) Murray, C. B.; Norris, D. J.; Bawendi, M. G. *J. Am. Chem. Soc.* **1993**, *115*, 8706–8715.

(30) LaMer, V. K.; Dinegar, R. H. *J. Am. Chem. Soc.* **1950**, *72*, 4847–4854.

(31) LaMer, V. K. *Ind. Eng. Chem.* **1952**, *44*, 1270–1277.

(32) Ostwald, W. *Z. Phys. Chem.* **1900**, *34*, 495–503.

(33) Watzky, M. A.; Finke, R. G. *J. Am. Chem. Soc.* **1997**, *119*, 10382–10400.

(34) Thanh, N. T. K.; Maclean, N.; Mahiddine, S. *Chem. Rev.* **2014**, *114*, 7610−7630

(35) Pruppacher, H. R.; Klett, J. D. *Microphysics of Clouds and Precipitation*, Kluwer: Massachusetts, 1997.

(36) Sear, R. P. *J. Phys.: Condens. Matter* **2007**, *19*, 033101.

(37) Guerra, J.; Herrero, M. A. *Nanoscale* **2010**, *2*, 1390−1400.

(38) Zhuo, Q.; Ma, Y.; Gao, J.; Zhang, P.; Xia, Y.; Tian, Y.; Sun, X.; Zhong, J.; Sun, X. *Inorg. Chem.* **2013**, *52*, 3141−3147.

(39) Shang, L.; Bian, T.; Zhang, B.; Zhang, D.; Wu, L. -Z.; Tung, C. -H.; Yin, Y.; Zhang, T. *Angew. Chem. Int. Ed. Engl.* **2014**, *53*, 250−254.

(40) White, R. J.; Luque, R.; Budarin, V. L.; Clark, J. H.; Macquarrie, D. J. *Chem. Soc. Rev.* **2009**, *38*, 481–494.

(41) Campelo, J. M.; Luna, D.; Luque, R.; Marinas, J. M.; Romero, A. A. *ChemSusChem* **2009**, *2*, 18–45.

(42) Ma, Z.; Yin, H.; Overbury, S. H.; Dai, S. *Catal. Lett.* **2008**, *126*, 20–30.

(43)   Gallezot, P.; Richard, D.; Bergeret, G. In *Novel Materials in Heterogeneous Catalysis*; Baker, R. T. K., Murrell, L. L., Eds.; ACS Symposium Series No. 437; American Chemical Society: Washington DC, 1990, 150–159.

(44)   Ley, S. V.; Mitchell, C.; Pears, D.; Ramarao, C.; Yu, J. -Q.; Zhou, W. -Z. *Org. Lett.* **2003**, *5*, 4665–4668.

(45)   Demir, M. M.; Gulgun, M. A.; Menceloglu, Y. Z.; Erman, B.; Abramchuk, S. S.; Makhaeva, E. E.; Khokhlov, A. R.; Matveeva, V. G.; Sullman, M. G. *Macromolecules* **2004**, *37*, 1787–1792.

(46)   Kidambi, S.; Dai, J. -H.; Lin, J.; Bruening, M. L. *J. Am. Chem. Soc.* **2004**, *126*, 2658–2659.

(47)   Chauhan, B. P. S.; Rathore, J. S.; Bandoo, T. *J. Am. Chem. Soc.* **2004**, *126*, 8493–8500.

(48)   Sanji, T.; Ogawa, Y.; Nakatsuka, Y.; Tanaka, M.; Sakurai, H. *Chem. Lett.* **2003**, 32, 980–981.

(49)   Drelinkiewicza, A.; Waksmundzka, A.; Makowski, W.; Sobczak, J. W.; Krol, A.; Zieba, A. *Catal. Lett.* **2004**, *94*, 143–156.

(50)   Liu, Y. -B.; Khemtong, C.; Hu, J. *Chem. Commun.* **2004**, 398–399.

(51)   Hu, J.; Liu, Y. -B. Langmuir 2005, 21, 2121–2123.

(52)   Pillai, U. R.; Sahle-Demessie, E. *J. Mol. Catal. A: Chem.* **2004**, *222*, 153–158.

(53)   Adlim, M.; Abu Bakar, M.; Liew, K. Y.; Ismail, J. *J. Mol. Catal. A: Chem.* **2004**, *212*, 141–149.

(54)   Tabuani, D.; Monticelli, O.; Chincarini, A.; Bianchini, C.; Vizza, F.; Moneti, S.; Russo, S. *Macromolecules* **2003**, *36*, 4294–4301.

(55)   Zhao, M.; Sun, L.; Crooks, R. M. *J. Am. Chem. Soc.* **1998**, *120,* 4877–4878.

(56)   Balogh, L.; Tomalia, D. A. *J. Am. Chem. Soc.* **1998**, *120*, 7355–7356.

(57)   Esumi, K.; Susuki, A.; Aihara, N.; Usui, K.; Torigoe, K. *Langmuir* **1998**, *14*, 3157–3159.

(58)   Pachón, L. D.; Rothenberg, G. *Appl. Organometal. Chem.* **2008**, *22*, 288–299.

(59)   Narayanan, R.; El-Sayed, M. A. *J. Phys. Chem. B* **2004**, *108*, 8572–8580.

(60)   Bönnemann, H.; Brijoux, W.; Brinkmann, R.; Dinjus, E.; Joussen, T.; Korall, B. *Angew. Chem. Int. Ed. Engl.* **1991**, *30*, 1312–1314.

(61)   Bönnemann, H.; Brijoux, W. In *Active Metals: Preparation, Characterization, Applications*; Fürstner, A. Ed.; VCH, Weinheim, 1996.

(62)   Niederer, J. P. M.; Arnold, A. B. J.; Hölderich, W. F.; Tesche, B.; Reetz, M.; Bönnemann, H. *Top. Catal.* **2002**, *18*, 265 269.

(63)   Luque, R.; Budarin, V.; Clark, J. H.; Macquarrie, D. J. *Appl. Catal. B* **2008**, *82*, 157–162.

(64)   Budarin, V.; Clark, J. H.; Hardy, J. J. E.; Luque, R.; Milkowski, K.; Tavener, S. J.; Wilson, A. J. *Angew. Chem. Int. Ed.* **2006**, *45*, 3782–3786.

(65)   Pan, X.; Bao, X. *Chem. Commun.* **2008**, 6271–6281.

(66)   Terrones, M. *Int. Mater. Rev.* **2004**, *49*, 325–377.

(67)   Wildgoose, G. G.; Banks, C. E.; Compton, R. G. *Small* **2006**, *2*, 182–193.

(68)   Wang, C.; Guo, S.; Pan, X.; Chen, W.; Bao, X. *J. Mater. Chem.* **2008**, *18*, 5782–5786.

(69)   Li, X.; Qin, Y.; Picraux, S. T.; Guo, Z. -X. *J. Mater. Chem.* **2011**, *21*, 7527–7547.

(70)   Subrahmanyam, K. S.; Manna, A. K.; Pati, S. K.; Rao, C. N. R. *Chem. Phys. Lett.*

2010, *497*, 70–75.

(71)   Kundu, P.; Anumol, E. A.; Ravishankar, N. *Nanoscale* **2013**, *5*, 5215–5224.

(72)   Oyama, M.; Chen, X.; Chen, X. *Anal. Sci.* **2014**, *30*, 529–538.

(73)   Muszynski, R.; Seger, B.; Kamat, P. V. *J. Phys. Chem. C* **2008**, *112*, 5263–5266.

(74)   Kamat, P. V. *J. Phys. Chem. Lett.* 2010, 1, 520–527.

(75)   Raghuveer, M. S.; Agrawal, S.; Bishop, N.; Ramanath, G. *Chem. Mater.* **2006**, *18*, 1390–1393.

(76)   Jasuja, K.; Berry, V. *ACS Nano* **2009**, *3*, 2358–2366.

(77)   Lu, L.; Randjelovic, I.; Capek, R.; Gaponik, N.; Yang, J.; Zhang, H.; Eychmuller, A. *Chem. Mater.* **2005**, *17*, 5731–5736.

(78)   Hassan, H. M. A.; Abdelsayed, V.; El-Rahman, A.; Khder, S.; AbouZeid, K. M.; Terner, J.; El-Shall, M. S.; Al-Resayes, S. I.; El-Azhary, A. A. *J. Mater. Chem.* **2009**, *19*, 3832–3837.

(79)   Li, J.; Liu, C. *Eur. J. Inorg. Chem.* **2010**, 1244–1248.

(80)   Yoo, E.; Okata, T.; Akita, T.; Kohyama, M.; Nakamura, J.; Honma, I. *Nano Lett.* 2009, 9, 2255–2259.

(81)   Bhandari, R.; Coppage, R.; Knecht, M. R. *Catal. Sci. Technol.* **2012**, *2*, 256–266.

(82)   Dickerson, M. B.; Sandhage, K. H.; Naik, R. R. *Chem. Rev.* **2008**, *108*, 4935–4978.

(83)   Guerra, J.; Burt, J. L.; Ferrer, D. A.; Mejía, S.; José-Yacamán, M. *J. Nanopart. Res.* **2011**, *13*, 1723–1735.

(84)   Behrens, S.; Heyman, A.; Maul, R.; Essig, S.; Steigerwald, S.; Quintilla, A.; Wenzel, W.; Bürck, J.; Dgany, O.; Shoseyov, O. *Adv. Mater.* **2009**, *21*, 3515–

3519.

(85)   Smith, G. P.; Baustian, K. J; Ackerson, C. J.; Feldheim, D. L. *J. Mater. Chem.*
         2009, *19*, 8299–8306.

(86)   Virkutyte, J.; Varma, R. S. *Chem. Sci.* **2011**, *2*, 837–846.

(87)   Ohara, S.; Hatakeyama, Y.; Umetsu, M.; Tan, Z.; Adschiri, T. *Adv. Power
         Technol.* **2011**, *22*, 559–565.

(88)   Chiu, C. -Y.; Li, Y.; Huang, Y. *Nanoscale* **2010**, *2*, 927–930.

(89)   Seker, U. O. S.; Demir, H. V. *Molecules* **2011**, *16*, 1426–1451.

(90)   Bhandari, R.; Knecht, M. R. *ACS Catal.* **2011**, *1*, 89–98.

(91)   Jakhmola, A.; Bhandari, R.; Pacardo, D. B.; Knecht, M. R. *J. Mater. Chem.* **2010**,
         20, 1522–1531.

(92)   Coppage, R.; Slocik, J. M.; Briggs, B. D.; Frenkel, A. I.; Heinz, H.; Naik, R. R.;
         Knecht, M. R. *J. Am. Chem. Soc.* **2011**, *133*, 12346–12349.

(93)   Pacardo, D. B.; Sethi, M.; Jones, S. E.; Naik, R. R.; Knecht, M. R. *ACS Nano*
         2009, *3*, 1288–1296.

(94)   Pacardo, D. B.; Knecht, M. R. *Catal. Sci. Technol.* **2013**, *3*, 745–753.

(95)   Briggs, B. D.; Pekarek, R. T.; Knecht, M. R. *J. Phys. Chem. C* **2014**, *118*,
         18543−18553.

(96)   Pacardo, D. B.; Slocik, J. M.; Kirk, K. C.; Naik, R. R.; Knecht, M. R. *Nanoscale*
         2011, *3*, 2194−2201.

(97)   Ramezani-Dakhel, H.; Mirau, P. A.; Naik, R. R.; Knecht, M. R.; Heinz, H. *Phys.
         Chem. Chem. Phys.* **2013**, *15*, 5488−5492.

(98)   Wu, H.; Wu, C.; He, Q.; Liao, X.; Shi, B. *Mater. Sci. Eng. C* **2010**, *30*, 770−776.

(99)   Hennebel, T.; Verhagen, P.; Simoen, H.; Gusseme, B. D.; Vlaeminck, S. E.; Boon, N.; Verstraete, W. *Chemosphere* **2009**, *76*, 1221−1225.

(100) Bennett, J. A.; Creamer, N. J.; Deplanche, K.; Macaskie, L. E.; Shannon, I. J.; Wood, J. *Chem. Eng. Sci.* **2010**, *65*, 282−290.

(101) Søbjerg, L. S.; Gauthier, D.; Lindhardt, A. T.; Bunge, M.; Finster, K.; Meyer, R. L.; Skrydstrup, T. *Green Chem.* **2009**, *11*, 2041−2046.

(102) Hennebel, T.; Gusseme, B. D.; Boon, N.; Verstraete, W. *Trends Biotechnol.* **2008**, *27*, 90−98.

(103) Søbjerg, L. S.; Lindhardt, A. T.; Skrydstrup, T.; Finster, K.; Meyer, R. L. *Colloids Surf. B* **2011**, *85*, 373−378.

(104) Murugesan, K.; Bokare, V.; Jeon, J. -R.; Kim, E. -J.; Kim, J. -H.; Chang, Y. -S. *Bioresour. Technol.* **2011**, *102*, 6019−6025.

(105) Manocchi, A. K.; Seifert, S.; Lee, B.; Yi, H. *Langmuir* **2011**, *27*, 7052−7058.

(106) Manocchi, A. K.; Horelik, N. E.; Lee, B.; Yi, H. *Langmuir* **2010**, *26*, 3670−3677.

(107) Yang, C.; Yi, H. *Biochem. Eng. J.* **2010**, *52*, 160−167.

(108) Yang, C.; Manocchi, A. K.; Lee, B.; Yi, H. *Appl. Catal. B* **2010**, *93*, 282−291.

(109) Bricout, H.; Hapiot, F.; Ponchel, A.; Tilloy, S.; Monflier, E. *Sustainability* **2009**, *1*, 924−945.

(110) Alvarez, J.; Liu, J.; Román, E.; Kaifer, A. E. *Chem. Commun.* **2000**, 1151−1152.

(111) Senra, J. D.; Malta, L. F. B.; Michel, R. C.; Cordeiro, Y.; Simão, R. A.; Simas, A. B. C.; Aguiar, L. C. S. *J. Mater. Chem.* **2011**, *21*, 13516−13523.

(112) Sreedhar, B.; Reddy, P. S.; Devi, D. K. *J. Org. Chem.* **2009**, *74*, 8806−8809.

(113) Bankar, A.; Joshi, B.; Kumar, A. R.; Zinjarde, S. *Mater. Lett.* **2010**, *64*,

1951−1953.

(114) Fenniri, H.; Mathivanan, P.; Vidale, K. L.; Sherman, D. M.; Hallenga, K.; Wood, K. V.; Stowell, J. G. *J. Am. Chem. Soc.* **2001**, *123*, 3854–3855.

(115) Fenniri, H.; Deng, B. -L.; Ribbe, A. E.; Hallenga, K.; Jacob, J.; Thiyagarajan, P. *Proc. Natl. Acad. Sci. USA* **2002**, *99*, 6487–6492.

(116) Fenniri, H.; Deng, B. -L.; Ribbe, A. E. *J. Am. Chem. Soc.* **2002**, *124*, 11064–11072.

(117) Moralez, J. G.; Raez, J.; Yamazaki, T.; Motkuri, R. K.; Kovalenko, A.; Fenniri, H. *J. Am. Chem. Soc.* **2005**, *127*, 8307–8309.

(118) Chhabra, R.; Moralez, J. G.; Raez, J.; Yamazaki, T.; Cho, J. -Y.; Myles, A. J.; Kovalenko, A. Fenniri, H. *J. Am. Chem. Soc.* **2010**, *132*, 32–33.

(119) Deraedt, C.; Astruc, D. *Acc. Chem. Res.* **2014**, *47*, 494–503.

(120) Li, G.; Tang, Z. *Nanoscale* **2014**, *6*, 3995–4011.

(121) Takale, B. S.; Bao, M.; Yamamoto, Y. *Org. Biomol. Chem.* **2014**, *12*, 2005–2027.

(122) Na, K.; Zhang, Q.; Somorjai, G. A. *J. Clust. Sci.* **2014**, *25*, 83–114.

(123) Sevonkaev, I.; Privman, V.; Goia, D. *J. Solid State Electrochem.* **2013**, *17*, 279–297.

(124) Lu, Z.; Yin, Y. Chem. Soc. Rev. **2012**, *41*, 6874–6887.

(125) Yan, N.; Xiao, C.; Kou, Y. *Coord. Chem. Rev.* **2010**, *254*, 1179–1218.

(126) Lee, Y. J.; Lee, Y.; Oh, D.; Chen, T.; Ceder, G.; Belcher, A. M. *Nano Lett.* **2010**, *10*, 2433–2440.

(127) Lee, Y. J.; Yi, H.; Kim, W. -J.; Kang, K.; Yun, D. S.; Strano, M. S.; Ceder, G.; Belcher, A. M. *Science* **2009**, *324*, 1051–1055.

(128) Varghese, O. K.; Paulose, M.; LaTempa, T. J.; Grimes, C. A. *Nano Lett.* **2009**, *9*, 731–737.

(129) Wang, L.; Yang, R. T. *Energy Environ. Sci.* **2008**, *1*, 268–279.

(130) Nam, K. T.; Kim, D. -W.; Yoo, P. J.; Chiang, C. -Y.; Meethong, N.; Hammond, P. T.; Chiang, Y. -M.; Belcher, A. M. *Science* **2006**, *312*, 885–888.

(131) Murphy, C. J.; San, T. K.; Gole, A. M.; Orendorff, C. J.; Gao, J. X.; Gou, L.; Hunyadi, S. E.; Li, T. *J. Phys. Chem. B* **2005**, *109*, 13857–138570.

(132) Jain, P. K.; Huang, X.; El-Sayed, I. H.; El-Sayed, M. A. *Acc. Chem. Res.* **2008**, *41*, 1578–1586.

(133) Seferos, D. S.; Giljohann, D. A.; Hill, H. D.; Prigodich, A. E.; Mirkin, C. A. *J. Am. Chem. Soc.* **2007**, *129*, 15477–15479.

(134) Rosi, N. L.; Mirkin, C. A. *Chem. Rev.* **2005**, *105*, 1547–1562.

(135) Rosi, N. L.; Giljohann, D. A.; Thaxton, C. S.; Lytton-Jean, A. K. R.; Han, M. S.; Mirkin, C. A. *Science* **2006**, *312*, 1027–1030.

(136) Jain, P. K.; Lee, K. S.; El-Sayed, I. H.; El-Sayed, M. A. *J. Phys. Chem. B* **2006**, *110*, 7238–7248.

(137) He, L.; Musick, M. D.; Nicewarner, S. R.; Salinas, F. G.; Benkovic, S. J.; Natan, M. J.; Keating, C. D. *J. Am. Chem. Soc.* **2000**, *122*, 9071–9077.

(138) Coronado, E.; Ridera, A.; García-Martinez, J.; Linares, N.; Liz-Marzán, L. M. *J. Mater. Chem.* **2008**, *18*, 5682–5688.

(139) Cui, H.; Feng, Y.; Ren, W.; Zeng, T.; Lv, H.; Pan, Y. *Rec. Pat. Nanotech.* **2009**, *3*, 32–41.

(140) Sethi, M.; Pacardo, D. B.; Knecht, M. R. *Langmuir* **2010**, *26*, 15121–15134.

(141) Ogi, T.; Honda, R.; Tamaoki, K.; Saitoh, N.; Konishi, Y. *Powder Technol.* **2011**, *205*, 143–148.

(142) Mao, C.; Solis, D. J.; Reiss, B. D.; Kottmann, S. T.; Sweeney, R. Y.; Hayhurst, A.; Georgiou, G.; Iverson, B.; Belcher, A. M. *Science* **2004**, *303*, 213–217.

(143) Lee, S. -W.; Mao, C.; Flynn, C. E.; Belcher, A. M. *Science* **2002**, *296*, 892–895.

(144) Pietsch, T.; Appelhans, D.; Gindy, N.; Voit, B.; Fahmi, A. *Colloids Surf. A* **2009**, *341*, 93–102.

(145) Sylvestre, J. -P.; Poulin, S.; Kabashin, A. V.; Sacher, E.; Meunier, M.; Luong, J. H. T. *J. Phys. Chem. B* **2004**, *108,* 16864–16869.

(146) Chen, R.; Jiang, Y.; Xing, W.; Jin, W. *Ind. Eng. Chem. Res.* **2013**, *52*, 5002−5008.

(147) Yen, M. -Y.; Teng, C. -C.; Hsiao, M. -C.; Liu, P. -I.; Chuang, W. -P.; Ma, C. -C. M.; Hsieh, C. -K.; Tsai, M. -C.; Tsai, C. -H. *J. Mater. Chem.* **2011**, *21*, 12880–12888.

(148) Kanvah, S.; Joseph, J.; Schuster, G. B.; Barnett, R. N.; Cleveland, C. L.; Landman, U. *Acc. Chem. Res.* **2010**, *43*, 280–287.

(149) Duarte, V.; Gasparutto, D.; Jaquinod, M.; Cadet, J. *Nucleic Acids Res.* **2000**, *28*, 1555–1563.

(150) Newman, J. D. S.; Blanchard, G. J. *Langmuir* **2006,** *22,* 5882–5887.

(151) Newman, J. D. S.; Blanchard, G. J. *J. Nanopart. Res.* **2007**, *9*, 861–868.

(152) Clukay, C. J.; Grabill, C. N.; Hettinger, M. A.; Dutta, A.; Freppon, D. J.; Robledo, A.; Heinrich, H.; Bhattacharya, A.; Kuebler, S. M. *Appl. Surf. Sci.* **2014**, *292*, 128–136.

(153) Subramaniam, C.; Tom, R. T.; Pradeep, T. *J. Nanopart. Res.* **2005**, *7*, 209–217.

(154) (a) Thiagarajan, S.; Yang, R. -F.; Chen, S. -M. *Bioelectrochemistry* **2009**, *75*, 163–169. (b) Haynes, W. M. Ed. *CRC Handbook of Chemistry and Physics*, 95th ed., 2014–2015. (c) (c) Okouchi, S.; Suzuki, M.; Sugano, K.; Kagamimori, S.; Ikeda, S. J. Food Sci. **2002**, *67*, 1594–1598.

(155) Steenken, S.; Jovanovic, S. V. *J. Am. Chem. Soc.* **1997**, *119*, 617–618.

(156) Fischer, A. Krozer, A. Schlapbach, L. *Surf. Sci.* **1992**, *269*, 737–742.

(157) Tura J. M.; Regull P.; Victori L.; Dolors D. C. M. *Surf. Interface Anal.* **1988**, *11*, 447–449.

(158) Shafeev G. A.; Themlin J. -M.; Bellard L.; Marine W.; Cros A. *J. Vac. Sci. Technol. A* **1996**, *14*, 319–326.

(159) Kim, K. S.; Gossmann, A. F.; Winograd, N. *Anal. Chem.* **1974**, *46*, 197–200.

(160) Kibis, L. S.; Stadnichenko, A. I.; Koscheev, S. V.; Zaikovskii, V. I.; Boronin, A. I. *J. Phys. Chem. C* **2012**, *116*, 19342–19348.

(161) Kumar G.; Blackburn, J. R.; Albridge R. G.; Moddeman W. E.; Jones M. M. *Inorg. Chem.* **1972**, *11*, 296–300.

(162) Brun, M.; Berthet, A.; Bertolini, J. C. *J. Electron Spectrosc. Relat. Phenom.* **1999**, 104, 55–60.

(163) Butler, I. B.; Schoonen, M. A. A.; Rickard, D. T. *Talanta* **1994**, *41*, 211–215.

(164) Hamerton, I.; Hay, J. N.; Howlin, B. J.; Jones, J. R.; Lu, S. -Y.; Webb, G. A. *Chem. Mater.* **1997**, *9,* 1972–1977.

(165) Souza, R. A. D.; Zehnpfenning, J.; Martin, M.; Maier, J. *Solid State Ionics* **2005**, *176*, 1465–1471.

(166) Subbaraman, R.; Tripkovic, D.; Strmcnik, D.; Chang, K. -C.; Uchimura, M.; Paulikas, A. P.; Stamenkovic, V.; Markovic, N. M. *Science* **2011**, *334*, 1256–1260.

(167) Yu, J. C.; Ho, W.; Yu, J.; Hark, S. K.; Iu K. *Langmuir* **2003,** *19,* 3889–3896.

(168) Knecht, M. R.; Weir, M. G.; Frenkel, A. I.; Crooks, R. M. *Chem. Mater.* **2008**, *20,* 1019–1028.

(169) Creighton, J. A.; Eadon, D. G. *J. Chem. Soc., Faraday Trans.* **1991**, *87*, 3881–3891.

(170) Scott, R. W. J.; Ye, H.; Henriquez, R. R.; Crooks, R. M. *Chem. Mater.* **2003**, *15*, 3873–3878.

(171) Scott, R. W. J.; Wilson, O. M.; Crooks, R. M. *J. Phys. Chem. B* **2005**, *109*, 692–704.

(172) Lamy, H.; Léger, J. -M.; Srinivasan, S. "Direct methanol fuel cells – from a 20th century electrochemists' dream to a 21st century emerging technology" In *Modern Aspects of Electrochemistry*, Bockris, J. Ó. M.; Conway, B. E. Eds., Plenum Press, New York, 2000, Chapter 3, page 53.

(173) Greenwood, R; Kendall, K *J. Eur. Ceram. Soc.* **1999**, *19,* 479–488.

(174) Hanaor, D. A. H.; Michelazzi, M.; Leonelli, C.; Sorrell, C. C. *J. Eur. Ceram. Soc.* **2012**, *32*, 235–244.

(175) Woehl, T. J.; Evans, J. E.; Arslan, I.; Ristenpart, W. D.; Browning, N. D. *ACS Nano* **2012**, *6,* 8599–8610.

(176) Paradies, J. *Angew. Chem. Int. Ed.* **2014**, *53*, 3552–3557.

(177) Hounjet, L. J.; Stephan, D. W. *Org. Process Res. Dev.* **2014**, *18*, 385–391.

(178) Nakao, R.; Rhee, H.; Uozumi, Y. *Org. Lett.* **2005**, *7*, 163–165.

(179) Narayanan, R.; Tabor, C.; El-Sayed, M. A. *Top Catal.* **2008**, *48*, 60–74.

(180) Pérez-Lorenzo, M. *J. Phys. Chem. Lett.* **2012**, *3*, 167–174.

(181) Horiuti, I.; Polanyi, M. *Trans. Faraday Soc.* **1934**, *30*, 1164–1172.

(182) Wang, Z. -J.; Zhou, H. -F.; Wang, T. -L.; He, Y. -M.; Fan, Q. -H. *Green Chem.* **2009**, *11*, 767–769.

(183) Simakova, I. L.; Semikolenov, V. A. *Kinet. Catal.* **2000**, *41*, 421–425.

(184) Bhandari, R.; Pacardo, D. B.; Bedford, N. M.; Naik, R. R.; Knecht, M. R. *J. Phys. Chem. C* **2013**, *117*, 18053−18062.

(185) Karhu, H.; Kalantar, A.; Väyrynen, I. J.; Salmi, T.; Murzin, D. Yu. *Appl. Catal. A* **2003**, *247*, 283−294.

(186) Badano, J.; Lederhos, C.; L'Argentière, M. Q. P.; Coloma-Pascual, F. *Quim. Nova* **2010**, *33*,48−51.

(187) Hugon, A.; Delannoy, L.; Louis, C. *Gold Bulletin* **2008**, *41*, 127−138.

(188) Li; D.; Kaner, R. B. *J. Am. Chem. Soc.* **2006**, *128*, 968−975.

(189) Nakano, T. *Polym. J.* **2010**, *42*, 103–123.

(190) Tinoco, I. *J. Am. Chem. Soc.* **1960**, *82*, 4785–4790.

(191) Rohdes, W. *J. Am. Chem. Soc.* **1961**, *83*, 3609–3617.

(192) Langeveld-Voss, B. M. W.; Janssen, R. A. J.; Meijer, E. W. *J. Mol. Struct.* **2000**, *521*, 285–301.

(193) Hoeben, F. J. M.; Jonkheijm, P.; Meijer, E. W.; Schenning, A. P. H. J. *Chem. Rev.* **2005**, *105*, 1491–1546.

(194)   Gottarelli, G.; Lena, S.; Masiero, S.; Pieraccini, S.; Spada, G. P. *Chirality* **2008**, *20*, 471–485.

(195)   Mateos-Timoneda, M. A.; Crego-Calama, M.; Reinhoudt, D. N. *Chem. Soc. Rev.* **2004**, *33*, 363–372.

(196)   Song, S.; Asher, S. A. *J. Am. Chem. Soc.* **1989**, *111*, 4295–4305.

(197)   Lermo, E. R.; Langeveld-Voss, B. M. W.; Janssen, R. A. J.; Meijer, E. W. *Chem. Commun.* **1999**, 791–792.

(198)   Ma, H.; Lin, D., Liu, H.; Yang, L.; Zhang, L.; Liu, J. Mater. Chem. Phys. 2013, 138, 573–580.

(199)   Lacaze, E.; Urdal, K.; Bodö, P.; Garbarz, J.; Salaneck, W. R.; Schott, M. *J. Polym. Sci., Part B: Polym. Phys.* **1993**, *31*, 111–114.

(200)   Wilson, O. M.; Knecht, M. R.; Garcia-Martinez, J. C.; Crooks, R. M *J. Am. Chem. Soc.* **2006**, *128*, 4510–4511.

(201)   Cremer, P. S.; Somorjai, G. A. *J. Chem. Soc., Faraday Trans.* **1995**, *91*, 3671−3677.

(202)   Astruc, D. *Organometallic Chemistry and Catalysis: Heterogeneous Catalysis*; Springer, 2007, Chapter 20.

(203)   Krüger, T.; Vorndran, K.; Linker, T. *Chem. Eur. J.* **2009**, *15*, 12082–12091.

(204)   MacNair, A. J.; Tran, M. -M.; Nelson, J. E.; Sloan, G. U.; Ironmonger, A.; Thomas, S. P. *Org. Biomol. Chem.* **2014**, *12*, 5082–5088.

(205)   Imada, Y.; Iida, H.; Kitagawa, T.; Naota, T. *Chem. Eur. J.* **2011**, *17*, 5908–5920.

(206)   Verho, O.; Nagendiran, A.; Johnston, E. V.; Tai, C. -W.; Bäckvall, J. -E. *ChemCatChem* **2013**, *5*, 612–618.

(207) Hu, Y. L.; Ge, Q.; He, Y.; Lu, M. *ChemCatChem* **2010**, *2*, 392–396.

(208) Brunel, J. M. *Tetrahedron* **2007**, *63*, 3899–3906.

(209) Martín, C.; Belderraín, T. R.; Pérez, P. J. *Org. Biomol. Chem.* **2009**, *7*, 4777–4781.

(210) Narayanan, R. *Molecules* **2010**, *15*, 2124–2138 and references therein.

(211) Ogasawara, S.; Kato, S. *J. Am. Chem. Soc.*, **2010**, *132*, 4608–4613.

(212) Piao, Y.; Jang, Y.; Shokouhimehr, M.; Lee, I. S.; Hyeon, T. *Small* **2007**, *3*, 255–260.

(213) Zhou, S.; Johnson, M; Veinot, J. G. C. *Chem. Commun* **2010**, *46*, 2411–2413.

(214) Chen, Y. -H.; Hung, H. -H.; Huong, M. H. *J. Am. Chem. Soc.*, **2009**, *131*, 9114–9121.

(215) Kovala-Demertzi, D.; Kourkoumelis, N.; Derlat, K.; Michalak, J.; Andreadaki, F. J.; Kostas, I. D. *Inorg. Chim. Acta* **2008**, *361*, 1562–1565.

(216) Meng, L. J.; Ren, L. Z. *eXPRESS Polym. Lett.* **2008**, *2*, 251–255.

(217) Proch, S.; Mei, Y.; Villanueva, J. M. R.; Lu, Y.; Karpov, A.; Ballauff, M. Kempe, R. *Adv. Synth. Catal.* **2008**, *350*, 493–500.

(218) Zhang, Z.; Wang, Z. *J. Org. Chem.* **2006**, *71*, 7485–7487.

(219) Lu, F.; Ruiz, J.; Astruc, D. *Tetrahedron Lett.* **2004**, *45*, 9443–9445.

(220) Gopidas, K. R.; Whitesell, J. K.; Fox, M. A. *Nano Lett.* **2003**, *3*, 1757–1760.

(221) Fihri, A.; Bouhrara, M.; Nekoueishahraki, B.; Basset, J. -M.; Polshettiwar V. *Chem. Soc. Rev.* **2011**, *40*, 5181–5203.

(222) Torborga, C.; Beller, M. *Adv. Synth. Catal.* **2009**, *351*, 3027–3043.

(223) Glasnova, T. N.; Kappe, C. O. *Adv. Synth. Catal.* **2010**, *352*, 3089–3097.

(224) Nowothnick, H.; Blum, J.; Schomäcker, R. *Angew. Chem. Int. Ed.* **2011**, *50*, 1918–1921.

(225) Alonso, D. A.; Cívicos, J. F.; Nájera, C. *Synlett.* **2009**, *18*, 3011–3015.

(226) Itoh, T.; Kato, S.; Nonoyama, N.; Wada, T.; Maeda, K.; Mase, T. *Org. Process Res. Dev.* **2006**, *10*, 822–828.

(227) Dey, R.; Sreedhar, B.; Ranu, B. C. *Tetrahedron* **2010**, *66*, 2301–2305.

(228) Coppage, R.; Slocik, J. M.; Sethi, M.; Pacardo, D. B.; Naik, R. R.; Knecht, M. R. *Angew. Chem., Int. Ed.* **2010**, *49*, 3767−3770.

(229) Coppage, R.; Slocik, J. M.; Briggs, B. D.; Frenkel, A. I.; Naik, R. R.; Knecht, M. R. *ACS Nano* **2012**, *6*, 1625−1636.

(230) Coppage, R.; Slocik, J. M.; Ramezani-Dakhel, H.; Bedford, N. M.; Heinz, H.; Naik, R. R.; Knecht, M. R. *J. Am. Chem. Soc.* **2013**, *135*, 11048−11054.

(231) Nan, G.; Ren, F.; Luo, M. *Beilstein J. Org. Chem.* **2010**, *6,* No. 70.

(232) Martin, R.; Buchwald, S. L. *Acc. Chem. Res.* **2008**, *41*, 1461−1473.

(233) Wang, J. -W.; Meng, F. -H.; Zhang, L. -F. *Organometallics* **2009**, *28*, 2334-2337.

(234) Barnard, C. *Platinum Metals Rev.* **2008**, *52*, 38–45.

(235) Miguez, J. M. A.; Adrio, L. A.; Sousa-Pedrares, A.; Vila, J. M.; Hii, K. K. *J. Org. Chem.* **2007**, *72*, 7771–7774.

(236) Borhade, S. R.; Waghmode, S. B. *Beilstein J. Org. Chem.* **2011**, *7*, 310–319.

(237) Zhang, X.; Liu, A.; Chen, W. *Org. Lett.* **2008**, *10*, 3849–3852.

(238) Chen, M.; Zhang, Z.; Li, L.; Liu, Y.; Wang, W.; Gao, J. *RSC Adv.* **2014**, *4*, 30914–30922.

(239) Suzuki, A. *J. Organomet. Chem.* **1999**, *576*. 147–168.

(240) Jang, S. H.; Tai, T. B.; Kim, M. K.; Han, J. W.; Kim, Y. -H.; Shin, S. C.; Yoon, Y. J.; Kwon, S. K.; Lee, S. -G. *Bull. Korean Chem. Soc.* **2009**, *30*, 618–622.

(241) Zhao, H.; Xu, C.; Wang, B.; Zhao, J.; Cui, C.; Zhang, X. *Int. J. Electrochem. Sci.* **2012**, *7*, 10685–10697.

(242) Habashneh, A. Y.; Dakhil, O. O.; Zein, A.; Georghiou, P. E. *Synth. Commun.* **2009**, *39*, 4221–4229.

(243) Urbaneja, X.; Mercier, A.; Besnard, C.; Kündig, E. P. *Chem. Commun.* **2011**, *47*, 3739–3741.

(244) Sato, M.; Maruyama, G.; Tanemura, A. *J. Organomet. Chem.* **2002**, *655*, 23–30.

(245) Ikeda, S.; Aratani, N.; Osuka, A. *Chem. Commun.* **2012**, *48*, 4317–4319.

(246) Handy, S. T.; Wilson, T.; Muth, A. *J. Org. Chem.* **2007**, *72*, 8496–8500.

(247) Magano, J.; Dunetz, J. R. *Chem. Rev.* **2011**, *111*, 2177–2250.

(248) Balaji, G.; Shim, W. L.; Parameswaran, M.; Valiyaveettil, S. Org. Lett. **2009**, *11*, 4450–4453.

(249) Akhtaruzzaman, M.; Kamata, N.; Nishida, J. -I.; Ando, S.; Tada, H.; Tomura, M.; Yamashita, Y. *Chem. Commun.* **2005**, 3183–3185.

(250) Akhtaruzzaman, M.; Tomura, M.; Nishida, J. -I.; Yamashita, Y. J. Org. Chem. **2004**, *69*, 2953–2958.

(251) Neto, B. A. D.; Lopes, A. S.; Ebeling, G.; Gonçalves, R. S.; Costa, V. E. U.; Quina, F. H.; Dupont, J. *Tetrahedron* **2005**, *61*, 10975–10982.

(252) Sandanayaka, A. S. D.; Taguri, Y.; Araki, Y.; Ishi-i, T.; Mataka, S.; Ito, O. *J. Phys. Chem. B* **2005**, *109*, 22502–22512.

(253)   Dou, C.; Chen, D.; Iqbal, J.; Yuan, Y.; Zhang, H.; Wang, Y. *Langmuir* **2011**, *27*, 6323–6329.

(254)   Zhang, X.; Yamaguchi, R.; Moriyama, K.; Kadowaki, M.; Kobayashi, T.; Ishi-i, T.; Thiemann, T.; Mataka, S. *J. Mater. Chem.* **2006**, *16*, 736–740.

(255)   Omer, K. M.; Ku, S. -Y.; Wong, K. -T.; Bard, A. J. *J. Am. Chem. Soc.* **2009**, *131*, 10733–10741.

(256)   Thomas, K. R. J.; Lin, J. T.; Velusamy, M.; Tao, Y. -T.; Chuen, C. -H. *Adv. Funct. Mater.* **2004**, *14*, 83–90.

(257)   Neto, B. A. D.; Lopes, A. S.; Wüst, M.; Costa, V. E. U.; Ebeling, G.; Dupont, J. *Tetrahedron Lett.* **2005**, *46*, 6843–6846.

(258)   Mancilha, F. S.; Neto, B. A. D.; Lopes, A. S.; Moreira Jr., P. F.; Quina, F. H.; Gonçalves, R. S.; Dupont, J. *Eur. J. Org. Chem.* **2006**, 4924–4933.

(259)   Ku, S. -Y.; Wong, K. -T.; Bard, A. J. *J. Am. Chem. Soc.* **2008**, *130*, 2392–2393.

(260)   Neto, B. A. D.; Lapis, A. A. M.; Mancilha, F. S.; Vasconcelos, I. B.; Thum. C.; Basso, L. A.; Santos, D. S.; Dupont, J. *Org. Lett.* **2007**, *9*, 4001–4004.

(261)   Aldakov, D.; Palacios, M. A.; Anzenbacher, Jr., P. *Chem. Mater.* **2005**, *17*, 5238–5241.

(262)   Zhang, X.; Gorohmaru, H.; Kadowaki, M.; Kobayashi, T.; Ishi-i, T.; Thiemann, T.; Mataka, S. *J. Mater. Chem.* **2004**, *14*, 1901–1904.

(263)   Fang, Y.; Pandey, A. K.; Nardes, A. M.; Kopidakis, N.; Burn, P. L.; Meredith, P. *Adv. Energy Mater.* **2013**, *3*, 54–59.

(264)   Chiu, S. -W.; Lin, L. -Y.; Lin, H. -W.; Chen, Y. -H.; Huang, Z. -Y.; Lin, Y. -T.; Lin, F.; Liu, Y. -H.; Wong, K. -T. *Chem. Commun.* **2012**, *48*, 1857–1859.

(265) Anthony, J. E. *Chem. Mater.* **2011**, *23*, 583–590.

(266) Lin, L. -Y.; Chen, Y. -H.; Huang, Z. -Y.; Lin, H. -W.; Chou, S. -H.; Lin, F.; Chen, C. -W.; Liu, Y. -H.; Wong, K. -T. *J. Am. Chem. Soc.* **2011**, *133*, 15822–15825.

(267) Chen, Y. -H.; Lin, L. -Y.; Lu, C. -W.; Lin, F.; Huang, Z. -Y.; Lin, H. -W.; Wang, P. -H.; Liu, Y. -H.; Wong, K. -T.; Wen, J.; Miller, D. J.; Darling, S. B. *J. Am. Chem. Soc.* **2012**, *134*, 13616−13623.

(268) Sun, Y.; Welch, G. C.; Leong, W. L.; Takacs, C. J.; Bazan, G. C.; Heeger, A. J. *Nature Mater.* **2012**, *11*, 44−48.

(269) Lin, L. -Y.; Lu, C. -W.; Huang, W. -C.; Chen, Y. -H.; Lin, H. -W.; Wong, K. -T. *Org. Lett.* **2011**, *13*, 4962–4965.

(270) Bernius, M.; Inbasekaran, M.; Woo, E.; Wu, W.; Wujkowski, L. *J. Mater. Sci.: mater. Electronics* **2002**, *11*, 111–116.

(271) Grey, J. K.; Kim, D. Y.; Donley, C. L.; Miller, W. L.; Kim, J. S.; Silva, C.; Friend, R. H.; Barbara, P. F. *J. Phys. Chem. B* **2006**, *110*, 18898–18903.

(272) Bernius, M. T.; Inbasekaran, M.; O'Brien, J.; Wu, W. *Adv. Mater.* **2000**, *12*, 1737–1750.

(273) Benedetto, F. D.; Camposeo, A.; Pagliara, S.; Mele, E.; Persano, L.; Stabile, R.; Cingolani, R.; Pisignano, D. *Nature Nanotech.* **2008**, *3*, 614–619.

(274) Edder, C.; Armstrong, P. B.; Prado, K. B.; Fréchet, J. M. J. *Chem. Commun.* **2006**, 1965–1967.

(275) Herguth, P.; Jiang, X.; Liu, M. S.; Jen, A. K. -Y. *Macromolecules* **2002**, *35*, 6094–6100.

(276) Kylmälä, T.; Kuuloja, N.; Xu, Y.; Rissanen, K.; Franzén, R. *Eur. J. Org. Chem.* **2008**, 4019–4024.

(277) Qin, C.; Lu, W. *J. Org. Chem.* **2008**, *73*, 7424–7427.

(278) Rottländer, M.; Palmer, N.; Knochel, P. *Synlett* **1996**, *6*, 573–575.

(279) Chen, H.; Huang, Z.; Hu, X.; Tang, G.; Xu, P.; Zhao, Y.; Cheng, C. -H. *J. Org. Chem.* **2011**, *76*, 2338–2344.

(280) Qiu, J.; Wang, L.; Liu, M.; Shen, Q.; Tang, J. *Tetrahedron Lett.* **2011**, *52*, 6489–6491.

(281) Li, P.; Wang, L.; Zhang, L.; Wang, G. -W. *Adv. Synth. Catal.* **2012**, *354*, 1307–1318.

(282) Felpin, F. -X.; Fouquet, E. *Adv. Synth. Catal.* **2008**, *350*, 863–868.

(283) Liu, N.; Liu, C.; Jin, Z. *Green Chem.* **2012**, *14*, 592–597.

(284) Seechurn, C. C. C. J.; Parisel, S. L.; Colacot, T. J. *J. Org. Chem.* **2011**, *76*, 7918–7932.

(285) Felpin, F. -X.; Fouquet, E.; Zakri, C. *Adv. Synth. Catal.* **2009**, *351*, 649–655.

(286) Alacid, E.; Nájera, C. *Org. Lett.* **2008**, *10*, 5011–5014.

(287) Hong, M. C.; Choi, M. C.; Chang, Y. W.; Lee, Y.; Kim, J.; Rhee, H. *Adv. Synth. Catal.* **2012**, *354*, 1257–1263.

(288) Sindhuja, E.; Ramesh, R.; Liu, Y. *Dalton Trans.* **2012**, *41*, 5351–5361.

(289) Jin, R.; Bian, Z.; Kang, C.; Guo, H.; Gao, L. *Synth. Commun*. **2005**, *35*, 1897–1902.

(290) Bolliger, J. L.; Frech, C. M. *Chem. Eur. J.* **2010**, *16*, 11072–11081.

(291) Bolliger, J. L.; Frech, C. M. *Adv. Synth. Catal.* **2010**, *352*, 1075–1080.

(292) Zhao, D; Ding, K. *ACS Catalysis* **2013**, *3*, 928–944.

(293) Mikami, K.; Lautens, M. Eds. *New Frontiers in Asymmetric Catalysis*, John Wiley & Sons Inc.: New York, 2007.

(294) Ojima, I. Ed. *Catalytic Asymmetric Synthesis,* 3rd ed., John Wiley & Sons Inc.: New York, 2010.

(295) Lühr, S; Holz, J.; Börner, A. *ChemCatChem* **2011**, *3*, 1708–1730.

(296) Blaser, H. -U.; Schmidt, S. Eds *Asymmetric Catalysis on Industrial Scale,* Wiley-VCH: Weinheim, 2004.

(297) Ohmatsu, K.; Ito, M.; Kunieda, T.; Ooi, T. *Nat. Chem.* **2012**, *4*, 473–477.

(298) Hamilton, G. L.; Kang, E. J.; Mba, M.; Toste, F. D. *Science* **2007**, *317*, 496–499.

(299) Mukherjee, S.; List, B. *J. Am. Chem. Soc.* **2007**, *129*, 11336–11337.

(300) Liao, S.; List, B. *Angew. Chem. Int. Ed.* **2010**, *49*, 628–631.

(301) Jiang, G.; List, B. *Angew. Chem. Int. Ed.* **2011**, *50*, 9471–9474.

(302) Jiang, G.; Halder, R.; Fang, Y.; List, B. *Angew. Chem. Int. Ed.* **2011**, *50*, 9752–9755.

(303) Meeuwissen, J.; Reek, J. N. H. *Nat. Chem.* **2010**, *2*, 615–621.

(304) Ringe, D.; Petsko, G. A. *Science* **2008**, *320*, 1428–1429.

(305) Gross, E.; Liu, J. H.; Alayoglu, S.; Marcus, M. A.; Fakra, S. C.; Toste, F. D. Somorjai, G. A. *J. Am. Chem. Soc.* **2013**, *135*, 3881–3886.

(306) Raynal, M.; Ballester, P.; Vidal-Ferran, A.; Leeuwen, P. W. N. M. V *Chem. Soc. Rev.* **2014**, *43*, 1734–1787.

(307) Park, S.; Sugiyama, H. *Molecules* **2012**, *17*, 12792–12803.

(308) Pluth, M. D.; Bergman, R. G.; Raymond, K. N. *Supramolecular Catalysis*, Chapter 8, Wiley-VCH: Weinheim, 2008, 165–191.

(309) Chin, J. *Acc. Chem. Res.* **1991**, *24*, 145–152.

(310) Uhlenbeck, O. C. *Nature* **1987**, *328*, 596–600.

(311) Zaug, A. J.; Michael, D. B.; Cech, T. R. *Nature* **1986**, *324*, 429–433.

(312) Chin, J.; Banaszczyk, M. *J. Am. Chem. Soc.* **1989**, *111*, 4103–4105.

(313) Benkovic, S. J.; Hammes-Schiffer, S. *Science* **2003**, *301*, 1196–1202.

(314) Marshall, S. T.; O'Brien, M.; Oetter, B.; Corpuz, A.; Richards, R. M.; Schwartz, D. K.; Medlin, J. W. *Nat. Mat.* **2010**, *9*, 853–858.

(315) Rod, T. H.; Norskov, J. K. *Surf. Sci.* **2002**, *500*, 678–698.

(316) Janssen, K. P. F.; Cremer, G. D.; Neely, R. K.; kubarev, A. V.; Loon, J. V.; Martens, J. A.; Vos, D. E. D.; Roeffaers, M. B. J.; Hofkens, J. *Chem. Soc. Rev.* **2014**, *43*, 990–1006.

(317) Sheldon, R. A. *Chem. Soc. Rev.* **2012**, *41*, 1437–1451.

(318) Boersma, A. J.; Klijn, J. E.; Feringa, B. L.; Roelfes, G. *J. Am. Chem. Soc.* **2008**, *130*, 11783–11790.

(319) Davies, R. R.; Distefano, M. D. *J. Am. Chem. Soc.* **1997**, *119*, 11643–11652.

(320) Collot, J.; Gradinaru, J.; Humbert, N.; Skander, M.; Zocchi, A.; Ward, T. R. *J. Am. Chem. Soc.* **2003**, *125*, 9030–9031.

(321) Wilson, M. E.; Whitesides, G. M. *J. Am. Chem. Soc.* **1978**, *100*, 306–307.

(322) Letondor, C.; Pordea, A.; Humbert, N.; Ivanova, A.; Mazurek, S.; Novic, M.; Ward, T. R. *J. Am. Chem. Soc.* **2006**, *128*, 8320–8328.

(323) Letondor, C.; Humbert, N.; Ward, T. R. *Proc. Natl. Acad. Sci. U.S.A.* **2005**, *102*, 4683–4687.

(324) Pierron, J.; Malan, C.; Creus, M.; Gradinaru, J.; Hafner, I.; Ivanova, A.; Sardo, A.; Ward, T. R. *Angew. Chem., Int. Ed.* **2008**, *47*, 701–705.

(325) Mahammed, A.; Gross, Z. *J. Am. Chem. Soc.* **2005**, *127*, 2883–2887.

(326) Carey, J. R.; Ma, S. K.; Pfister, T. D.; Garner, D. K.; Kim, H. K.; Abramite, J. A.; Wang, Z.; Guo, Z.; Lu, Y. *J. Am. Chem. Soc.* **2004**, *126*, 10812–10813.

(327) Velde, F. V. D.; Könemann, L.; Rantwijk, F. V.; Sheldon, R. A. *Chem. Commun.* **1998**, 1891–1892.

(328) Sugimoto, T.; Kokubo, T.; Miyazaki, J.; Tanimoto, S.; Okano, M. *J. Chem. Soc., Chem. Commun.* **1979**, 402–404.

(329) Okrasa, K.; Kazlauskas, R. J. *Chem. Eur. J.* **2006**, *12*, 1587–1596.

(330) Fernández-Gacio, A.; Codina, A.; Fastrez, J.; Riant, O.; Soumillion, P. *ChemBioChem* **2006**, *7*, 1013–1016.

(331) Kokubo, T.; Sugimoto, T.; Uchida, T.; Tanimoto, S.; Okano, M. *J. Chem. Soc., Chem. Commun.* **1983**, 769–770.

(332) Reetz, M. T.; Jiao, N. *Angew. Chem., Int. Ed.* **2006**, *45*, 2416–2419.

(333) Colonna, S.; Manfredi, A.; Annunziata, R. *Tetrahedron Lett.* **1988**, *29*, 3347–3350.

(334) Roy, R. S.; Imperiali, B. *Protein Eng.* **1997**, *10*, 691–698.

(335) Roelfes, G. *Mol. Biosys.* **2007**, *3*, 126–135.

(436) Stuhlmann, F.; Jäschke, A. *J. Am. Chem. Soc.* **2002**, *124*, 3238–3244.

(337) Li, X.; Liu, D. R. *J. Am. Chem. Soc.* **2003**, *125*, 10188–10189.

(338)   Seelig, B.; Keiper, S.; Stuhlmann, F.; Jäschke, A. *Angew. Chem., Int. Ed.* **2000**, *39*, 4576–4579.

(339)   Kozlov, I. A.; Politis, P. K.; Pitsch, S.; Herdewijn, P.; Orgel, L. E. *J. Am. Chem. Soc.* **1999**, *121*, 1108–1109.

(340)   Schmidt, J. G.; Nielsen, P. E.; Orgel, L. E. *J. Am. Chem. Soc.* **1997**, *119*, 1494–1495.

(341)   Bolli, M.; Micura, R.; Eschenmoser, A. *Chem. Biol.* **1997**, *4*, 309–320.

(342)   Joyce, G. F.; Visser, G. M.; Boeckel, C. A. A. V.; Boom, J. H. V.; Orgel, L. E.; Westrenen, J. V. *Nature* **1984**, *310*, 602–604.

(343)   Roelfes, G.; Feringa, B. L. *Angew. Chem. Int. Ed.* **2005**, *44*, 3230–3232.

(344)   Roelfes, G.; Boersma, A. J.; Feringa, B. L. *Chem. Commun.* **2006**, 635–637.

(345)   Boersma, A. J.; Feringa, B. L.; Roelfes, G. *Org. Lett.* **2007**, *9*, 3647–3650.

(346)   Coquière, D.; Feringa, B. L.; Roelfes, G. *Angew. Chem. Int. Ed.* **2007**, *46*, 9308–9311.

(347)   Boersma, A. J.; Feringa, B. L.; Roelfes, G. *Angew. Chem. Int. Ed.* **2009**, *48*, 3346–3348.

(348)   Boersma, A. J.; Coquière, D.; Greerdink, D.; Rosati, F.; Feringa, B. L.; Roelfes, G. *Nat. Chem.* **2010**, *2*, 991–995.

(349)   Boersma, A. J.; Bruin, B.; Feringa, B. L.; Roelfes, G. *Chem. Commun.* **2012**, *48*, 2394–2396.

(350)   Oltra, N. S.; Roelfes, G. *Chem. Commun.* **2008**, 6039–6041.

(351)   Fournier, P.; Fiammengo, R.; Jäschke, A. *Angew. Chem. Int. Ed.* **2009**, *48*, 4426–4429.

(352) Shibata, N.; Yasui, H.; Nakamura, S.; Toru, T. *Synlett* **2007**, 1153–1157.

(353) Park, S.; Ikehata, K.; Watabe, R.; Hidaka, Y.; Rajendran, A.; Sugiyama, H. *Chem. Commun.* **2012**, 10398–10400.

(354) Roe, S.; Ritson, D. J.; Garner, T.; Searle, M.; Moses, J. E. *Chem. Commun.* **2010**, 4309–4311.

(355) Wang, C.; Li, Y.; Jia, G.; Liu, Y.; Lu, S.; Li, C. *Chem. Commun.* **2012**, 6232–6234.

(356) Wang, C.; Jia, G.; Zhou, J.; Li, Y.; Liu, Y.; Lu, S.; Li, C. *Angew. Chem. Int. Ed.* **2012**, *51*, 9352–9355.

(357) Megens, R. P.; Roelfes, G. *Org. Biomol. Chem.* **2010**, *8*, 1387–1393.

(358) Rozenman, M. M.; Liu, D. R. *ChemBioChem* **2006**, *7*, 253–256.

(359) Oila, M. J.; Koskinen, A. M. P. *ARKIVOC* **2006**, *xv*, 76–83.

(360) Huang, Y.; Xu, S.; Lin, V. S. -Y. *ChemCatChem* **2011**, *3*, 690–694.

(361) Gross, E.; Liu, J. H. -C.; Toste, F. D.; Somorjai, G. A. *Nat. Chem.* **2012**, *4*, 947–952.

(362) Bringmann, G.; Mortimer, A. J. P.; Keller, P. A.; Gresser, M. J.; Garner, J.; Breuning, M. *Angew. Chem. Int. Ed.* **2005**, *44*, 5384–5427.

(363) Mikami, K.; Miyamoto, T.; Hatano, M. *Chem. Commun.* **2004**, 2082–2083.

(364) Colobert, F.; Valdivia, V.; Choppin, S.; Leroux, F. R.; Fernández, I.; Alvarez, E.; Khiar, N. *Org. Lett.* **2009**, *11*, 5130–5133.

(365) Shen, X.; Jones, G. O.; Watson, D. A.; Bhayana, B.; Buchwald, S. L. *J. Am. Chem. Soc.* **2010**, *132*, 11278–11287.

(366) Tang, W.; Patel, N. D.; Xu, G.; Xu, X.; Savoie, J.; Ma, S.; Hao, M. -H.; Keshipeddy, S.; Capacci, A. G.; Wei, X.; Zhang, Y.; Gao, J. J.; Li, W.; Rodriguez, S.; Lu, B. Z.; Yee, N. K.; Senanayake, C. H. *Org. Lett.* **2012**, *14*, 2258–2261.

(367) Karthikeyan, T.; Sankararaman, S. *Tetrahedron Lett.* **2009**, *50*, 5834–5837.

(368) Cammidge, A. N.; Crépy, K. V. L. *J. Org. Chem.* **2003**, *68*, 6832–6835.

(369) Suau, R.; Rico, R.; Nájera, F.; Ortiz-López, F. J.; López-Romero, J. M.; Moreno-Mañas, M.; Roglans, A. *Tetrahedron* **2004**, *60*, 5725–5735.

(370) Bari, L. D.; Pescitelli, G.; Salvadori, P. *J. Am. Chem. Soc.* **1999**, *121*, 7998–8004.

(371) Kubinyi, M.; Pál, K.; Baranyai, P.; Grofcsik, A.; Bitter, I.; Grün, A. *Chirality* **2004**, *16*, 174–179.

(372) Nishizaka, M.; Mori, T.; Inoue, Y. *J. Phys. Chem. A* **2011**, *115*, 5488–5495.

(373) Nakai, Y.; Nishizaka, M.; Yang, C.; Fukuhara, G.; Mori, T.; Inoue, Y. *Chirality* **2011**, *23*, E22–E27.

(374) Richardson, J. M.; Jones, C. W. *J. Catal.* **2007**, *251*, 80–93.

(375) Trost, B. M.; Fandrick, D. R. *Aldrichimica Acta* **2007**, *40*, 59–72.

(376) Walsh, P. J.; Kozlowski, M. C. *Fundamentals of Asymmetric Catalysis*, Chapter 4, University Science Books: Virginia, 2009.

(377) Hsu, Y. -C.; Datta, S.; Ting, C. -M.; Liu, R. -S. *Org. Lett.* **2008**, *10*, 521–524.

(378) Shen, H. -C.; Pal, S.; Lian, J. -J.; Liu, R. -S. *J. Am. Chem. Soc.* **2003**, *125*, 15762–15763.

(379) Toummini, D.; Ouazzani, F.; Taillefer, M. *Org. Lett.* **2013**, *15*, 4690–4693.